CARL VON OSSIETZKY universität OLDENBURG

Controlling Ultracold Atoms with Modulated Standing Light Waves: Present Status and Future Perspectives

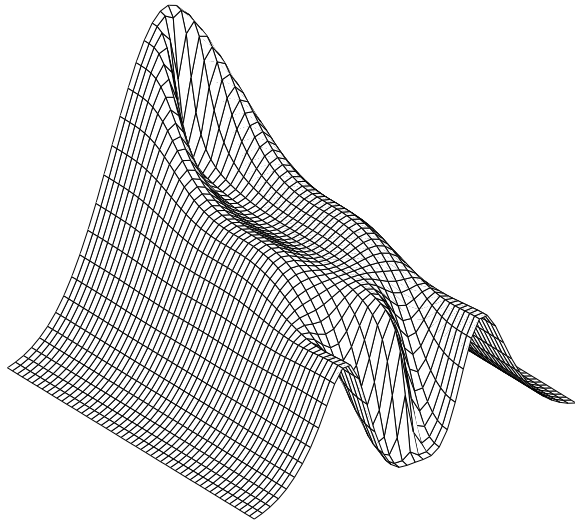

Von der Fakultät für Mathematik und Naturwissenschaften der Carl von Ossietzky Universität Oldenburg zur Erlangung des Grades und Titels eines Doktors der Naturwissenschaften (Doctor rerum naturalium, abgekürzt: Dr. rer. nat.) angenommene Dissertation von Herrn

Dipl.-Phys. Stephan Arlinghaus

geboren am 08. Juni 1983 in Vechta, Deutschland.

Referee:	Prof. Dr. Martin Holthaus
Second referee:	Prof. Dr. Andreas Engel
Day of defense:	May 3, 2012

Abstract

The scope of the present publication-based thesis on periodically forced optical lattices is twofold: In the first part, the reader is introduced to the main concepts required to formulate the central results of this thesis, and a review is given of landmark papers on coherently controlling ultracold atoms by subjecting them to periodic forces. The second part provides the author's own results of original research on the subject and consists of four publications and a preprint.

The central object of this thesis is a cloud of noninteracting ultracold atoms or a Bose-Einstein condensate that is trapped in a standing wave of laser light. In the first chapter the reader is familiarized with the effect of Bose-Einstein condensation and the mechanisms are discussed to tune the interaction between the atoms to zero. In addition, various protocols are sketched for cooling down the atoms to the temperature regime in which they are trapped by laser light. The chapter closes with the introduction of Bloch oscillations emerging due to an external constant force acting on the system.

In the second chapter, the constraint of a constant force is lifted, switching the focus to time-periodic forces. The concept of "dressing" the system by a periodic force is central here and the reader is introduced to basic elements of Floquet theory, a powerful tool to describe periodically driven systems, which is crucial for exerting control in a precise and efficient way. The first experimental realizations of periodically modulated optical

lattices are landmarks in the field and a selection of papers is discussed representing most recent efforts to exploit external forces for exerting control. The end of the chapter contains recent theoretical investigations by the author on multiphoton-like transitions.

The section "Publications" constitutes the central part of this thesis and contains its main results. Ultracold atoms in optical lattices are much more flexible systems than the solid state counterpart they are emulating. On the one hand, the parameters of the system can be varied almost arbitrarily, such as the interaction strength between the atoms or the spacing of the lattice. With the interaction strength tuned to zero, even single-particle models can accurately be realized experimentally without any effects present due to the interaction. This allows for a detailed investigation of single-particle dynamics on a quantum level, whereas many-body effects can be disentangled at a later stage. On the other hand, these systems can be subjected to external forces with exceptionally high scaled amplitudes that would induce polarization effects in traditional crystalline solids or might even cause them to disintegrate. Hence, driven optical lattices can be used as strong-field simulators, as discussed in Paper I, and offer the unique possibility to study effects such as multiphoton-like processes in their purest form as described in preprint V. In the book chapter "Dynamic localization in optical lattices", see Publication II, the effect of hampering or even completely stopping quantum tunnelling by applying a periodic force to the atoms is discussed in detail. It is shown that this effect can be utilized to coherently control the "metal-insulator"–like transition occurring in sufficiently deep quasiperiodic lattices.

For protocols aiming at driving-induced control, the particle is subjected to pulsed driving: The amplitude of the external force is not kept constant, but endowed with a smooth envelope function that varies sufficiently slowly in time. In the generic case, the particle is initially prepared

in a state pertaining to the lowest energy band of the lattice with a Gaussian momentum distribution. A convenient method to monitor transitions to higher bands is to subject the particle to a pulse with fixed driving frequency and a certain maximum driving amplitude, and to measure the probability of finding the particle in any but the lowest band after the pulse. By repeating this procedure for different driving frequencies ω, resonances are revealed when the energy $\hbar\omega$ matches gaps in the dispersion relation of the undriven lattice. But most importantly, additional resonances occur since the bands "dressed" by the driving are ac-Stark-shifted.

The central theoretical concept for understanding the dynamics of a particle subjected to pulsed driving is the quasienergy surface. According to Floquet theory, if the lattice system is driven with a fixed frequency and amplitude measured by K, the energy bands $E_n(k)$ of the undriven lattice with wavenumber k and band index n are replaced by quasienergy bands $\varepsilon_n(k)$, which are defined only modulo $\hbar\omega$. In the limit of a vanishing driving amplitude, that is $K \to 0$, the quasienergy bands are continuously connected to the dispersion relation $E_n(k)$. If a pulsed driving scenario is employed instead of a constant amplitude, the quasienergy bands change in the course of time just as the driving amplitude, thus forming quasienergy surfaces $\varepsilon_n(k, K)$. The initial wave packet is generically prepared in a single energy band and hence on a single quasienergy surface. The wave packet is parallel transported on that surface during the pulse if its envelope varies sufficiently slowly. The dynamics of the wave packet on the quasienergy surface can be monitored by using a family of bases, each given by a set of spatiotemporal Bloch waves, which are solutions to the Schrödinger equation with a Hamiltonian periodic both in space and in time, and which pertain to the instantaneous driving amplitudes during the pulse. Such a representation of the wave-packet's dynamics can be favorable when compared to the traditional crystal-momentum represen-

tation, which resorts to the static basis of Bloch waves: On the one hand, the wave-packet's motion in k space according to the semi-classical acceleration theorem is already incorporated in the bases of spatiotemporal Bloch waves, which are themselves time-dependent. On the other hand, during the pulse, the crystal-momentum representation might exhibit transient excitations, which are caused by the heavily Stark-shifted bands. While these transient excitations are hard to explain in this setting, the family of instantaneous spatiotemporal Bloch waves constitutes a set of bases more adapted to the symmetries of the system and the dynamics remain fully adiabatic in this representation.

This is true as long the quasienergy surfaces do not anti-cross in the regions explored by the wave packet during the pulse. The fact that excitations of the wave packet to higher quasienergy surfaces are closely linked to their morphology can be exploited by choosing the driving frequency (and hence the quasienergy surfaces) such that the momentum distribution of the particle is changed deliberately. This allows to exploit interband transitions to transport parts of the wave-packet's momentum distribution selectively to higher bands, thus creating exotic states, as elaborated on in Paper IV. This concept is vastly expanded by adding a second constant force, which acts homogeneously on the entire system. As detailed in Paper III, the combination of both forces grants the freedom to move the wave-packet's momentum distribution on its quasienergy surface in any direction, so regions of avoided crossings can deliberately be accessed or avoided during a single pulse. This is rendered possible by a generalization of the well known acceleration theorem by F. Bloch to the Floquet setting, for which the instantaneous bases for spatiotemporal Bloch waves turn out to be crucial. In addition, this generalized acceleration theorem facilitates an efficient theoretical explanation of super Bloch oscillations, which reduce to the case of "almost resonant tilting" within this context.

Apart from a preprint, three papers are already published in international peer-reviewed journals and one manuscript is printed as a chapter of the book “Dynamical Tunneling – Theory and Experiment”.

Zusammenfassung

Die vorliegende publikationsbasierte Dissertation über periodisch angetriebene optische Gitter verfolgt zwei Ziele: Im ersten Teil wird der Leser in die für die Formulierung der zentralen Ergebnisse erforderlichen Konzepte dieser Arbeit eingeführt, und es wird eine Übersicht herausragender Veröffentlichungen zur kohärenten Kontrolle ultrakalter Atome durch periodische Kräfte gegeben. Der zweite Teil liefert die Ergebnisse selbstständiger Forschung des Autors zu diesem Themengebiet und besteht aus vier Publikationen sowie einem Preprint.

Das zentrale Objekt der Dissertation ist eine Wolke nicht wechselwirkender ultrakalter Atome oder eines Bose-Einstein Kondensates, die in einer stehenden Welle aus Laserlicht gefangen ist. Im ersten Kapitel wird der Leser mit dem Phänomen der Bose-Einstein Kondensation vertraut gemacht und es werden die Mechanismen beschrieben, mit denen die Wechselwirkung zwischen den Atomen künstlich ausgeschaltet werden kann. Zusätzlich werden verschiedene Kühlverfahren skizziert, mit deren Hilfe die Atome in jenen Temperaturbereich gebracht werden, der das Einfangen der Atome durch Laserlicht ermöglicht. Das Kapitel endet mit der Einführung von Bloch-Oszillationen, die durch eine externe konstante Kraft verursacht werden.

Im zweiten Kapitel wird die Einschränkung einer konstanten Kraft aufgehoben und der Fokus liegt auf zeitperiodischen Kräften. Das Konzept, ein System durch eine periodische Kraft zu „dressen“ steht hier im Mittel-

punkt. Der Leser wird dabei in die grundlegenden Elemente der Floquet-Theorie eingeführt, die ein leistungsfähiges Werkzeug zur Beschreibung periodisch angetriebener Systeme darstellt und ausschlaggebend ist, um das System präzise und effizient zu kontrollieren. Die ersten experimentellen Realisierungen periodisch modulierter optischer Gitter sind Meilensteine des Forschungsfeldes, und eine Auswahl an Veröffentlichungen zur Ausübung von Kontrolle mittels externer Kräfte wird diskutiert. Am Ende des Kapitels werden jüngste theoretische Forschungsarbeiten des Autors zu Multiphoton-Übergängen präsentiert.

Der Abschnitt „Publikationen“ stellt den zentralen Teil dieser Dissertation dar und enthält ihre Hauptergebnisse. Ultrakalte Atome in optischen Gittern sind weitaus flexiblere Systeme als ihre Gegenstücke aus der Festkörperphysik, die sie emulieren. Auf der einen Seite lassen sich die Systemparameter wie beispielsweise die Wechselwirkungsstärke oder der Gitterabstand fast beliebig variieren. Bei verschwindender Wechselwirkung sind sogar Einteilchen-Modelle experimentell exakt umsetzbar, ohne dass sich wechselwirkungsinduzierte Effekte bemerkbar machen. Dies erlaubt eine genaue Untersuchung der quantenmechanischen Einteilchen-Dynamik; Vielteilchen-Effekte können so zu einem späteren Zeitpunkt von Einteilchen-Effekten getrennt werden. Auf der anderen Seite können diese Systeme externen Kräften mit außergewöhnlich hohen skalierten Amplituden ausgesetzt werden, die in herkömmlichen kristallinen Festkörpern zu Polarisationseffekten oder sogar zur Auflösung des Materials führen. Daher können, wie in Publikation I beschrieben, angetriebene optische Gitter auch als Starkfeld-Simulatoren verwendet werden und bieten die einzigartige Möglichkeit, Effekte wie zum Beispiel Multiphoton-Prozesse in Reinform zu studieren, siehe Preprint V. Das Buchkapitel, dessen Titel sich mit „Dynamische Lokalisierung in optischen Gittern“ übersetzt und als Publikation II in diese Arbeit eingebunden ist, enthält eine de-

taillierte Diskussion darüber, wie mit Hilfe einer periodischen Kraft das quantenmechanische Tunneln der Atome im Gitter eingeschränkt oder sogar ganz unterbunden werden kann. Es wird aufgezeigt, wie dieser Effekt zur kohärenten Kontrolle des „Metall-Isolator“-ähnlichen Überganges in hinreichend tiefen quasiperiodischen Gittern genutzt werden kann.

Bei Verfahren, die auf eine antriebsinduzierte Kontrolle abzielen, wird das Teilchen häufig einem gepulsten Antrieb ausgesetzt: Die Amplitude der externen Kraft wird nicht konstant gehalten, sondern mit einer glatten Einhüllenden versehen, die sich zeitlich hinreichend langsam ändert. Dabei ist das Teilchen typischerweise in einem Zustand präpariert, der sich lediglich auf das unterste Energieband des Gitters bezieht und eine Gauß'sche Impulsverteilung besitzt. Übergänge in höhere Bänder können auf einfache Art und Weise gemessen werden, indem das Teilchen einem gepulsten Antrieb mit einer festen Antriebsfrequenz und einer gewissen Maximalamplitude unterworfen wird, und anschließend die Wahrscheinlichkeit gemessen wird, das Teilchen in irgendeinem außer dem untersten Band zu finden. Wird diese Prozedur für verschiedene Antriebsfrequenzen ω wiederholt, so treten Resonanzen auf, wenn die Energie $\hbar\omega$ genau den Energielücken in der Dispersionsrelation des ungetriebenen Gitters entspricht. Noch wichtiger ist jedoch das Auftreten weiterer Resonanzen aufgrund der ac-Stark-Verschiebung der durch den Antrieb „gedressten“ Bänder.

Das zentrale theoretische Konzept zum Verständnis der Dynamik eines Teilchens, das einem gepulsten Antrieb unterworfen ist, ist die Quasienergiefläche. Wenn das Gittersystem mit einer festen Frequenz und einer mit K bezeichneten Amplitude angetrieben wird, so werden gemäß der Floquet-Theorie die Energiebänder $E_n(k)$ des ungetriebenen Gitters mit Wellenzahl k und Bandindex n durch Quasienergiebänder $\varepsilon_n(k)$ ersetzt, die lediglich modulo $\hbar\omega$ definiert sind. Im Grenzfall verschwindender An-

triebsamplitude, das heißt $K \to 0$, sind die Quasienergiebänder kontinuierlich mit der Dispersionsrelation $E_n(k)$ verbunden. Wird das System jedoch nicht mit einer konstanten Amplitude angetrieben, sondern stattdessen ein gepulster Antrieb verwendet, so ändern sich die Antriebsamplituden und mit ihnen die Quasienergiebänder im Laufe der Zeit, und bilden nun Quasienergieflächen $\varepsilon_n(k, K)$. Das Anfangswellenpaket ist typischerweise nur in einem einzigen Energieband und damit auf einer einzigen Quasienergiefläche präpariert, und das Wellenpaket wird während des Pulses auf dieser Fläche paralleltransportiert, vorausgesetzt die Pulseinhüllende variiert hinreichend langsam. Die Dynamik des Wellenpaketes auf der Quasienergiefläche kann mit Hilfe einer Schar von Basen verfolgt werden. Dabei besteht jede einzelne Basis aus raumzeitlichen Blochwellen, die sich als Lösung der Schrödingergleichung mit einem räumlich und zeitlich periodischen Hamilton-Operator ergeben und zu einer instantanen Antriebsamplitude während des Pulses gehören. Eine solche Darstellung der Dynamik des Wellenpaketes kann der traditionellen Kristallimpulsdarstellung (engl. crystal-momentum representation) vorzuziehen sein, die sich auf eine Basis von statischen Blochwellen bezieht: Einerseits ist die Bewegung des Wellenpaketes im k-Raum gemäß dem semiklassischen Beschleunigungstheorem bereits in die Basen der raumzeitlichen Blochwellen eingebaut, welche ihrerseits schon zeitabhängig sind. Andererseits kann die Kristallimpulsdarstellung vorübergehende Anregungen anzeigen, die durch eine ausgeprägte Stark-Verschiebung der Energiebänder hervorgerufen werden, und in diesem Rahmen nicht zu erklären sind. Die instantanen raumzeitlichen Blochwellen bilden dagegen eine Schar von Basen, die den Symmetrien des Systems besser angepasst sind. Eine auf ihnen fußende Beschreibung der Systemdynamik bleibt in dieser Darstellung vollständig adiabatisch.

Dies ist korrekt, solange sich die Quasienergieflächen in den Regionen,

die vom Wellenpaket während des Pulses sondiert werden, nicht antikreuzen. Die Tatsache, dass Anregungen des Wellenpaketes in höhere Quasienergieflächen eng an deren Morphologie gebunden sind, kann durch die Wahl der Antriebsfrequenz (und damit die der Quasienergiefläche) ausgenutzt werden, so dass die Impulsverteilung des Teilchens gezielt verändert werden kann. Dies erlaubt es, Interbandübergänge selektiv für den Transport von Teilen der Impulsverteilung des Wellenpaketes in höhere Bänder zu nutzen, und so exotische Zustände zu erzeugen, wie in Veröffentlichung IV ausgeführt wird. Dieses Konzept wird durch das Hinzufügen einer zweiten konstanten Kraft, die homogen auf das gesamte System wirkt, stark erweitert. Wie in Veröffentlichung III detailliert beschrieben ist, erlaubt es die Kombination beider Kräfte, die Impulsverteilung des Wellenpaketes auf dessen Quasienergiefläche in beliebige Richtungen zu verschieben, so dass vermiedene Kreuzungen während eines Pulses zielgerichtet angesteuert oder umgangen werden können. Dies wird durch eine Verallgemeinerung des bekannten Beschleunigungstheorems von F. Bloch auf den Rahmen der Floquet-Theorie ermöglicht, wobei sich die instantanen Basen der raumzeitlichen Blochwellen als zentral erweisen. Ferner erlaubt dieses generalisierte Beschleunigungstheorem eine effiziente theoretische Beschreibung der sogenannten Super-Bloch-Oszillationen, die sich in diesem Kontext auf den Fall der „fast resonanten Verkippung“ reduzieren.

Abgesehen von einem Preprint sind drei im Rahmen der Dissertation entstandene Arbeiten bereits in internationalen, von Experten begutachteten Zeitschriften veröffentlicht. Ein weiteres Manuskript ist als ein Kapitel des Buches „Dynamical Tunneling – Theory and Experiment“ erschienen.

Contents

List of Publications

I. Stephan Arlinghaus and Martin Holthaus,
Driven optical lattices as strong-field simulators,
Phys. Rev. A **81**, 063612 (2010).

II. Stephan Arlinghaus, Matthias Langemeyer, and Martin Holthaus,
Dynamic localization in optical lattices,
Chapter 12 of the volume "Dynamical Tunneling – Theory and Experiment",
(Taylor and Francis, 2010).

III. Stephan Arlinghaus and Martin Holthaus,
Generalized acceleration theorem for spatiotemporal Bloch waves,
Phys. Rev. B **84**, 054301 (2011).

IV. Stephan Arlinghaus and Martin Holthaus,
Controlled wave-packet manipulation with driven optical lattices,
Phys. Rev. A **84**, 063617 (2011).

V. Stephan Arlinghaus and Martin Holthaus,
ac Stark shift and multiphoton-like resonances in low-frequency driven optical lattices,
Preprint.

In addition to the publications contained in this thesis, a further publication

- Bettina Gertjerenken, Niklas Teichmann, Stephan Arlinghaus, and Christoph Weiss,
  Reproducible mesoscopic superpositions of Bose-Einstein condensates and mean-field chaos,
  Phys. Rev. A **82**, 023620 (2010)

was written, to which I contributed by providing an optimization procedure programmed as an independent cross-check to a similar program designed by the first author Bettina Gertjerenken. Both procedures yielded identical results, which were thus confirmed by independent coding. In addition, I helped improving the manuscript by revising it in detail in company with the other authors of the paper, and took part in discussing its scope and structure.

Preface

The world of quantum mechanics is extremely fascinating and richly interspersed with effects far from everyday experience. When the domain of classical physics is left behind, expectations are often turned upside down. For example, a quantum particle in a periodic structure starts *oscillating* in response to a constant force. An analogous situation governed by classical physics might be the often cited example of a marble in an egg carton. In this setting, the idea that the marble starts oscillating in response to gravity appears absurd. Yet, in quantum mechanics this effect known as "Bloch oscillations" has been observed in experiments with extremely high accuracy. This was rendered possible due to a new tool for studying quantum mechanical effects, which emerged only recently: the Bose-Einstein condensate.

In the 1990s, the first experimental realization of Bose-Einstein condensates greatly enhanced the ability to directly observe and experiment with systems governed by quantum mechanics. A new branch of physics evolved and many systems known from solid state physics can now be emulated in an extremely "clean" way. Moreover, the high tunability of these systems grants much more experimental freedom and the systems' parameters can be varied up to domains unattainable to their solid state counterparts: For example, monitoring the system's response to a continuous change of the lattice spacing over a wide range is impossible with traditional solids yet easily realized with Bose-Einstein condensates.

As already pointed out, many of the systems realized with Bose-Einstein condensates involve periodic potentials. In current experimental setups, the atoms are trapped in a standing wave of laser light. But how can atoms be trapped with light? At room temperature, the motion of the atoms is barely affected by the laser light and the atoms remain untrapped. This changes, however, if the atoms are cooled down sufficiently. In this context, the notion of "cold" differs greatly from its usual meaning in everyday life: The atoms – generally heavy atoms such as ^{87}Rb – need to be cooled down to temperatures of up to a microkelvin. Although this is about an order of magnitude higher than the critical temperature for Bose-Einstein condensation, these temperatures were long out of reach of experimental realization. Yet due to a number of new cooling mechanisms, cryogenic temperatures even down to 500 pK are now possible. These extreme or *ultracold* temperatures, even small when compared to the characteristic temperature of the universe of about 2.7 K [1], may be grasped by a simple analogy: Consider a room which is cooled down linearly from 300 K (slightly above room temperature) to absolute zero in a year, starting at January 1st, 0:00 am. Then the temperature needed for Bose-Einstein condensation to set in at about 200 nanokelvin is reached about 20 milliseconds before midnight on New Year's Eve.

Ultracold atoms and Bose-Einstein condensates in periodic fields lend themselves to far more than just neat emulations of other systems, though very valuable by themselves. A door towards a new area of research is opened up by varying one or more parameters of the system dynamically. In the newly emerging field of periodically driven atoms in optical lattices researchers seek to utilize effects induced by the driving to gain control over these quantum systems. The feasibility to subject particles in an optical lattice to periodic driving has been demonstrated already, and with advancing experimental techniques in the past few years, more and

more complex driving protocols can be implemented, leading to a broad spectrum of new approaches to control atoms on a quantum level.

This is exactly the scope of the present work, which is divided into three parts. In the first section, the reader is familiarized with the concept of Bose-Einstein condensation and introduced to basic mechanisms to explore the single-particle regime. After some remarks on how particles can be trapped in optical potentials, the section closes with a first example of external forces: a constant and homogeneous force, which gives rise to Bloch oscillations. One of the cornerstones of the present work is the second section which is devoted to time-periodic forces and the Floquet approach. Here, landmark experiments in the field of Bose-Einstein condensates in periodically forced optical lattices are reviewed, and at the end of the section, multiphoton-like transitions are discussed. The section "Publications" is the second cornerstone of this work, wherein new approaches to gain control over the dynamics of forced systems are presented and the implications of these approaches are illustrated. In conjunction with new analytical results derived in this thesis, the present work aims at opening up new vistas for understanding and utilizing periodically forced systems, and points out future perspectives to achieve these goals.

Chapter 1.

Bose-Einstein Condensation and Optical Potentials

In the mid-1920s, Einstein, building on previous work by Bose, predicted the existence of a new quantum phase emerging when bosonic systems are cooled below a certain critical temperature: the Bose-Einstein condensate [2, 3, 4]. Definitive for bosonic (fermionic) systems is the symmetry of its many-body wave function, which is of even (odd) parity under the exchange of two particles, respectively. These symmetry relations are a direct consequence of the indistinguishability of the particles. In other words, it is *in principle* impossible to label the particles, for example by assigning a number to each of them. This concept of identical particles lies at the core of the statistical properties of both bosonic and fermionic systems, as introduced by Bose and Einstein. The latter remarked in 1925 that this "indirectly implies some hypothesis about a mutual interaction of the molecules, which for the present is of entirely enigmatical nature" [5]; this became known as exchange interaction. Yet, already in 1911 the Polish physicist Natanson brought up the notion of the indistinguishability of particles by writing "Yet we regard the elements or entities of energy as indiscriminative. If we were able to perceive each one of them separately, the conditions would change fundamentally. This needs to be

pointed out first and foremost" [6], and in 1915 Ehrenfest and Kamerlingh Onnes remarked on indistinguishability in a work about Planck's law [7]. Furthermore, the statistical properties of the system are fundamentally [8] linked to the spin of its constituents by means of the spin-statistics theorem [9, 10], which associates bosons with integer spin (in units of $\hbar$) and fermions with half-integer spin.

Crucial for the gas to eventually form a Bose-Einstein condensate is the possibility of the particles to occupy a single energy eigenstate with an arbitrary number of atoms, a characteristic property of all bosonic particles, elementary or composite. Yet, massive particles condense only at extremely low temperatures of a few microkelvin, which is why pure Bose-Einstein condensation evaded experimental realization for about seven decades. The experimental observation of Bose-Einstein condensation was rendered possible due to substantial efforts in the development of new laser cooling techniques, which use the force of the laser light that acts on the atoms to slow them down, thus cooling the atoms: After the first independent proposals for laser cooling by Hänsch and Schawlow [11] in 1975, Wineland and Dehmelt [12] in 1975, and Ashkin [13] in 1978, the first observation of radiation-pressure cooling was reported by Wineland and co-workers, who cooled ions somewhat below 40 Kelvin with what became known as Doppler cooling [14]. This scheme cools only those atoms which are resonant to the laser radiation and was improved by Phillips and Metcalf in 1982 with the Zeeman slower [15], which involves additional magnetic fields to exploit the Zeeman effect for changing the resonance frequency of the atoms. The commonly accepted temperature limit for Doppler cooling [16] was first reported to be violated by the group around Phillips in 1988, who took up a technique developed earlier in 1985 by Chu and co-workers [17] and measured the temperature of a gas of sodium atoms to be as low as 43 microkelvin [18]. In the same year,

another assumed limit on cooling was shattered: the recoil limit. Cohen-Tannoudji and his colleagues used metastable ^{4}He atoms to beat the recoil limit of 4 microkelvin and cooled the atoms down to 2 microkelvin [19]. At this temperature, the mean velocity of the atoms is reduced to about 4 cm/s. So in only ten years, neutral atoms had gotten a million times colder! For the "development of methods to cool and trap atoms with laser light" Phillips, Chu, and Cohen-Tannoudji won the Nobel Prize in Physics in 1997.

These advances in trapping and cooling techniques of atoms finally culminated in the experimental observation of the first "pure" Bose-Einstein condensate created in 1995 by Cornell, Wieman and co-workers [20] using ^{87}Rb. Independently, only a few months later, the group around Ketterle at MIT generated a condensate with ^{23}Na [21]. All three of them were awarded the Nobel Prize in Physics in 2001 "for the achievement of Bose-Einstein condensation in dilute gases of alkali atoms, and for early fundamental studies of the properties of the condensates" [22]. These seminal works triggered further experiments on this fascinating quantum state of matter. A whole new area of research was born.

Soon, this exciting field spawned a multitude of experimental realizations of quantum systems, hitherto unavailable in such a clear and versatile form: Early seminal experiments include the observations of interference of two Bose-Einstein condensates [23] in 1997, of quantized vortices [24, 25] at the turn of 1999, of long-range phase coherence [26] in 2000, and of vortex lattices [27] in 2001. Whereas the early experiments were conducted with about half a million atoms, today more than 120 million atoms [28] can be used in experiments with Bose-Einstein condensates, rendering quantum mechanical effects visible and explorable on a macroscopic scale.

It should not go unnoticed that the discovery of superfluidity in 1937 by Kapitza [29] and Allen and Misener [30] is linked with Bose-Einstein

condensation: A superfluid sample of ^{4}He can be regarded as a partially condensed system, where complete condensation is impeded by the strong interaction between the atoms. Helium-4 is thus an example of an atomic species which, although bosonic, does not display complete condensation.

Since 1995, Bose-Einstein condensates have been obtained for a multitude of bosonic atoms, mostly alkalies due to their suitability for working with traps, but in the search for less massive particles to use in experiments, condensation was even achieved with atomic hydrogen [31]. Only recently, Weitz and co-workers [32] managed to Bose-condense photons in a dye-filled optical microcavity. The cavity provides the confining potentials and induces a non-vanishing effective photon mass, so the system can be mapped to a two-dimensional gas of trapped, massive bosons. With the Bose-condensation of dysprosium reported in October 2011, the properties of strongly dipolar Bose-Einstein condensates can be studied experimentally [33, 34].

But even fermionic systems, though the particles are bound by the exclusion principle not to occupy a single quantum state more than once, can be made to form "fermionic condensates" by coaxing the particles into bosonic molecules, which then undergo Bose-Einstein condensation albeit at even lower temperatures than their truly bosonic analog, as first shown independently by the groups of Jin [35], Grimm [36], and Ketterle [37] in 2004. A further example of a fermionic condensate is a fermionic superfluid, where electrons form weakly bound pairs below a certain critical temperature. The condensation of these so-called Cooper pairs is theoretically founded in the BCS transition, discovered 1957 by Bardeen, Cooper, and Schrieffer [38, 39].

In this chapter, the main concepts this work is founded on are briefly introduced: First of all, the statistical background describing the transition to a Bose-Einstein condensate at the critical temperature is discussed.

The subsequent section focuses on the feasibility of tuning the interaction of the particles in a gas of ultracold or Bose-condensed atoms. The case of vanishing interactions is most important for the present work: Since this is experimentally feasible by tuning the interaction strength to zero, single-particle dynamics can be enforced in a many-body system. The notion of a Feshbach resonance is presented, by which the interaction strength between the atoms can be shifted almost arbitrarily between the strongly repulsive, noninteracting, and strongly attractive regimes. The third section introduces the optical lattice, which enables one to trap the atoms in a perfectly periodic potential with no defects present. The theoretical description within the dipole approximation is introduced and experimental prerequisites for optical lattices are considered.

1.1. Bose-Einstein Condensation

In everyday experience, gases behave classically, show particle-like behavior, and their quantum features remain veiled by relatively high temperatures. The wave-like nature of the particles emerges due to a substantial overlap of the waves of two particles. The thermodynamical length scale of those waves – the thermal de Broglie wavelength λ – is connected with the temperature T of the gas via

$$\lambda = \frac{h}{\sqrt{2\pi m k_{\mathrm{B}} T}} \,, \tag{1.1.1}$$

where h is the Planck constant, m is the mass of the particle, and k_{B} denotes the Boltzmann constant. Whether the waves of particles in a gas overlap (on average) is determined by the relation between the thermal wave length λ and the density n of the particles: A gas can be described classically if the interparticle separation is large when compared to the thermal wavelength, that is as long as $n\lambda^3 \ll 1$. Thus, the quantum nature of the gas becomes visible for low temperatures or high densities; the

classical Maxwell-Boltzmann statistics does no longer describe the gas correctly and is replaced by the corresponding bosonic (or fermionic) quantum statistics. In this section, the discussion remains restricted to ideal, that is noninteracting, gases and the calculation of the critical temperature for the onset of Bose-Einstein condensation is sketched.

Within the grand canonical ensemble, the bosonic partition function of a gas of N particles with one-particle energies ε_j contained in a volume V and in contact with a bath at temperature T and chemical potential μ is without any approximations given by

$$\mathcal{Z}(\mu, V, T) = \prod_j \frac{1}{1 - z\mathrm{e}^{-\beta\varepsilon_j}} \,, \tag{1.1.2}$$

where $z = \exp(\beta\mu)$ is the fugacity with $\beta = 1/(k_\mathrm{B}T)$. The expectation value of the occupation number of a given state with energy ε_j then reads ([40], §54)

$$\langle n_j \rangle = \frac{1}{\mathrm{e}^{\beta(\varepsilon_j - \mu)} - 1} \,, \tag{1.1.3}$$

where the restriction $\mu < \varepsilon_0$ of the chemical potential with respect to the single-particle ground-state energy ε_0 ensures positive occupation numbers. Already at this step it can clearly be seen that the ground state is macroscopically occupied, that is $\langle n_0 \rangle = \mathcal{O}(N)$, when the chemical potential tends to ε_0.

For calculating the critical temperature T_c, the grand canonical equations of state

$$\frac{pV}{k_\mathrm{B}T} = \ln \mathcal{Z} \qquad = -\sum_j \ln\left(1 - z\mathrm{e}^{-\beta\varepsilon_j}\right) \tag{1.1.4}$$

$$N = \sum_j \langle n_j \rangle = \quad \sum_j \frac{1}{z^{-1}\mathrm{e}^{\beta\varepsilon_j} - 1} \,. \tag{1.1.5}$$

are needed, which are valid without any approximation. For sufficiently high temperatures, which imply the occupation of many energy levels,

these equations can be evaluated by replacing the sum over j by integrals. For this so-called continuum approximation the density of states $D(\varepsilon)$ is needed, which is system specific just as the single-particle spectrum. For particles moving freely in a box of volume V the density of states is

$$D_{\text{free}}(\varepsilon) = \frac{2\pi V}{h^3} (2m)^{3/2} \varepsilon^{1/2} , \tag{1.1.6}$$

whereas a three-dimensional harmonic trapping potential leads to [41, 42]

$$D_{\text{harm}}(\varepsilon) \approx \frac{1}{2} \frac{\varepsilon^2}{(\hbar\bar{\omega})^3} , \tag{1.1.7}$$

where $\bar{\omega} \equiv (\omega_x \omega_y \omega_z)^{1/3}$ is the geometric mean of the oscillator frequencies and $\hbar = h/(2\pi)$. When evaluating (1.1.5) a subtlety comes into play: With $\varepsilon_0 = 0$ the occupation number of the ground state

$$N_0 \equiv \langle n_0 \rangle = \frac{1}{z^{-1} - 1} \tag{1.1.8}$$

is very large for $\mu \to 0$, yet its weight in the density of states is zero. So this term needs to be treated separately yielding

$$N_{\text{ex}} \equiv N - N_0 = \frac{2\pi V}{h^3} (2m)^{3/2} \int_0^\infty \mathrm{d}\varepsilon \, \frac{\varepsilon^{1/2}}{\mathrm{e}^{\beta(\varepsilon-\mu)} - 1} . \tag{1.1.9}$$

The integral is known as Bose-Einstein integral function, defined in general by[1]

$$g_n(z) = \frac{1}{\Gamma(n)} \int_0^\infty \mathrm{d}x \, \frac{x^{n-1}}{z^{-1} e^x - 1} , \tag{1.1.10}$$

so the number of excited particles is

$$N_{\text{ex}} = \frac{V}{\lambda^3} g_{3/2}(z) . \tag{1.1.11}$$

The fugacity can be written as $z = N_0/(N_0 + 1)$ as a consequence of Eq. (1.1.8), so it is obvious that z is restricted to $0 \leq z < 1$. Since the

[1] In mathematics, the function $g_n(z)$ is known as an integral representation of the polylogarithm, which reduces to the Riemann zeta function $\zeta(n)$ for $z = 1$.

function $g_{3/2}(z)$ is monotonically increasing in this interval and bounded by $g_{3/2}(1) = \zeta(3/2) \approx 2.612$, the number of excited particles remains restricted as well:

$$N_{\mathrm{ex}} \leq V \left(\frac{2\pi m k_{\mathrm{B}} T}{h^2} \right)^{3/2} \zeta(3/2) \, . \tag{1.1.12}$$

Consequently, as soon as

$$N > V \left(\frac{2\pi m k_{\mathrm{B}} T}{h^2} \right)^{3/2} \zeta(3/2) \, , \tag{1.1.13}$$

the number of excited particles is less than the total particle number and particles are collectively forced to the ground state. This macroscopic occupation sets in at $n\lambda^3 = \zeta(3/2)$ and yields the critical temperature

$$T_{\mathrm{c}}^{\mathrm{free}} = \frac{h^2}{2\pi m k_{\mathrm{B}}} \left(\frac{N}{V \zeta(3/2)} \right)^{2/3} \tag{1.1.14}$$

for a gas moving freely in a box of volume V. For the harmonically trapped gas, the critical temperature can be calculated in the same manner using the density of states given by Eq. (1.1.7). In this case, the critical temperature reads

$$T_{\mathrm{c}}^{\mathrm{harm}} = \frac{\hbar \bar{\omega}}{k_{\mathrm{B}}} \left(\frac{N}{\zeta(3)} \right)^{1/3} \tag{1.1.15}$$

with $\zeta(3) \approx 1.202$. Similar to the previous case, at the temperature $T_{\mathrm{c}}^{\mathrm{harm}}$ the thermal de Broglie wavelength reaches the mean interparticle distance at the center of the trap.

Considering harmonic trapping potentials is not just a theoretical exercise since they are experimentally indispensable for the cooling process during which the atoms need to be spatially confined. Additionally, three-dimensional harmonic trapping opens up the possibility of realizing systems which are confined in one or more dimensions: By increasing, for instance, the trapping frequency ω_z with respect to the others, the atoms

remain confined in the x-y plane and the system becomes approximately two-dimensional. If the dynamics are frozen in y-direction as well, effectively one-dimensional systems can be studied. Here, typical trapping frequencies along the tube are on the order of 10–200 Hz, whereas the radial trapping frequencies can become as high as 100 kHz [43]. But low-dimensionality leads to obstacles, which even emerge in the argument sketched above, where two-dimensional systems without a trapping potential require the function $g_{2/2}(z)$ in the limit $z \to 1$, for which the Bose-Einstein integral function reduces to a harmonic series which diverges. Although in a two-dimensional gas a true condensate emerges only at $T = 0\,K$, at sufficiently low temperatures there exists a Kosterlitz-Thouless transition [44, 45], which, in the Bose-gas framework, is characterized by a quasicondensate with fluctuating phase [46] and has been realized experimentally in the group of Dalibard and co-workers [47] in 2006.

Only two years prior to the bosonic Kosterlitz-Thouless transition, the hard-core limit of the Lieb-Liniger model [48, 49], which describes a one-dimensional Bose gas and is known as Tonks-Girardeau gas [50], was realized experimentally using strong optical lattices [51, 52]. In this gas, strong repulsive interactions between the atoms dominate the dynamics and in this one-dimensional system, the hard-core limit prevents the bosons from passing each other or occupying the same position in space. The latter feature is similar to the exclusion principle for fermions, but although the system can be mapped to a gas of noninteracting fermions by the Jordan-Wigner transformation [53], not all fermionic characteristics, such as its momentum distribution [54], emerge in the Tonks-Girardeau gas.

For further details the reader is referred to the review article by Petrov *et al.* on low-dimensional trapped gases and references therein [55].

1.2. Tuning the Interaction

Apart from the symmetry-induced exchange interaction, which is not mediated by a potential, the particles interact by scattering. In dilute gases three-particle scattering becomes negligible[2] and the scattering processes are dominated by two-body collisions. In the low-energy regime, implying very cold atoms and temperatures in the sub-millikelvin range, usually the collisions with the lowest angular momentum dominate the interaction. In the bosonic case, all scattering events with nonzero angular momentum are negligible so only s-wave scattering takes place in good approximation.[3] These scattering events can be described by a single parameter, the s-wave scattering length a_{sc} [56, 57]: Due to the long wavelength of the scattering particles, the low-scale structure of the interaction potential remains unresolved and only the lowest order in a partial-wave expansion has significant influence on the scattering event. The magnitude of the scattering length gives the strength of the interactions, whereas its sign determines its kind: positive (negative) scattering lengths describe repulsive (attractive) interactions, respectively. In the dilute limit, that is if the interparticle separation is larger than the scattering length, the complicated interaction potential can be replaced by a pseudopotential ([58], §10 and [59]). It usually takes on the form of a delta function and is proportional to the s-wave scattering length, which is the only parameter entering from the actual scattering potential.

The concept of a Feshbach resonance was put forward 1958 by H. Feshbach in the framework of nuclear physics [60] and independently three years later by Fano [61] on the background of atomic physics. About two

[2] An important exception arises in the context of Feshbach resonances and is discussed below.

[3] For identical fermions p-wave scattering dominates since Pauli's exclusion principle rules out s-wave scattering.

decades later, it was considered by Stwalley [62] in the context of ultracold gases, but only 1998 Feshbach resonances were experimentally observed in a Bose-Einstein condensate by the Ketterle group [63] (for a review see [64]): An external magnetic field couples the state of two free colliding atoms to a molecular bound state, as schematically depicted in Fig. 1.1a. By tuning the strength of the magnetic field, the scattering length of the atoms can artificially be changed to almost arbitrary values, including positive and negative values as well as vanishing scattering lengths. In the vicinity of such a magnetic Feshbach resonance, which occurs at a certain value of the magnetic field $B = B_0$ and is characterized by the width Δ, the scattering length can be given as a function of the magnetic field as first introduced by Moerdijk *et al.* [65],

$$a_{\mathrm{sc}} = \widetilde{a}_{\mathrm{sc}} \left(1 - \frac{\Delta}{B - B_0} \right) , \tag{1.2.1}$$

where $\widetilde{a}_{\mathrm{sc}}$ is the background scattering length far from the resonance. As depicted in Fig. 1.1b, no scattering occurs at $B = B_0 + \Delta$. This is most important for the present work: By adjusting the scattering length to zero, noninteracting systems can be realized, which are modeled theoretically as one-particle systems. In this way, genuine effects of one-particle quantum mechanics can be studied in the laboratory without being masked by interaction effects.

On the one hand, this powerful technique enables easy access to the regime of strong interactions: Positive scattering lengths of more than 9,000 Bohr radii have been observed using atoms of ^{85}Rb [66]. Yet, magnetic Feshbach resonances suffer from high particle losses close to the resonance since particle losses due to three-body collisions are proportional to a_{sc}^4 (see [67, 68]) and are thus highly increased. This downside can be attenuated by the so-called optical Feshbach resonance [69], which has been realized by Bauer *et al.* in 2009 using a laser which is near-resonant

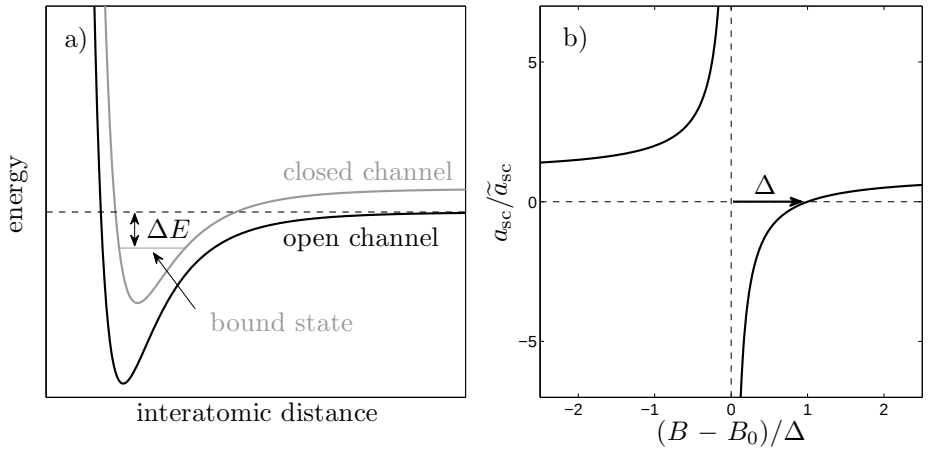

Figure 1.1.: Left panel: The atoms are prepared in the open channel and scatter at low kinetic energies. The open channel is coupled to a bound state with energy ΔE in the closed channel. A Feshbach resonance occurs if the bound molecular state in the closed channel matches the scattering state in the open channel. This can be controlled by applying a magnetic field to modify ΔE. Right panel: The scattering length a_{sc} as a function of the magnetic field B according to Eq. (1.2.1). The Feshbach resonance occurs at $B = B_0$; noninteracting condensates can be realized by tuning the magnetic field to $B = B_0 + \Delta$.

to the bound-to-bound transition [70]. Furthermore, strong coupling to the bound channel leads to the emergence of weakly bound dimers, so-called Feshbach molecules [71]. Thus, by forming bosonic bound pairs of fermions, even condensates with fermionic constituents – "fermionic Bose-Einstein condensates" – can be observed, as first realized by the Grimm group [72]. In these systems, the study of the transition from a Bose-Einstein condensate at repulsive interactions to a fermionic superfluid at

attractive interactions, continuously connected by a Feshbach resonance, has attracted considerable attention (see [73, 74] for reviews). The positions B_0 of the resonances vary strongly with atomic species, an overview is given in the appendix of [64]. Resonances are found in ^{87}Rb at about 400 Gauss and up to 1000 Gauss, whereas in ^{85}Rb they occur at about 160 Gauss [75], which is still large when compared to the earth's magnetic field of about 0.5 Gauss. Negative scattering lengths open up the exciting field of attractive interactions. By rapidly switching the scattering length of a stable Bose-Einstein condensate from repulsive to attractive, a controlled collapse of a condensate can be induced as shown by Cornell, Wieman, and co-workers [76], which causes fragmentation of the condensate into bright solitons [77].

On the other hand, by tuning the scattering length close to zero – values on the order of and even less than the Bohr radius have been observed – the weak interaction regime can be explored. It needs to be mentioned, though, that the cross section for elastic collisions between bosons is proportional to a_{sc}^2, so too small values of the scattering length suppress these collisions, which are needed for evaporative cooling, so the condensate needs to be created first. Typical scattering lengths are in the regime of ten to a few hundred Bohr radii [64].

One prominent example of a system that can be realized by exploiting a Feshbach resonance to generate a noninteracting system is a single particle moving in a periodic potential. The spatial freedom of the particles can be restricted to one spatial dimension, for example by confining the atoms in the other directions as discussed before, and the dynamics of these systems will be discussed in Section 1.4, where the focus is on a single particle in an optical lattice subjected to a constant homogeneous force.

1.3. Trapping Atoms with Light

Naturally, cooling the atoms is closely linked to trapping them. In order to cool the atoms they have to be spatially confined and for the atoms to "feel" a trapping potential they need to be sufficiently cool. Traps can generally be distinguished by the kind of particles they trap. In ion traps the Coulomb interaction is exploited to confine the atoms with electric or electromagnetic fields. The most prominent types of ion traps are the Paul trap and the Penning trap. For the former, alternating[4] electric fields are used whose potential surfaces form a saddle surface to trap the ions, a technique for which Dehmelt and Paul were awarded the Nobel Prize in Physics in 1989 [79, 80]. The Penning trap uses static fields only: An electric quadrupole field and an additional magnetostatic field trap the particles spatially. For neutral atoms, traps can be categorized as radiation-pressure, magnetic, or optical dipole traps (see [81]), the most prominent example is the magneto-optical trap (MOT). For the purpose of this work, these traps will not be discussed in detail. In this section, the focus is on optical lattices and how they can be used as trapping potentials for ultracold atoms [82, 83]. In particular, the dipole force laser light exerts on the atoms and the concept of a one-dimensional optical lattice are introduced.

To understand the basic physics within the framework of a simple model, the one-dimensional laser field remains unquantized[5] and thus acts semiclassically on a single atom which is modeled as a two-level system, con-

[4] Charged particles cannot be held in a stable stationary equilibrium by electrostatic fields only, which is known as Earnshaw's theorem [78].

[5] This approximation is justified for a high number of photons in the laser mode and thus for high laser amplitudes, allowing for a semiclassical description of the radiation field. Its quantization is discussed by Dalibard and Cohen-Tannoudji in [84]; see [85] §5 as well.

taining a ground state $|\mathrm{g}\rangle$ and an excited state $|\mathrm{e}\rangle$, each associated with the energy E_g and E_e, respectively. The energy gap between the levels is denoted as $\hbar\omega_0 \equiv E_\mathrm{e} - E_\mathrm{g}$ and they are connected by a dipole transition characterized by the dipole matrix element $\mu \equiv \langle \mathrm{e}|\hat{d}|\mathrm{g}\rangle$, where $\hat{d}$ denotes the dipole operator in the direction of the field. The dipole moment is induced by the standing light wave $E(x,t) = E_0 \cos(k_\mathrm{L} x)\cos(\omega_\mathrm{L} t)$, where k_L and ω_L denote the wavenumber and angular frequency of the laser light, respectively, and is determined by the gradient of its time-averaged intensity [86]. The model Hamiltonian reads

$$H = \frac{p^2}{2m}\mathbb{1} + \hbar\omega_0 \left|\mathrm{e}\right\rangle\left\langle\mathrm{e}\right| - \mu E(x,t)\left(\left|\mathrm{g}\right\rangle\left\langle\mathrm{e}\right| + \left|\mathrm{e}\right\rangle\left\langle\mathrm{g}\right|\right) \ , \tag{1.3.1}$$

where p and m denote the atom's momentum and mass, respectively, and $\mathbb{1} = |\mathrm{g}\rangle\langle\mathrm{g}| + |\mathrm{e}\rangle\langle\mathrm{e}|$. In order to derive an effective potential for the atom, the laser frequency is tuned such that the absolute value of the detuning

$$\delta_\mathrm{L} = \omega_0 - \omega_\mathrm{L} \tag{1.3.2}$$

is small compared to ω_0, that is $|\delta_\mathrm{L}| = |\omega_0 - \omega_\mathrm{L}| \ll \omega_0$. In this case of main practical interest, the time-dependence of the amplitudes in the ansatz

$$|\Psi(x,t)\rangle = \psi_\mathrm{g}(x,t)\left|\mathrm{g}\right\rangle + \psi_\mathrm{e}(x,t)\mathrm{e}^{-\mathrm{i}\omega_\mathrm{L} t}\left|\mathrm{e}\right\rangle \tag{1.3.3}$$

is only weak, assuming that the laser perturbs the atom only slightly, that is $\mu E_0 \ll \hbar\omega_0$. The Schrödinger equation then yields the equations of motion for the amplitudes

$$\mathrm{i}\hbar\partial_t\psi_\mathrm{g}(x,t) = -\frac{\hbar^2}{2m}\partial_x^2\psi_\mathrm{g}(x,t) - \frac{\mu E_0}{2}\cos(k_\mathrm{L}x)\psi_\mathrm{e}(x,t) \ , \tag{1.3.4}$$

$$\mathrm{i}\hbar\partial_t\psi_\mathrm{e}(x,t) = -\frac{\hbar^2}{2m}\partial_x^2\psi_\mathrm{e}(x,t) - \frac{\mu E_0}{2}\cos(k_\mathrm{L}x)\psi_\mathrm{g}(x,t) + \hbar\delta_\mathrm{L}\psi_\mathrm{e}(x,t) \ , \tag{1.3.5}$$

where the rotating-wave approximation [87, 88] has been used, discarding all components oscillating with twice the laser frequency. The occupation probability of the two levels oscillates between the ground state and the excited state with the Rabi frequency $\Omega = \mu E_0/\hbar$, which is characteristic for two-level systems [89]. If the system is initially prepared in the ground state and a separation of time scales by

$$\Omega \ll |\delta_{\mathrm{L}}| \ll \omega_{\mathrm{L}}, \omega_0 \ , \tag{1.3.6}$$

is assumed, then for times that are small compared to the Rabi period the first term on the right hand side of Eq. (1.3.5) remains negligible. Furthermore, $\psi_{\mathrm{e}}(x,t)$ changes slowly in this time interval and Eq. (1.3.5) yields

$$\psi_{\mathrm{e}}(x,t) \approx \frac{\mu E_0}{2\hbar\delta_{\mathrm{L}}} \cos(k_{\mathrm{L}} x)\psi_{\mathrm{g}}(x,t) \ . \tag{1.3.7}$$

Now, the excited amplitude can be "adiabatically eliminated" in the equation of motion for the ground state amplitude (1.3.4), so that

$$\mathrm{i}\hbar\partial_t\psi_{\mathrm{g}}(x,t) \approx \left(-\frac{\hbar^2}{2m}\partial_x^2 - \frac{(\mu E_0)^2}{4\hbar\delta_{\mathrm{L}}} \cos^2(k_{\mathrm{L}} x) \right) \psi_{\mathrm{g}}(x,t) \ . \tag{1.3.8}$$

Utilizing $\cos^2(x) = [1 + \cos(2x)]/2$ and neglecting constant energy shifts finally yields

$$\mathrm{i}\hbar\partial_t\psi_{\mathrm{g}}(x,t) \approx \left(-\frac{\hbar^2}{2m}\partial_x^2 - \frac{\hbar\Omega^2}{8\delta_{\mathrm{L}}} \cos(2k_{\mathrm{L}} x) \right) \psi_{\mathrm{g}}(x,t) \ . \tag{1.3.9}$$

Denoting the lattice depth by $V_0 = (\hbar\Omega^2)/(4\delta_{\mathrm{L}})$, the atom in a standing light wave "sees" an effective potential

$$V_{\mathrm{eff}}(x) = -\frac{V_0}{2} \cos(2k_{\mathrm{L}} x) \ , \tag{1.3.10}$$

which is spatially periodic and the depth is proportional to the Rabi frequency squared and thus to the laser intensity. The sign of the detuning δ_{L}

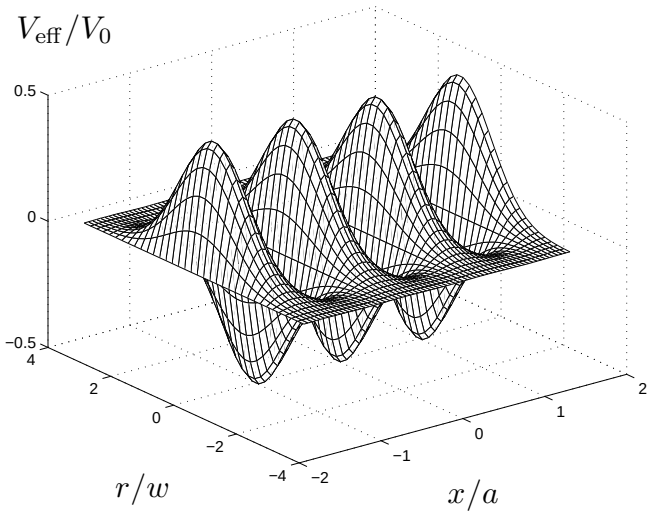

Figure 1.2.: The effective potential $V_{\mathrm{eff}}(x, r)$ includes a Gaussian radial profile, which is characterized by the spot size (waist) w. It reduces to Eq. (1.3.10) for $r = 0$.

determines whether the atom is attracted to the nodes or antinodes of the field: For red (blue) detuning δ_{L} is positive (negative) and the atom moves to regions of high (low) laser intensity, respectively. This is also referred to as high-field or low-field seeking. So the electric field $E(x, t)$ induces an effective potential for the atoms, which then move in an "optical lattice": a spatially periodic potential. Its lattice period denoted by a is connected to the laser wavelength and wavenumber via $k_{\mathrm{L}} = \pi/a = 2\pi/\lambda_{\mathrm{L}}$, where the laser wavelength $\lambda_{\mathrm{L}} = 2a$ is typically in the regime of 600 nm to 1100 nm.

Of course, in the laboratory, the standing light wave is not perfectly one-dimensional but has a Gaussian radial profile with a beam waist w as shown in Fig. 1.2. The variation of the waist with x has been neglected

here;[6] this corresponds to an infinite Rayleigh length x_R. With the lattice period in the nanometer regime and a Rayleigh length which under realistic conditions is on the order of a few millimeters [43], the approximation $x_\mathrm{R} \to \infty$ is justified and $w = w_0$ in good approximation. Typical beam waists figure at about $100\,\mu$m.

As evident from the Schrödinger equation for the ground-state amplitude, Eq. (1.3.9), the characteristic energy of a particle in a standing light wave is given by the single-particle recoil energy

$$E_\mathrm{r} = \frac{\hbar^2 k_\mathrm{L}^2}{2m}\,, \tag{1.3.11}$$

which corresponds to the energy an atom at rest gains from emitting a photon with wavenumber k_L. The recoil energy typically is on the order of $10^{-10}\,$eV, so the corresponding recoil frequencies are in the kHz regime. Experimentally, moderate lattice depths range from 5 to 10 recoil energies and are thus ten orders of magnitude smaller than those encountered in traditional solids.

If the lattice-generating beams are not counterpropagating but enclose an angle of less than 180°, lattices with an increased lattice constant can be erected [90, 91]. Two- and three-dimensional lattices are created by four or six beams and with additional harmonic potentials confining the motion in two directions; an ensemble of approximately one-dimensional tubes, even in mutual isolation, can be generated [92, 93, 94].

Due to the theoretical predictions concerning the combination of Bose-Einstein condensates and optical lattices on the one hand and first experimental verifications of these in the laboratory on the other, the field of Bose-Einstein condensates and ultracold atoms in optical lattices began to evolve rapidly. It has already been pointed out that the lattice parameters

[6] The beam waist varies according to $w(x) = w_0\sqrt{1 + (x/x_\mathrm{R})^2}$ with the Rayleigh length $x_\mathrm{R} = w_0^2\pi/\lambda_\mathrm{L}$.

can be controlled almost perfectly and the lattice can even be switched off during experiments. With the lattice depth as a tuning knob, very deep lattices lead to the emergence of isolated "condensates" in the individual wells – the Mott-insulating state – whereas shallow lattices allow for a superfluid phase where the condensate is extended over the lattice. The transition from the superfluid to the Mott insulator is a quantum phase transition and can be realized by varying the lattice depth during the experiment; this will be detailed in Section 2.4.

The difference between loading a Bose-Einstein condensate or just ultracold atoms into the lattice is a question of both temperature and density. Whereas for ultracold atoms these are in the regime of microkelvin and $10^{10}\,\mathrm{cm}^{-3}$, for Bose-Einstein condensates lower temperatures in the nanokelvin regime and higher densities around $10^{14}\,\mathrm{cm}^{-3}$ are needed. Higher densities lead to higher filling factors[7] of the lattice and to enhanced interaction effects. Although these *can* be reduced by means of Feshbach resonances if unwanted, they open up more general concepts of nonlinear systems [95] and the field of strongly interacting systems. For now, the focus is on weakly interacting systems, where interaction-induced effects do not destroy those of single-particle quantum mechanics. One prominent example is discussed in the following section.

1.4. Time-Independent Forces and Bloch Oscillations

After observing key quantum signatures of Bose-Einstein condensation such as the interference between two condensates and the experimental realization of models from solid-state physics, the desire for enhancing control over these systems grew. This was rooted not only in the striving for a more careful state preparation but also in the quest for understanding

[7] (particles per lattice site)

phenomena such as high-temperature superconductivity and the long-time goal of quantum computing, for which careful quantum control is crucial.

A very promising approach for increasing control is an additional force acting homogeneously on the entire lattice system. More complex forcing protocols are discussed in Chapter 2 and in the Chapter "Publications". In the simplest case, the homogeneous force is constant in time so that the atoms in the now "tilted" lattice are experiencing a constant acceleration. This situation was already studied in 1929 by F. Bloch in the framework of the motion of electrons in solids [96]. The key features of his semiclassical "acceleration theorem" and the emergence of Bloch oscillations in one dimension[8] are briefly recapitulated in this section, a detailed derivation is provided in the Appendix A.

The acceleration theorem is derived on the basis of single-particle quantum mechanics and hinges on the assumption that the dynamics of a wave packet initially prepared in a single energy band remains restricted to this band. To be definite, the Hamiltonian of the system, describing a particle of mass m in a periodic lattice potential $V_{\mathrm{lat}}(x)$ accelerated by an inertial force F in x-direction is given by

$$H(x) = \frac{p^2}{2m} + V_{\mathrm{lat}}(x) - Fx \,, \tag{1.4.1}$$

where the lattice potential is spatially periodic, that is $V_{\mathrm{lat}}(x) = V_{\mathrm{lat}}(x+a)$ with the lattice constant a. With the force absent, that is for $F = 0$, the energy eigenvalues of the Hamiltonian are given by the dispersion relation $E_n(k)$, where n is the band index and the wavenumber k can be restricted to the first Brillouin zone $[-\pi/a, \pi/a[$, as known from basic quantum mechanics. Given an initial single-band wave packet $\psi(k, t_0)$ in momentum space[9] centered around some value k_{c}, Bloch's acceleration

[8] The results can easily be generalized to higher dimensions.

[9] For brevity the band index has been dropped.

theorem states that its time evolution is governed semiclassically by

$$\hbar \dot{k}_{\mathrm{c}}(t) = F \ . \tag{1.4.2}$$

Sole requirement for the acceleration theorem is the validity of the single-band approximation. Obviously, for constant forces F this equation can easily be solved, yielding a linear growth of k_{c} in time. So the wave packet traverses the Brillouin zone periodically, since this zone itself is periodic in quasimomentum k.

The motion in k space can be transformed to a motion in real space, as has been shown by Jones and Zener [97]; they used the group velocity $v_{\mathrm{g}}(t)$ of the wave packet to derive its motion. Here, in contrast to Bloch's approach in momentum space, additional requirements are needed. Most importantly, the procedure given by Jones and Zener works the better, the narrower the k-space distribution of the wave packet is. The group velocity is determined by the derivative of the dispersion relation according to

$$v_{\mathrm{g}}(t) = \frac{1}{\hbar} \left. \frac{\mathrm{d}E}{\mathrm{d}k} \right|_{k_{\mathrm{c}}(t)} \ . \tag{1.4.3}$$

Within the tight-binding approximation [98], the dispersion relation simply reads $E(k) = -(W/2)\cos(ka)$ with the band width W extracted from the tight-binding Hamiltonian or determined numerically, so that in this case the group velocity is given by

$$v_{\mathrm{g}}(t) = \frac{Wa}{2\hbar} \sin\left[k_{\mathrm{c}}(t)a\right] \ . \tag{1.4.4}$$

Writing $k_{\mathrm{L}}(t)a = \omega_{\mathrm{B}}t$ with the Bloch frequency [99]

$$\omega_{\mathrm{B}} = \frac{Fa}{\hbar} \ , \tag{1.4.5}$$

the position of the wave packet's center is given by

$$x_{\mathrm{g}}(t) = -\frac{W}{2F} \cos\left(\omega_{\mathrm{B}}t\right) \tag{1.4.6}$$

with appropriate choice of the origin of the x-axis. So the particle's motion due to a constant homogeneous force is periodic in real space. The amplitude of the oscillation is inversely proportional to the external force; huge oscillations mimic extended Bloch waves in the limit $F \to 0$. The somewhat counterintuitive result that a constant force causes the wave packet to oscillate can be explained qualitatively: If $\varphi_n(x)$ is a solution of the stationary Schrödinger equation

$$\left(\frac{p^2}{2m} + V_{\text{lat}}(x) - Fx\right)\varphi_n(x) = E_n\varphi_n(x)\ , \tag{1.4.7}$$

then the functions $\varphi_n(x + ma)$, shifted by m lattice constants, solve the same equation but with shifted energies $E_n + mFa$, known as the Wannier-Stark ladder [100]. So the external force splits each unperturbed energy band into a series of energies, equally spaced by Fa. In analogy to the quantum harmonic oscillator, the equidistant spectrum implies periodic oscillations of the wave packet and the frequency of these Bloch oscillations is given by the energy spacing as in Eq. (1.4.5).

From the first theoretical formulation of Bloch oscillations in the 1930s it took several decades until evidence for the existence of Bloch oscillators was observed in experiments. In traditional solids their verification is hampered by electron scattering by phonons and by lattice defects, which break the translational symmetry of the lattice and lead to decoherence on a time scale much shorter than the period of the oscillations. Encouraged by further theoretical efforts [101] and by the idea to focus on semiconductor superlattices [102, 103], in 1992 Bloch oscillations were predicted to generate terahertz radiation [104] and were observed for a few cycles in the same year [105, 106]. With the availability of ultracold atoms and Bose-Einstein condensates in optical lattices, the observation of Bloch oscillations was first reported in 1996 with ultracold but non-condensed caesium atoms [107]. Long-lived oscillations of several seconds were measured and

proposed to be used for sensitive gravity measurements in 2006 by Ferrari and co-workers [108]. Being a single-particle phenomenon, Bloch oscillations are most pronounced in weakly to noninteracting systems as the group around H.-C. Nägerl confirmed by monitoring Bloch oscillations for over 20,000 cycles [109] and Fattori *et al.* suggested exploiting them for atom interferometry [110].

Chapter 2.

Driving Atoms and Exerting Control: Time-Periodic Forces

In 2002, the experimental realization of the superfluid-to-Mott insulator transition with ^{87}Rb atoms in an optical lattice by I. Bloch and coworkers [111] demonstrated unprecedented control over parameters such as the spacing or the depth of the lattice, the latter being most important for observing the quantum phase transition. The precision with which the parameters can be controlled in the laboratory directly reflects the control over the quantum system itself. The clear-cut observation of the superfluid-to-Mott insulator transition with Bose-Einstein condensates is a landmark in the field.

The possibilities of coherent control of the system are hinted at by techniques used in atomic and molecular physics. Here, the field has been enriched by the use of lasers, which spawned new spectroscopic methods and enabled deliberate control of atomic and molecular states. Many of the tools developed there can be transferred directly to the framework of ultracold atoms. A step towards this has already been done with the introduction of a time-periodic drive into the system. Working with condensates, Lignier *et al.* achieved a periodic driving of a lattice system in 2007 by inducing a periodic frequency difference between the two counterprop-

agating laser beams [112], whereas already in 1998, Madison *et al.* used a periodically driven lattice with cold sodium atoms to study the dynamical Bloch band suppression [113]. In current experiments, a lattice-generating laser beam is retroreflected into itself by a mirror, which is mounted onto a piezoelectric crystal. The periodic shaking of the mirror induces the periodic driving of the lattice as realized by the Pisa group [114]. With the position of the mirror oscillating with amplitude L, in the laboratory frame of reference the lattice potential takes the form

$$\frac{V_0}{2}\cos\{k_{\mathrm{L}}[x - L\cos(\omega t)]\}\ . \tag{2.0.1}$$

As a meaningful dimensionless measure of the driving strength,

$$K_0 = \frac{Fa}{\hbar\omega} = \frac{\pi^2}{2}\frac{\omega}{\omega_{\mathrm{r}}}\frac{L}{a} \tag{2.0.2}$$

is employed with the usual notation, $\omega_{\mathrm{r}} = E_{\mathrm{r}}/\hbar$ being the recoil frequency, and $F = ML\omega^2$ [115]. With $\omega/\omega_{\mathrm{r}}$ and L/a on the order of unity, K_0 can easily exceed unity and then corresponds to quite strong forcing, see Paper I.

By introducing basic elements of Floquet theory, this chapter provides the theoretical background needed for a systematic understanding of the physics of periodically driven quantum systems, and additionally reviews some of the landmark experiments driving this newly developing field.

2.1. The Floquet Approach: Dressing the System

The external drive with frequency ω, which in the generic case gives rise to an additional term to some (static) Hamiltonian H_0, introduces a new periodicity to the system; the Hamiltonian, now explicitly time dependent, becomes invariant to shifts of $T = 2\pi/\omega$ in time, $H(t) = H(t+T)$. On the one hand, this invalidates the concept of energy conservation: The

driving force performs (positive or negative) work on the system and energy conservation is no longer given. From a theorist's point of view, the Schrödinger equation cannot be treated with separation of variables anymore and thus no stationary Schrödinger equation and energy eigenvalues exist. On the other hand, the external forcing is not arbitrary but periodic in time. Consequently, a differential equation with periodic coefficients needs to be treated. For this case, already in 1883 G. Floquet developed a mathematical theory [116], basic features of which are briefly introduced here from a physicist's point of view. Further reference can be found in [117, 118] among others.

Starting point is the Schrödinger equation with a Hamiltonian periodic in time,

$$\mathrm{i}\hbar\partial_t \left|\psi(t)\right\rangle = H(t) \left|\psi(t)\right\rangle \ . \tag{2.1.1}$$

The particular solutions $|\psi_\alpha(t)\rangle$ to this equation, called "Floquet states" in this context, can be written as (cf. [119])

$$\left|\psi_\alpha(t)\right\rangle = \exp\left(-\mathrm{i}\varepsilon_\alpha t/\hbar\right) \left|u_\alpha(t)\right\rangle \ , \tag{2.1.2}$$

where the Floquet functions $|u_\alpha(t)\rangle$ are T-periodic. In analogy to energy eigenvalues in the time-independent framework, the factors ε_α determining the linear growth of the phase are dubbed quasienergies, see papers by Zel'dovich [119] and Ritus [120]. Yet, the quasienergies as well as the Floquet functions are not defined unambiguously by Eq. (2.1.2), since with integer m the functions $|u_n(t)\rangle \exp\left(\mathrm{i}m\omega t\right)$ are T-periodic as well and lead to the identity

$$\exp\left(-\mathrm{i}\varepsilon_n t/\hbar\right) \left|u_n(t)\right\rangle = \exp\left[-\mathrm{i}\left(\varepsilon_n + m\hbar\omega\right) t/\hbar\right] \left[\left|u_n(t)\right\rangle \exp\left(\mathrm{i}m\omega t\right)\right] \ . \tag{2.1.3}$$

So the index in Eq. (2.1.2) has to be considered as a double-index $\alpha = (n, m)$ and for each solution labeled by n, there exist a countably infinite

number of representatives labeled by m. This richness in solutions can be described by a different but equivalent approach as first introduced by Sambe [121] in 1973. Inserting the Floquet states into the Schrödinger equation leads to an eigenvalue equation for the quasienergies:

$$[H(t) - \mathrm{i}\hbar\partial_t]\,|u_\alpha(t)\rangle = \varepsilon_\alpha\,|u_\alpha(t)\rangle \ . \tag{2.1.4}$$

If the Hilbert space spanned by the eigenfunctions of the unperturbed Hamiltonian H_0 is denoted by $\mathcal{H}$, the emerging quasienergy operator $H(t) - \mathrm{i}\hbar\partial_t$ is associated with an extended Hilbert space

$$\mathcal{K} = L_2\,[0,T] \otimes \mathcal{H}\ , \tag{2.1.5}$$

in which time and the spatial coordinates are explicitly treated on the same footing and hence time is integrated over in the scalar product in $\mathcal{K}$ given by

$$\langle\!\langle v|w\rangle\!\rangle = \frac{1}{T}\int_0^T \mathrm{d}t\ \langle v(t)|w(t)\rangle\ , \tag{2.1.6}$$

where $\langle\cdot|\cdot\rangle$ denotes the usual scalar product in $\mathcal{H}$. A few words regarding completeness and orthonormality: As eigenstates of the quasienergy operator, the Floquet functions $|u_n(t)\rangle\exp(im\omega t)$ constitute a complete orthonormal system in $\mathcal{K}$ with respect to the extended scalar product (2.1.6). All Floquet functions from the same class, that is with n fixed, are orthonormal. Additionally, completeness and orthonormality in the original Hilbert space $\mathcal{H}$ holds for the set of Floquet functions $|u_n(t)\rangle$ generated by picking an arbitrary representative from each class for each fixed time t.

Although the argument leading to Eq. (2.1.3) requires α to be treated as a double-index and induces the extended Hilbert space $\mathcal{K}$, it simultaneously reveals the physical identity of states differing in m only: Floquet functions from the same class are physically equivalent. This is also true for the quasienergies and consequently, the unbounded spectrum of

quasienergies can be divided into identical zones of width $\hbar\omega$, each zone containing a single representative of each class of quasienergies. In analogy to the Brillouin zone scheme in solid-state physics, arising from a *spatial* periodicity resulting in quasimomenta defined only modulo $\hbar \cdot 2\pi/a$, the *temporal* periodicity leads to quasienergies defined modulo $\hbar \cdot 2\pi/T = \hbar\omega$. Here, the fundamental Brillouin zone for quasienergies is agreed to be $[-\hbar\omega/2, \hbar\omega/2[$.

The power of the Floquet formalism is connected to the possibility to express every solution $|\psi(t)\rangle$ of the Schrödinger equation as

$$|\psi(t)\rangle = \sum_n c_n \, |u_n(t)\rangle \exp\left(-\mathrm{i}\varepsilon_n t/\hbar\right) \ , \tag{2.1.7}$$

where no index m labeling the representatives arises and, most importantly, the occupation amplitudes are *time-independent*. In other words: If a basis of Floquet states is used for describing the time evolution of a state $|\psi(t)\rangle$, the corresponding occupation probabilities $|c_n|^2$ remain constant in time. This is in complete analogy to a state expansion into the eigenstates of the Hamiltonian of time-independent systems.

Apart from the drawback that the Floquet picture remains restricted to the description of classical fields, and the mathematical difficulty to decide even for seemingly simple systems whether the quasienergy spectrum is continuous or a dense point spectrum [122], both only marginal issues for the present work, the main difficulties with the Floquet formalism in the context discussed here arise from two points:

(i) How can the quasienergy spectrum for a given system be calculated numerically? The short answer is that, after an inevitable truncation of the basis for numerical manageability, the quasienergies can be calculated by diagonalizing the monodromy operator – the time evolution operator $U(T, 0)$ for one period T – in the given basis, for which

$$U(T, 0) \, |u_\alpha(0)\rangle = \exp\left(-\mathrm{i}\varepsilon_\alpha T/\hbar\right) |u_\alpha(0)\rangle \tag{2.1.8}$$

holds due to the T-periodicity of the Floquet functions $|u_\alpha(t)\rangle$. For a detailed description of the calculation of quasienergies the reader is referred to the Appendix C, where the scheme is exemplified for a lattice system.

(*ii*) The Floquet formalism describes perfectly periodic systems. In the physical context of laser radiation interacting with matter, this interaction and hence the laser radiation itself, when described by Floquet theory, has never been switched on in the past and will never be turned off in the future, otherwise the temporal periodicity – the key element in Floquet theory – will be broken. This is obviously highly unsatisfactory from the experimental point of view but even theoretically speaking it is likely that the switching on/off process and its specific protocol can (and indeed will) change the evolution of a given state of the system. On the one hand, this makes a theoretical treatment of a more realistic setup with included switching on and off processes mandatory. On the other hand, these processes, if understood in detail, can be exploited to deliberately *control* the evolution of a given state of the system.

The second key problem, the process of switching the laser on (or off), can be treated with adiabatic techniques even in the Floquet framework, provided the relevant parameter – the laser radiation's amplitude in this case – is varied slowly with respect to the period of the laser radiation. This separation of periodic and parametric time scales is close in spirit to the Born-Oppenheimer approximation [123, 124]. Then, for each point in time an instantaneous basis of Floquet states can be defined for each instantaneous amplitude of the laser; a procedure that is derived from the treatment of parametrically but not periodically varying Hamiltonians, see [125, 126]. The system dynamics can now be monitored with respect to this set of Floquet bases despite the loss of formal periodicity of the Hamiltonian. If the state of the system is connected to a single quasienergy, for example, its variation with a change of parameters deter-

mines whether or not the state is able to follow these changes adiabatically. As is turns out, the concept of an adiabatic transport even holds for lattice systems, where entire momentum distributions are transported according to the rules of adiabaticity, as detailed in Publication IV. This concept, when applied to the framework of Floquet states [127, 128], is called an adiabatic principle in contrast to the adiabatic theorem. The latter requires an energy gap between the transported state and all other states, a condition not necessarily met in the Floquet context.

If the Hamiltonian changes such that the evolution is not perfectly adiabatic, transitions between different quasienergies occur. For parametric but not periodic changes of the Hamiltonian, the most prominent model to describe transition probabilities between two anticrossing energy lines is the Landau-Zener approach,[1] see [132]. This technique can be transferred to the setup of a periodically changing Hamiltonian, where transitions between anticrossing quasienergies occur, as discussed (among others) by Shirley [133].

In the case of periodically changing external fields acting on an atom, the radiation field is said to be "dressing" the bare atom [134] (that is the atom without the field present). This terminology of a dressed-atom picture was coined by Cohen-Tannoudji and co-workers, who were able to manipulate Landé g-factors by applying an oscillating magnetic field to the atoms. With the field with amplitude B and frequency ω present, the

[1] This theory specifies the anticrossing to be linear, that is far from the anticrossing the energy lines approach straight lines, and the coupling elements are constant in time. Other models consider different anticrossing geometries (such as tanh-anticrossings in the second Demkov-Kunike model [129]), time-dependent coupling elements as in the Rosen-Zener model [130], or a combination of both as in the first Demkov-Kunike model. For further details the reader is referred to [131] and references therein.

effective g-factor g_{eff} is connected to the original one by

$$g_{\text{eff}} = g\, \mathcal{J}_0 \left(\frac{\gamma B}{\omega} \right) , \tag{2.1.9}$$

where $\mathcal{J}_0$ denotes the zero-order Bessel function of the first kind and γ is the gyromagnetic ratio [135]. Eckardt *et al.* transferred the dressed-atom picture to periodically driven ultracold atoms and Bose-Einstein condensates, and suggest to view them as "dressed matter waves" [136]. First steps have been made to explore the exciting prospect of dressed matter waves on theoretical as well as experimental grounds. The following sections review some of the efforts already undertaken to gain insight into driven matter waves.

2.2. Dynamic Localization

One of the effects induced by an external periodic driving of a lattice system is "dynamic localization". In particular, and in contrast to the pulsed driving scenarios described in detail in the Publications I, III, and IV, it resorts to schemes with constant driving amplitudes. This section gives a short review of the effect and its explanation in terms of Floquet theory. The line of thought is kept close to the one adopted in Publication II, which in addition discusses the necessity of semiclassical approximations – in particular with respect to "extended" wave packets – as well as applications to bichromatic lattices and the coherent control of the "metal-insulator"–like transition occurring in the Harper model [137, 138].

Consider a particle moving in a lattice potential. For simplicity the lattice is assumed to be one-dimensional, but the following discussion can easily be generalized to higher dimensions. If the wave function of the particle is initially localized around some lattice site, the width of its envelope will grow in time since quantum tunneling enables the particle to

explore its neighborhood as known from basic quantum mechanics. This dispersive behaviour of the wave packet can be eliminated deliberately by shaking the lattice in a specific way. This impeded dispersion by an external force is, in short, dynamic localization.

The term was introduced by Dunlap and Kenkre in 1986, who considered a charged particle moving in a single-band tight-binding lattice with sites labeled by m under the influence of a spatially homogeneous but explicitly time-dependent sinusoidal electric field $E(t)$ [139]. The characteristic energy scale associated with the field's amplitude, $\mathcal{E} = qEa$, is proportional to the charge q of the particle and to the lattice constant a. Dunlap and Kenkre discovered that for times that are long compared to the driving period, that is for $t \gg 2\pi/\omega$, the mean square displacement of the particle is given by

$$\left\langle m^2 \right\rangle = 2\left(V_{\text{eff}}\, t\right)^2 \ . \tag{2.2.1}$$

The electric field rescales the tunneling energy V connecting neighboring sites and leads to an effective intersite matrix element

$$V_{\text{eff}} = V \mathcal{J}_0\left(\frac{\mathcal{E}}{\hbar\omega}\right) \ , \tag{2.2.2}$$

which reduces to V in the limit $\mathcal{E} \to 0$. Interestingly, though, V_{eff} can vanish if the ratio between field amplitude and frequency reaches a zero of the Bessel function $\mathcal{J}_0$. In this case $\left\langle m^2 \right\rangle$ vanishes, displaying explicit localization. Dunlap and Kenkre conjectured in 1986 that this effect might be exploited in higher dimensional systems "for inducing an anisotropy in the transport properties in ordinarily isotropic material" [139].

The term "coherent destruction of tunneling", coined in 1991 by Grossmann *et al.* (cf. [140]), describes a closely related concept in double-well systems. There, by applying a suitable oscillating external force, a state initially prepared in only one of the wells remains localized in the same well: The tunneling contact between the wells is "cut".

With the experimental realization of lattice as well as double-well systems in the framework of ultracold atoms and the viability of shaking these system periodically, driving-induced localization mechanisms could be put to the test with mesoscopic matter waves. On the many-body level, Eckardt *et al.* showed theoretically in 2005 that the superfluid-to-Mott insulator transition can be induced by an external forcing [141]. The tunneling matrix element gets renormalized by a Bessel function and again the tunneling contact between neighboring sites can be reduced almost arbitrarily. The details of this transition and the connection to external driving forces are discussed in Sec. 2.4. The first observation of dynamical suppression of tunneling as predicted by Eckardt *et al.* [141] and Creffield and Monteiro [142] was reported by the Pisa group in 2007: The experimental results confirmed the theoretical considerations [112]. Although only the absolute value $|J_{\text{eff}}/J|$ could be measured at the time, later experiments allowed to extract the sign of the Bessel function by monitoring the phase coherence of the condensate [143].

On the single-particle level, Holthaus *et al.* approached dynamic localization in 1992/93 theoretically by using Floquet theory [144, 145]. In this language, localization takes place due to a field-induced collapse of quasienergy bands: Consider the simple model of a one-dimensional tight-binding system described by the Hamiltonian

$$H_0 = -J \sum_m \left(|m+1\rangle \langle m| + |m\rangle \langle m+1| \right) \ , \tag{2.2.3}$$

where $|m\rangle$ denotes a Wannier state localized at the mth lattice site and $J > 0$ is the hopping matrix element between two neighboring sites, spatially separated by the lattice constant a. In this case, the dispersion relation is exactly given by

$$E(k) = -2J \cos(ka) \ , \tag{2.2.4}$$

where k is a wavenumber. By adding a term

$$H_1(t) = -F_1 \cos(\omega t) \sum_m |m\rangle \, am \, \langle m| \tag{2.2.5}$$

describing a homogeneous external force $F_1 \cos(\omega t)$ acting on the system, the Hamiltonian $H = H_0 + H_1$ becomes periodic in time and – within the single-band approximation – the Schrödinger equation is solved by the functions

$$|\psi_k(t)\rangle = \exp\left\{-\frac{\mathrm{i}}{\hbar}\int_0^t \mathrm{d}\tau \; E\left[q_k\left(\tau\right)\right]\right\} \sum_m |m\rangle \exp\left[\mathrm{i}m q_k(t) a\right] \tag{2.2.6}$$

known as "accelerated Bloch waves" (or Houston states [146] when discussed in the context of crystal electrons), provided the time-dependent wave numbers $q_k(t)$ obey[2]

$$q_k(t) = k + \frac{1}{\hbar}\int_0^t \mathrm{d}\tau \; F(\tau) \tag{2.2.7}$$

$$= k + \frac{F_1}{\hbar\omega}\sin(\omega t) \; . \tag{2.2.8}$$

Now, the energies $E[q_k(t)]$ are periodic because the force $F(t)$ is, but the Houston states are not. But they can be cast into the form of Floquet states simply by rewriting their exponential part as

$$\exp\left\{-\frac{\mathrm{i}}{\hbar}\int_0^t \mathrm{d}\tau \; E\left[q_k\left(\tau\right)\right]\right\} = \exp\left\{-\frac{\mathrm{i}}{\hbar}\int_0^t \mathrm{d}\tau \; \left[E\left(q_k\left(\tau\right)\right) - \varepsilon(k)\right]\right\} \times \exp\left[-\mathrm{i}\varepsilon(k)t/\hbar\right] \tag{2.2.9}$$

using the one-cycle average

$$\varepsilon(k) \equiv \frac{1}{T}\int_0^T \mathrm{d}t \; E\left[q_k\left(t\right)\right] \tag{2.2.10}$$

$$= -2J_{\mathrm{eff}} \cos(ka) \tag{2.2.11}$$

[2] This results from the relation $\hbar\dot{q}_k(t) = F(t)$ obtained by inserting (2.2.6) into the Schrödinger equation, plus the demand that $q_k(t)$ is equal to k at $t = 0$.

involving an effective hopping matrix element given by

$$J_{\text{eff}} = J\mathcal{J}_0\left(\frac{F_1 a}{\hbar\omega}\right) . \tag{2.2.12}$$

The Houston states are now in the form of Floquet states and the averages (2.2.11) are exactly the quasienergies. But regardless of whether the detour involving Houston states is taken or the Floquet theory is directly applied to the problem, both ways result in a Floquet expansion where the width of the quasienergy band $\varepsilon(k)$ changes according to Eq. (2.2.11) when the driving amplitude changes. If the scaled driving amplitude $F_1 a/(\hbar\omega)$ reaches a zero of the Bessel function, the quasienergy band is completely flat. Consequently, all elements in the Floquet expansion of the wave function gather the same dynamical phase factors. This results in a "prohibited dephasing" at the collapse point.

2.3. Photon-Assisted Tunneling

An external periodic force can be used to suppress the tunneling contact between adjacent sites in a lattice system by dynamic localization or in double-well potentials by coherent destruction of tunneling, but quite the opposite effect can be realized with the same tool: External forces can be used to enhance tunneling contact; an effect which has become known as "photon-assisted tunneling". The term originates from solid state physics, where, at certain voltages, a photon-irradiated superconducting Josephson junction exhibits steps in the quasiparticle current [147]. Photon-assisted tunneling has already been observed in quantum dots [148, 149], superconducting diodes [150], semiconductor superlattices [151, 152], and has recently been seen in double-well and lattice systems with ultracold atoms and Bose-Einstein condensates as elaborated on in the following.

The scheme of photon-assisted tunneling was transferred to the frame-

work of ultracold atoms in a double-well potential by Eckardt and co-workers in 2005, considering individual wells which are modulated periodically in time [153]. In this so-called "bosonic Josephson junction", the frequency associated with the "photons" is in the lower kilohertz regime. For lattice systems, multiphoton processes which increase the tunneling contact were studied theoretically by Creffield *et al.* in 2006, who proposed to exploit these processes for controlling the superfluid-to-Mott insulator transition [142] and considered effects of the initial driving phase in a consecutive study [154].

But before photon-assisted tunneling was observed experimentally three years after the theoretical proposal, an effect similar to photon-assisted tunneling was realized with Bose-Einstein condensates, which does not rely on a periodically modulated driving force but on a constant acceleration leading to a homogeneous "tilting" of the entire lattice. For certain values of the tilt, spatially separated lattice sites become resonantly coupled as Sias and co-workers showed experimentally in 2007 [155]. But whereas this time-independent resonantly enhanced tunneling is mediated by a tilting force tuned to a difference in the site-dependent energy levels (see Fig. 2.1a), for photon-assisted tunneling an additional driving force is needed. In a tilted system the tunneling contact can (partially) be restored by an external drive with a frequency that is resonantly tuned to bridge the gap between otherwise uncoupled sites as depicted in Fig. 2.1b. If the tilting force F is acting on the lattice with wells separated by a distance a, then the potential difference between adjacent wells is $\Delta E = Fa$. Now, the resonance condition for photon-assisted tunneling reads

$$m\hbar\omega = Fa \tag{2.3.1}$$

and denotes what is called an m-photon resonance or a photon-assisted resonance of the order m. Generally speaking, photon-assisted tunneling

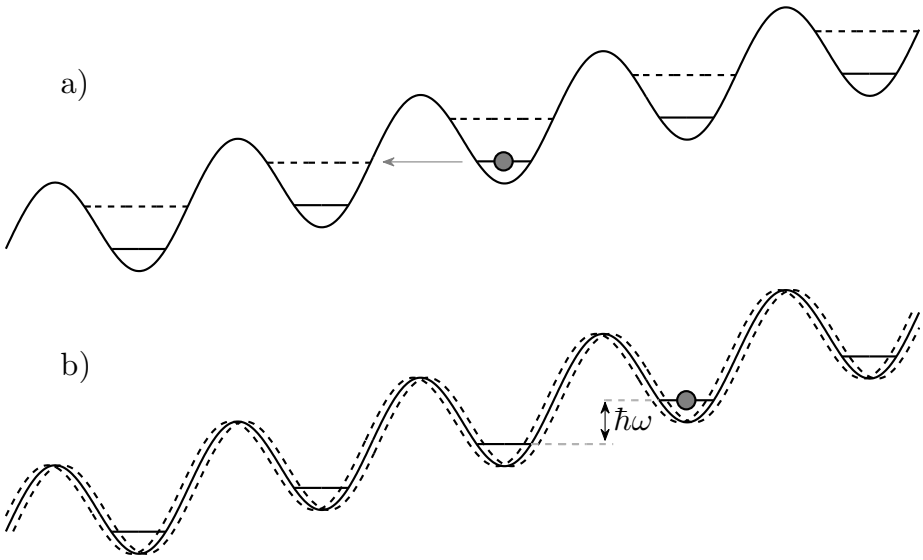

Figure 2.1.: Upper panel: Resonance enhanced tunneling. The tilting is tuned such that two states in adjacent sites match energetically. For different tiltings, even wells that are several sites apart can be resonantly coupled. Lower panel: Photon-assisted tunneling. The lowest states are tilted out of resonance. The tunneling contact is restored by shaking the lattice resonantly with frequency ω, thus bridging the tilting-induced level separation.

is achieved when the driving frequency bridges the energy gap between two modes; tilting the lattice is just one way to create off-resonant modes.

This scheme of photon-assisted tunneling in a lattice system was experimentally realized for the first time by the Pisa group in 2008 [156] with a Bose-Einstein condensate in a one-dimensional optical lattice described by the Hamiltonian

$$\begin{aligned} H = &- J \sum_{\langle i,j \rangle} \left(c_i^\dagger c_j + c_j^\dagger c_i \right) + \frac{U}{2} \sum_j n_j \left(n_j - 1 \right) \\ &+ \Delta E \sum_j j n_j + K \cos\left(\omega t \right) \sum_j j n_j \ , \end{aligned} \tag{2.3.2}$$

where the first line is the Bose-Hubbard Hamiltonian,[3] J is the tunneling energy between adjacent sites, U is the on-site interaction energy, $c_i^{(\dagger)}$ denote the bosonic annihilation (creation) operators, respectively, and n_j is the particle number operator for the jth site. The third and fourth term additionally introduce the tilting associated with an energy difference ΔE as described previously and the external driving with amplitude K and frequency ω. As predicted by Eckardt *et al.*, the periodic driving dresses the system and leads to a rescaled effective tunneling matrix element

$$J_{\text{eff}} = J \mathcal{J}_n(K_0) \ , \tag{2.3.3}$$

where the nth Bessel function is evaluated at the dimensionless driving amplitude $K_0 = K/(\hbar\omega)$. The experiment was performed with a Bose-Einstein condensate of ^{87}Rb in a lattice with spacing $\lambda_{\text{L}} = 852\,\text{nm}$ and depth of five recoil energies. The acceleration was implemented by adding a frequency difference $\delta\nu$ between the two lattice-generating laser beams, which additionally was modulated sinusoidally to induce the time-dependent force. The ratio $|J_{\text{eff}}/J|$ was extracted by measuring the *in*

[3] See Section 2.4 for details.

situ width of the condensate with and without accelerating and/or shaking the lattice. Both the suppression of tunneling in the homogeneously accelerated lattice and the photon-assisted restoration of tunneling are evident in the experimental results shown in [156]. The lower panel of Fig. 2.2 (taken from Creffield *et al.* [157]) depicts[4] the experimental data for photon-assisted tunneling as analyzed by Sias *et al.*. Seemingly, the data interpolates between a linear and quadratic scaling with the Bessel function. This results from the assumption that the width of the condensate $\sigma(t)$ scales linearly in time. However, this is justified only for long expansion times, as recently pointed out by Creffield *et al.*: If the correct scaling (cf. [157, 158])

$$\begin{aligned}\sigma(t) &= \sqrt{\langle x^2\rangle - \langle x\rangle^2} \\ &= \sigma_0\sqrt{1+(t/t_\mathrm{c})^2}\end{aligned} \tag{2.3.4}$$

with the initial width σ_0 and $t_\mathrm{c} \propto |J_\mathrm{eff}|^{-1}$ is employed to calculate $|J_\mathrm{eff}/J|$, the agreement between theory and experiment is improved noticeably, as shown in Fig. 2.2a.

Similar results were obtained in tilted, driven double-well systems [159]. Recent theoretical work by Teichmann *et al.* even points to fractional photon-assisted tunneling in a system of a Bose-Einstein condensate in a double-well potential. Unlike their integer valued predecessor, fractional photon-assisted tunneling processes cannot be explained by a mere driving-induced renormalization of the tunneling frequencies [160]. In 2011, Esmann and co-workers analyzed the contribution of fractional photon-assisted tunneling in a double-well superlattice to the particle transfer [161].

[4] © 2010 by the American Physical Society.

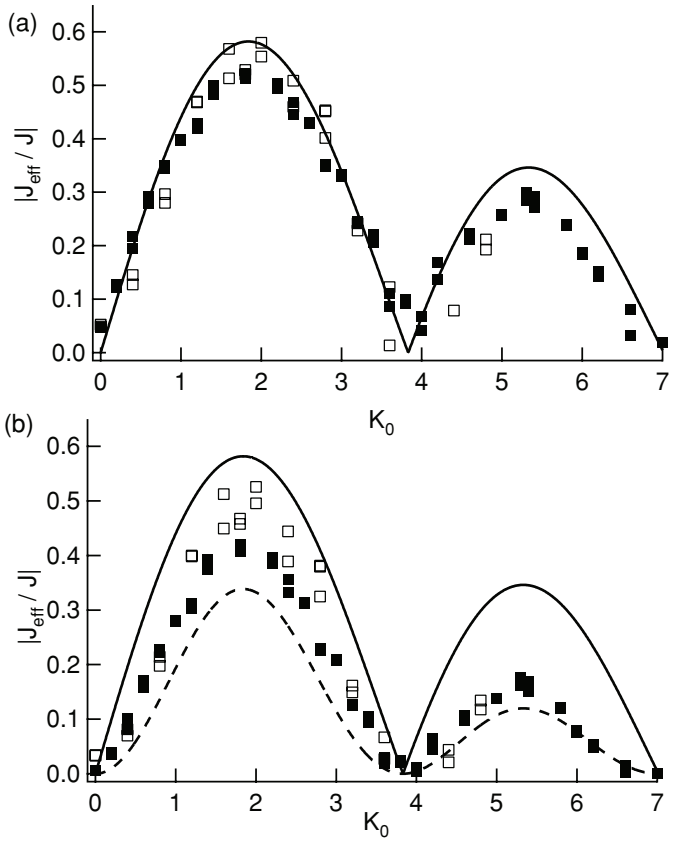

Figure 2.2.: Photon-assisted tunneling in theory and experiment. For a one-photon resonance, in (a) the theoretically expected (first-order Bessel function, solid line) and the experimentally measured effective tunneling are juxtaposed for two different initial condensate sizes [15 μm (open squares), 17 μm (solid squares)]. The effective tunneling matrix element is extracted using the correct scaling given by Eq. (2.3.4). Panel (b) depicts the same experimental data, but now a linear scaling is assumed, that is $t \gg t_c$. The data clearly interpolates between a linear (solid line) and quadratic (dashed line) scaling in the Bessel function. From [157] with kind permission of Dr. C. Creffield.

2.4. The Superfluid-to-Mott Insulator Transition

As one of the landmark experiments with Bose-Einstein condensates, the superfluid-to-Mott insulator transition has already been mentioned in the previous sections. The present one focuses on this quantum phase transition, which emerges naturally in the Bose-Hubbard model, as well as on its experimental realization, achieved for the first time in 2001. The Bose-Hubbard model has been studied extensively in the literature. Inevitably, only an incomplete selection can be given here and the reader is referred to [111, 141, 162, 163, 164, 165, 166, 167, 168] and references therein. A description of the superfluid-to-Mott insulator transition can be found in Sachdev's "*Quantum Phase transitions*", see [169].

The transition itself can easily be sketched: Consider a Bose-Einstein condensate in a static optical lattice, which is neither accelerated nor externally driven. Suppose two atoms interact only with each other when they are in the same well; quantum tunneling is restricted to adjacent wells only and additionally single-band dynamics are assumed. Then, the ratio between the energy J associated with a single tunneling event on the one hand and the (repulsive) on-site interaction energy U on the other determines the phase of the system. Two cases can be distinguished:

- If the interaction energy scale dominates as in the case of very deep lattice wells, $J/U \ll 1$, quantum tunneling is suppressed and the system is in a Mott-insulating state. All of the wells are isolated and phase coherence between the individual condensates is lost.

- If the tunneling energy scale dominates as in the case of rather shallow lattice wells, $J/U \gg 1$, quantum tunneling events dominate and the system is in the superfluid state. The condensate is no longer fractioned and extends phase-coherently over the entire lattice.

Obviously, when slowly increasing the depth of the wells in an initially

rather shallow lattice, the state of the system changes from the superfluid to the Mott-insulating state. Although by no means apparent, the transition takes place at a certain critical value $(J/U)_\mathrm{c}$ and is driven by quantum rather than statistical fluctuations and hence poses an example for a quantum phase transition, which takes place even at zero temperature.

The physics of the scenario sketched above is enclosed in the Bose-Hubbard model. It is closely related to the Hubbard model known from solid state physics, which describes the very similar "hopping" and interaction of electrons in a lattice system [170]. To be definite, the Bose-Hubbard model reads

$$\hat{H} = -J \sum_{\langle i,j \rangle} \left(\hat{c}_i^\dagger \hat{c}_j + \hat{c}_j^\dagger \hat{c}_i \right) + \frac{U}{2} \sum_j \hat{n}_j \left(\hat{n}_j - 1 \right) \ , \tag{2.4.1}$$

where $-J$ ($J > 0$) denotes the hopping matrix element between adjacent lattice sites, which are summed over in the first term. Note that their number depends on the dimension d of the lattice; for a simple cubic lattice each site has $2d$ nearest neighbors. The second term accounts for the on-site interaction associated with the energy U and $n_j(n_j - 1)/2$ is exactly the number of pairs in the jth well. This second-quantized form of the Hamiltonian with the bosonic annihilation (creation) operators $\hat{c}_j^{(\dagger)}$, respectively, which obey the bosonic commutation rules

$$\left[\hat{c}_i, \hat{c}_j^\dagger \right] = \delta_{ij} \qquad \left[\hat{c}_i, \hat{c}_j \right] = \left[\hat{c}_i^\dagger, \hat{c}_j^\dagger \right] = 0 \ , \tag{2.4.2}$$

refers to a Fock basis of states with occupation numbers n_j,

$$\left\{ |n_1, n_2, \ldots, n_M\rangle \,|\, \sum_{i=1}^{M} n_i = N \right\} \ , \tag{2.4.3}$$

where M is the number of lattice sites. This basis explicitly contains the particle number N, in contrast to the Hamiltonian (2.4.1). At a first

glance, the Bose-Hubbard model seems to be a rather simple model with only the basic tunneling and interaction effects incorporated. Yet it evades an analytical solution and the existence of a quantum phase transition, too, indicates the nontrivial physics involved. But even exact numerical approaches are feasible only for rather small systems with a few particles and lattice sites (at the most up to ten each). This is due to the dimension $\mathcal{D}$ of the Hilbert space, which grows exponential with the system size:

$$\mathcal{D} = \binom{N+M-1}{N} \sim \mathrm{e}^{hM} \ , \tag{2.4.4}$$

with $h = (n+1)\ln(n+1) - n\ln n$ and the filling factor $n \equiv N/M$.

To understand the mechanisms of the quantum phase transition, consider a one dimensional lattice ($d = 1$) ...

- in the limit of weak interactions, $U/J \to 0$. The Hamiltonian (2.4.1) is now diagonal in the basis of Bloch waves

$$|\psi_k\rangle = \frac{1}{\sqrt{M}} \sum_{\ell=1}^{M} |\ell\rangle \, \mathrm{e}^{\mathrm{i}k\ell a} \tag{2.4.5}$$

  where $|\ell\rangle$ denotes a Wannier function [171] at the ℓth site and a is the lattice constant. The many body ground state is then superfluid (SF) and can be created from the vacuum $|0\rangle$:

$$|\mathrm{SF}\rangle = \frac{1}{\sqrt{N!}} \left(\frac{1}{\sqrt{M}} \sum_{\ell=1}^{M} \hat{c}_\ell^\dagger \right)^N |0\rangle \ . \tag{2.4.6}$$

  In the limit of weak interactions *all* particles occupy the single particle ground state

$$|\psi_0\rangle = \frac{1}{\sqrt{M}} \sum_{\ell=1}^{M} |\ell\rangle \ , \tag{2.4.7}$$

  which is extended over the entire lattice and corresponds to $k = 0$ of the single particle dispersion relation

$$E(k) = -2J\cos(ka) \tag{2.4.8}$$

of the Bose-Hubbard Hamiltonian in the limit $U/J \to 0$. The ground state obviously is not separated from the spectrum by an energy gap, thus elementary excitations are ungapped.

- in the limit of strong interactions, $J/U \to 0$, where the Hamiltonian (2.4.1) is now diagonal in the basis of (localized) Wannier states. For integer n, the many body ground state of the system reads

$$|\mathrm{MI}\rangle = \prod_{\ell=1}^{M} \frac{\left(\hat{c}_\ell^\dagger\right)^n}{\sqrt{n!}} |0\rangle \ . \tag{2.4.9}$$

  Since no tunneling occurs, the particles cannot move to different lattice sites and the system is in a Mott-insulating state. Due to the repulsive interactions it is energetically favorable for the atoms to be spread out homogeneously over the entire lattice. For integer filling factors n a perfectly homogeneous distribution is possible: Each site is filled with n atoms. In this case, elementary excitations are particle-hole excitations, which are energetically gapped from the ground state by $\Delta E = U$.

At the critical value $(J/U)_\mathrm{c}$, the elementary excitations change character from ungapped to gapped. For understanding the superfluid-to-Mott insulator transition it is helpful to extend the system to the grand canonical ensemble, thus allowing fluctuations in particle number. The Hamiltonian then reads

$$\hat{H}_\mathrm{gc} = -J \sum_{\langle i,j \rangle} \left(\hat{c}_i^\dagger \hat{c}_j + \hat{c}_j^\dagger \hat{c}_i \right) + \frac{U}{2} \sum_j \hat{n}_j \left(\hat{n}_j - 1 \right) - \mu \hat{N} \ , \tag{2.4.10}$$

with the chemical potential μ and $\hat{N} = \sum_i \hat{n}_i$ is the particle number operator.

In the limit $J/U \to 0$ the system is in the Mott-insulating regime, where

the (integer) occupation numbers n_i for the ground state minimize the on-site energy $E(n) = Un(n-1)/2 - \mu N$, leading to

$$n = \begin{cases} 0 & \text{if } \mu/U < 0 \\ g & \text{if } (g-1) < \mu/U < g \\ g \text{ or } (g-1) & \text{if } \mu/U = g - 1 \, . \end{cases} \tag{2.4.11}$$

with integer $g \geq 1$. Hence the system is incompressible for noninteger μ/U,

$$\frac{\partial \langle \hat{n}_i \rangle}{\partial \mu} = 0 \, . \tag{2.4.12}$$

In the limit $J/U \to 0$, particle-hole excitations increase the energy of the system by a finite amount $E_0(N \pm 1) - E_0(N)$. If J/U is slowly increased, the energy levels are shifted continuously and the energy gap between the ground state and a particle-hole excited state decreases. When the energy lines cross, the previous excited state is energetically favored and becomes the new ground state: The particle number of the system changes. This takes place when the energy cost of the excitation is compensated by a gain in energy due to the delocalization induced by the tunneling. Perturbative calculations in J/U lead to a phase diagram for the superfluid-to-Mott insulator transition as sketched in Fig. 2.3. The "Mott lobes" dominate for small values of J/U except near integer values of μ/U where the system is superfluid just as in the $J/U \gg 1$ regime. The lobes are calculated for a square $2d$ lattice geometry in 9th order perturbation theory [according to Kato, extrapolated (for details see [172])].

When a mean-field approach is used to determine the critical point of the quantum phase transition, the grand canonical Hamiltonian (2.4.10) is replaced by the mean-field Hamiltonian

$$\hat{H}_{\mathrm{mf}}(\psi) = \sum_i \hat{H}_{\mathrm{S}}^{(i)} \, , \tag{2.4.13}$$

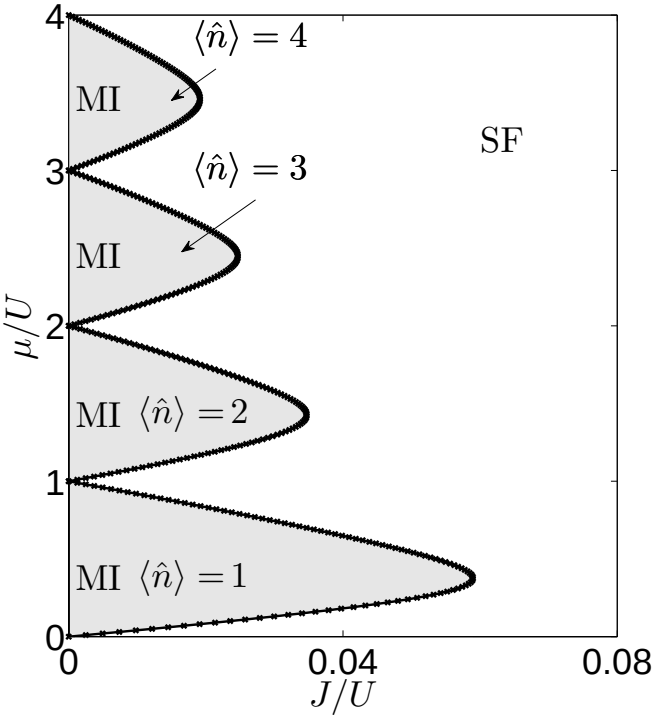

Figure 2.3.: Phase diagram for the superfluid-to-Mott insulator transition for a square lattice in $d = 2$ dimensions. In the superfluid regime (SF) with integer values of $\langle\hat{n}\rangle$, the lines of constant density $\langle\hat{n}\rangle$ hit the phase boundary to the Mott-insulating regime (MI) at the tips of the Mott lobes. For noninteger $\langle\hat{n}\rangle$ these lines end at integer values of μ/U in the limit $J/U \to 0$. Data by courtesy of D. Hinrichs.

where the single-site Hamiltonian

$$\hat{H}_{\mathrm{S}}^{(i)} = -2dJ\left(\psi^*\hat{c}_i + \psi\hat{c}_i^\dagger - |\psi|^2\right) + \frac{U}{2}\hat{n}_i(\hat{n}_i - 1) - \mu\hat{n}_i \qquad (2.4.14)$$

is equipped with a complex parameter ψ (ψ^*) which controls the strength with which a particle is coupled "into (out of) the site", respectively. But for what values of ψ is the mean-field Hamiltonian a proper replacement for the grand canonical one? The mean-field ground state is reached for

$$\psi = \langle\hat{c}\rangle_\psi \ , \qquad (2.4.15)$$

that is, this choice for ψ is optimal in the sense that it minimizes the expectation value $E_{\mathrm{mf}}(\psi) \equiv \left\langle \hat{H}_{\mathrm{mf}}(\psi)\right\rangle_\psi$. Since the expectation value of the difference between mean-field and grand canonical Hamiltonian

$$\left\langle \hat{H}_{\mathrm{gc}} - \hat{H}_{\mathrm{mf}}(\psi)\right\rangle_\psi = -2dJM\left(\langle\hat{c}\rangle_\psi - \psi\right)^2 \qquad (2.4.16)$$

depends on the fluctuations $(\hat{c}_i - \psi)$, substituting $\hat{H}_{\mathrm{gc}}$ with $\hat{H}_{\mathrm{mf}}$ is equivalent to neglecting the correlation of those fluctuations.

The trial function $E_{\mathrm{mf}}(\psi)$ now is characteristically different for the different phases, as depicted in Fig. 2.4. In the Mott-insulating regime, the mean-field ground state energy is minimized for $\psi^0 = 0$ (upper panel). If the tunneling contact is now slowly turned on, the minimum gets broader until the phase transition $(J/U)_{\mathrm{c}}$ is passed. After passing the transition point the order parameter ψ^0 is nonzero and the mean-field energy as a function of ψ is double-well shaped and exhibits two minima, provided ψ is chosen real. This is possible since a complex phase factor of ψ can be absorbed in the definition of the annihilation operator without changing the commutation relations. For systems with complex order parameters (which cannot be transformed to real values as it is the case here), the trial energy has a characteristic "Mexican hat" geometry. This leads to gapped

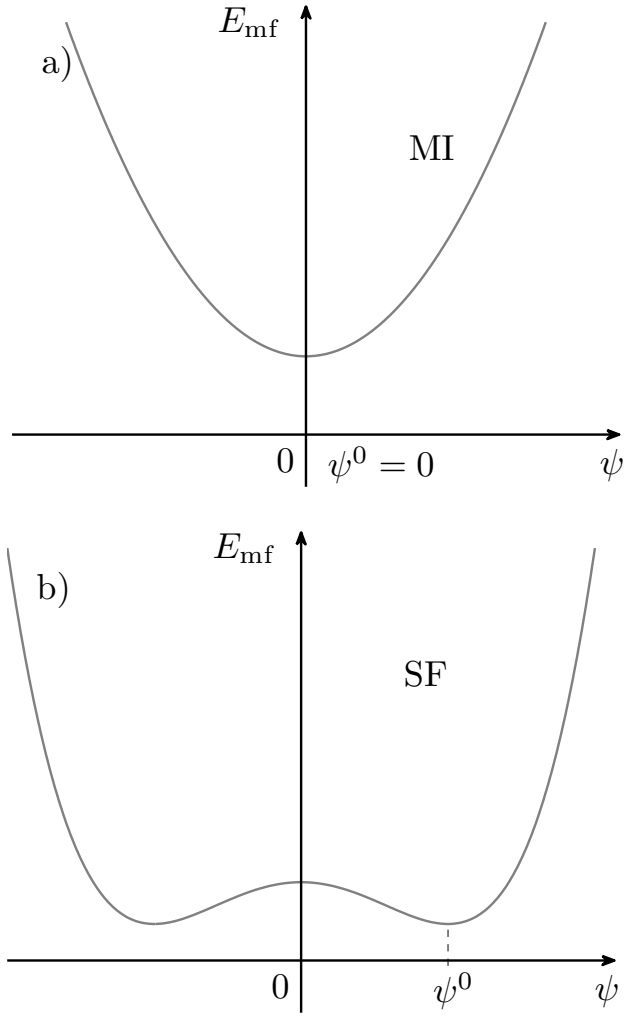

Figure 2.4.: Trial mean-field energies as a function of the parameter ψ (sketched). a) For $J/U = 0$ the mean-field energy minimum is at $\psi^0 = \langle \hat{c} \rangle = 0$. This implies $\langle \hat{c}_i^\dagger \hat{c}_j \rangle = \langle \hat{c}_i^\dagger \rangle \langle \hat{c}_j \rangle$, so no long-range correlations exist and the system is in the Mott-insulating state (MI). These correlations do exist in the compressible regime (b) as indicated by the order parameter ψ^0, which is nonzero for a state in the superfluid regime (SF).

excitations in radial direction just as in the Mott phase, but there are additional gapless excitations along the "trough" of the Mexican hat, which are associated with Goldstone modes. This behaviour known as "spontaneous symmetry breaking" [173] is characteristic for phase transitions and can be found in a variety of different physical systems.

The experimental realization of the superfluid-to-Mott insulator transition with ultracold atoms was first achieved in 3d by Greiner *et al.* in 2002 [111], four years after the theoretical proposal by Jaksch and coworkers [163]. Subsequent experiments observed the superfluid-to-Mott insulator transition in 2d [174] and 1d [167] as well. The experimental signature used to determine whether the system is in the superfluid or Mott-insulating state is its momentum distribution, which exhibits a pronounced interference pattern in the superfluid regime due to phase coherence of the superfluid state, whereas in the Mott-insulating regime the interference pattern vanishes since phase coherence is lost. Notably, phase coherence of the Mott insulator can be restored by crossing the phase transition to the superfluid regime, as depicted in Fig. 2.5. The seminal experimental observation of the phase transition clearly demonstrates the feasibility to emulate complex model systems known from solid state physics with Bose-Einstein condensates in an extremely transparent and controlled way, as performed with the Bose-Hubbard model. The model itself and its range were put to the test and both experimental and theoretical efforts included the study of facets of the model such as the in-trap density distributions [175, 176, 177], the number statistics [177, 178], the detailed shape of the phase diagram [162, 172, 179], the excitation spectrum [111, 180, 181], and more.

As in the case of the already discussed dynamic localization and photon-assisted tunneling, an additional periodic force acting on the system can coherently and in a controlled way alter the dynamics of the Bose-Hubbard

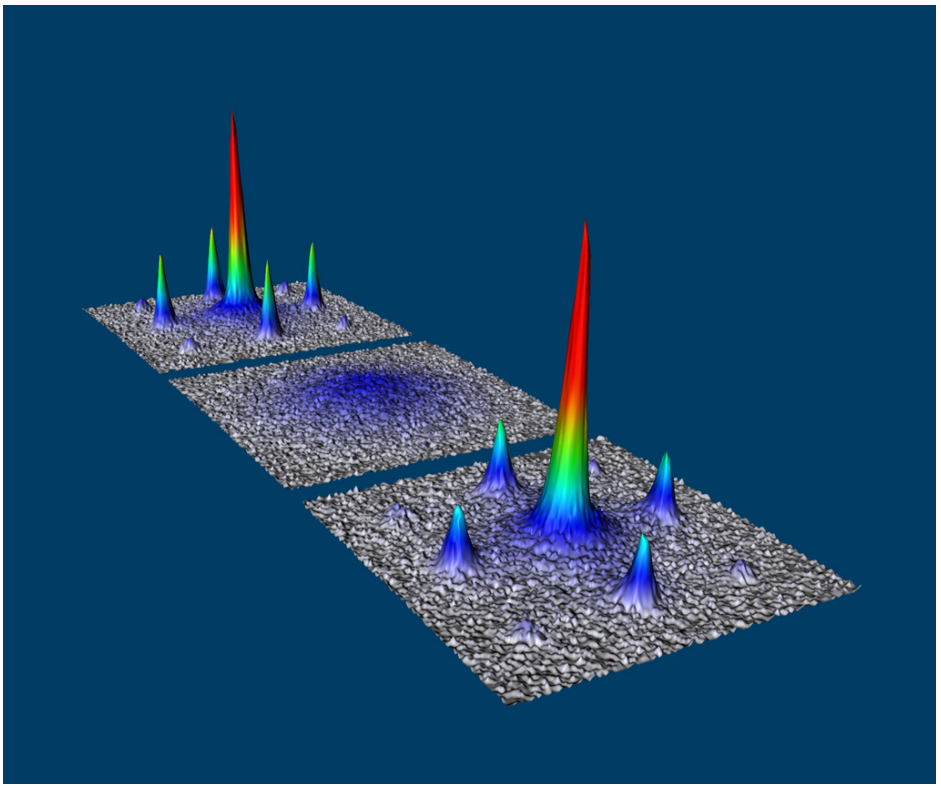

Figure 2.5.: The pronounced interference patterns indicating the superfluid state (left) vanish in the Mott-insulating regime due to a loss of phase coherence (middle), but can be restored by transitioning back to the superfluid regime (right). Shown here is experimental data for a three-dimensional optical lattice with more than 100,000 occupied lattice sites. Figure by courtesy of I. Bloch.

model and literally drive its phase transition: For simplicity, consider a 1d Bose-Hubbard model with an additional driving term as done by Eckardt and Holthaus in 2008 [136], so that the Hamiltonian of the system is given by

$$\hat{H}(t) = -J \sum_{i=1}^{M-1} \left(\hat{c}_i^\dagger \hat{c}_{i+1} + \hat{c}_{i+1}^\dagger \hat{c}_i \right) + \frac{U}{2} \sum_{i=1}^{M} \hat{n}_i \left(\hat{n}_i - 1 \right) + \left[K_0 + K_\omega \sin(\omega t) \right] \sum_{i=1}^{M} i \, \hat{n}_i \ , \quad (2.4.17)$$

where M denotes the number of lattice sites. Now, without any interaction between the particles, that is $U/J = 0$, and tuning the constant force resonant to the driving by setting

$$K_0 = m\hbar\omega \qquad (\text{integer } m) \ , \quad (2.4.18)$$

the driven system approximately behaves like an undriven one, but again the hopping matrix element is renormalized by a Bessel function according to

$$J_{\text{eff}} = (-1)^m \mathcal{J}_m \left(\frac{K_\omega}{\hbar\omega} \right) J \ . \quad (2.4.19)$$

If the system is in the high frequency regime ($\hbar\omega \gg U$ and $\hbar\omega \gg J$), Eq. (2.4.19) remains valid even for nozero U (cf. [141]).

Now, since the phase of the system is determined by the parameter J/U and this parameter gets "renormalized" by the presence of the driving force, the phase transition can be crossed by varying the driving strength K_ω. Note that, experimentally, the ground state of the undriven system needs to be transported to the effective ground state of the driven system – a nontrivial task as discussed in [136]: An adiabatic following of the many-body wave function imposes conditions on the driving protocol. a) The quasienergy spectrum has to remain "smooth", that is without exhibiting major resonances in the spectrum, so the driving frequency has

to be chosen accordingly. b) To ensure proper adiabaticity, the driving amplitude needs to vary sufficiently slowly on the one hand, but still fast enough on the other to pass minor resonances in the spectrum without them inducing tangible interband transitions.

With these difficulties it was by no means clear whether the Mott-insulator transition in a periodically driven lattice could be observed experimentally. This changed in 2009, when the Pisa group demonstrated the feasibility to induce the phase transition reversibly by changing the strength of the driving [114], thus extending the range of applicability of cold atoms in optical lattices. Again, driving the atoms opened up new vistas for controlling cold atoms on a quantum level.

2.5. Quantum Simulation of Frustrated Classical Magnetism

Only very recently an article written by the Hamburg group entitled "Quantum simulation of frustrated classical magnetism in triangular optical lattices" has been published in Science [182]. The paper is appealing on several levels: Firstly, it provides another example of the fruitful exploitation of the highly flexible system of Bose-Einstein condensates in optical lattices to emulate other physical systems with a purity unequaled by other means. Struck *et al.* succeeded in finding a way to simulate the XY model on a triangular lattice, a basic spin system which allows for frustration due to the lattice geometry [183, 184, 185, 186, 187, 188]. Just as with the observation of Bloch oscillations and basically for the same reasons, an experimental realization with ordinary solid-state devices poses a major challenge, yet Bose-Einstein condensates can fill the gap. Secondly, it is again the external *driving* of the system that is crucial. In the scheme adopted by Struck *et al.* the sign of the hopping matrix elements was

manipulated by the driving force, thus deliberately rendering the nearest-neighbor coupling ferro- or antiferromagnetic. The successful utilization of a driving force again hints at the still latent possibilities to be explored in periodically driven quantum systems.

The concept of "geometrical frustration", in the following short "frustration", can easily be sketched with the help of the plaquettes the lattice is build of. Consider the spins, for the moment, to have just two alignments: up and down. With antiferromagnetic interactions, adjacent spins on the lattice tend to align antiparallelly to minimize the system's energy. If the lattice is build of rectangular plaquettes (a single one is sketched in Fig. 2.6a), then all four antiferromagnetic bonds between the spins can be respected by alternating the spins orientation from site to site. If all

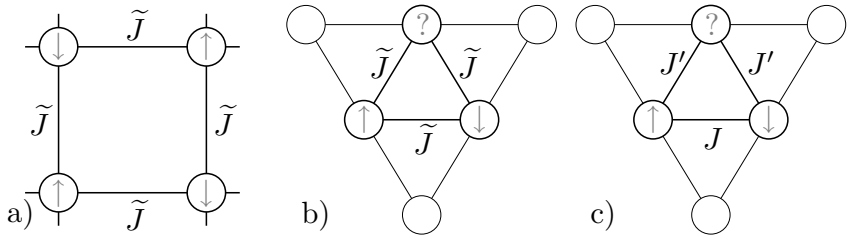

Figure 2.6.: For quadratic plaquettes, a), all antiferromagnetic bonds ($\widetilde{J} < 0$) can be respected in contrast to triangular plaquettes, b), where for J, $J' < 0$ the third spin is frustrated since it cannot respect both bonds simultaneously. In the driven lattice, c), the horizontal and diagonal bonds can be tuned independently so that different phases can be modeled.

the spins on the entire lattice are aligned in this fashion, the system is in its (twofold degenerate) ground state. For a lattice build of triangular plaquettes, on the other hand, this scheme does not work out. One pair of spins can always be aligned correctly, but not matter how the third one is oriented, it will violate one of the antiferromagnetic bonds and is hence

called frustrated, compare Fig. 2.6b. If the lattice is just a single plaquette, the ground state now is threefold degenerate. In general, frustrated systems allow for highly degenerate ground states, leading to a nonzero entropy even at zero temperature, to give an example of the intriguing physics of frustrated systems.

But now back to the XY model [189, 190], the physics of which were simulated with Bose-Einstein condensates by Struck and co-workers. It consists of classical vector spins $\vec{S}_i = [\cos(\theta_i), \sin(\theta_i)]$ located at the nodes of a (triangular) lattice and interacting by nearest-neighbor couplings J_{ij}: ferromagnetic (antiferromagnetic) interactions are modeled by positive (negative) J_{ij}, respectively. Since the spin degree of freedom is no longer restricted to $\theta_i = \pm\pi/2$ but can explore the the entire plane, $\theta_i \in [0, 2\pi[$, the XY model is also known as rotor model. The Hamiltonian of the system is given by

$$\begin{aligned} H(\{\theta_i\}) &= -\sum_{\langle i,j\rangle} J_{ij} \vec{S}_i \cdot \vec{S}_j \\ &= -\sum_{\langle i,j\rangle} J_{ij} \cos(\theta_i - \theta_j) \ , \end{aligned} \tag{2.5.1}$$

where the sum runs over all pairs $\langle i, j\rangle$ of adjacent spins. This model can be mapped to weakly interacting bosons on a triangular lattice forming a superfluid state. For a lattice depth of $5.6\, E_\mathrm{r}$, on-site interaction $U = 0.004\, E_\mathrm{r}$, homogeneous tunneling $J_{ij} = J$, and $\widetilde{J}/U = 0.5$ as used by Struck and co-workers, the system is deep in the superfluid regime.[5] In the weakly interacting regime, the superfluid ground state can locally be approximated by [186]

$$\prod_i \exp\left(\psi_i \hat{c}_i^\dagger\right) |0\rangle \tag{2.5.2}$$

[5] Note that the phase diagram naturally depends on the geometry of the system, so a direct comparison with Fig. 2.3 calculated for a quadratic lattice cannot be made and the reader is referred to reference [191].

with the discrete local order parameter $\psi_i = \sqrt{n_i}\exp(\mathrm{i}\theta_i)$; the mean number of atoms at the ith site is n_i, and θ_i denotes the local phase. The energy of the system without interactions reads in the tight binding limit

$$E(\{\theta_i\}) = -\sum_{\langle i,j\rangle} \sqrt{n_i}\sqrt{n_j} J_{ij} \cos(\theta_i - \theta_j) \ , \tag{2.5.3}$$

which is in the homogeneous case, $n_i \equiv n$ for all i, equivalent – up to a constant factor – to the energy of the XY model given by Eq. (2.5.1). Next to this formal mapping of both systems, their similarity becomes evident in the language of phase transitions, too, since both systems belong to the same universality class [162, 192].

The feature described as "most important"[6] to the approach used by Struck and co-workers is the possibility to tune the parameters J and J' (see Fig. 2.6c) independently by shaking the lattice elliptically according to

$$\vec{F}(t) = F_\mathrm{c}\cos(\omega t)\vec{e}_y + F_\mathrm{s}\cos(\omega t)\vec{e}_x \ , \tag{2.5.4}$$

resulting in the typical renormalization

$$J = \mathcal{J}_0\left(\frac{d|F_\mathrm{c}|}{\hbar\omega}\right)\widetilde{J} \tag{2.5.5}$$

$$J' = \mathcal{J}_0\left(\frac{d\sqrt{F_\mathrm{c}^2/4 + 3F_\mathrm{s}^2/4}}{\hbar\omega}\right)\widetilde{J} \tag{2.5.6}$$

of the bare coupling element $\widetilde{J}$ by a Bessel function $\mathcal{J}_0(z)$. Thus, J and J' can each independently and deliberately be adjusted to zero or ferromagnetic or antiferromagnetic, leading to different cases as labeled in Tab. 2.1. The tunability of the hopping matrix elements now is extremely useful for studying the transition between different phases. Consider, for example, a perfectly ferromagnetic setting ($J = 1$ and $J' = 1$) and then slowly

[6] cf.[182], p. 997

Table 2.1.: Different phases in the triangular XY model are labeled according the signs of the coupling parameters J and J', defined as in Fig. 2.6c.

	ferromag.	rhombic	Sp1	Sp2	staggered 1d chains
sign(J)	1	1	-1	-1	1
sign(J')	1	-1	-1	1	0

decrease J' to -1 while keeping J fixed. At some value of J' the phase of the system will turn from ferromagnetic to rhombic. This is accompanied by a certain critical value of J' and can be understood by calculating the energy (cf. supplementary material of [182])

$$E(J, J') = \begin{cases} -J - 2|J'| & \text{if } |J'| \geq -2J \\ J + J'^2/(2J) & \text{if } |J'| < -2J \end{cases} \tag{2.5.7}$$

of a single plaquette for a homogeneous system. In Fig. 2.7 the energy function is shown and the corresponding phases are indicated.[7] Since the first derivative of $E(J, J')$ is discontinuous at the boundary between the ferromagnetic (F) and rhombic (R) phase, the transition is of first order. The phase transition between the ferromagnetic and spiral 1 (Sp1) phase and the one between rhombic and spiral 2 (Sp2) are of second order, since the second derivative of the energy function is discontinuous. Since each spin configuration is uniquely associated with a quasimomentum distribution, which closely reflects the dispersion relation of the lowest band, each spin configuration and hence the different phase transitions can be identified experimentally by time-of-flight absorption imaging.

[7] The design of Fig. 2.7 is kept close to Fig. S2, which can be found in the supplementary material of [182].

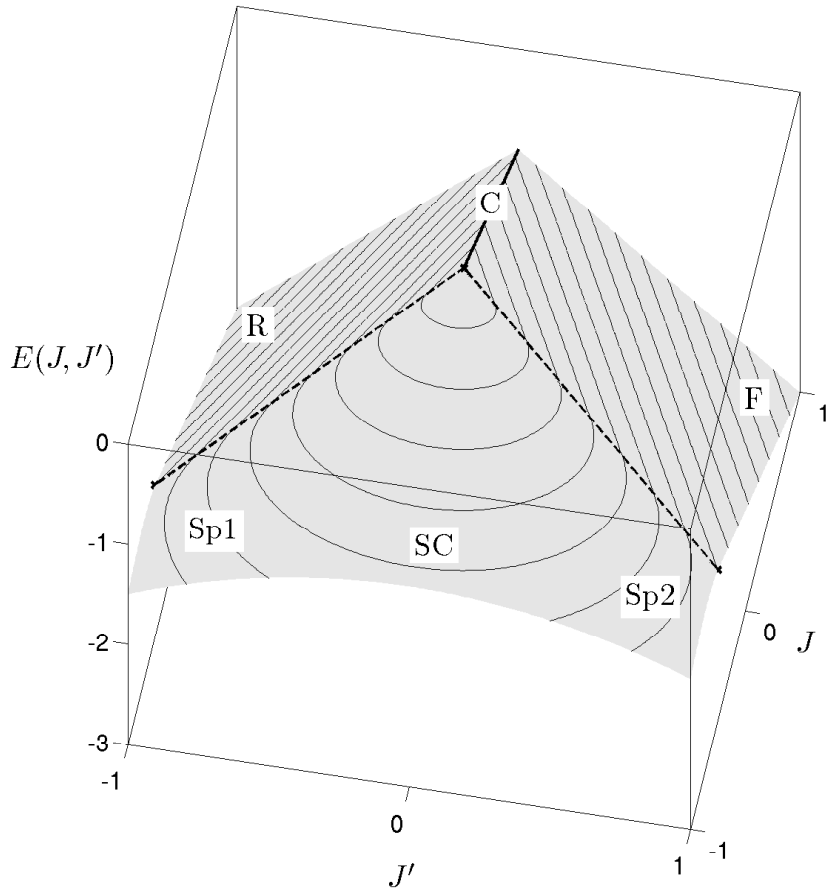

Figure 2.7.: The different phases from Tab. 2.1 can be mapped to the graph of the energy function $E(J, J')$. Its first derivative shows a discontinuity at the ferromagnetic-to-rhombic transition (bold black line) and hence indicates a phase transition of first order. The transition from the ferromagnetic or rhombic phase to the spiral phases (dashed lines) are of second order due to a discontinuity of the second derivative of the energy function.

Driving ultracold atoms in optical lattices are a powerful tool, which allows for a clean realization of various spin systems. The recent advances in controlling the driving parameters and the application of driving forces to emulate a wide range of solid-state systems point to a new emerging subfield in the area of ultracold atoms and Bose-Einstein condensates.

2.6. Multiphoton Transitions

So far, multiphoton excitations and the closely related ionization processes have been investigated in detail in atomic and molecular physics [193, 194, 195, 196, 197]. Advances in the generation of ultrashort laser pulses opened up new vistas for exploring and understanding these mechanisms on a fundamental level [198, 199, 200, 201]. With Bose-Einstein condensates as well as ultracold atoms in optical lattices being routinely realized in current experiments, and with the advent of periodically modulating these systems, the study of multiphoton excitations becomes applicable for ultracold atoms and Bose-Einstein condensates in optical lattices subjected to pulsed forcing. Although a transfer of methods as well as a "clean" realization of multiphoton transitions with optical lattices is of interest in its own right, there is more to gain than just selling the proverbial old wine in new skins. For example, switching the driving force off during the pulse becomes feasible in this new framework, thus providing insight into the dynamics of multiphoton excitations during a single pulse; a possibility that remains inaccessible with the traditional atomic or molecular counterpart. For the prefix "multi" to be appropriate, the characteristic energy gap ΔE between coupled bands needs to be much larger than the energy $\hbar\omega$ given by the driving. Hence, the driving is restricted to the low frequency regime, defined by $\omega \ll \Delta E/\hbar$.

On the theoretical level, the multiphoton character of the dynamics is

directly visible in the Floquet description: One of its key elements are the quasienergies $\varepsilon_n(k)$, which are defined only up to an integer multiple of the "photon" energy $\hbar\omega$, where ω is the driving frequency. Using the Floquet approach, multiphoton excitations are nothing but quasienergy-state transitions. The number of photons needed for a specific transition is given by the distance in $\hbar\omega$ of the corresponding quasienergies. These are continuously connected to the energy dispersion relation $E_n(k)$ in the limit of vanishing driving amplitudes, $K \to 0$, and are ac-Stark-shifted due to the driving. Since they depend on both the wavenumber k and the driving amplitude K for each band n, the quasienergies form "quasienergy surfaces" $\varepsilon_n(k, K)$, which determine the dynamics of an initial wave packet, which, without loss of generality, is assumed to be prepared within a single band. If such a wave packet is subjected to pulsed driving, the driving amplitude K changes during the pulse from zero to some maximum value $K_{\max}$ and then back to zero. Consequently, the basis of spatiotemporal Bloch waves that is used to describe the wave packet changes as well, and during the pulse, a family of bases is needed, one basis for each instantaneous amplitude. To enable parallel transport of the wave packet on its quasienergy surface during the pulse (stipulating smoothness of the envelope and a duration of the pulse much longer than the period $T = 2\pi/\omega$ of the driving), a special connection is required between different instantaneous bases. This connection is established by the Schrödinger equation. The concept of parallel transport is used here as equivalent to the notion of an adiabatic transport of the wave packet. Whether the wave packet is transported adiabatically on its quasienergy surface, hinges on its morphology: An adiabatic transport is possible provided those parts of the quasienergy surface explored by the wave packet remain undisturbed by any avoided crossings. If, on the other hand, the wave packet passes any regions with avoided crossings, transitions to the anticrossing surfaces oc-

cur. The amplitude of the transitions can be estimated for example with the Landau-Zener transition formula and hinges on the velocity with which the avoided crossing is passed as well as on its width [99, 128, 202]. In conjunction with the control mechanisms investigated in Publication III, where the effects of a homogeneous tilting in addition to the external driving has been considered, the morphology of quasienergy surfaces can – once known – deliberately be exploited for the preparation of exotic states, the principles of which are sketched in Publication IV. But apart from numerical calculations, can the structure of the quasienergy surfaces be measured experimentally?

In principle, yes. Multiphoton transitions in combination with pulsed driving allow for a "spectroscopy" of the quasienergy surfaces. The procedure is twofold:

(i) The morphology of a quasienergy surface can be screened and an avoided crossings can be *located* by subjecting an initial wave packet prepared on a specific band to a pulse and monitoring the final population of the band the wave packet was initially prepared in (called 'survival probability' in the following). Repeating the experiment with an increased maximum driving amplitude, deviations from adiabaticity become visible as soon as avoided crossings on the quasienergy surface are explored. But since working with driven optical lattices allows for monitoring the dynamics within a single pulse, a faster approach suggests itself: Instead of repeating the experiment with pulses of different maximum driving amplitudes, it is possible to monitor deviations from adiabaticity within the first half of a single pulse. The times at which transitions occur can be mapped to the corresponding instantaneous driving amplitudes, thus indicating the position of the avoided crossings. The information at which wavenumber the avoided crossing occurs can be isolated by preparing an initial wave packet with a very narrow k-space distribution centered around some value

$\langle k \rangle$. Thus, during the pulse the wave packet explores only a small range of the quasienergy surface and the avoided crossing can be located. If the width Δk of the initial wave packet is much less than the width of the Brillouin zone, that is $\Delta k \ll 2k_{\mathrm{L}}$, the excitation is determined by a section $\varepsilon_n(\langle k \rangle, K)$ of the quasienergy surfaces in good approximation.

(*ii*) In a second step the *width* of the avoided crossing can be estimated with asymmetric pulses. Just as for locating the avoided crossing and for the same reasons, this works the better the narrower the initial wave packet can be prepared in k space. The initial wave packet is subjected to an asymmetric pulse and the survival probability is monitored after the pulse. During the switch-on time $T_{\mathrm{p}}^{(1)}/2$ the amplitude rises to its maximum value $K_{\max}$ and then decreases back to zero during $T_{\mathrm{p}}^{(2)}/2$ with $T_{\mathrm{p}}^{(2)} \geq T_{\mathrm{p}}^{(1)}$. Needless to say, the value of $K_{\max}$ is chosen such that an avoided crossing is traversed during the pulse. On the one hand, the switch-on time needs to be substantially larger than the driving period T for the adiabatic principle to hold, on the other hand it should be so small that the first transition at the avoided crossing is almost complete. During the switch-off time, the wave packet hits the avoided crossing a second time and the final survival probability is formed. When repeating the experiment, always with a rapid switch-on and an ever larger ramp-down duration, the transition probability during the switch-off time will steadily decrease until for $T_{\mathrm{p}}^{(2)} \gg T_{\mathrm{p}}^{(1)}$ most of the wave packet stays in the continuously connected quasienergy states. If the survival probability is monitored as a function of the switch-off time, an exponential decay is expected since the transition probability for the second passage of the avoided crossing reads

$$P_{\mathrm{LZ}} = \exp\left(-\frac{\alpha\pi^2}{2}\frac{T_{\mathrm{p}}^{(2)}}{T}\right) \tag{2.6.1}$$

with

$$\alpha \equiv \frac{\left[\delta\varepsilon/(\hbar\omega)\right]^2}{\Delta\varepsilon/(\hbar\omega)} \,, \tag{2.6.2}$$

where $\delta\varepsilon$ is the width of the avoided crossing and $\Delta\varepsilon$ denotes the diabatic distance in quasienergy as sketched in Fig. 2.8. With the ratio α extracted experimentally, the width of the avoided crossing is known assuming the distance in quasienergy is. Note that equation (2.6.1) holds for an initial wave packet with only a single wavenumber k rather than a distribution and pertains to the Landau-Zener scenario of a symmetric and asymptotically linear avoided crossing, which is traversed with constant speed (cf. [99, 203]).

The protocol with steps (i) and (ii) has been implemented numerically for parameters directly accessible with current experimental setups: A Bose-Einstein condensate of Cs atoms is loaded into a 1d optical lattice $V(x) = V_0/2\cos(2k_{\mathrm{L}}x)$, with $k_{\mathrm{L}} = 2\pi/\lambda_{\mathrm{L}}$ and λ_{L} denoting the wavelength of the lattice-generating laser light; the lattice period is $a = \pi/k_{\mathrm{L}}$. To explore the single-particle regime, the interaction of the atoms is tuned to zero by means of a Feshbach resonance, cf. Section 1.2. Introducing an external force acting periodically on the atoms with some maximum driving amplitude $F_{\max}$, the system is described by the Hamiltonian

$$H(t) = \frac{p^2}{2m} + V(x) - s(t)F_{\max}x\sin(\omega t) \,, \tag{2.6.3}$$

where the dimensionless shape function $s(t)$ defines the envelope of the pulse. Using a rather shallow lattice with depth $V_0 = 2.3\,E_{\mathrm{r}}$, where E_{r} is the single-photon recoil energy [95], and laser wavenumber $\lambda_{\mathrm{L}} = 1064.49\,\mathrm{nm}$, the driving frequency is with $\omega/(2\pi) = 300\,\mathrm{Hz}$ fixed in the low frequency regime, since $\hbar\omega = 0.23\,E_{\mathrm{r}}$. The smallest gap between the first and second band figures as $5.05\,\hbar\omega$, so that more than five "photons" are required to excite particles from the initially occupied lowest band to the first excited band.

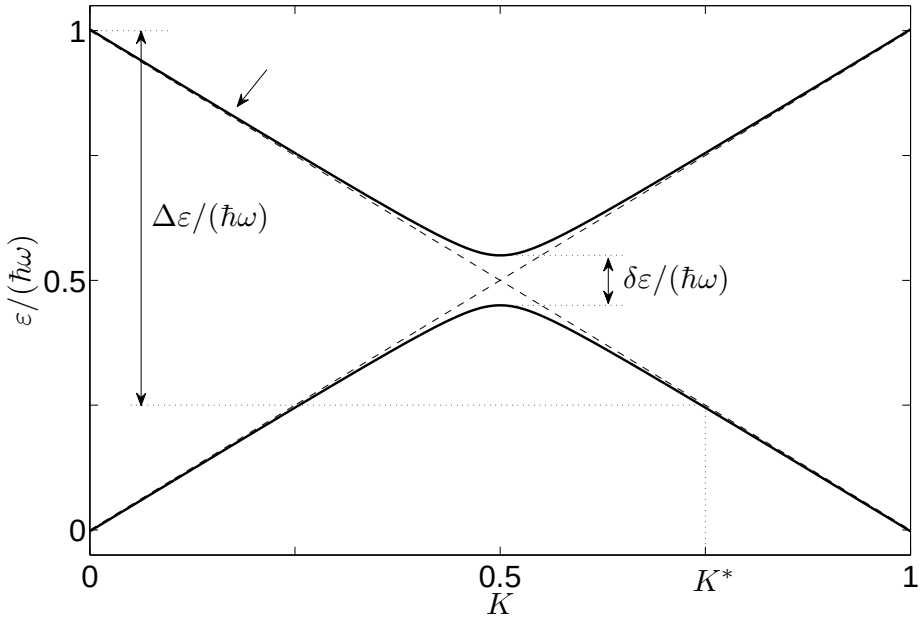

Figure 2.8.: Sketch of a Landau-Zener scenario with symmetric and asymptotically linear quasienergies, separated by $\delta\varepsilon/(\hbar\omega)$ at closest approach. The diabatic distance in quasienergy traversed when the parameter K is varied from zero to some value K^* is denoted $\Delta\varepsilon/(\hbar\omega)$; for example, starting at $K = 0$ on the quasienergy line marked by the arrow and setting $K^* = 0.75$ yields $\Delta\varepsilon/(\hbar\omega) = 0.75$. If the parameter K is varied with constant velocity, the probability to "jump over" the avoided crossing is given by Eq. (2.6.1).

(i) Excitations during a single pulse are monitored by plotting the survival probability of the atoms in the lowest band obtained by numerically solving the Schrödinger equation with an initial state

$$\psi(x,0) = \sqrt{\frac{a}{2\pi}} \int \mathrm{d}k \; g_1(k,0)\chi_{1,k}(x) \; , \tag{2.6.4}$$

where $\chi_{1,k}(x)$ are the Bloch states of the lowest band, and the initial momentum distribution

$$g_1(k,0) = \left(\sqrt{\pi}\Delta k\right)^{-1/2} \exp\left(-\frac{[k - \langle k\rangle\,(0)]^2}{2(\Delta k)^2}\right) \tag{2.6.5}$$

is, for this example, centered around $\langle k\rangle\,(0)/k_\mathrm{L} = 0.8$ with width $\Delta k/k_\mathrm{L} = 0.1$. The wave packet is now subjected to pulsed driving, with the envelope of the pulse given by

$$s(t) = \sin^2(\pi t/T_\mathrm{p}) \quad ; \quad 0 \le t \le T_\mathrm{p} \; ; \tag{2.6.6}$$

the duration of the pulse is fixed to 60 cycles, $T_\mathrm{p} = 60\,T$, so the condition $T_\mathrm{p} \gg T$ is met. After the pulse, that is at $t = T_\mathrm{p}$, the probability to find the particle in the lowest band is determined; in an experimental realization the atom number loss from the lattice after the pulse might be measured. This procedure is now repeated for different maximum driving amplitudes $K_\mathrm{max} \equiv F_\mathrm{max}a/(\hbar\omega)$, yielding the escape probability as a function of K_max. The results of the numerical simulation are displayed in Fig. 2.9. The excitations visible in this figure can be mapped to avoided crossings in the quasienergy spectrum, which is available numerically as well. Since the initial wave packet is with $\Delta k/k_\mathrm{L} = 0.1$ rather narrow in k space, a section of the quasienergy surfaces at k/k_L should suffice to explain the main features of the escape probability visible in Fig. 2.9. Yet only an approximate correspondence can be expected, since the initial wave packet still is extended in momentum space and explores parts of the

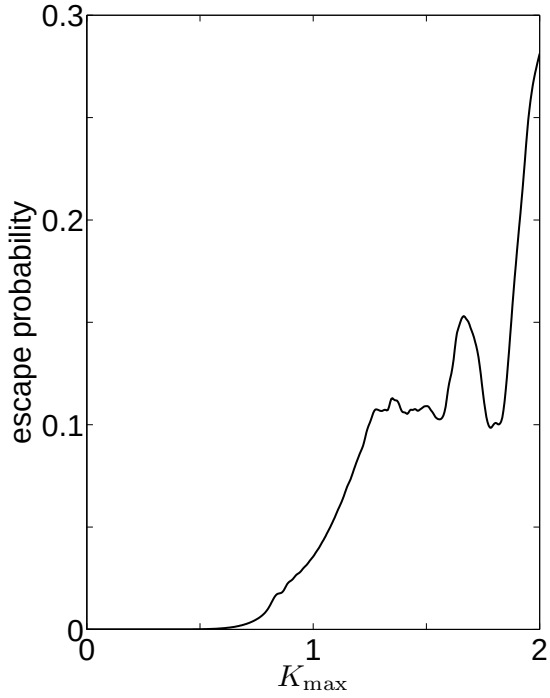

Figure 2.9.: The wave packet given by Eqs. (2.6.4) and (2.6.5) is subjected to a squared-sine pulse of length $T_\mathrm{p} = 60\,T$ and driving frequency $\omega/(2\pi) = 300\,\mathrm{Hz}$. After the pulse, the escape probability is monitored as a function of the maximum driving amplitude K_max. No excitations are visible after the pulse for maximum driving amplitudes below $K_\mathrm{max} \approx 0.7$, indicating an adiabatic transport on the quasienergy surface the initial wave packet is prepared on. Larger values of K_max result in excitations which hint at avoided crossings in the underlying quasienergy spectrum.

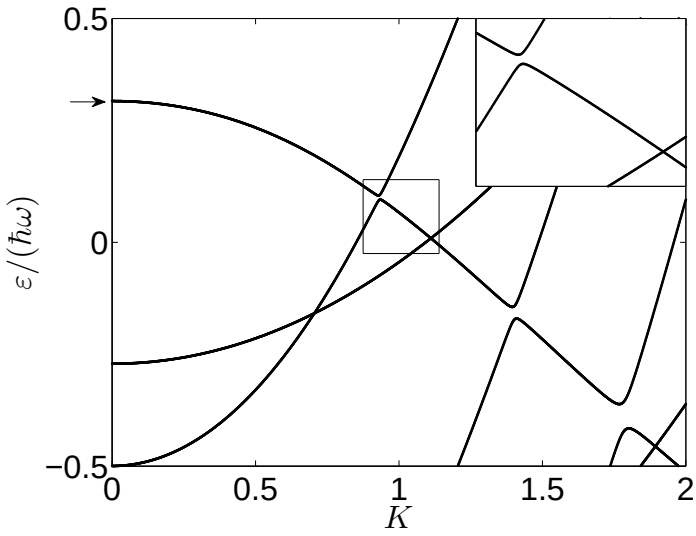

Figure 2.10.: Quasienergies $\varepsilon_n(k)$ for $k/k_\mathrm{L} = 0.8$ and $n = 1, 2, 3$. The quasienergy band originating from the lowest energy band $n = 1$ is indicated by the arrow and exhibits avoided crossings at $K \approx 0.95$, 1.4, and 1.8. These cause the transitions observed in Fig. 2.9.

quasienergy surfaces other than $k/k_\mathrm{L} = 0.8$. This reasoning is confirmed in Fig. 2.10. The locations of the avoided crossings visible in the quasienergy band connected to the lowest energy band approximately coincide with an increased escape probability. Even an effect of the first and rather narrow avoided crossing at $K \approx 0.95$ is, though weak, visible in Fig. 2.9. Since the avoided crossings shift to lower (higher) values of K when the section is displayed not at $k/k_\mathrm{L} = 0.8$ but at lower (higher) wavenumbers, respectively, the increase in escape probability is rather smeared over K. With the availability of wave packets with a much narrower k-space distribution, the signatures of the escape probability should be more pronounced.

(*ii*) To extract information about the width of the avoided crossing, asymmetric pulses are used as described. These are characterized by a rising part given by the first half of the envelope (2.6.6) with a fixed switch-on time $T_\mathrm{p}^{(1)}/2 = 5\,T$, while the decreasing part is squared-sine shaped as well but with a switch-off time $T_\mathrm{p}^{(2)}/2$. The initial wave packet already employed in part (i) is now subjected to asymmetric pulses and the survival probability after the pulse is depicted in Fig. 2.11 as a function of $T_\mathrm{p}^{(2)}$. The maximum driving amplitudes $K_\mathrm{max} = 0.6$, 1.2, and 1.6 are tuned such that not one, only one, and two avoided crossings, respectively, are traversed during the pulse, cf. Fig. 2.10. With the quasienergy spectrum and thus $\Delta\varepsilon/(\hbar\omega)$ and $\delta\varepsilon/(\hbar\omega)$ already known for the parameters used in the simulations, the numerically extracted widths of the avoided crossings can be compared to the actual ones given by the spectrum. The results are shown in Tab. 2.2, revealing that the numerically determined widths of the avoided crossings match the ones read off from the spectrum rather well. This is the more surprising, since many of the assumptions needed to apply Eq. (2.6.1) are, in fact, violated: Neither are the avoided crossings asymptotically linear and symmetric (cf. Fig. 2.10), nor are they traversed at constant speed (due to the squared-sine envelope). In addition, the

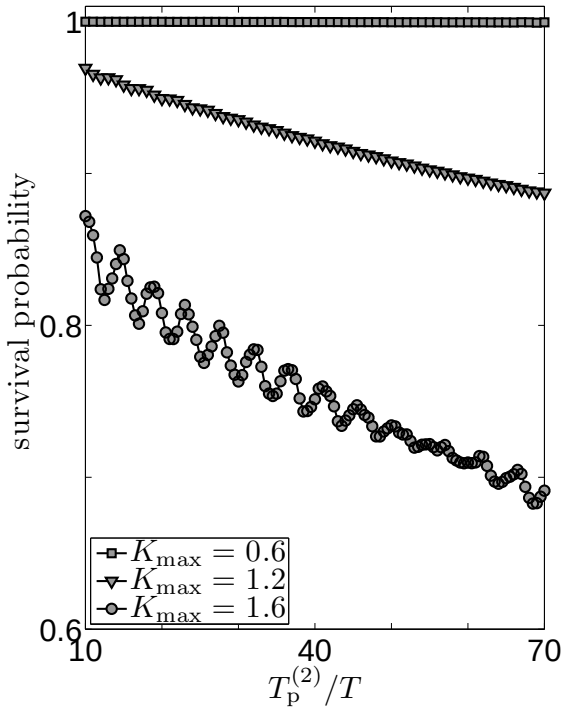

Figure 2.11.: Survival probability of atoms in the lowest band for three different maximum driving amplitudes K_max after asymmetric pulses with fast switch-on time $T_\mathrm{p}^{(1)}/2 = 5\,T$, and with varying switch-off durations $T_\mathrm{p}^{(2)}/2$. Again, the wave packet is initially centered around $\langle k \rangle\,(0)/k_\mathrm{L} = 0.8$. The spectrum determining the dynamics is given by Fig. 2.10. The expected exponential decay allows for an extraction of the constant α employed in Eq. (2.6.2), which in turn yields the width $\delta\varepsilon/(\hbar\omega)$ of the avoided crossing if the distance $\Delta\varepsilon/(\hbar\omega)$ is known.

Table 2.2.: Widths $\delta\varepsilon$ of the avoided crossings for various driving amplitudes $K_{\max}$ as read off from the spectrum displayed in Fig. 2.10, and as calculated from spectral quasienergy distance and from the data seen in Fig. 2.11. The numerical values match the exact ones surprisingly well.

$K_{\max}$	$\delta\varepsilon^{\mathrm{exact}}/(\hbar\omega)$	$\delta\varepsilon^{\mathrm{num}}/(\hbar\omega)$	$\delta\varepsilon^{\mathrm{exact}}/\delta\varepsilon^{\mathrm{num}}$
0.6	0	3.7×10^{-4}	0
1.2	0.01	0.00991	1.0030
1.6	0.03	0.02006	1.4955

restriction to only a single quasienergy spectrum at $k/k_{\mathrm{L}} = 0.8$ draws a drastically simplified picture, since the initial wave packet is actually still occupying about ten percent of the Brillouin zone.

In this section, a way has been outlined to use periodically driven matter waves for a kind of "quasienergy spectroscopy". This once again underlines the various ways in which exerting a periodic drive on ultracold atoms or Bose-Einstein condensates can be used as a tool to investigate fundamental properties of these systems. The schemes discussed here form the content of Publication V.

Appendix A.

Acceleration Theorem and Group Velocity

Already in 1929 Felix Bloch discussed in "Über die Quantenmechanik der Elektronen in Kristallgittern" [96] the acceleration of electrons in a periodic potential endowed with an additional homogeneous field. However, the occurrence of Bloch oscillations within the single band approximation was first mentioned by Zener [99]: The presence of a constant force F_0 leads to oscillations of an initial wave packet in real space with the Bloch frequency, which is proportional to the force acting on the particle. The group velocity of a wave packet, that is well centered around k_c in momentum space in the nth band, is connected with the derivative of the dispersion relation of the untilted potential via

$$v_\mathrm{g}(t) \equiv \frac{\mathrm{d}}{\mathrm{d}t} \langle x \rangle = \frac{1}{\hbar} \left. \frac{\mathrm{d}E_n(k)}{\mathrm{d}k} \right|_{k_\mathrm{c}(t)} , \tag{A.1}$$

whereas in k space the expectation value evolves in a semiclassical manner according to the "acceleration theorem"

$$\hbar \frac{\mathrm{d}}{\mathrm{d}t} \langle k \rangle (t) = F_0 . \tag{A.2}$$

In this appendix, the acceleration theorem (A.2) is derived using the crystal-momentum representation [204, 205]. An effective Schrödinger

equation for the k-space distribution is presented. As it turns out, the only restriction necessary is the single-band approximation, whereas Eq. (A.1) additionally requires the wave packet to be extended in real space over at least a few lattice constants. These results are generalized in App. B to time-periodically driven systems and it is shown that the wave packet follows the external force in the Floquet picture as well. The general techniques used to derive the acceleration theorem in the framework of not explicitly time-dependent Hamiltonians can almost directly be transferred to time-periodic Hamiltonians.

In a first step, the acceleration theorem as well as the expression (A.1) of the group velocity are derived. The discussion is focused on requirements for as well as limitations of the theorems. After discussing the acceleration theorem in the first section, the expression for the group velocity is reviewed subsequently. The appendix closes with numerical data, which visualizes the previous reasoning.

A.1. Acceleration Theorem

The discussion is splitted in two parts. Firstly, the untilted Hamiltonian with the external force absent, that is $F_0 = 0$, is considered. After deriving the acceleration theorem, the Hamiltonian is extended by the additional force term in a second step, thus breaking translational symmetry.

The eigenvalue equation of the Hamiltonian of the untilted lattice reads

$$\left(\frac{p^2}{2m} + V(x)\right) \varphi_{n,k}(x) = E_n(k)\varphi_{n,k}(x) \ , \tag{A.3}$$

where the operator on the left hand side is denoted $H_0(x)$. The potential $V(x)$ is assumed to be periodic with period a, so that $V(x+a) = V(x)$. Thus, the Hamiltonian inherits the periodicity of the potential $V(x)$, that is $H_0(x+a) = H_0(x)$. The Bloch waves $\varphi_{n,k}(x) = \exp(\mathrm{i}kx)u_{n,k}(x)$ with

a-periodic functions $u_{n,k}(x)$ are normalized such that

$$\int_{-\infty}^{\infty} \mathrm{d}x\ \varphi^*_{n',k'}(x)\varphi_{n,k}(x) = \frac{2\pi}{a}\delta(k-k')\delta_{nn'}\ , \tag{A.4}$$

where all wavenumbers are within the fundamental Brillouin zone $\mathcal{B}$, ranging from $-\pi/a$ to π/a. As a direct consequence of Eq. (A.4),

$$\begin{aligned}\frac{2\pi}{a}\delta(k-k')\delta_{nn'} &= \int_{-\infty}^{\infty} \mathrm{d}x\ \mathrm{e}^{\mathrm{i}(k-k')x}\, u^*_{n',k'}(x)\, u_{n,k}(x) \\ &= \sum_{m=-\infty}^{\infty} \mathrm{e}^{\mathrm{i}(k-k')ma} \int_0^a \mathrm{d}x\ \mathrm{e}^{\mathrm{i}(k-k')x}\, u^*_{n',k'}(x)\, u_{n,k}(x)\ ,\end{aligned} \tag{A.5}$$

and with the series representation of the $(2\pi/a)$-periodic delta distribution

$$\sum_{m=-\infty}^{\infty} \mathrm{e}^{\mathrm{i}(k-k')ma} = \frac{2\pi}{a}\delta(k-k') \tag{A.6}$$

this yields

$$\big\langle u_{n',k}(x) | u_{n,k}(x) \big\rangle = \int_0^a \mathrm{d}x\ u^*_{n',k}(x)\, u_{n,k}(x) = \delta_{nn'} \tag{A.7}$$

for $k = k'$. This is just the natural scalar product of the a-periodic functions $u_{n,k}(x)$.

The key for deriving the acceleration theorem is the validity of the the single-band approximation, which neglects all interband transitions. Within this approximation, the band index n is obsolete and omitted in the following. The initial wave packet is constructed out of the Bloch waves of a single band:

$$\psi(x,t_0) = \sqrt{\frac{a}{2\pi}} \int_{\mathcal{B}} \mathrm{d}k\ g(k,t_0)\varphi_k(x)\ . \tag{A.8}$$

The normalization of the Bloch waves given by Eq. (A.4) and the prerequisite of a normalized wave function, that is $\|\psi\|^2 = 1$, directly yields

$$\int_{\mathcal{B}} \mathrm{d}k\ \ |g(k,t_0)|^2 = 1\ . \tag{A.9}$$

The k-space distribution is understood to be initially centered around

$$k_{\mathrm{c}}(t_0) \equiv \langle k \rangle (t_0) = \int_{\mathcal{B}} \mathrm{d}k \; k \, |g(k, t_0)|^2 \; . \tag{A.10}$$

The time evolution of $\langle k \rangle$ is given by the evolution of $g(k,t)$, which in turn is stipulated to be generated by an effective Schrödinger equation with an effective Hamiltonian $\mathcal{H}_0$ according to

$$\mathrm{i}\hbar \frac{\mathrm{d}}{\mathrm{d}t} g(k,t) = \mathcal{H}_0 \, g(k,t) \; . \tag{A.11}$$

With the operator $\mathcal{H}_0$ known, the evolution of the expectation value $\langle k \rangle$ is consequently given by

$$\begin{aligned} \frac{\mathrm{d}}{\mathrm{d}t} \langle k \rangle &= \int_{\mathcal{B}} \mathrm{d}k \; \left(\frac{\mathrm{d}}{\mathrm{d}t} g^*(k,t) \right) k \, g(k,t) + \int_{\mathcal{B}} \mathrm{d}k \; g^*(k,t) k \left(\frac{\mathrm{d}}{\mathrm{d}t} g(k,t) \right) \\ &= \frac{\mathrm{i}}{\hbar} \langle [\mathcal{H}_0, k] \rangle \; . \end{aligned} \tag{A.12}$$

The operator $\mathcal{H}_0$ is determined in the following.

To begin with, note that $H_0(x)$ is not explicitly time-dependent. Hence, the solution of the Schrödinger equation is given by

$$\begin{aligned} \psi(x,t) &= \exp\left(-\frac{\mathrm{i}}{\hbar} H_0(x)(t - t_0) \right) \psi(x, t_0) \\ &= \sqrt{\frac{a}{2\pi}} \int_{\mathcal{B}} \mathrm{d}k \; g(k, t_0) \exp\left(-\frac{\mathrm{i}}{\hbar} H_0(x)(t - t_0) \right) \varphi_k(x) \\ &= \sqrt{\frac{a}{2\pi}} \int_{\mathcal{B}} \mathrm{d}k \; g(k,t) \varphi_k(x) \; , \end{aligned} \tag{A.13}$$

where

$$g(k,t) \equiv \exp\left(-\frac{\mathrm{i}}{\hbar} E(k)(t - t_0) \right) \, g(k, t_0) \; . \tag{A.14}$$

In other words, the time evolution operator for the distribution $g(k,t)$ is given by the exponential in (A.14) and thus the effective Hamiltonian is

precisely a multiplication with the dispersion relation: $\mathcal{H}_0 = E(k)$. Note that the diagonal character of the Hamiltonian expressed in the Bloch basis is crucial for this.[1] The effective Hamiltonian obviously commutes with k, resulting in

$$\hbar \frac{\mathrm{d}}{\mathrm{d}t} \langle k \rangle = 0 \tag{A.15}$$

as anticipated. The expectation value $\langle k \rangle$ of a wave packet remains constant in time as long as the homogeneous force is absent.

The situation is altered, though, if the force is present. Now the Hamiltonian of the system

$$H(x) = H_0(x) - F_0 x \tag{A.16}$$

is no longer periodic in space. Yet it remains explicitly time-independent and thus the solution of the Schrödinger equation is given by

$$\begin{aligned} \psi(x,t) &= \exp\left(-\frac{\mathrm{i}}{\hbar} H(x)(t-t_0)\right) \psi(x,t_0) \\ &= \sqrt{\frac{a}{2\pi}} \int_{\mathcal{B}} \mathrm{d}k \, \exp\left(-\frac{\mathrm{i}}{\hbar} H(x)(t-t_0)\right) g(k,t_0)\varphi_k(x) \, . \end{aligned} \tag{A.17}$$

Previously, with $F_0 = 0$, the wave function had been constructed out of eigenfunctions of the system's Hamiltonian. Hence, the Hamiltonian in the time evolution operator had been replaced by the dispersion relation. Since the wave function in Eq. (A.17) is given in terms of the eigenfunctions of the *untilted* lattice and the Hamiltonian (A.16) is no longer diagonal in the Bloch basis, this replacement is no longer feasible. In order to calculate the effective Hamiltonian $\mathcal{H}$, which governs the time evolution of the envelope functions $g(k,t)$, the wave function (A.17) is projected onto the Bloch waves: With

$$\sqrt{\frac{a}{2\pi}} \int_{\mathcal{B}} \mathrm{d}k' \, g(k',t) \int_{-\infty}^{\infty} \mathrm{d}x \, \varphi_k^*(x)\varphi_{k'}(x) = \sqrt{\frac{2\pi}{a}} g(k,t) \, , \tag{A.18}$$

[1] Alternatively, the same result can be obtained by projecting the Schrödinger equation with the wave function (A.13) onto the Bloch wave $\varphi_k(x)$.

the evolution of $g(k,t)$ is given by

$$\begin{aligned} \mathrm{i}\hbar \frac{\mathrm{d}}{\mathrm{d}t} g(k,t) &= \sqrt{\frac{a}{2\pi}} \left\langle \varphi_k(x) \right| H_0(x) \left| \psi(t) \right\rangle - F_0 \sqrt{\frac{a}{2\pi}} \left\langle \varphi_k(x) \right| x \left| \psi(t) \right\rangle \\ &= E(k) g(k,t) - F_0 \sqrt{\frac{a}{2\pi}} \int_{-\infty}^{\infty} \mathrm{d}x \; \varphi_k^*(x)\, x\, \psi(x,t) \; . \end{aligned} \tag{A.19}$$

Together with the identity

$$\mathrm{i}\partial_k \varphi_k^*(x) = x \varphi_k^*(x) + \mathrm{i} \mathrm{e}^{-\mathrm{i}kx} \, \partial_k u_k^*(x) \; , \tag{A.20}$$

this yields

$$\begin{aligned} \mathrm{i}\hbar \frac{\mathrm{d}}{\mathrm{d}t} g(k,t) = E(k) g(k,t) &- \mathrm{i} F_0 \, \partial_k \, g(k,t) \\ &+ \mathrm{i} \frac{F_0 a}{2\pi} \int_{\mathcal{B}} \mathrm{d}k' \; g(k',t) \int_{-\infty}^{\infty} \mathrm{d}x \; \mathrm{e}^{\mathrm{i}(k'-k)x} \, u_{k'}(x) \, \partial_k u_k^*(x) \; . \end{aligned} \tag{A.21}$$

So the expectation value of x with respect to the Bloch functions, cf. Eq. (A.19), can be expressed in terms of a derivative with respect to k. This is crucial for the derivation of the acceleration theorem and rendered possible due to the spatial structure of the Bloch waves. As shown below, exactly this derivative occurs in the effective Hamiltonian $\mathcal{H}$ and eventually leads to a nonvanishing commutator $[\mathcal{H}, k]$.

The remaining integrals in Eq. (A.21) can be simplified by (i) performing a translation of x by $-a$, (ii) rewriting the spatial integral as a sum

over integrals (cf. Eq. (A.5)), and (*iii*) applying Eq. (A.6):

$$\begin{aligned}
&\int_{\mathcal{B}} \mathrm{d}k'\; g(k',t) \int_{-\infty}^{\infty} \mathrm{d}x\; \mathrm{e}^{\mathrm{i}(k'-k)x}\, u_{k'}(x)\, \partial_k u_k^*(x) \\
&\qquad \overset{(i)}{=} \int_{\mathcal{B}} \mathrm{d}k'\; g(k',t)\, \mathrm{e}^{\mathrm{i}(k'-k)a} \int_{-\infty}^{\infty} \mathrm{d}x\; \mathrm{e}^{\mathrm{i}(k'-k)x}\, u_{k'}(x)\, \partial_k u_k^*(x) \\
&\qquad \overset{(ii)}{=} \int_{\mathcal{B}} \mathrm{d}k'\; g(k',t)\, \mathrm{e}^{\mathrm{i}(k'-k)a} \sum_{m=-\infty}^{\infty} \mathrm{e}^{\mathrm{i}(k'-k)ma} \\
&\qquad\qquad \times \int_{\mathcal{B}} \mathrm{d}x\; \mathrm{e}^{\mathrm{i}(k'-k)x}\, u_{k'}(x)\, \partial_k u_k^*(x) \\
&\qquad \overset{(iii)}{=} \frac{2\pi}{a} g(k,t)\, \langle \partial_k u | u \rangle
\end{aligned} \tag{A.22}$$

Due to $\langle \partial_k u|u\rangle^* = \langle u|\partial_k u\rangle$ and Eq. (A.7), $\langle \partial_k u|u\rangle$ is purely imaginary. With this, the effective Hamiltonian of the tilted system is

$$\mathcal{H} = E(k) - \mathrm{i}F_0\partial_k - F_0\,\mathrm{Im}\,\langle \partial_k u|u\rangle \ . \tag{A.23}$$

The occurrence of ∂_k in the effective Hamiltonian effectuates a nonvanishing commutator with k and the rate of change in the expectation value is given by

$$\begin{aligned}
\hbar \frac{\mathrm{d}}{\mathrm{d}t} \langle k \rangle &= \mathrm{i}\, \langle [\mathcal{H}, k] \rangle \\
&= F_0\, \langle [\partial_k, k] \rangle \\
&= F_0 \ .
\end{aligned} \tag{A.24}$$

This is exactly the acceleration theorem as stated by Bloch. Note that no assumptions are made but the validity of the single band approximation.

Note that multiplying

$$\mathrm{i}\hbar \frac{\mathrm{d}}{\mathrm{d}t} g(k,t) = \left[E(k) - \mathrm{i}F_0\partial_k - F_0\,\mathrm{Im}\,\langle \partial_k u|u\rangle\right] g(k,t) \tag{A.25}$$

by $g^*(k,t)$ from the left and subtracting the complex conjugate of this equation leads directly to

$$\left[\frac{\mathrm{d}}{\mathrm{d}t} + \frac{F_0}{\hbar}\frac{\mathrm{d}}{\mathrm{d}k}\right] |g(k,t)|^2 = 0 \,, \tag{A.26}$$

so that $|g(k,t)|^2$ does not in fact depend on k and t separately but rather on the combination $k - F_0 t/\hbar$ and

$$|g(k,t)|^2 = f(k - F_0 t/\hbar) \,. \tag{A.27}$$

This is in concurrence with the acceleration theorem, yet Eq. (A.27) states much more for the absolute square of $g(k,t)$: The whole envelope traverses the Brillouin zone collectively and in a form-invariant manner.

A.2. Group Velocity

The expression (A.1) for the group velocity can be derived using the Hellmann-Feynman theorem. The single-band approximation in is force again and the band index is dropped. The Schrödinger equation for the tilted system reads

$$\mathrm{i}\hbar\frac{\mathrm{d}}{\mathrm{d}t}\psi(x,t) = H(x)\psi(x,t) \,, \tag{A.28}$$

where $H(x) = H_0(x) - F_0 x$. The Baker-Campbell-Hausdorff formula for x and p reads

$$\mathrm{e}^{-\mathrm{i}kx} p\, \mathrm{e}^{\mathrm{i}kx} = p - \mathrm{i}k\,[x,p] = p + \hbar k \,. \tag{A.29}$$

Thus, the periodic part of the eigenfunctions of the untilted system is given by

$$\left(\frac{1}{2m}\left(p + \hbar k\right)^2 + V(x)\right) u_k(x) = E(k) u_k(x) \,, \tag{A.30}$$

where the operator on the left-hand side is denoted H_k. Switching to bra-ket notation, multiplying Eq. (A.30) by $\langle u_k(x)|$ from the left and taking the derivative with respect to k yields the Hellmann-Feynman theorem

$$\begin{aligned}\frac{\mathrm{d}E(k)}{\mathrm{d}k} &= \frac{\mathrm{d}}{\mathrm{d}k}\langle u_k(x)|\, H_k\, |u_k(x)\rangle \\ &= \left\langle u_k(x)\left|\frac{\mathrm{d}H_k}{\mathrm{d}k}\right|u_k(x)\right\rangle + E(k)\frac{\mathrm{d}}{\mathrm{d}k}\langle u_k(x)|u_k(x)\rangle \\ &= \left\langle u_k(x)\left|\frac{\mathrm{d}H_k}{\mathrm{d}k}\right|u_k(x)\right\rangle \ ,\end{aligned} \tag{A.31}$$

where Eq. (A.7) has been used in the last step. The integral in Eq. (A.31) can be represented in terms of Bloch waves by utilizing Eq. (A.29). This yields

$$\frac{1}{\hbar}\frac{\mathrm{d}E(k)}{\mathrm{d}k} = \left\langle \varphi_k(x)\left|\frac{p}{m}\right|\varphi_k(x)\right\rangle \ . \tag{A.32}$$

On the other hand, using $[p^n, x] = -\mathrm{i}\hbar\partial_p\, p^n$, the group velocity is given by

$$\begin{aligned}v_g(t) &\equiv \frac{\mathrm{d}}{\mathrm{d}t}\langle x\rangle_{\psi(x,t)} = \frac{\mathrm{i}}{\hbar}\langle [H_0, x]\rangle_{\psi(x,t)} = \frac{1}{m}\langle p\rangle_{\psi(x,t)} \\ &= \frac{a}{2\pi}\int_{\mathcal{B}}\mathrm{d}k\int_{\mathcal{B}}\mathrm{d}k'\ g^*(k',t)g(k,t)\left\langle \varphi_{k'}(x)\left|\frac{p}{m}\right|\varphi_k(x)\right\rangle \ .\end{aligned} \tag{A.33}$$

The envelope function $g(k, t_0)$ is assumed to be well localized in k space around k_c, cf. (A.10). If the characteristic width ξ of $g(k, t_0)$ is small compared to the width of the fundamental Brillouin zone, that is $\xi \ll 2\pi/a$, the group velocity is approximately given by

$$v_\mathrm{g}(t) \approx \frac{1}{\hbar}\left.\frac{\mathrm{d}E(k)}{\mathrm{d}k}\right|_{k_\mathrm{c}(t)} \ . \tag{A.34}$$

The approximation becomes exact for $g(k, t_0) = \sqrt{2\pi/a}\,\delta(k - k_\mathrm{c})$. Of course, "exact" is still to be understood within the limits of the validity of the single-band approximation. An analogous argument holds for the tilted system.

A.3. Numerical Confirmation of the Concepts

The tilted lattice is treated numerically by implementing the Hamiltonian (A.16) with a periodic potential of the form

$$V(x) = \frac{V_0}{2}\cos\left(2k_{\mathrm{L}}x\right) \ , \tag{A.35}$$

with $k_{\mathrm{L}} \equiv \pi/a$. To ensure the validity of the single-band approximation, the depth of the lattice is set to $V_0 = -5.7\,E_{\mathrm{r}}$, where E_{r} denotes the recoil energy, resulting in a band gap $\Delta E \approx 2.76\,E_{\mathrm{r}}$ at $k = k_{\mathrm{L}}$ and the band width of the lowest band is $W \approx 0.22\,E_{\mathrm{r}}$. The strength of the external force figures as $F_0 a/\pi = 0.01\,E_{\mathrm{r}}$, chosen such that the oscillation of the wave packet extends over several lattice periods. This choice of parameters renders transitions to higher bands impalpable for at least a few Bloch periods T_{B}: The Landau-Zener transition probability for a single Bloch cycle is approximately given by [99, 206]

$$|T|^2 \approx \exp\left(-2\zeta\right) \tag{A.36}$$

with the Zener parameter

$$\zeta = \frac{\pi^2}{16}\frac{\left(\Delta E/E_{\mathrm{r}}\right)^2}{F_0 a/E_{\mathrm{r}}} \ . \tag{A.37}$$

For the parameters studied here, the Zener parameter figures as $\zeta \approx 150$, resulting in a diminutive transition probability. With a lattice depth of $-5.7\,E_{\mathrm{r}}$, the dynamics remain restricted to nearest neighbor tunneling in good approximation. Hence, the dispersion relation is well approximated by

$$\widetilde{E}(k) = -\frac{W}{2}\cos(ka) \ . \tag{A.38}$$

According to Eq. (A.24), the expectation value $k_{\mathrm{c}}(t)$ grows linearly in time,

$$k_{\mathrm{c}}(t) = \frac{1}{\hbar}F_0 t + k_0 \ . \tag{A.39}$$

This yields, together with Eq. (A.34),

$$\begin{aligned} v_{\mathrm{g}}(t) &= \frac{1}{\hbar} \left. \frac{\mathrm{d}\widetilde{E}(k)}{\mathrm{d}k} \right|_{k_{\mathrm{c}}(t)} \\ &= \frac{Wa}{2\hbar} \sin\left(\omega_{\mathrm{B}} t + k_0 a\right) \ , \end{aligned} \tag{A.40}$$

where

$$\omega_{\mathrm{B}} \equiv \frac{F_0 a}{\hbar} \tag{A.41}$$

is the Bloch frequency. Thus, the position of the wave packet's center in real space evolves according to

$$x_{\mathrm{g}}(t) = -\frac{W}{2F_0} \cos\left(\omega_{\mathrm{B}} t + k_0 a\right) \tag{A.42}$$

with appropriate choice of the origin of the x-axis.

Figure A.1 depicts the time evolution for two wave functions in real space as well as in k space. Both wave functions are initially, that is at $t_0 = 0$, prepared in the lowest band of the untilted lattice, so the initial wave function reads

$$\psi(x,0) = \sqrt{\frac{a}{2\pi}} \int_{\mathcal{B}} \mathrm{d}k \, g_1(k,0) \varphi_k(x) \ . \tag{A.43}$$

The initial k-space distribution

$$g_1(k,0) = \left(\sqrt{\pi}\Delta k\right)^{-1/2} \exp\left(-\frac{k^2}{2\left(\Delta k\right)^2}\right) \tag{A.44}$$

is centered around $k_{\mathrm{c}}/k_{\mathrm{L}} = 0$ with $\Delta k = 0.1\, k_{\mathrm{L}}$, so the initial wave packet carries no net momentum. In the upper row of Fig. A.1, the initial wave packet is with $\Delta k/k_{\mathrm{L}} = 0.1$ well centered in k space. The linear growth of $\langle k \rangle\,(t)$ is apparent and the group velocity is well captured by the semiclassical relation (A.34). As demonstrated in the lower row of the figure, lifting the condition of a localized wave packet in k space by setting $\Delta k = k_{\mathrm{L}}$

does not affect the validity of the acceleration theorem (A.24), but the group velocity is no longer accurately described by (A.34), which requires $\Delta k \ll k_{\mathrm{L}}$. Note that, in accordance with Eq. (A.27), in both cases the momentum wave packet is transported through the Brillouin zone as a whole without changing its envelope.

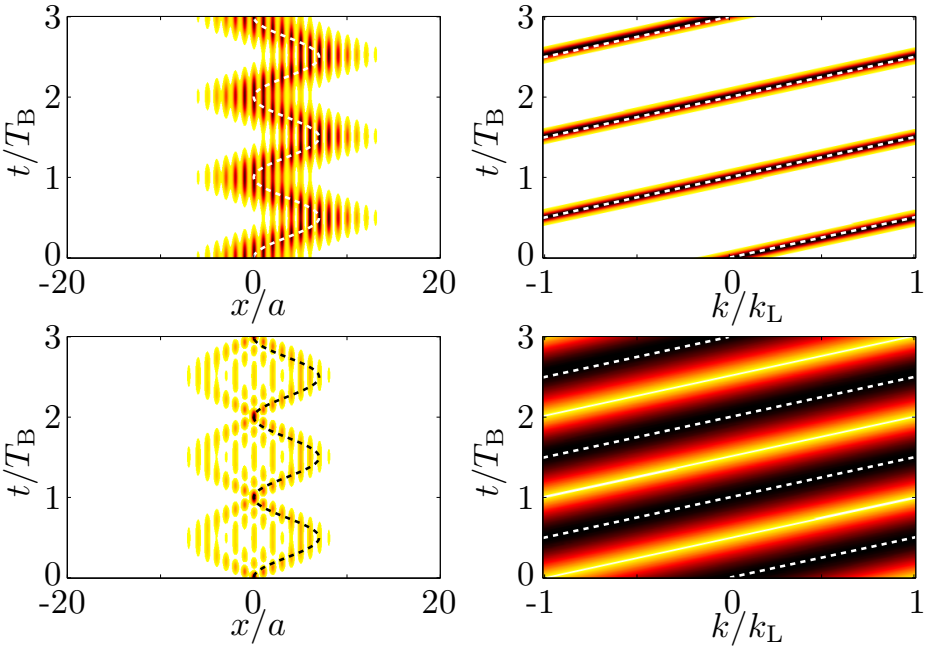

Figure A.1.: Density plots of two wave packets, differing initially in the width Δk of the Gaussian distribution in k space and evolving in a tilted cosine lattice with $V_0 = -5.7\,E_\mathrm{r}$ and $F_0 a/\pi = 0.01\,E_\mathrm{r}$. The left (right) column depicts the evolution in real (k) space, respectively; dashed lines mark the semiclassical results. Upper row: With $\Delta k/k_\mathrm{L} = 0.1$ the condition $\Delta k \ll k_\mathrm{L}$ for the applicability of (A.34) is met in contrast to the lower row with $\Delta k = k_\mathrm{L}$. The acceleration theorem (A.24) remains valid in both cases, whereas the group velocity (A.34) does not.

Appendix B.

Acceleration Theorem for Hamiltonians Periodic in Time

After deriving the acceleration theorem as well as the group velocity in App. A for time independent Hamiltonians, the discussion is now generalized to explicitly time dependent Hamiltonians with temporal periodicity, see Publication III. A derivation of a generalized acceleration theorem along the lines of reasoning of the undriven case is given.

The restriction of a constant force F_0 already discussed in App. A is now lifted: The external force is assumed to be periodic in time with period T and zero average, so that $F(t+T) = F(t)$ and

$$\frac{1}{T}\int_0^T \mathrm{d}t\; F(t) = 0\;. \tag{B.1}$$

The Hamiltonian

$$\widetilde{H}_0(x,t) = \frac{p^2}{2m} + V(x) - F(t)x \tag{B.2}$$

is thus explicitly time dependent and inherits the temporal periodicity of the driving force. To restore spatial periodicity, the solution $\widetilde{\psi}(x,t)$ of the Schrödinger equation is transformed unitarily by means of $\psi(x,t) = U\widetilde{\psi}(x,t)$ with

$$U \equiv \exp\left(-\frac{\mathrm{i}}{\hbar}x\int_0^t \mathrm{d}t'\; F(t')\right)\;, \tag{B.3}$$

so the Schrödinger equation for the transformed wave function reads

$$\mathrm{i}\hbar\frac{\mathrm{d}}{\mathrm{d}t}\psi(x,t) = \left(\frac{1}{2m}\left(p + \int_0^t \mathrm{d}t'\ F(t')\right)^2 + V(x)\right)\psi(x,t)\ . \tag{B.4}$$

Now the Hamiltonian $H_0(x,t)$ on the right-hand side is periodic both in space and in time, that is $H(x+a,t) = H(x,t+T) = H(x,t)$. Thus, there are solutions of Eq. (B.4), which take the form of spatiotemporal Bloch waves

$$\begin{aligned}\psi_{n,k}(x,t) &= \mathrm{e}^{-\mathrm{i}\varepsilon_n(k)t/\hbar}\mathrm{e}^{\mathrm{i}kx}w_{n,k}(x,t)\\ &\equiv \mathrm{e}^{-\mathrm{i}\varepsilon_n(k)t/\hbar}\varphi_{n,k}(x,t)\ ,\end{aligned} \tag{B.5}$$

where the functions $w_{n,k}(x,t)$ inherit the periodicity of $H_0(x,t)$, namely $w_{n,k}(x,t) = w_{n,k}(x+a,t) = w_{n,k}(x,t+T)$. In analogy to the undriven case, for the periodic part of the spatiotemporal Bloch waves

$$\int_0^a \mathrm{d}x\ w^*_{n',k}(x)w_{n,k}(x) = \delta_{nn'} \tag{B.6}$$

holds (cf. Eq. (A.7)). Their spatial parts are then normalized according to

$$\int_{-\infty}^{\infty}\mathrm{d}x\ \varphi_{n',k'}(x,t)\varphi_{n,k}(x,t) = \frac{2\pi}{a}\delta_{nn'}\delta(k-k')\ . \tag{B.7}$$

The initial wave function at $t=0$ is constructed out of Floquet functions

$$\psi(x,0) = \sqrt{\frac{a}{2\pi}}\int_{\mathcal{B}}\mathrm{d}k\ g(k,0)\varphi_k(x,0)\ , \tag{B.8}$$

where the k-space envelope is normalized and centered around k_c (as in Eqs. (A.9) and (A.10)). The wave function evolves according to

$$\psi(x,t) = \sqrt{\frac{a}{2\pi}}\int_{\mathcal{B}}\mathrm{d}k\ g(k,t)\varphi_k(x,t)\ , \tag{B.9}$$

with $g(k,t) \equiv g(k,0)\mathrm{e}^{-\mathrm{i}\varepsilon(k)t/\hbar}$. Again, the evolution of $g(k,t)$ is demanded to be governed by an equation of Schrödinger type,

$$\mathrm{i}\hbar\frac{\mathrm{d}}{\mathrm{d}t}g(k,t) = \mathcal{H}_0 g(k,t) \tag{B.10}$$

with an effective Hamiltonian $\mathcal{H}_0$. For its determination, the Schrödinger equation (B.4) is projected onto the Floquet function $\varphi_k^*(x,t)$. Utilizing Eq. (A.18) and omitting the argument x for brevity yields

$$\begin{aligned}
\mathrm{i}\hbar\frac{\mathrm{d}}{\mathrm{d}t}\int_{-\infty}^{\infty}\mathrm{d}x\;\varphi_k^*(t)\,\psi &= \mathrm{i}\hbar\frac{\mathrm{d}}{\mathrm{d}t}\sqrt{\frac{2\pi}{a}}g(k,t)\\
&= \int_{-\infty}^{\infty}\mathrm{d}x\;\left(\mathrm{i}\hbar\frac{\mathrm{d}\varphi_k^*(t)}{\mathrm{d}t}\psi(t)+\varphi_k^*(t)H_0\psi(t)\right)\\
&= \int_{-\infty}^{\infty}\mathrm{d}x\;\left[\left(H_0-\mathrm{i}\hbar\frac{\mathrm{d}}{\mathrm{d}t}\right)\varphi_k(t)\right]^*\psi(t)\\
&= \varepsilon(k)\int_{-\infty}^{\infty}\mathrm{d}x\;\varphi_k^*(t)\psi(t)\\
&= \varepsilon(k)\sqrt{\frac{2\pi}{a}}g(k,t)\;,
\end{aligned}\tag{B.11}$$

and hence

$$\mathrm{i}\hbar\frac{\mathrm{d}}{\mathrm{d}t}g(k,t)=\varepsilon(k)g(k,t)\;.\tag{B.12}$$

In close analogy to the time-independent case, the effective Hamiltonian governing the evolution of $g(k,t)$ is just a multiplication with the quasienergy dispersion relation:

$$\mathcal{H}_0=\varepsilon(k)\;.\tag{B.13}$$

The evolution of $\langle k\rangle$ is determined by the expectation value of the commutator of $\mathcal{H}_0$ with k. Since $[\mathcal{H}_0,k]=0$, this results in

$$\frac{\mathrm{d}}{\mathrm{d}t}\langle\hbar k\rangle=0\;,\tag{B.14}$$

so that a generalized acceleration theorem holds for the untilted but periodically driven lattice.

Now, the Hamiltonian (B.2) is extended by an additional term $-F_0x$ with a constant force F_0. After subjecting the solution of the Schrödinger

equation to the transformation given by Eq. (B.3), the transformed Hamiltonian $H(x,t) = H_0 - F_0 x$ is periodic in time only. Nonetheless, the solution of the Schrödinger equation is expanded into the Floquet states of the untilted system H_0, that is

$$\psi(x,t) = \sqrt{\frac{a}{2\pi}} \int_{\mathcal{B}} \mathrm{d}k \; g(k,t)\varphi_k(x,t) \; . \tag{B.15}$$

Since the Floquet functions $\varphi_k(x,t)$ are of Bloch type, the relation

$$\mathrm{i}\partial_k \varphi_k^*(x,t) = x\varphi_k^*(x,t) + \mathrm{i}\mathrm{e}^{-\mathrm{i}kx}\partial_k w_k^*(x,t) \tag{B.16}$$

can be exploited to find an expression for the matrix elements of x:

$$\begin{aligned}\int_{-\infty}^{\infty} \mathrm{d}x \; \varphi_k^*(x,t) x \varphi_{k'}(x,t) &= \mathrm{i}\partial_k \int_{-\infty}^{\infty} \mathrm{d}x \; \varphi_k^*(x,t)\varphi_{k'}(x,t) \\ &\quad - \mathrm{i}\int_{-\infty}^{\infty} \mathrm{d}x \; \mathrm{e}^{\mathrm{i}(k'-k)x} w_{k'}(x,t)\partial_k w_k^*(x,t) \\ &= \mathrm{i}\partial_k \frac{2\pi}{a}\delta(k-k') - \mathrm{i}\frac{2\pi}{a}\delta(k-k') \left\langle \partial_k w | w \right\rangle \; ,\end{aligned} \tag{B.17}$$

with

$$\left\langle \partial_k w | w \right\rangle = \int_0^a \mathrm{d}x \; w_k(x,t)\partial_k w_k^*(x,t) \; . \tag{B.18}$$

Again, $\left\langle \partial_k w | w \right\rangle = \mathrm{i}\,\mathrm{Im}\left\langle \partial_k w | w \right\rangle$ is purely imaginary. Now, projecting the

Schrödinger equation onto the Floquet function $\varphi_k^*(x,t)$ yields

$$\begin{aligned}
&\mathrm{i}\hbar\frac{\mathrm{d}}{\mathrm{d}t}\sqrt{\frac{a}{2\pi}}\int_{-\infty}^{\infty}\mathrm{d}x\;\varphi_k^*(x,t)\psi(x,t)\\
&\qquad=\mathrm{i}\hbar\frac{\mathrm{d}}{\mathrm{d}t}g(k,t)\\
&\qquad=\sqrt{\frac{a}{2\pi}}\int_{-\infty}^{\infty}\mathrm{d}x\;\left(\mathrm{i}\hbar\frac{\mathrm{d}\varphi_k^*(x,t)}{\mathrm{d}t}\psi+\varphi_k^*(x,t)\mathrm{i}\hbar\frac{\mathrm{d}\psi(x,t)}{\mathrm{d}t}\right)\\
&\qquad=\sqrt{\frac{a}{2\pi}}\int_{-\infty}^{\infty}\mathrm{d}x\;\left[\left(H_0-\mathrm{i}\hbar\frac{\mathrm{d}}{\mathrm{d}t}\right)\varphi_k(x,t)\right]^*\psi(x,t)\\
&\qquad\quad-\sqrt{\frac{a}{2\pi}}F_0\int_{-\infty}^{\infty}\mathrm{d}x\;\varphi_k^*(x,t)\,x\,\psi(x,t)\;.
\end{aligned}\tag{B.19}$$

Together with Eq. (B.17), the last term in Eq. (B.19) is given by

$$\begin{aligned}
&\sqrt{\frac{a}{2\pi}}F_0\int_{-\infty}^{\infty}\mathrm{d}x\;\varphi_k^*(x,t)\,x\,\psi(x,t)\\
&\qquad=\frac{a}{2\pi}F_0\int_{\mathcal{B}}\mathrm{d}k'\;g(k',t)\int_{-\infty}^{\infty}\mathrm{d}x\;\varphi_k^*(x,t)\,x\varphi_{k'}(x,t)\\
&\qquad=\mathrm{i}F_0\partial_k g(k,t)+F_0\mathrm{Im}\,\langle\partial_k w|w\rangle\,g(k,t)\;,
\end{aligned}\tag{B.20}$$

so that the evolution of $g(k,t)$ is governed by

$$\mathrm{i}\hbar\partial_t g(k,t)=\mathcal{H}g(k,t)\tag{B.21}$$

with the effective Hamiltonian

$$\mathcal{H}=\varepsilon(k)-\mathrm{i}F_0\partial_k-F_0\mathrm{Im}\,\langle\partial_k w|w\rangle\;.\tag{B.22}$$

Again, the occurrence of a partial derivative with respect to k in the effective Hamiltonian gives rise to a nonvanishing commutator with k, which results in a generalized acceleration theorem for Floquet states

$$\hbar\frac{\mathrm{d}}{\mathrm{d}t}\,\langle k\rangle=\mathrm{i}\,\langle[\mathcal{H},k]\rangle=F_0.\tag{B.23}$$

The analogy to the standard acceleration theorem (A.24) for the crystal-momentum representation is evident. Multiplying Eq. (B.21) by $g^*(k,t)$ and subtracting the complex conjugate of the resulting equation yields

$$\left(\frac{\partial}{\partial t} + \frac{F_0}{\hbar}\frac{\partial}{\partial k}\right)|g(k,t)|^2 = 0\,, \tag{B.24}$$

which implies that $|g(k,t)|^2$ depends on the combination $k - F_0 t/\hbar$, so that – in close analogy to the undriven case – the distribution $g(k,t)$ moves through Floquet k space without change of shape.

Note that the seemingly simple dynamics of the wave packet when monitored in the Floquet representation might be unrecognizable in the customary crystal-momentum representation due to a multitude of interband transitions. These are untangled in the Floquet picture, which provides a transparent view of the wave-packet dynamics. Yet, on the numerical level, it requires the calculation of Floquet functions as well as quasienergies. A detailed procedure is given in the subsequent appendix.

Appendix C.

Calculation of Quasienergy Spectra for a Periodically Driven Lattice

After introducing fundamental properties of Floquet theory in Section 2.1, this appendix focuses on the numerical calculation of quasienergies for a periodically driven lattice. The key element here is the one-cycle propagator $U(T,0)$ of the system, since the quasienergies can be read off directly from its eigenvalues. The procedure is divided in two steps: Firstly, each element of a given basis set of functions is propagated according to the Schrödinger equation yielding a matrix representation of the one-cycle propagator. Secondly, diagonalizing $U(T,0)$ yields the quasienergies. To improve efficiency of the numerical scheme, the symmetries of the system can be exploited.

Starting point is the Hamiltonian of a single particle of mass m moving in an optical lattice of depth V_0 and laser wavenumber k_L within the dipole approximation. If the lattice is erected by retroreflecting the lattice-generating laser radiation with a mirror into itself, then modulating the mirror's position in space periodically leads to the Hamiltonian within the Kramers-Henneberger gauge [115, 207],

$$H^{(1)}(x,t) = \frac{p^2}{2m} + \frac{V_0}{2}\cos\left\{2k_\mathrm{L}\left[x + \Delta L \sin\left(\omega t\right)\right]\right\} \ , \tag{C.1}$$

where the driving amplitude and frequency, denoted by ΔL and ω, respectively, induce an inertial force $F(t) = F\sin(\omega t)$ with $F \equiv m\Delta L\omega^2$. Transforming the wave functions $\Psi^{(1)}(x,t)$ associated with $H^{(1)}_{\text{eff}}(x,t)$ according to

$$\Psi^{(1)}(x,t) = \exp\left[\frac{\mathrm{i}}{\hbar}\Delta L\sin(\omega t)p + \frac{\mathrm{i}}{8\hbar}m(\Delta L)^2\omega\sin(2\omega t)\right]\Psi^{(2)}(x,t)\ , \tag{C.2}$$

the new functions $\Psi^{(2)}(x,t)$ are solutions to the Schrödinger equation with the Hamiltonian in the velocity gauge

$$H^{(2)}(x,t) = \frac{1}{2m}\left[p + m\Delta L\omega\cos(\omega t)\right]^2 + \frac{V_0}{2}\cos\left(2k_{\mathrm{L}}x\right) - \frac{1}{4}m\left(\Delta L\omega\right)^2\ , \tag{C.3}$$

where the first term in the exponent of Eq. (C.2) shifts the spatial coordinate x by $-\Delta L\sin(\omega t)$ and leads to a term proportional to p. Completing the square, the remaining terms are combined with those emerging from the second term in the exponent of Eq. (C.2). This results in the ponderomotive energy $m\left(\Delta L\omega\right)^2/4$ of the particle, being its averaged kinetic energy due to the quiver motion of the particle. Since the transformation (C.2) is unitary and periodic (such that the frequencies involved are integer multiples of the driving frequency), the quasienergy spectrum remains unchanged. The velocity gauge is favorable when computing the quasienergy spectrum, since the Hamiltonian is now additionally periodic in space as well. Due to the periodicity of the Hamiltonian, $H^{(2)}(x,t) = H^{(2)}(x+a,t) = H^{(2)}(x,t+T)$, according to Floquet theory, the Schrödinger equation admits quasi-periodic solutions of the form $\Psi^{(2)}(x,t) = \exp\left[\mathrm{i}\left(kx - \varepsilon_n(k)t/\hbar\right)\right]w_{n,k}(x,t)$ with periodic functions $w_{n,k}(x,t) = w_{n,k}(x+a,t) = w_{n,k}(x,t+T)$, where the spatial and temporal period are denoted by $a = \pi/k_{\mathrm{L}}$ and $T = 2\pi/\omega$, respectively. In conjunction with $\Psi^{(2)}(x,t) = U(t,0)\Psi^{(2)}(x,0)$, the eigenvalue equation for the

one-cycle propagator

$$U(T,0)w_{n,k}(x,T) = \mathrm{e}^{-\mathrm{i}\varepsilon_n(k)T/\hbar}w_{n,k}(x,T) \tag{C.4}$$

reveals that the quasienergies are known as soon as the eigenvalues are.

A matrix representation of $U(T,0)$ can be found by propagating a suitable basis over one period T for each wavenumber k. This is done numerically by implementing the Schrödinger equation with the Hamiltonian (C.3). Due to its temporal periodicity, the solutions can be written as $\Psi_{n,k}(x,t) = \exp(\mathrm{i}kx)u_{n,k}(x,t)$, where the spatially periodic functions $u_{n,k}(x,t) := \exp(-\mathrm{i}\varepsilon_n(k)t/\hbar)w_{n,k}(x,t)$ are governed by the Schrödinger equation

$$\mathrm{i}\hbar\frac{\mathrm{d}}{\mathrm{d}t}u_{n,k}(x,t) = \left[\frac{1}{2m}\left(p+\hbar k+\frac{F}{\omega}\cos(\omega t)\right)^2 + \frac{V_0}{2}\cos(2k_\mathrm{L}x)\right]u_{n,k}(x,t)\,; \tag{C.5}$$

or equivalently, after switching to proper dimensionless variables $z = k_\mathrm{L}x$, $\tau = \omega t$, and $\widetilde{k} = k/k_\mathrm{L}$,

$$\begin{aligned}\mathrm{i}\frac{\hbar\omega}{E_\mathrm{r}}\frac{\mathrm{d}}{\mathrm{d}\tau}u_{n,\widetilde{k}}(z,\tau) = \Big[&-\partial_z^2 + \beta^2\cos^2\tau - 2\mathrm{i}\left(\beta\cos\tau+\widetilde{k}\right)\partial_z \\ &+\widetilde{k}^2 + 2\beta\widetilde{k}\cos\tau + \frac{V_0}{2E_\mathrm{r}}\cos(2z)\Big]u_{n,\widetilde{k}}(z,\tau)\,,\end{aligned} \tag{C.6}$$

where $E_\mathrm{r} = \hbar^2k_\mathrm{L}^2/(2m)$ is the recoil energy and $\beta := (F/k_\mathrm{L})/(\hbar\omega)$. Without changing the quasienergy spectrum, yet another periodic transformation of the functions u eliminates the squared-cosine term $\beta^2\cos^2\tau = \beta^2/2[\cos(2\tau)+1]$ (apart from its zero-mode $\beta^2/2$) as well as the term $2\beta\widetilde{k}\cos\tau$ yielding

$$\begin{aligned}&\mathrm{i}\frac{\hbar\omega}{E_\mathrm{r}}\frac{\mathrm{d}}{\mathrm{d}\tau}u_{n,\widetilde{k}}(z,\tau) = \\ &\left[-\partial_z^2 + \frac{\beta^2}{2} - 2\mathrm{i}\left(\beta\cos\tau+\widetilde{k}\right)\partial_z + \widetilde{k}^2 + \frac{V_0}{2E_\mathrm{r}}\cos(2z)\right]u_{n,\widetilde{k}}(z,\tau)\,,\end{aligned} \tag{C.7}$$

For numerical implementation, a set $\{f_\nu(z) : \nu = 0, 1, 2, \dots\}$ of basis functions given by

$$\begin{aligned} f_0(z) &= \sqrt{\frac{1}{\pi}} \\ f_1(z) &= \sqrt{\frac{2}{\pi}}\sin(2z) & f_2(z) &= \sqrt{\frac{2}{\pi}}\cos(2z) \\ f_3(z) &= \sqrt{\frac{2}{\pi}}\sin(4z) & f_4(z) &= \sqrt{\frac{2}{\pi}}\cos(4z) \\ &\vdots \end{aligned} \tag{C.8}$$

is chosen. On the one hand, this automatically ensures the spatial periodicity of the functions $u_{n,\widetilde{k}}(z,\tau)$. On the other hand, the operators occurring in Eq. (C.7) become sparse matrices in this basis:

The matrix representation of $\partial^2/\partial z^2$ is diagonal

$$\frac{\partial^2}{\partial z^2} \to \begin{pmatrix} 0 & & & & & & \\ & -4 & & & & & \\ & & -4 & & & & \\ & & & -16 & & & \\ & & & & -16 & & \\ & & & & & \ddots & \end{pmatrix}. \tag{C.9}$$

The operator $\partial/\partial z$ is represented by the tridiagonal matrix

$$\frac{\partial}{\partial z} \to \begin{pmatrix} 0 & & & & & & \\ & 0 & -2 & & & & \\ & 2 & 0 & & & & \\ & & & 0 & -4 & & \\ & & & 4 & 0 & & \\ & & & & & \ddots & \end{pmatrix}, \tag{C.10}$$

whereas the operator $\cos(2z)$ yields a pentadiagonal matrix:

$$\cos(2z) \to \frac{1}{2}\begin{pmatrix} 0 & 0 & \sqrt{2} & & & \\ 0 & 0 & 0 & 1 & & \\ \sqrt{2} & 0 & 0 & 0 & 1 & \\ & 1 & 0 & 0 & 0 & \ddots \\ & & 1 & 0 & 0 & \\ & & & \ddots & & \end{pmatrix} . \tag{C.11}$$

Now, the scheme can easily be implemented numerically: The columns of the one-cycle propagator $U(T,0)$ are given by propagating the basis functions (C.8) over a single period. Diagonalizing $U(T,0)$ yields the Floquet multipliers $\exp(-i\varepsilon_n(k)T/\hbar)$ and hence the quasienergies $\varepsilon_n(k)$ themselves. Exploiting special symmetries of the system allows for a more efficient calculation of the one-cycle propagator.

Bibliography

[1] J. C. Mather, E. S. Cheng, D. A. Cottingham, R. E. Eplee, Jr., and D. J. Fixsen. Measurement of the cosmic microwave background spectrum by the COBE FIRAS instrument. *Astrophys. J.* **420**, 439–444 (1994).

[2] S. N. Bose. Plancks Gesetz und Lichtquantenhypothese. *Z. Phys.* **26**, 178–181 (1924).

[3] A. Einstein. Quantentheorie des einatomigen idealen Gases. *Sitzungsberichte der preussischen Akademie der Wissenschaften*, 261–267 (1924).

[4] A. Einstein. Quantentheorie des einatomigen idealen Gases. Zweite Abhandlung. *Sitzungsberichte der preussischen Akademie der Wissenschaften*, 3–14 (1925).

[5] The original wording is "Diese Formel drückt also indirekt eine gewisse Hypothese über eine gegenseitige Beeinflussung der Moleküle von vorläufig ganz rätselhafter Art aus (. . .)", see Ref. [4].

[6] The original wording is "Die Elemente oder Einheiten der Energie betrachten wir aber als unterschiedslos gleich. Würden wir jede einzelne von ihnen für sich wahrnehmen können, so würden sich damit die Bedingungen des Falles von Grund auf ändern. Hierauf muss in allererster Linie aufmerksam gemacht werden." ([208], p. 660).

[7] P. Ehrenfest and H. Kamerlingh Onnes. Vereinfachte Ableitung der kombinatorischen Formel, welche der Planckschen Strahlungstheorie zugrunde liegt. *Annalen der Physik* **351**, 1021–1024 (1915).

[8] Feynman noted: "An explanation has been worked out by Pauli from complicated arguments of quantum field theory and relativity. He has shown that the two [spin and statistics] must necessarily go together, but we have not been able to find a way of reproducing his arguments on an elementary level. It appears to be one of the few places in physics where there is a rule which can be stated very simply, but for which no one has found a simple and easy explanation. The explanation is deep down in relativistic quantum mechanics. This probably means that we do not have a complete understanding of the fundamental principle involved." ([209], chap. 4-3).

[9] M. Fierz. Über die relativistische Theorie kräftefreier Teilchen mit beliebigem Spin. *Helv. Phys. Acta.* **12**, 3–37 (1939).

[10] W. Pauli. The connection between spin and statistics. *Phys. Rev.* **58**, 716–722 (1940).

[11] T. W. Hänsch and A. L. Schawlow. Cooling of gases by laser radiation. *Opt. Comm.* **13**, 68–69 (1975).

[12] D. J. Wineland and H. Dehmelt. Proposed $10^{14}\,\Delta\nu < \nu$ laser fluorescence spectroscopy on TI^+ mono-ion oscillator III. *Bull. Am. Phys. Soc.* **20**, 637 (1975).

[13] A. Ashkin. Trapping of atoms by resonance radiation pressure. *Phys. Rev. Lett.* **40**, 729–732 (1978).

[14] D. J. Wineland, R. E. Drullinger, and F. L. Walls. Radiation-

pressure cooling of bound resonant absorbers. *Phys. Rev. Lett.* **40**, 1639–1642 (1978).

[15] W. D. Phillips and H. Metcalf. Laser deceleration of an atomic beam. *Phys. Rev. Lett.* **48**, 596–599 (1982).

[16] Y. Castin, H. Wallis, and J. Dalibard. Limit of Doppler cooling. *J. Opt. Soc. Am. B* **6**, 2046–2057 (1989).

[17] S. Chu, L. Hollberg, J. E. Bjorkholm, A. Cable, and A. Ashkin. Three-dimensional viscous confinement and cooling of atoms by resonance radiation pressure. *Phys. Rev. Lett.* **55**, 48–51 (1985).

[18] P. D. Lett, R. N. Watts, C. I. Westbrook, W. D. Phillips, P. L. Gould, and H. J. Metcalf. Observation of atoms laser cooled below the Doppler limit. *Phys. Rev. Lett.* **61**, 169–172 (1988).

[19] A. Aspect, E. Arimondo, R. Kaiser, N. Vansteenkiste, and C. Cohen-Tannoudji. Laser cooling below the one-photon recoil energy by velocity-selective coherent population trapping. *Phys. Rev. Lett.* **61**, 826–829 (1988).

[20] M. H. Anderson, J. R. Ensher, M. R. Matthews, C. E. Wieman, and E. A. Cornell. Observation of Bose-Einstein condensation in a dilute atomic vapor. *Science* **269**, 198–201 (1995).

[21] K. B. Davis, M.-O. Mewes, M. R. Andrews, N. J. von Druten, D. S. Durfee, D. M. Kurn, and W. Ketterle. Bose-Einstein condensation in a Gas of Sodium Atoms. *Phys. Rev. Lett.* **75**, 3969–3973 (1995).

[22] B. G. Levi. Cornell, Ketterle, and Wieman share Nobel Prize for Bose-Einstein condensates. *Physics Today* **54**, 14–16 (2001).

[23] M. R. Andrews, C. G. Townsend, H.-J. Miesner, D. S. Durfee, D. M. Kurn, and W. Ketterle. Observation of interference between two Bose condensates. *Science* **275**, 637–641 (1997).

[24] M. R. Matthews, B. P. Anderson, P. C. Haljan, D. S. Hall, C. E. Wieman, and E. A. Cornell. Vortices in a Bose-Einstein condensate. *Phys. Rev. Lett.* **83**, 2498–2501 (1999).

[25] K. W. Madison, F. Chevy, W. Wohlleben, and J. Dalibard. Vortex formation in a stirred Bose-Einstein condensate. *Phys. Rev. Lett.* **84**, 806–809 (2000).

[26] I. Bloch, T. W. Hänsch, and T. Esslinger. Measurement of the spatial coherence of a trapped Bose gas at the phase transition. *Nature* **403**, 166–170 (2000).

[27] J. R. Abo-Shaeer, C. Raman, J. M. Vogels, and W. Ketterle. Observation of vortex lattices in Bose-Einstein condensates. *Science* **292**, 476–479 (2001).

[28] K. M. R. van der Stam, R. van Ooijen, R. Meppelink, J. M. Vogels, and P. van der Straten. Large atom number Bose-Einstein condensate of sodium. *Rev. Sci. Instrum.* **78**, 013102 (2007).

[29] P. Kapitza. Viscosity of liquid Helium below the λ-point. *Nature* **141**, 74–74 (1938).

[30] J. F. Allen and A. D. Misener. Flow of liquid Helium II. *Nature* **141**, 75–75 (1938).

[31] D. G. Fried, T. C. Killian, L. Willmann, D. Landhuis, S. C. Moss, D. Kleppner, and T. J. Greytak. Bose-Einstein condensation of atomic hydrogen. *Phys. Rev. Lett.* **81**, 3811–3814 (1998).

[32] J. Klaers, J. Schmitt, F. Vewinger, and M. Weitz. Bose-Einstein condensation of photons in an optical microcavity. *Nature* **468**, 545–548 (2010).

[33] M. Lu, S. H. Youn, and B. L. Lev. Trapping ultracold dysprosium: A highly magnetic gas for dipolar physics. *Phys. Rev. Lett.* **104**, 063001 (2010).

[34] M. Lu, N. Q. Burdick, S. H. Youn, and B. L. Lev. Strongly dipolar Bose-Einstein condensate of dysprosium. *Phys. Rev. Lett.* **107**, 190401 (2011).

[35] C. A. Regal, M. Greiner, and D. S. Jin. Observation of resonance condensation of fermionic atom pairs. *Phys. Rev. Lett.* **92**, 040403 (2004).

[36] M. Bartenstein, A. Altmeyer, S. Riedl, S. Jochim, C. Chin, J. Hecker Denschlag, and R. Grimm. Crossover from a molecular Bose-Einstein condensate to a degenerate Fermi gas. *Phys. Rev. Lett.* **92**, 120401 (2004).

[37] S. Gupta, Z. Hadzibabic, J. R. Anglin, and W. Ketterle. Collisions in zero temperature Fermi gases. *Phys. Rev. Lett.* **92**, 100401 (2004).

[38] J. Bardeen, L. N. Cooper, and J. R. Schrieffer. Microscopic theory of superconductivity. *Phys. Rev.* **106**, 162–164 (1957).

[39] J. Bardeen, L. N. Cooper, and J. R. Schrieffer. Theory of superconductivity. *Phys. Rev.* **108**, 1175–1204 (1957).

[40] L. D. Landau and E. M. Lifshitz. *Course of Theoretical Physics V: Statistical Physics, Part 1.* Butterworth Heinemann, Oxford, 3rd edition (1980).

[41] F. Dalfovo, S. Giorgini, L. P. Pitaevskii, and S. Stringari. Theory of Bose-Einstein condensation in trapped gases. *Rev. Mod. Phys.* **71**, 463–512 (1999).

[42] S. Grossmann and M. Holthaus. On Bose-Einstein condensation in harmonic traps. *Phys. Lett. A* **208**, 188–192 (1995).

[43] I. Bloch, J. Dalibard, and W. Zwerger. Many-body physics with ultracold gases. *Rev. Mod. Phys.* **80**, 885–964 (2008).

[44] V. L. Berezinskii. Destruction of long-range order in one-dimensional and two-dimensional systems possessing a continuous symmetry group. II. Quantum systems. *Sov. Phys. JETP* **34**, 610–616 (1972).

[45] J. M. Kosterlitz and D. J. Thouless. Ordering, metastability and phase transitions in two-dimensional systems. *J. Phys. C* **6**, 1181–1203 (1973).

[46] Y. Kagan, B. V. Svistunov, and G. V. Shlyapnikov. Influence on inelastic processes of the phase transition in a weakly collisional two-dimensional Bose gas. *Sov. Phys. JETP* **66**, 314–323 (1987).

[47] Z. Hadzibabic, P. Krüger, M. Cheneau, B. Battelier, and J. Dalibard. Berezinskii-Kosterlitz-Thouless crossover in a trapped atomic gas. *Nature* **441**, 1118–1121 (2006).

[48] E. H. Lieb and W. Liniger. Exact analysis of an interacting Bose gas. I. The general solution and the ground state. *Phys. Rev.* **130**, 1605–1616 (1963).

[49] E. H. Lieb. Exact analysis of an interacting Bose gas. II. The excitation spectrum. *Phys. Rev.* **130**, 1616–1624 (1963).

[50] M. Girardeau. Relationship between systems of impenetrable Bosons and Fermions in one dimension. *J. Math. Phys.* **1**, 516–523 (1960).

[51] T. Kinoshita, T. Wenger, and D. S. Weiss. Observation of a one-dimensional Tonks-Girardeau gas. *Science* **305**, 1125–1128 (2004).

[52] B. Paredes, A. Widera, V. Murg, O. Mandel, S. Fölling, I. Cirac, G. V. Shlyapnikov, T. W. Hänsch, and I. Bloch. Tonks-Girardeau gas of ultracold atoms in an optical lattice. *Nature* **429**, 277–281 (2004).

[53] P. Jordan and E. Wigner. Über das Paulische Äquivalenzverbot. *Z. Phys.* **47**, 631–651 (1928).

[54] A. Lenard. Momentum distribution in the ground state of the one-dimensional system of impenetrable Bosons. *J. Math. Phys.* **5**, 930–943 (1964).

[55] D. S. Petrov, D. M. Gangardt, and G. V. Shlyapnikov. Low-dimensional trapped gases. *J. Phys. IV France* **116**, 5–44 (2004).

[56] G. F. Gribakin and V. V. Flambaum. Calculation of the scattering length in atomic collisions using the semiclassical approximation. *Phys. Rev. A* **48**, 546–553 (1993).

[57] V. V. Flambaum, G. F. Gribakin, and C. Harabati. Analytical calculation of cold-atom scattering. *Phys. Rev. A* **59**, 1998–2005 (1999).

[58] K. Huang. *Statistical mechanics*. John Wiley & Sons, 2nd edition (1987).

[59] K. Huang and C. N. Yang. Quantum-mechanical many-body problem with hard-sphere interaction. *Phys. Rev.* **105**, 767–775 (1957).

[60] H. Feshbach. Unified theory of nuclear reactions. *Ann. Phys. (N.Y.)* **5**, 357–390 (1958).

[61] U. Fano. Effects of configuration interaction on intensities and phase shifts. *Phys. Rev.* **124**, 1866–1878 (1961).

[62] W. C. Stwalley. Stability of spin-aligned hydrogen at low temperatures and high magnetic fields: New field-dependent scattering resonances and predissociations. *Phys. Rev. Lett.* **37**, 1628–1631 (1976).

[63] S. Inouye, M. R. Andrews, J. Stenger, H.-J. Miesner, D. M. Stamper-Kurn, and W. Ketterle. Observation of Feshbach resonances in a Bose-Einstein condensate. *Nature* **392**, 151–154 (1998).

[64] C. Chin, R. Grimm, P. Julienne, and E. Tiesinga. Feshbach resonances in ultracold gases. *Rev. Mod. Phys.* **82**, 1225–1286 (2010).

[65] A. J. Moerdijk, B. J. Verhaar, and A. Axelsson. Resonances in ultracold collisions of ^{6}Li, ^{7}Li, and ^{23}Na. *Phys. Rev. A* **51**, 4852–4861 (1995).

[66] S. L. Cornish, N. R. Claussen, J. L. Roberts, E. A. Cornell, and C. E. Wieman. Stable ^{85}Rb Bose-Einstein condensates with widely tunable interactions. *Phys. Rev. Lett.* **85**, 1795–1798 (2000).

[67] P. O. Fedichev, M. W. Reynolds, and G. V. Shlyapnikov. Three-body recombination of ultracold atoms to a weakly bound s level. *Phys. Rev. Lett.* **77**, 2921–2924 (1996).

[68] E. Braaten and H.-W. Hammer. Universality in few-body systems with large scattering length. *Phys. Rep.* **428**, 259–390 (2006).

[69] P. O. Fedichev, Y. Kagan, G. V. Shlyapnikov, and J. T. M. Walraven. Influence of nearly resonant light on the scattering length

in low-temperature atomic gases. *Phys. Rev. Lett.* **77**, 2913–2916 (1996).

[70] D. M. Bauer, M. Lettner, C. Vo, G. Rempe, and S. Dürr. Control of a magnetic Feshbach resonance with laser light. *Nature* **5**, 339–342 (2009).

[71] T. Köhler, K. Goral, and P. S. Julienne. Production of cold molecules via magnetically tunable Feshbach resonances. *Rev. Mod. Phys.* **78**, 1311–1361 (2006).

[72] S. Jochim, M. Bartenstein, A. Altmeyer, G. Hendl, S. Riedl, C. Chin, J. Hecker Denschlag, and R. Grimm. Bose-Einstein condensation of molecules. *Science* **302**, 2101–2103 (2003).

[73] Q. Chen, J. Stajic, S. Tan, and K. Levin. BCS-BEC crossover: From high temperature superconductors to ultracold superfluids. *Phys. Rep.* **412**, 1–88 (2005).

[74] S. Giorgini, L. P. Pitaevskii, and S. Stringari. Theory of ultracold atomic Fermi gases. *Rev. Mod. Phys.* **80**, 1215–1274 (2008).

[75] P. Courteille, R. S. Freeland, D. J. Heinzen, F. A. van Abeelen, and B. J. Verhaar. Observation of a Feshbach resonance in cold atom scattering. *Phys. Rev. Lett.* **81**, 69–72 (1998).

[76] E. A. Donley, N. R. Claussen, S. L. Cornish, J. L. Roberts, E. A. Cornell, and C. E. Wieman. Dynamics of collapsing and exploding Bose-Einstein condensates. *Nature* **412**, 295–299 (2001).

[77] S. L. Cornish, S. T. Thompson, and C. E. Wieman. Formation of bright matter-wave solitons during the collapse of attractive Bose-Einstein condensates. *Phys. Rev. Lett.* **96**, 170401 (2006).

[78] S. Earnshaw. On the nature of the molecular forces which regulate the constitution of the luminiferous ether. *Trans. Camb. Phil. Soc.* **7**, 97–116 (1839).

[79] W. Paul. Electromagnetic traps for charged and neutral particles. *Rev. Mod. Phys.* **62**, 531–540 (1990).

[80] H. Dehmelt. Experiments with an isolated subatomic particle at rest. *Rev. Mod. Phys.* **62**, 525–530 (1990).

[81] R. Grimm, M. Weidemüller, and Y. B. Ovchinnikov. Optical dipole traps for neutral atoms. *Adv. Atom. Mol. Opt. Phys.* **42**, 95–170 (2000).

[82] D. R. Meacher. Optical lattices – crystalline structures bound by light. *Contemp. Phys.* **39**, 329–350 (1998).

[83] G. Grynberg and C. Robilliard. Cold atoms in dissipative optical lattices. *Phys. Rep.* **355**, 335–451 (2001).

[84] J. Dalibard and C. Cohen-Tannoudji. Dressed-atom approach to atomic motion in laser light: the dipole force revisited. *J. Opt. Soc. Am. B* **2**, 1707–1720 (1985).

[85] L. D. Landau and E. M. Lifshitz. *Course of Theoretical Physics IV: Quantum Electrodynamics.* Butterworth Heinemann, Oxford, 2nd edition (1982).

[86] J. P. Gordon and A. Ashkin. Motion of atoms in a radiation trap. *Phys. Rev. A* **21**, 1606–1607 (1980).

[87] I. I. Rabi, N. F. Ramsey, and J. Schwinger. Use of rotating coordinates in magnetic resonance problems. *Rev. Mod. Phys.* **26**, 167–171 (1954).

[88] S. Haroche and J.-M. Raimond. *Exploring the Quantum*. Oxford University Press, New York, 1st edition (2006).

[89] J. J. Sakurai. *Modern Quantum Mechanics*. Addison-Wesley, revised edition edition (2006).

[90] S. Peil, J. V. Porto, B. Laburthe Tolra, J. M. Obrecht, B. E. King, M. Subbotin, S. L. Rolston, and W. D. Phillips. Patterned loading of a Bose-Einstein condensate into an optical lattice. *Phys. Rev. A* **67**, 051603(R) (2003).

[91] L. Fallani, C. Fort, J. E. Lye, and M. Inguscio. Bose-Einstein condensate in an optical lattice with tunable spacing: transport and static properties. *Optics Express* **13**, 4303–4313 (2005).

[92] M. Greiner, I. Bloch, O. Mandel, T. W. Hänsch, and T. Esslinger. Exploring phase coherence in a 2D lattice of Bose-Einstein condensates. *Phys. Rev. Lett.* **87**, 160405 (2001).

[93] H. Moritz, T. Stöferle, M. Köhl, and T. Esslinger. Exciting collective oscillations in a trapped 1d gas. *Phys. Rev. Lett.* **91**, 250402 (2003).

[94] Z. Hadzibabic, S. Stock, B. Battelier, V. Bretin, and J. Dalibard. Interference of an array of independent Bose-Einstein condensates. *Phys. Rev. Lett.* **93**, 180403 (2004).

[95] O. Morsch and M. Oberthaler. Dynamics of Bose-Einstein condensates in optical lattices. *Rev. Mod. Phys.* **78**, 179–215 (2006).

[96] F. Bloch. Über die Quantenmechanik der Elektronen in Kristallgittern. *Z. Phys.* **52**, 555–600 (1929).

[97] H. Jones and C. Zener. A general proof of certain fundamental

equations in the theory of metallic conduction. *Proc. R. Soc. Lond. A* **144**, 101–117 (1934).

[98] C. J. Pethick and H. Smith. *Bose-Einstein condensation in dilute gases*. Cambridge University Press, 2nd edition (2008).

[99] C. Zener. A theory of the electrical breakdown of solid dielectrics. *Proc. R. Soc. Lond. A* **145**, 523–529 (1934).

[100] G. H. Wannier. Wave functions and effective Hamiltonian for Bloch electrons in an electric field. *Phys. Rev.* **117**, 432–439 (1960).

[101] J. B. Krieger and G. J. Iafrate. Time evolution of Bloch electrons in a homogeneous electric field. *Phys. Rev. B* **33**, 5494–5500 (1986).

[102] L. Esaki and R. Tsu. Superlattice and negative differential conductivity in semiconductors. *IBM J. Res. Dev.* **14**, 61–65 (1970).

[103] G. von Plessen and P. Thomas. Method for observing Bloch oscillations in the time domain. *Phys. Rev. B* **45**, 9185–9191 (1992).

[104] A. M. Bouchard and M. Luban. Semiconductor superlattices as terahertz generators. *Phys. Rev. B* **47**, 6815–6818 (1993).

[105] K. Leo, P. H. Bolivar, F. Brüggemann, R. Schwedler, and K. Köhler. Observation of Bloch oscillations in a semiconductor superlattice. *Solid State Commun.* **84**, 943–946 (1992).

[106] J. Feldmann, K. Leo, J. Shah, D. A. B. Miller, J. E. Cunningham, T. Meier, G. von Plessen, A. Schulze, P. Thomas, and S. Schmitt-Rink. Optical investigation of Bloch oscillations in a semiconductor superlattice. *Phys. Rev. B* **46**, 7252–7255 (1992).

[107] M. B. Dahan, E. Peik, J. Reichel, Y. Castin, and C. Salomon. Bloch oscillations of atoms in an optical potential. *Phys. Rev. Lett.* **76**, 4508–4511 (1996).

[108] G. Ferrari, N. Poli, F. Sorrentino, and G. M. Tino. Long-lived Bloch oscillations with bosonic Sr atoms and application to gravity measurement at the micrometer scale. *Phys. Rev. Lett.* **97**, 060402 (2006).

[109] M. Gustavsson, E. Haller, M. J. Mark, J. G. Danzl, G. Rojas-Kopeinig, and H.-C. Nägerl. Control of interaction-induced dephasing of Bloch oscillations. *Phys. Rev. Lett.* **100**, 080404 (2008).

[110] M. Fattori, C. D'Errico, G. Roati, M. Zaccanti, M. Jona-Lasinio, M. Modugno, M. Inguscio, and G. Modugno. Atom interferometry with a weakly interacting Bose-Einstein condensate. *Phys. Rev. Lett.* **100**, 080405 (2008).

[111] M. Greiner, O. Mandel, T. Esslinger, T. W. Hänsch, and I. Bloch. Quantum phase transition from a superfluid to a Mott insulator in a gas of ultracold atoms. *Nature* **415**, 39–44 (2002).

[112] H. Lignier, C. Sias, D. Ciampini, Y. Singh, A. Zenesini, O. Morsch, and E. Arimondo. Dynamical control of matter-wave tunneling in periodic potentials. *Phys. Rev. Lett.* **99**, 220403 (2007).

[113] K. W. Madison, M. C. Fischer, R. B. Diener, Qian Niu, and M. G. Raizen. Dynamical Bloch band suppression in an optical lattice. *Phys. Rev. Lett.* **81**, 5093–5096 (1998).

[114] A. Zenesini, H. Lignier, D. Ciampini, O. Morsch, and E. Arimondo. Coherent control of dressed matter waves. *Phys. Rev. Lett.* **102**, 100403 (2009).

[115] K. Drese and M. Holthaus. Ultracold atoms in modulated standing light waves. *Chem. Phys.* **217**, 201–219 (1997).

[116] G. Floquet. Sur les équations différentielles linéaires à coefficients périodiques. *Ann. École Norm. Sup.* **12**, 47–88 (1883).

[117] M. S. P. Eastham. *The Spectral Theory of Periodic Differential Equations*. Scottish Academic Press, Edinburgh (1973).

[118] P. Kuchment. *Floquet Theory for Partial Differential Equations*. Birkhäuser, Basel (1993).

[119] Y. B. Zel'dovich. The quasienergy of a quantum-mechanical system subjected to a periodic action. *Zh. Eksp. Theor. Fiz.* **51**, 1492 (1966). [*Sov. Phys. JETP* **24**, 1006 (1967)].

[120] V. I. Ritus. *Zh. Eksp. Theor. Fiz.* **51**, 1544 (1966). [*Sov. Phys. JETP* **24**, 1041 (1967)].

[121] H. Sambe. Steady states and quasienergies of a quantum-mechanical system in an oscillating field. *Phys. Rev. A* **7**, 2203 (1973).

[122] J. S. Howland. Quantum stability. Published in: Schrödinger operators: The quantum mechanical many-body problem. Proceedings of a workshop held at Aarhus, Denmark 15 May - 1 August 1991. *Lecture Notes in Physics* **403**, 100–122 (1992).

[123] M. Born and W. Heisenberg. Zur Quantentheorie der Molekeln. *Annalen der Physik* **379**, 1–31 (1924).

[124] M. Born and R. Oppenheimer. Zur Quantentheorie der Molekeln. *Annalen der Physik* **389**, 457–484 (1927).

[125] M. Born and V. Fock. Beweis des Adiabatensatzes. *Z. Phys.* **51**, 165–180 (1928).

[126] J. E. Avron, R. Seiler, and L. G. Yaffe. Adiabatic theorems and applications to the quantum Hall effect. *Commun. Math. Phys.* **110**, 33–49 (1987). [Erratum: *ibid.* **156**, 649–650 (1993)].

[127] H. P. Breuer and M. Holthaus. Adiabatic processes in the ionization of highly excited hydrogen atoms. *Z. Phys. D* **11**, 1–14 (1989).

[128] H. P. Breuer and M. Holthaus. Quantum phases and Landau-Zener transitions in oscillating fields. *Phys. Lett. A* **140**, 507–512 (1989).

[129] Y. N. Demkov and M. Kunike. *Vestn. Leningr. Univ. Fis. Khim.* **16**, 39 (1969). (In part reproduced in [131]).

[130] N. Rosen and C. Zener. Double Stern-Gerlach experiment and related collision phenomena. *Phys. Rev.* **40**, 502–507 (1932).

[131] K.-A. Suominen and B. M. Garraway. Population transfer in a level-crossing model with two time scales. *Phys. Rev. A* **45**, 374–386 (1992).

[132] C. Zener. Non-adiabatic crossing of energy levels. *Proc. R. Soc. Lond. A* **137**, 696–702 (1932).

[133] J. H. Shirley. Solution of the Schrödinger equation with a Hamiltonian periodic in time. *Phys. Rev.* **138**, B979–B987 (1965).

[134] C. Cohen-Tannoudji. *Atoms in electromagnetic fields.* World Scientific, Singapore (2005).

[135] S. Haroche, C. Cohen-Tannoudji, C. Audoin, and J. P. Schermann. Modified Zeeman hyperfine spectra observed in H^1 and Rb^{87} ground states interacting with a nonresonant rf field. *Phys. Rev. Lett.* **24**, 861–864 (1970).

[136] A. Eckardt and M. Holthaus. Dressed matter waves. *J. Phys.: Conf. Ser.* **99**, 012007 (2008).

[137] P. G. Harper. Single band motion of conduction electrons in a uniform magnetic field. *Proc. Phys. Soc. A* **68**, 874–878 (1955).

[138] J. B. Sokoloff. Unusual band structure, wave functions and electrical conductance in crystals with incommensurate periodic potentials. *Phys. Rep.* **126**, 189–244 (1985).

[139] D. H. Dunlap and V. M. Kenkre. Dynamic localization of a charged particle moving under the influence of an electric field. *Phys. Rev. B* **34**, 3625–3633 (1986).

[140] F. Grossmann, T. Dittrich, P. Jung, and P. Hänggi. Coherent destruction of tunneling. *Phys. Rev. Lett.* **67**, 516–519 (1991).

[141] A. Eckardt, C. Weiss, and M. Holthaus. Superfluid-insulator transition in a periodically driven optical lattice. *Phys. Rev. Lett.* **95**, 260404 (2005).

[142] C. E. Creffield and T. S. Monteiro. Tuning the Mott transition in a Bose-Einstein condensate by multiple photon absorption. *Phys. Rev. Lett.* **96**, 210403 (2006).

[143] A. Zenesini, H. Lignier, C. Sias, O. Morsch, D. Ciampini, and E. Arimondo. Tunneling control and localization for Bose-Einstein condensates in a frequency modulated optical lattice. *Laser Physics* **20**, 1182–1189 (2010).

[144] M. Holthaus. Collapse of minibands in far-infrared irradiated superlattices. *Phys. Rev. Lett.* **69**, 351–354 (1992).

[145] M. Holthaus and D. Hone. Quantum wells and superlattices in strong time-dependent fields. *Phys. Rev. B* **47**, 6499–6508 (1993).

[146] W. V. Houston. Acceleration of electrons in a crystal lattice. *Phys. Rev.* **57**, 184–186 (1940).

[147] A. Barone and G. Paterno. *Physics and applications of the Josephson effect*. Wiley, New York (1982).

[148] L. P. Kouwenhoven, S. Jauhar, J. Orenstein, P. L. McEuen, Y. Nagamune, J. Motohisa, and H. Sakaki. Observation of photon-assisted tunneling through a quantum dot. *Phys. Rev. Lett.* **73**, 3443–3446 (1994).

[149] T. H. Oosterkamp, L. P. Kouwenhoven, A. E. A. Koolen, N. C. van der Vaart, and C. J. P. M. Harmans. Photon sidebands of the ground state and first excited state of a quantum dot. *Phys. Rev. Lett.* **78**, 1536–1539 (1997).

[150] P. K. Tien and J. P. Gordon. Multiphoton process observed in the interaction of microwave fields with the tunneling between superconductor films. *Phys. Rev.* **129**, 647–651 (1963).

[151] P. S. S. Guimarães, B. J. Keay, J. P. Kaminski, S. J. Allen, Jr., P. F. Hopkins, A. C. Gossard, L. T. Florez, and J. P. Harbison. Photon-mediated sequential resonant tunneling in intense terahertz electric fields. *Phys. Rev. Lett.* **70**, 3792–3795 (1993).

[152] B. J. Keay, S. J. Allen, Jr., J. Galán, J. P. Kaminski, K. L. Campman, A. C. Gossard, U. Bhattacharya, and M. J. W. Rodwell. Photon-assisted electric field domains and multiphoton-assisted tunneling in semiconductor superlattices. *Phys. Rev. Lett.* **75**, 4098–4101 (1995).

[153] A. Eckardt, T. Jinasundera, C. Weiss, and M. Holthaus. Analog of photon-assisted tunneling in a Bose-Einstein condensate. *Phys. Rev. Lett.* **95**, 200401 (2005).

[154] C. E. Creffield and F. Sols. Controlled generation of coherent matter currents using a periodic driving field. *Phys. Rev. Lett.* **100**, 250402 (2008).

[155] C. Sias, A. Zenesini, H. Lignier, S. Wimberger, D. Ciampini, O. Morsch, and E. Arimondo. Resonantly enhanced tunneling of Bose-Einstein condensates in periodic potentials. *Phys. Rev. Lett.* **98**, 120403 (2007).

[156] C. Sias, H. Lignier, Y. P. Singh, A. Zenesini, D. Ciampini, O. Morsch, and E. Arimondo. Observation of photon-assisted tunneling in optical lattices. *Phys. Rev. Lett.* **100**, 040404 (2008).

[157] C. E. Creffield, F. Sols, D. Ciampini, O. Morsch, and E. Arimondo. Expansion of matter waves in static and driven periodic potentials. *Phys. Rev. A* **82**, 035601 (2010).

[158] A. Galindo and P. Pascual. *Quantum Mechanics I.* Springer-Verlag, Berlin, 2nd edition (1990).

[159] E. Kierig, U. Schnorrberger, A. Schietinger, J. Tomkovic, and M. K. Oberthaler. Single-particle tunneling in strongly driven double-well potentials. *Phys. Rev. Lett.* **100**, 190405 (2008).

[160] N. Teichmann, M. Esmann, and C. Weiss. Fractional photon-assisted tunneling for Bose-Einstein condensates in a double well. *Phys. Rev. A* **79**, 063620 (2009).

[161] M. Esmann, N. Teichmann, and C. Weiss. Fractional-photon-assisted tunneling in an optical superlattice: Large contribution to particle transfer. *Phys. Rev. A* **83**, 063634 (2011).

[162] M. P. A. Fisher, P. B. Weichman, G. Grinstein, and D. S. Fisher. Boson localization and the superfluid-insulator transition. *Phys. Rev. B* **40**, 546–570 (1989).

[163] D. Jaksch, C. Bruder, J. I. Cirac, C. W. Gardiner, and P. Zoller. Cold bosonic atoms in optical lattices. *Phys. Rev. Lett.* **81**, 3108–3111 (1998).

[164] N. Elstner and H. Monien. Dynamics and thermodynamics of the Bose-Hubbard model. *Phys. Rev. B* **59**, 12184–12187 (1999).

[165] D. van Oosten, P. van der Straten, and H. T. C. Stoof. Quantum phases in an optical lattice. *Phys. Rev. A* **63**, 053601 (2001).

[166] G. G. Batrouni, V. Rousseau, R. T. Scalettar, M. Rigol, A. Muramatsu, P. J. H. Denteneer, and M. Troyer. Mott domains of bosons confined on optical lattices. *Phys. Rev. Lett.* **89**, 117203 (2002).

[167] T. Stöferle, H. Moritz, C. Schori, M. Köhl, and T. Esslinger. Transition from a strongly interacting 1D superfluid to a Mott insulator. *Phys. Rev. Lett.* **92**, 130403 (2004).

[168] F. E. A. dos Santos and A. Pelster. Quantum phase diagram of bosons in optical lattices. *Phys. Rev. A* **79**, 013614 (2009).

[169] S. Sachdev. *Quantum Phase Transitions.* Cambridge University Press, 2nd edition (2011).

[170] J. Hubbard. Electron correlations in narrow energy bands. III. An improved solution. *Proc. Roy. Soc. Lond. A* **281**, 401–419 (1964).

For the preceding papers see *Ibid.* **276**, 238 (1963) and **277**, 237 (1964).

[171] W. Kohn. Analytic properties of Bloch waves and Wannier functions. *Phys. Rev.* **115**, 809–821 (1959).

[172] N. Teichmann, D. Hinrichs, M. Holthaus, and A. Eckardt. Process-chain approach to the Bose-Hubbard model: Ground-state properties and phase diagram. *Phys. Rev. B* **79**, 224515 (2009).

[173] J. Goldstone, A. Salam, and S. Weinberg. Broken symmetries. *Phys. Rev.* **127**, 965–970 (1962).

[174] I. B. Spielman, W. D. Phillips, and J. V. Porto. Mott-insulator transition in a two-dimensional atomic Bose gas. *Phys. Rev. Lett.* **98**, 080404 (2007).

[175] B. DeMarco, C. Lannert, S. Vishveshwara, and T.-C. Wei. Structure and stability of Mott-insulator shells of bosons trapped in an optical lattice. *Phys. Rev. A* **71**, 063601 (2005).

[176] S. Foelling, A. Widera, T. Müller, F. Gerbier, and I. Bloch. Formation of spatial shell structure in the superfluid to Mott insulator transition. *Phys. Rev. Lett.* **97**, 060403 (2006).

[177] G. K. Campbell, J. Mun, M. Boyd, P. Medley, A. E. Leanhardt, L. G. Marcassa, D. E. Pritchard, and W. Ketterle. Imaging the Mott insulator shells by using atomic clock shifts. *Science* **313**, 649–652 (2006).

[178] F. Gerbier, S. Fölling, A. Widera, O. Mandel, and I. Bloch. Probing number squeezing of ultracold atoms across the superfluid-Mott insulator transition. *Phys. Rev. Lett.* **96**, 090401 (2006).

[179] B. Capogrosso-Sansone, N. V. Prokof'ev, and B. V. Svistunov. Phase diagram and thermodynamics of the three-dimensional Bose-Hubbard model. *Phys. Rev. B* **75**, 134302 (2007).

[180] A. M. Rey, P. B. Blakie, G. Pupillo, C. J. Williams, and C. W. Clark. Bragg spectroscopy of ultracold atoms loaded in an optical lattice. *Phys. Rev. A* **72**, 023407 (2005).

[181] C. Kollath, A. Iucci, T. Giamarchi, W. Hofstetter, and U. Schollwöck. Spectroscopy of ultracold atoms by periodic lattice modulations. *Phys. Rev. Lett.* **97**, 050402 (2006).

[182] J. Struck, C. Ölschläger, R. Le Targat, P. Soltan-Panahi, A. Eckardt, M. Lewenstein, P. Windpassinger, and K. Sengstock. Quantum simulation of frustrated classical magnetism in triangular optical lattices. *Science* **333**, 996–999 (2011).

[183] G. H. Wannier. Antiferromagnetism. The triangular Ising net. *Phys. Rev.* **79**, 357–364 (1950).

[184] R. Moessner and A. P. Ramirez. Geometrical frustration. *Phys. Today* **59**, 24–29 (2006).

[185] M. Lewenstein, A. Sanpera, V. Ahufinger, B. Damski, A. Sen(De), and U. Sen. Ultracold atomic gases in optical lattices: mimicking condensed matter physics and beyond. *Adv. Phys.* **56**, 243–379 (2007).

[186] A. Eckardt, P. Hauke, P. Soltan-Panahi, C. Becker, K. Sengstock, and M. Lewenstein. Frustrated quantum antiferromagnetism with ultracold bosons in a triangular lattice. *Europhys. Lett.* **89**, 10010 (2010).

[187] C. Becker, P. Soltan-Panahi, J. Kronjäger, S. Dörscher, K. Bongs, and K. Sengstock. Ultracold quantum gases in triangular optical lattices. *New J. Phys.* **12**, 065025 (2010).

[188] J. Simon, W. S. Bakr, R. Ma, M. E. Tai, P. M. Preiss, and M. Greiner. Quantum simulation of antiferromagnetic spin chains in an optical lattice. *Nature* **472**, 307–312 (2011).

[189] E. Barouch, B. M. McCoy, and M. Dresden. Statistical Mechanics of the XY Model. I. *Phys. Rev. A* **2**, 1075–1092 (1970).

[190] E. Lieb, T. Schultz, and D. Mattis. Two soluble models of an antiferromagnetic chain. *Ann. Phys.* **16**, 407–466 (1961).

[191] N. Teichmann, D. Hinrichs, and M. Holthaus. Reference data for phase diagrams of triangular and hexagonal bosonic lattices. *EPL* **91**, 10004 (2010).

[192] M.-C. Cha, M. P. A. Fisher, S. M. Girvin, M. Wallin, and A. P. Young. Universal conductivity of two-dimensional films at the superconductor-insulator transition. *Phys. Rev. B* **44**, 6883–6902 (1991).

[193] J. E. Bayfield. Excited atomic and molecular states in strong electromagnetic fields. *Phys. Rep.* **51**, 317–391 (1978).

[194] N. L. Manakov, V. D. Ovsiannikov, and L. P. Rapoport. Atoms in a laser field. *Phys. Rep.* **141**, 320–433 (1986).

[195] G. Mainfray and G. Manus. Multiphoton ionization of atoms. *Rep. Prog. Phys.* **54**, 1333–1372 (1991).

[196] N. B. Delone and V. P. Krainov. *Multiphoton Processes in Atoms*. Springer-Verlag, Berlin, 2nd edition (2000).

[197] S. I. Chu and D. A. Telnov. Beyond the Floquet theorem: generalized Floquet formalisms and quasienergy methods for atomic and molecular multiphoton processes in intense laser fields. *Phys. Rep.* **390**, 1–131 (2004).

[198] D. Meshulach and Y. Silberberg. Coherent quantum control of multiphoton transitions by shaped ultrashort optical pulses. *Phys. Rev. A* **60**, 1287–1292 (1999).

[199] V. Prasad, B. Dahiya, and K. Yamashita. Ionization of the H atom in ultrashort chirped laser pulses. *Phys. Scr.* **82**, 055302 (2010).

[200] M. Richter, S. V. Bobashev, A. A. Sorokin, and K. Tiedtke. Multiphoton ionization of atoms with soft x-ray pulses. *J. Phys. B: At. Mol. Opt. Phys.* **43**, 194005 (2010).

[201] P. Lambropoulos, G. M. Nikolopoulos, and K. G. Papamihail. Route to direct multiphoton multiple ionization. *Phys. Rev. A* **83**, 021407(R) (2011).

[202] H. P. Breuer, K. Dietz, and M. Holthaus. Adiabatic evolution, quantum phases, and Landau-Zener transitions in strong radiation fields. *Radiation Effects and Defects in Solids* **122/123**, 91–106 (1991).

[203] K. Drese and M. Holthaus. Floquet theory for short laser pulses. *Eur. Phys. J. D* **5**, 119–134 (1999).

[204] J. Callaway. *Quantum Theory of the Solid State.* Academic Press, New York (1976).

[205] V. Grecchi and A. Sacchetti. Acceleration theorem for Bloch oscillators. *Phys. Rev. B* **63**, 212303 (2001).

[206] M. Holthaus. Bloch oscillations and Zener breakdown in an optical lattice. *J. Opt. B: Quantum Semiclass. Opt.* **2**, 589–604 (2000).

[207] W. C. Henneberger. Perturbation method for atoms in intense light beams. *Phys. Rev. Lett.* **21**, 838–841 (1968).

[208] W. Natanson. Über die statistische Theorie der Strahlung. *Phys. Zeit.* **12**, 659 (1911).

[209] R. P. Feynman. *The Feynman Lectures on Physics*, volume III. Addison-Wesley, Reading (1965).

Publications

The present dissertation is based upon the following contributions to scientific research conducted from April 2009 to March 2012 at the Carl von Ossietzky University of Oldenburg, Germany. This section states my contributions to each work, consisting of four papers published in international peer-reviewed journals of the Physical Review, a chapter of the book "Dynamical Tunneling – Theory and Experiment" published by CRC Press, and a manuscript for a paper that is presently under review for publication.

The first paper resulting from my studies on periodically driven optical lattices is titled "**Driven optical lattices as strong-field simulators**". The idea to investigate the deviations from an adiabatic transport of a quantum state in a periodically driven lattice was carried over from previous investigations on many-body dynamics in double-well systems conducted for my diploma thesis. With the dynamics of the lattice system enriched by the Brillouin-zone structure due to the spatial periodicity of the lattice, the decision to focus on single-particle dynamics and to disentangle effects induced by the interaction at a later stage came naturally. This course of action was confirmed by the richness of effects displayed by the seemingly simple model systems as well as the multitude of modes to deliberately manipulate the dynamics. Publication I focuses on relevant parameters for an experimental realization of the proposed scenario. All numerical work was done by me and an existing source code for the calcu-

lation of quasienergies as well as another one for wave-packet propagation was carefully checked for errors and expanded to fulfill the requirements to pulsed driving. I created and prepared all visual data presented in the paper and wrote the first draft, which was then improved and revised together with Martin Holthaus.

The publication "**Dynamic localization in optical lattices**" is printed as chapter 12 of the book "Dynamical Tunneling – Theory and Experiment" edited by Srihari Keshavamurthy and Peter Schlagheck and published by CRC Press in March 2011. The first part provides a basic description of how quantum tunneling can deliberately be impeded by driving the system – an effect known as dynamic localization. This introduction is followed by an application of this theory to atoms in a bichromatic optical lattice, where the "metal-insulator"–like transition can be controlled by adjusting the amplitude of the driving. With the exception of Figs. 1 and 2, which were provided by Matthias Langemeyer, and Figs. 12 and 13 being credited to Oliver Morsch, all numerical work was performed by me. This includes extending already existing routines and tuning the system's parameters as well as selecting and preparing the final figures for the manuscript. Martin Holthaus and I planned and structured the chapter, after which Martin Holthaus wrote the draft. I improved and carefully revised the manuscript.

In August 2011, the paper "**Generalized acceleration theorem for spatiotemporal Bloch waves**" was published in Physical Review B. The idea to investigate what turned out to be a generalization of Bloch's familiar acceleration theorem to the Floquet setting was born earlier that year: At the time I was working on the controlled manipulation of k-space distributions by subjecting an initial wave packet to pulsed driving, and I experimented with a homogeneous force acting on the system in addition to the purely periodic driving. The numerical work to monitor the

wave-packet's dynamics in the set of bases provided by the instantaneous spatiotemporal Bloch waves was already accomplished. This proved to be extremely useful for the study and manipulation of wave packets and revealed the potentials inherent in the then found "dressing and probing" strategy. These results encouraged me to formulate the generalized acceleration theorem, I worked out its mathematical formulation in the following weeks. Its predictions are in full agreement with the numerical results and in addition it allows for a self-contained explanation of the so-called super Bloch oscillations. The manuscript for the paper was planned and drafted mainly by me, and revised together with Martin Holthaus, who penned the section on super Bloch oscillations. I conducted all numerical work and provided all figures. This includes the extension of existing programs as well as the conception and coding of new ones.

Directly after Paper III was published, I focused on finalizing the investigations already undertaken in coherently controlling dressed matter waves. The results are printed in "**Controlled wave-packet manipulation with driven optical lattices**" and relate strongly to the previous publications. For a periodically driven lattice system, the paper provides figures of quasienergy surfaces, depicted for the first time in scientific literature, and utilizes these to explain and predict the dynamics of particles in those systems. I had already accomplished most of the work when I paused it to focus on the formulation and implications of the generalized acceleration theorem. The work on the controlled wave-packet manipulation was resumed and finished in mid-2011, when I planned and wrote the entire manuscript for which all numerical calculations had already been completed. Together with Martin Holthaus I revised the manuscript, which was published in December 2011.

At about the same time, Dr. Elmar Haller, then at the University of Innsbruck, Austria, visited our group and reported on recent experimental

investigations on periodically driven lattices in the low-frequency regime conducted by the Innsbruck group around Prof. Dr. Hanns-Christoph Nägerl. This prompted an investigation of low-frequency driven optical lattices and the interrelated multiphoton-like processes with parameters closely adapted to the Innsbruck experiment. In addition to these considerations, the resulting preprint titled "**ac Stark shift and multiphoton-like resonances in low-frequency driven optical lattices**" contains a proposal to perform avoided quasienergy crossing spectroscopy with asymmetric pulses. Preliminary experimental measurements performed by E. Haller confirmed the viability of the theoretical suggestions. All numerical work – including writing and extending the source code, evaluating the data, and preparing the figures – was performed by me. I sketched and planned the manuscript together with Martin Holthaus, who wrote the draft, which was then revised and improved by both of us.

I

I. Driven optical lattices as strong-field simulators

Stephan Arlinghaus and Martin Holthaus,
Driven optical lattices as strong-field simulators,
Phys. Rev. A **81**, 063612 (2010).

PHYSICAL REVIEW A **81**, 063612 (2010)

Driven optical lattices as strong-field simulators

Stephan Arlinghaus and Martin Holthaus
Institut für Physik, Carl von Ossietzky Universität, D-26111 Oldenburg, Germany
(Received 24 March 2010; published 8 June 2010)

We argue that ultracold atoms in strongly shaken optical lattices can be subjected to conditions similar to those experienced by electrons in laser-irradiated crystalline solids, but without introducing secondary polarization effects. As a consequence, one can induce nonperturbative multiphoton-like resonances due to the mutual penetration of ac-Stark-shifted Bloch bands. These phenomena can be detected with a combination of currently available laboratory techniques.

DOI: 10.1103/PhysRevA.81.063612 PACS number(s): 67.85.−d, 32.80.Xx, 42.50.Hz

I. INTRODUCTION

The investigation of ultracold atoms in optical lattices constitutes a major area of topical research [1–4]. One of the long-term visions driving this trend stems from the prospect of using these well-controllable and flexible systems for "emulating" important quantum many-body problems which still are not fully understood, such as high-T_c superconductivity [5,6], and of obtaining information on these by observing their cold-atom-emulated versions in the laboratory, rather than attempting necessarily imperfect computer simulations. So far, interest has been focused mainly on systems governed by a time-independent Hamiltonian operator, a hallmark example being provided by the Bose-Hubbard model [7]. However, it is feasible to subject the lattice atoms to time-dependent external forces, and thus to study explicitly time-dependent phenomena [8,9]. Already in 1998 Madison *et al.* have obtained evidence for Bloch band narrowing with cold sodium atoms in time-periodically forced optical lattices [10]; more recently, dynamic localization [11,12], photon-assisted tunneling [13], and coherent control of the superfluid-to-Mott insulator transition [14] have been demonstrated with Bose-Einstein condensates in such strongly shaken periodic potentials. Moreover, it has been suggested to employ oscillating optical lattices for realizing frustrated quantum antiferromagnetism [15]. In this article we argue that ultracold atoms in forced optical lattices also lend themselves to the study of multiphoton-like transitions under strong-field conditions which are barely accessible with electrons in solids irradiated by high-power lasers; in particular, they provide an exceptionally clean testing ground for the investigation of nonperturbative multiphoton-like resonances. We first sketch in Sec. II the required setup, and specify the orders of magnitude of the relevant parameters which characterize the optical-lattice analogs of strong laser fields. We then present numerical model calculations in Sec. III, demonstrating how both perturbative and nonperturbative resonances manifest themselves. The explanation of these phenomena makes use of both the spatial periodicity of the optical lattice and the temporal periodicity of the driving force: Effectively, one encounters a spatiotemporal crystal, the band structure of which is controlled by the parameters of the driving force. This viewpoint is emphasized in the concluding Sec. IV.

II. SIMULATING STRONG LASER FIELDS

A one-dimensional (1D) optical lattice is created, for example, by shining laser radiation with wavelength $\lambda = 2\pi/k_L$ against a mirror and retroreflecting the beam into itself. An atom of mass M moving in this standing light wave then experiences a periodic potential with a depth V_0 which is proportional to the laser intensity [2]. Mounting the mirror on a piezoelectric actuator now allows one to let it oscillate sinusoidally with a precisely controlled angular frequency ω and amplitude L, thus shaking the lattice back and forth [14]. In the laboratory frame, the Hamiltonian describing the particle's center-of-mass motion along the lattice direction then reads

$$H_{\mathrm{lab}} = \frac{p^2}{2M} + \frac{V_0}{2}\cos\{2k_L[x - L\cos(\omega t)]\}. \tag{1}$$

The relevant characteristic energy scale is given by the single-photon recoil energy,

$$E_r = \frac{\hbar^2 k_L^2}{2M}; \tag{2}$$

typical scaled lattice depths V_0/E_r range between about 5 and 10. For example, with ^{87}Rb atoms in a lattice erected by light with wavelength $\lambda = 842$ nm one has $E_r = 1.34 \times 10^{-11}$ eV, as corresponding to the recoil frequency $\nu_r = E_r/(2\pi\hbar) = 3.23$ kHz.

Performing a unitary transformation to a frame co-moving with the lattice, the Hamiltonian acquires the suggestive form [10,16]

$$H = \frac{p^2}{2M} + \frac{V_0}{2}\cos(2k_L x) - Fx\cos(\omega t), \tag{3}$$

with $F = ML\omega^2$ denoting the amplitude of the inertial force appearing in this oscillating frame. A meaningful measure for the strength of this force is the dimensionless parameter [12]

$$K_0 = \frac{Fd}{\hbar\omega}, \tag{4}$$

where $d = \lambda/2$ specifies the lattice constant. In terms of quantities directly accessible in the laboratory, one has

$$K_0 = \frac{\pi^2}{2}\frac{\nu}{\nu_r}\frac{L}{d}, \tag{5}$$

with the driving frequency $\nu = \omega/(2\pi)$, showing that one may easily realize values $K_0 > 1$ when both ratios ν/ν_r and L/d are on the order of unity [11–14]. To appreciate what this means, consider an atomic analog: A common KrF exciplex laser provides photons with energy $\hbar\omega = 5.0$ eV. Inserting this into the expression (4), taking the Bohr radius for the length d, and solving for the electric field strength $\mathcal{E} = F/e$ acting on an electronic charge, one finds that $K_0 = 1$ is reached only for $\mathcal{E} = 9.45 \times 10^{10}$ V/m, which is roughly one-fifth

of the field formally experienced by a ground-state electron in the hydrogen atom. In this sense, time-periodically forced optical lattices can serve even as superstrong-field simulators: Shaking a lattice with large amplitudes L according to the Hamiltonian (1) simulates perfectly homogeneous fields acting on particles in periodic potentials in the regime $K_0 > 1$ of the parameter (4) which is hard to reach with laser-driven electrons in traditional solids, without introducing, for example, detrimental polarization effects. Thus, ultracold atoms in driven optical lattices offer the unique possibility to study superstrong-field–induced multiphoton-like processes in periodic potentials in their purest form.

III. PERTURBATIVE AND NONPERTURBATIVE MULTIPHOTON TRANSITIONS

For illustrating the dynamics that become explorable in this way, we consider a 1D lattice with depth $V_0 = 5.7E_r$. Its single-particle eigenstates are Bloch waves [17],

$$\varphi_{n,k}(x) = \exp(\mathrm{i}kx)u_{n,k}(x), \tag{6}$$

with lattice-periodic functions $u_{n,k}(x) = u_{n,k}(x+d)$ labeled by a band index n and a wave number k; Fig. 1 depicts the energy dispersion relations $E_n(k)$ for the lowest bands $n = 1,2,3$. In the center of the Brillouin zone, that is, at $k/k_L = 0$, one has $E_2(0) - E_1(0) = 4.690E_r$, and $E_3(0) - E_1(0) = 5.544E_r$. We now take an initial state exclusively populating the lowest band, as described by

$$\psi(x,t_0) = \int_{-k_L}^{+k_L} dk g_1(k,t_0)\varphi_{1,k}(x,t_0) \tag{7}$$

with a Gaussian k-space distribution

$$g_1(k,t_0) = (2k_L\sqrt{\pi}\,\Delta k)^{-1/2}\exp\left(-\frac{k^2}{2(\Delta k)^2}\right) \tag{8}$$

centered around $k/k_L = 0$, and set $\Delta k = 0.1k_L$ for its width, as appropriate for an initial ensemble of noninteracting ultracold atoms. This state then is subjected to pulsed forcing with an amplitude $F(t)$ which rises from zero to a maximum value, stays constant for a while, and decreases back to zero. For the sake of definiteness, we consider conditions as already realized experimentally in Ref. [14]: We take ^{87}Rb as atomic species in a lattice with $\lambda = 842$ nm, and design the envelope of the pulse such that $F(t)$ rises linearly within 10 ms, stays constant for a holding time of 2 ms, and then is linearly switched off in another 10 ms. For a driving frequency of 5 kHz, say, the ramp time of 10 ms corresponds to 50 cycles, so that the relatively slowly changing envelope $F(t)$ may enable adiabatic following under nonresonant conditions.

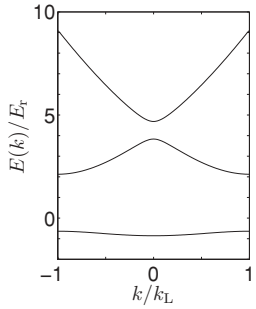

FIG. 1. Lowest three Bloch bands of a 1D optical lattice with depth $V_0 = 5.7E_r$. The lowest band gap is $2.763E_r$ at $k = k_L$.

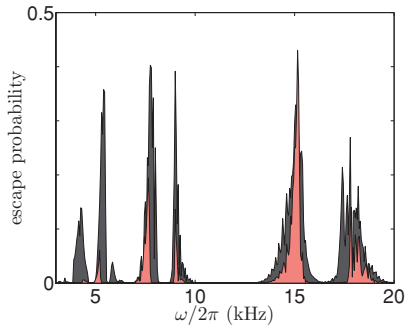

FIG. 2. (Color online) Escape probabilities from the lowest Bloch band after pulses with linear switch-on and switch-off ramps of 10-ms duration each, and a holding time of 2 ms, during which a specified value $K_0^{\max}$ of the scaled amplitude (4) is reached. Driving frequencies $\omega/(2\pi)$ correspond to ^{87}Rb in an optical lattice with $\lambda = 842$ nm. Light, $K_0^{\max} = 0.7$; black, $K_0^{\max} = 1.3$. Of particular interest is the unexpected, strong, and narrow resonance at $\omega/(2\pi) = 5.3$ kHz.

Moreover, we rely on the fact that the fraction of atoms surviving in the lowest band can be accurately determined, as demonstrated by the Landau-Zener measurements reported in Ref. [18]. We therefore compute the escape probability from the lowest band after each pulse, for specified values of $K_0^{\max}$ reached during the plateau phase. Figure 2 shows results thus obtained for $K_0^{\max} = 0.7$ and $K_0^{\max} = 1.3$, as functions of the driving frequency $\omega/(2\pi)$. The pronounced peak pattern depends markedly on the maximum driving amplitude; for instance, a further peak has appeared for $K_0^{\max} = 1.3$ at $\omega/(2\pi) \approx 4$ kHz which was not visible for $K_0^{\max} = 0.7$. A more complete picture is provided by Fig. 3, which shows a two-dimensional plot of the escape probability considered as function of both $\omega/(2\pi)$ and $K_0^{\max}$, for the same pulse shape as taken in Fig. 2.

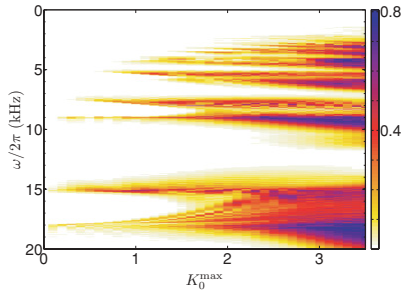

FIG. 3. (Color online) Escape probability versus both driving frequency $\omega/(2\pi)$ and maximum scaled amplitude $K_0^{\max}$, for the same pulse shape as employed in Fig. 2.

TABLE I. Expected and computed resonance frequencies: $\nu_{\rm res}$ is an m-photon transition frequency according to Eq. (9), $\nu_{\rm peak}$ is the position of the corresponding peak where it becomes apparent in Fig. 3. The entry NV indicates that no peak is visible for the pulse profile employed here.

m	n	$\Delta E_{n,1}/(mE_{\rm r})$	$\nu_{\rm res}$ (kHz)	$\nu_{\rm peak}$ (kHz)
1	3	5.544	17.932	18.00
1	2	4.690	15.170	15.15
2	3	2.772	8.966	9.00
2	2	2.345	7.585	7.60
3	3	1.848	5.977	5.85
		–	–	5.30
3	2	1.563	5.057	NV

The positions of most of the peaks in Figs. 2 and 3 (i.e., most of the system's resonant frequencies) are easily explained: Because the initial state is narrowly centered around $k/k_{\rm L}=0$, its response is mainly determined by the energies $E_n(0)$ in the Brillouin-zone center. Hence, one expects ordinary m-photon-like resonances between the initial band $n=1$ and higher bands $n=2,3,\ldots$ when the driving frequency complies with the condition

$$\Delta E_{n,1} \equiv E_n(0) - E_1(0) = m\hbar\omega \tag{9}$$

for integer m. Indeed, listing these expected m-photon transition frequencies in Table I and comparing them to the frequencies of the peaks observed in Fig. 3, one generally finds quite good agreement.

In some instances, however, the numerical solution of the Schrödinger equation produces a peak which does *not* fit into this naive pattern. Most notably, the sharp spike visible in Fig. 2 at $\omega/(2\pi)=5.3$ kHz does not match Eq. (9) for any reasonable combination of n and m. Such "nonperturbative" events are our main concern; we predict that they can be detected experimentally in already existing setups. These particular resonances admit a systematic explanation which forces us to go way beyond the perturbative reasoning underlying Eq. (9).

Because the Hamiltonian (1) is periodic *both* in space (with lattice period $d=\pi/k_{\rm L}=\lambda/2$) *and* in time (with driving period $T=2\pi/\omega$), it gives rise to spatiotemporal Bloch waves [16],

$$\psi_{n,k}(x,t) = u_{n,k}(x,t)\exp\{{\rm i}[kx - \varepsilon_n(k)t/\hbar]\}, \tag{10}$$

with functions $u_{n,k}(x,t)=u_{n,k}(x+d,t)=u_{n,k}(x,t+T)$ reflecting translational invariance in space and time on equal footing, and quasienergies $\varepsilon_n(k)$, in generalization of the usual Bloch waves (6). While quasimomenta $\hbar k$ are determined up to an integer multiple of $2\pi\hbar/d=2\hbar k_{\rm L}$, quasienergies are likewise determined up to an integer multiple of the photon energy $2\pi\hbar/T=\hbar\omega$. Figure 4 shows one "quasienergy Brillouin zone" (of height $\hbar\omega$) with states originating from the lowest three Bloch bands for $\omega/(2\pi)=5.30$ kHz, the frequency of the extraordinary peak in Fig. 2, and $K_0=0.7$, 1.0, and 1.3. There are various avoided crossings indicating multiphoton-like couplings between the bands; however, with $\Delta k=0.1k_{\rm L}$ the wave packet evolving from the initial distribution (8) mainly explores the interval of quasimomenta indicated by the shaded areas. The quasienergy band originating from the lowest

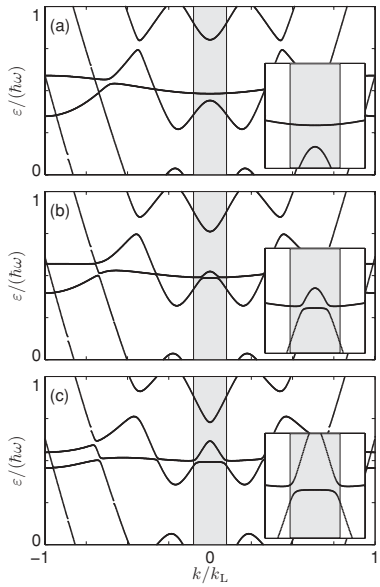

FIG. 4. Quasienergies $\varepsilon_n(k)$ for the 1D optical lattice driven with frequency $\omega/(2\pi)=5.30$ kHz, and scaled amplitudes $K_0=0.7$ (a), 1.0 (b), and 1.3 (c). The areas shaded in gray, extending from $k=-0.1k_{\rm L}$ to $k=+0.1k_{\rm L}$, mark the range of wave numbers explored by the initial wave packet. The insets show how the quasienergy band $n=1$ (above) is pinched through with increasing K_0 by the band $n=2$, displaced downward by $3\hbar\omega$. This causes the nonperturbative resonance observed in Fig. 2.

unperturbed energy band $n=1$ is shown enlarged in the insets; with increasing K_0 this band is pierced through from below by the quasienergy band $n=2$, displaced down in energy by $3\hbar\omega$ against that representative which is continuously connected to the bare $n=2$ Bloch band. This penetration results in "active" avoided crossings signaling a strong-field–induced three-photon resonance; this is responsible for the anomalous peak at $\omega/(2\pi)=5.30$ kHz.

The dynamics underlying that peak should thus be discussed in terms of the morphology of the surfaces which emerge when the quasienergies are considered as functions of both the wave number k and the instantaneous amplitude F (or K_0): When the driving amplitude $F(t)$ increases during the upward ramp of a pulse, the initial distribution is shifted almost adiabatically on its quasienergy surface, parallel to the K_0 axis. As long as the maximum value of K_0 lies below the critical regime where this surface is first being pierced by another one, the initial distribution is restored with only minor distortion when the amplitude returns to zero, resulting in negligible escape probability. However, when the moving distribution hits an avoided-crossing regime, part of the wave function undergoes a Landau-Zener-type transition to the anticrossing band. Both parts of the wave function then evolve separately on their respective surfaces, until they meet for a second time during the downward ramp, when they interfere and thereby establish the final occupation probabilities of the bands

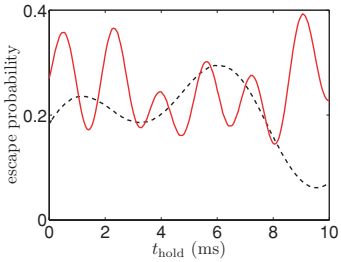

FIG. 5. (Color online) Stückelberg oscillations of the escape probability in response to prolongation of the plateau duration t_{hold}, for $\omega/(2\pi) = 5.30$ kHz, and $K_0^{\mathrm{max}} = 1.0$ (dashed) and 1.3 (solid line).

involved. This mechanism of splitting and interference implies that there should be Stückelberg-like oscillations when the final occupation probabilities are monitored while the length of the pulses' plateau segment is varied, because varying the plateau duration means varying the relative phase picked up by the two interfering components. Indeed, these oscillations are clearly visible in Fig. 5.

We remark that the standard perturbative m-photon resonances can be grasped in a similar manner: For frequencies such that Eq. (9) holds, two quasienergy surfaces are degenerate already at $F = 0$, so that adiabaticity is disabled and the wave function splits right at the beginning of a pulse [19]. Seen against this background, a perturbative resonance corresponds to the removal of a quasienergy degeneracy already present at $F = 0$, while a nonperturbative one emerges when ac-Stark-shifted Bloch bands penetrate each other at a certain finite driving strength.

IV. CONCLUSIONS

When viewing a time-periodically forced optical lattice as a spatiotemporal crystal, the natural basis states are the spatiotemporal Bloch waves (10); the energy bands $E_n(k)$ of the undriven lattice turn into quasienergy bands $\varepsilon_n(k)$. The latter depend not only on the lattice parameters, but also on the parameters of the driving force. While they differ barely from the unperturbed energy bands as long as the driving amplitude is weak, corresponding to values $K_0 \ll 1$ of the dimensionless parameter (4), they become strongly distorted, and even penetrate each other, in the nonperturbative regime.

When subjected to pulsed forcing with an amplitude which changes slowly compared to the period $T = 2\pi/\omega$ of the drive, a wave packet can adjust itself adiabatically to a mere distortion of its quasienergy band. However, when the wave packet explores a part of a quasienergy band which is pierced by another one, as exemplified in Fig. 4, Landau-Zener transitions occur; this mechanism leads to strong nonperturbative resonances at frequencies not given by the simple condition (9). In principle, such resonances should also occur in solids irradiated by strong laser pulses; however, there they would be masked by a host of competing effects. The experimentally proven good controllability of ultracold atoms in forced optical lattices makes such systems a far better testing ground for these dynamics.

Our study has been restricted to the single-particle level; it is reasonable to expect that the phenomena exemplarily discussed in the present work can immediately be detected with sufficiently dilute or close-to-ideal Bose-Einstein condensates in driven optical lattices [12]. Even more, it appears equally feasible to perform the experiments suggested here under conditions of sizable interparticle interactions, or even of strong correlations. The question how the single-particle scenario outlined above is modified then opens up far-reaching further lines of investigation, concerning both experiment and theory.

ACKNOWLEDGMENTS

We thank Oliver Morsch for continuing in-depth discussions of the Pisa experiments [11–14,18]. This work was supported by the Deutsche Forschungsgemeinschaft under Grant No. Ho 1771/6.

[1] D. Jaksch and P. Zoller, Ann. Phys. (NY) **315**, 52 (2005).
[2] O. Morsch and M. Oberthaler, Rev. Mod. Phys. **78**, 179 (2006).
[3] M. Lewenstein, A. Sanpera, V. Ahufinger, B. Damski, A. Sen, and U. Sen, Adv. Phys. **56**, 243 (2007).
[4] I. Bloch, J. Dalibard, and W. Zwerger, Rev. Mod. Phys. **80**, 885 (2008).
[5] W. Hofstetter, J. I. Cirac, P. Zoller, E. Demler, and M. D. Lukin, Phys. Rev. Lett. **89**, 220407 (2002).
[6] I. Bloch, Science **319**, 1202 (2008).
[7] M. Greiner, O. Mandel, T. Esslinger, T. W. Hänsch, and I. Bloch, Nature **415**, 39 (2002).
[8] S. D. Huber, E. Altman, H. P. Büchler, and G. Blatter, Phys. Rev. B **75**, 085106 (2007).
[9] C. Gaul, R. P. A. Lima, E. Díaz, C. A. Müller, and F. Domínguez-Adame, Phys. Rev. Lett. **102**, 255303 (2009).
[10] K. W. Madison, M. C. Fischer, R. B. Diener, Q. Niu, and M. G. Raizen, Phys. Rev. Lett. **81**, 5093 (1998).
[11] H. Lignier, C. Sias, D. Ciampini, Y. Singh, A. Zenesini, O. Morsch, and E. Arimondo, Phys. Rev. Lett. **99**, 220403 (2007).
[12] A. Eckardt, M. Holthaus, H. Lignier, A. Zenesini, D. Ciampini, O. Morsch, and E. Arimondo, Phys. Rev. A **79**, 013611 (2009).
[13] C. Sias, H. Lignier, Y. P. Singh, A. Zenesini, D. Ciampini, O. Morsch, and E. Arimondo, Phys. Rev. Lett. **100**, 040404 (2008).
[14] A. Zenesini, H. Lignier, D. Ciampini, O. Morsch, and E. Arimondo, Phys. Rev. Lett. **102**, 100403 (2009).
[15] A. Eckardt, P. Hauke, P. Soltan-Panahi, C. Becker, K. Sengstock, and M. Lewenstein, Europhys. Lett. **89**, 10010 (2010).
[16] K. Drese and M. Holthaus, Chem. Phys. **217**, 201 (1997).
[17] N. W. Ashcroft and N. D. Mermin, *Solid State Physics* (Harcourt College Publishers, Fort Worth etc., 1976).
[18] A. Zenesini, H. Lignier, G. Tayebirad, J. Radogostowicz, D. Ciampini, R. Mannella, S. Wimberger, O. Morsch, and E. Arimondo, Phys. Rev. Lett. **103**, 090403 (2009).
[19] M. Holthaus and B. Just, Phys. Rev. A **49**, 1950 (1994).

II

II. Dynamic localization in optical lattices

Stephan Arlinghaus, Matthias Langemeyer, and Martin Holthaus,
Dynamic localization in optical lattices,
Chapter 12 of the volume "Dynamical Tunneling – Theory and Experiment", (Taylor and Francis, 2010).

Dynamic localization in optical lattices[1]

Stephan Arlinghaus, Matthias Langemeyer, and Martin Holthaus[2]

March 23, 2011

[1]Chapter 12 of the volume: **Dynamical Tunneling - Theory and Experiment**, edited by S. Keshavamurthy and P. Schlagheck (Taylor and Francis CRC, 2011)

[2]Carl von Ossietzky Universität
Institut für Physik
D - 26111 Oldenburg, Germany

Contents

Chapter 1

Dynamic localization in optical lattices

The concept of dynamic localization goes back to an observation reported by Dunlap and Kenkre in 1986: The wave packet of a single particle moving on a single-band tight-binding lattice endowed with only nearest-neighbor couplings remains perpetually localized when driven by a spatially homogeneous ac force, provided the amplitude and the frequency of that force obey a certain condition [1]. When trying to overcome the limitations of the model, it is comparatively straightforward to deal with an arbitrary form of the dispersion relation — thus abandoning the nearest-neighbor approximation — and with arbitrary time-periodic forces, thus doing away with the restriction to purely sinusoidal driving [2]. But in any real lattice system an external time-periodic force will induce interband transitions, and it is by no means obvious whether dynamic localization can survive when these come into play.

In this chapter we consider ultracold atoms in driven optical lattices, which provide particularly attractive, experimentally well accessible examples of quantum particles in spatially periodic structures exposed to time-periodic forcing [3, 4, 5]. Such systems are much cleaner, and more easy to control, than electrons in crystal lattices under the influence of ac electric fields, for which the original idea had been developed [1]. With the help of results obtained

by numerical calculations we illustrate that such ultracold atoms in kHz-driven optical lattices exhibit dynamic localization in almost its purest form if the parameters are chosen judiciously, despite the potentially devastating presence of interband transitions.

When viewing dynamic localization as resulting from a band collapse [6, 7], far-reaching further possibilities emerge. Namely, the actual strength of deviations from exact spatial periodicity, be they isolated [8], random [9], or quasiperiodic [10, 11], is measured relative to the effective band width. Thus, when the band in question almost collapses in response to time-periodic driving, the effects of even slight deviations from exact lattice periodicity are strongly enhanced. This allows one, in particular, to coherently control the "metal-insulator"-like incommensurability transition occurring in sufficiently deep quasiperiodic optical lattices [10, 11, 12]. While the very transition has already been observed with Bose-Einstein condensates in bichromatic optical potentials [13], its coherent control by means of time-periodic forcing still awaits its experimental verification.

1.1 The basic idea

The one-dimensional tight-binding system described by the Hamiltonian

$$H_0 = -J \sum_{\ell} \left(|\ell+1\rangle\langle\ell| + |\ell\rangle\langle\ell+1| \right) , \tag{1.1}$$

where $|\ell\rangle$ denotes a Wannier state localized at the ℓth lattice site, and J is the hopping matrix element connecting neighboring sites, is about the simplest model for the formation of Bloch bands. Assuming that the unspecified number of sites is so large that finite-size effects may be neglected, its energy eigenstates are Bloch waves

$$|\varphi_k\rangle = \sum_{\ell} |\ell\rangle \exp(\mathrm{i}\ell k a) \tag{1.2}$$

labeled by a wave number k; the lattice period is given by a. The corresponding energy dispersion relation reads

$$E(k) = -2J \cos(ka) \; ; \tag{1.3}$$

here we assume $J > 0$, so that its minimum is located at $k = 0 \bmod 2\pi/a$. Now we let an external time-dependent, spatially homogeneous force $F(t)$ act on the system, such that the total Hamiltonian becomes

$$H(t) = H_0 + H_1(t) \tag{1.4}$$

with

$$H_1(t) = -F(t) \sum_\ell |\ell\rangle a\ell\langle\ell| \; . \tag{1.5}$$

It is easy to verify that the wave functions

$$|\psi_k(t)\rangle = \exp\Big(-\frac{\mathrm{i}}{\hbar}\int_0^t \mathrm{d}\tau \, E(q_k(\tau))\Big) \sum_\ell |\ell\rangle \exp\left(\mathrm{i}\ell q_k(t) a\right) \tag{1.6}$$

then are solutions to the time-dependent Schrödinger equation, provided the time-dependent wave numbers $q_k(t)$ introduced here obey the "semiclassical" relation

$$\hbar \dot{q}_k(t) = F(t) \; . \tag{1.7}$$

We demand that $q_k(t)$ be equal to k at time $t = 0$, and therefore set

$$q_k(t) = k + \frac{1}{\hbar}\int_0^t \mathrm{d}\tau \, F(\tau) \; . \tag{1.8}$$

These wave functions (1.6), originally considered by Houston in the context of crystal electrons exposed to a uniform electric field superimposed on a periodic lattice potential [14], are known as "accelerated Bloch waves", or Houston states.

In the particular case of a monochromatic force with angular frequency ω and amplitude F_1, given by

$$F(t) = F_1 \cos(\omega t) \; , \tag{1.9}$$

one has

$$q_k(t) = k + \frac{F_1}{\hbar\omega} \sin(\omega t) \; , \tag{1.10}$$

so that $q_k(t)$ naturally acquires the temporal period $T = 2\pi/\omega$ of the driving force. Then also $E(q_k(t))$ is T-periodic, but the Houston state (1.6) is not, because the integral appearing

in the exponential prefactor acquires a contribution which grows linearly with time. In order to extract that contribution, we calculate the one-cycle average

$$\begin{aligned} \varepsilon(k) &\equiv \frac{1}{T}\int_0^T \mathrm{d}\tau\, E(q_k(\tau)) \\ &= -2J_{\mathrm{eff}}\cos(ka)\ , \end{aligned} \tag{1.11}$$

thus obtaining an effective hopping matrix element given by

$$J_{\mathrm{eff}} = J\,\mathrm{J}_0\Big(\frac{F_1 a}{\hbar\omega}\Big)\ , \tag{1.12}$$

with $\mathrm{J}_0(z)$ denoting the Bessel function of zero order. We then write

$$\exp\Big(-\frac{\mathrm{i}}{\hbar}\int_0^t \mathrm{d}\tau\, E(q_k(\tau))\Big) = \exp\Big(-\frac{\mathrm{i}}{\hbar}\int_0^t \mathrm{d}\tau\,\Big[E(q_k(\tau)) - \varepsilon(k)\Big]\Big)\exp\Big(-\mathrm{i}\varepsilon(k)t/\hbar\Big)\ , \tag{1.13}$$

so that the first exponential on the right hand side now is T-periodic by construction. Hence, for the T-periodic force (1.9) the Houston states (1.6) can be cast into a form

$$|\psi_k(t)\rangle = |u_k(t)\rangle\exp\Big(-\mathrm{i}\varepsilon(k)t/\hbar\Big) \tag{1.14}$$

with T-periodic functions $|u_k(t)\rangle$,

$$|u_k(t)\rangle = |u_k(t+T)\rangle\ . \tag{1.15}$$

This leads to a remarkable conclusion. Any wave packet governed by the full Hamiltonian (1.4) with periodic forcing (1.9) can be expanded with respect to these states (1.14) with coefficents that are constant in time, because the time-dependence already is fully incorporated into the states themselves. After each cycle T the T-periodic functions $|u_k(t)\rangle$ are restored, so that the time evolution of the wave packet, when viewed stroboscopically at intervals T, is determined by the different "speed" of rotation of the complex phase factors $\exp(-\mathrm{i}\varepsilon(k)t/\hbar)$ of the packet's individual components. But if all quantities $\varepsilon(k)$ are equal, which according to Eqs. (1.11) and (1.12) occurs when the scaled driving amplitude

$$K_0 \equiv \frac{F_1 a}{\hbar\omega} \tag{1.16}$$

equals a zero of the Bessel function J_0, all phase factors evolve at the same speed, so that the wave packet reproduces itself exactly after each period: There is some T-periodic wiggling, but no long-term motion. This, in short, is dynamic localization [1].

The above argument appears so special, and the decisive step (1.13) so swift, that it is not easy to see how to transfer this finding to more realistic situations: How can one incorporate deviations from exact lattice periodicity into this reasoning? How to proceed when several bands are coupled by interband transitions? The answer to these questions is provided by the Floquet picture, which does not directly take recourse to the spatial lattice periodicity, but rather builds on the temporal periodicity of the Hamiltonian: When $H(t) = H(t+T)$, there exists a complete set of solutions to the time-dependent Schrödinger equation of the particular form

$$|\psi_n(t)\rangle = |u_n(t)\rangle \exp(-\mathrm{i}\varepsilon_n t/\hbar) \;, \tag{1.17}$$

where the functions $|u_n(t)\rangle = |u_n(t+T)\rangle$ inherit the T-periodicity of the underlying Hamiltonian. These states are known as Floquet states; the quantities ε_n are dubbed as quasienergies [15, 16, 17, 18]. Obviously the Houston states (1.6) with time-periodic forcing are particular examples of such Floquet states; from now on we employ an abstract state label n instead of the wave number k in order to also admit settings without lattice periodicity. In the case of the Houston-Floquet states, the determination of their quasienergies (1.11) essentially was a by-product of the solution of an initial value problem. The general case, however, has to proceed along a more sophisticated route: Floquet states and quasienergies are determined by solving the eigenvalue problem

$$\left(H(t) - \mathrm{i}\hbar\frac{\partial}{\partial t}\right) |u_n(t)\rangle\!\rangle = \varepsilon_n |u_n(t)\rangle\!\rangle \;, \tag{1.18}$$

posed in an *extended Hilbert space* of T-periodic functions; in that space time plays the role of a *coordinate*. Therefore, if $\langle u_1(t)|u_2(t)\rangle$ is the scalar product of two T-periodic functions in the usual physical Hilbert space, their scalar product in the extended space reads [18]

$$\langle\!\langle u_1|u_2\rangle\!\rangle \equiv \frac{1}{T}\int_0^T \mathrm{d}t\, \langle u_1(t)|u_2(t)\rangle \;. \tag{1.19}$$

Hence, we write $|u_n(t)\rangle$ for a Floquet eigenfunction when viewed in the physical Hilbert

space, and $|u_n(t)\rangle\!\rangle$ when that same function is regarded as an element of the extended space.

A most important consequence of this formalism stems from the fact that when $|u_n(t)\rangle\!\rangle$ is a solution to the problem (1.18) with eigenvalue ε_n, then $|u_n(t)\exp(\mathrm{i}m\omega t)\rangle\!\rangle$ is a further solution with eigenvalue $\varepsilon_n + m\hbar\omega$, where we have set $\omega = 2\pi/T$, and m is any (positive, zero, or negative) integer, in order to comply with the required T-periodic boundary condition. For $m \neq 0$ these two solutions are orthogonal with respect to the scalar product (1.19). But when going back to the physical Hilbert space, one has

$$|u_n(t)\exp(\mathrm{i}m\omega t)\rangle \exp\Big(-\mathrm{i}(\varepsilon_n + m\hbar\omega)/\hbar\Big) = |u_n(t)\rangle \exp(-\mathrm{i}\varepsilon_n t/\hbar)\ , \tag{1.20}$$

so that the two different solutions represent *the same* Floquet state (1.17). We conclude that a physical Floquet state does not simply correspond to an individual solution to the eigenvalue problem (1.18), but rather to a whole class of such solutions labeled by the state index n, whereas the "photon" index m distinguishes different representatives of such a class. Likewise, a quasienergy should not be regarded as a single eigenvalue, but rather as a set $\{\varepsilon_n + m\hbar\omega \mid m = 0, \pm 1, \pm 2, \ldots\}$ associated with one particular state n, while m ranges through all integers. Therefore, each "quasienergy Brillouin zone" of width $\hbar\omega$ contains one quasienergy representative of each state.

The time evolution of any wave function can then be written as a Floquet-state expansion,

$$|\psi(t)\rangle = \sum_n c_n |u_n(t)\rangle \exp(-\mathrm{i}\varepsilon_n t/\hbar)\ , \tag{1.21}$$

where the coefficients c_n remain constant in time. This is one of the main benefits offered by the Floquet picture, and allows one to draw many parallels to the evolution of systems governed by a time-independent Hamiltonian.

Equipped with this set of tools, it is now clear how to investigate the possible occurrence of dynamic localization in realistic lattice structures: One has to solve the eigenvalue problem (1.18) for the Hamiltonian with the respective full lattice potential, and to enquire whether the resulting quasienergy bands collapse at least approximately, that is, acquire negligible widths for certain parameters. If so, any wave packet prepared in a quasienergy

band at a collapse point will suffer from "prohibited dephasing", as in the archetypal model specified by Eqs. (1.1), (1.5), and (1.9); and thus remain dynamically localized. Interband transitions then are automatically included, with multiphoton-like resonances manifesting themselves through quasienergy-curve anticrossings [19].

In the following section we will carry through this program for ultracold atoms in driven one-dimensional optical lattices.

1.2 Does it work?

A one-dimensional optical lattice is created by two counterpropagating laser beams with wave number k_{L}, suitably detuned from a dipole-allowed transition of the atomic species moving in this standing light wave. By means of the ac Stark effect, the spatially periodic electric field experienced by the atoms then translates into a cosine potential

$$V_{\mathrm{lat}}(x) = \frac{V_0}{2}\cos(2k_{\mathrm{L}}x) \tag{1.22}$$

for their translational motion along the lattice, with a depth V_0 that is proportional to the laser intensity [20, 21]. The characteristic energy scale then is given by the single-photon recoil energy

$$E_{\mathrm{rec}} = \frac{\hbar^2 k_{\mathrm{L}}^2}{2M}\,, \tag{1.23}$$

where M denotes the atomic mass. To give a numerical example, when working with ^{87}Rb in a lattice generated by laser radiation with wavelength $\lambda = 2\pi/k_{\mathrm{L}} = 842$ nm [4, 5] one has $E_{\mathrm{rec}} = 1.34 \cdot 10^{-11}$ eV. Thus, typical lattice depths of 5 to 10 recoil energies are on the order of 10^{-10} eV — which means that one encounters many phenomena with ultracold atoms in optical lattices which are known from traditional solid-state physics, but scaled down in energy by no less than 10 orders of magnitude.

This also tells us what "ultracold" means. Taking an ensemble of atoms with a temperature T_{ens} such that $k_{\mathrm{B}}T_{\mathrm{ens}}$ is roughly equal to E_{rec}, say, where k_{B} is Boltzmann's constant,

the de Broglie wavelength of these atoms, given by

$$\lambda_{\mathrm{deBroglie}} = \frac{h}{\sqrt{2\pi M k_{\mathrm{B}} T_{\mathrm{ens}}}} \approx \frac{2}{\sqrt{\pi}} \frac{\lambda}{2} \,, \tag{1.24}$$

is barely longer than the lattice constant $a = \lambda/2$. But in order to experience quantum mechanical lattice effects, the particles have to be able to "feel" the periodic structure, so that $\lambda_{\mathrm{deBroglie}}$ should cover *at least* a few lattice constants — which means that being this cold is not cold enough: We even require $k_{\mathrm{B}} T_{\mathrm{ens}} \ll E_{\mathrm{rec}}$.

With hardly any thermal excitation energy left the atoms occupy only the lowest Bloch band of their optical lattice, so that the single-particle Hamiltonian with the lattice potential (1.22) translates directly into the single-band tight-binding model (1.1) when working in a basis of Wannier functions pertaining to that lowest band, and neglecting all couplings other than those between nearest neighbors, denoted as J. The accuracy of this approximation increases with increasing lattice depth [4, 12]: For $V_0/E_{\mathrm{rec}} = 5$ the magnitude of the ratio of the neglected matrix element connecting next-to-nearest neighbors to J still reaches about 5%, but it decreases to about 1% when $V_0/E_{\mathrm{rec}} = 10$. Moreover, when expressing the exact band structure of a cosine lattice in terms of characteristic values of the Mathieu equation, and noting that the width W of the cosine energy band (1.3) is $4J$, one finds the approximation [21]

$$J/E_{\mathrm{rec}} \sim \frac{4}{\sqrt{\pi}} \left(\frac{V_0}{E_{\mathrm{rec}}}\right)^{3/4} \exp\left(-2\sqrt{\frac{V_0}{E_{\mathrm{rec}}}}\right) \qquad \text{for} \quad V_0/E_{\mathrm{rec}} \gg 1 \,. \tag{1.25}$$

The requisite still missing now is the time-periodic force corresponding to the model (1.5). This can be effectuated either by introducing a small oscillating frequency difference between the two lattice-generating laser beams, as detailed later, or by retro-reflecting one such beam off an oscillating mirror back into itself [3, 4, 5]. In a frame of reference co-moving with the oscillating lattice, one then obtains the single-particle Hamiltonian

$$H(t) = \frac{p^2}{2M} + V_{\mathrm{lat}}(x) - F_1 x \cos(\omega t + \phi) \,, \tag{1.26}$$

where p is the atomic center-of-mass momentum in the lattice direction, the driving force is

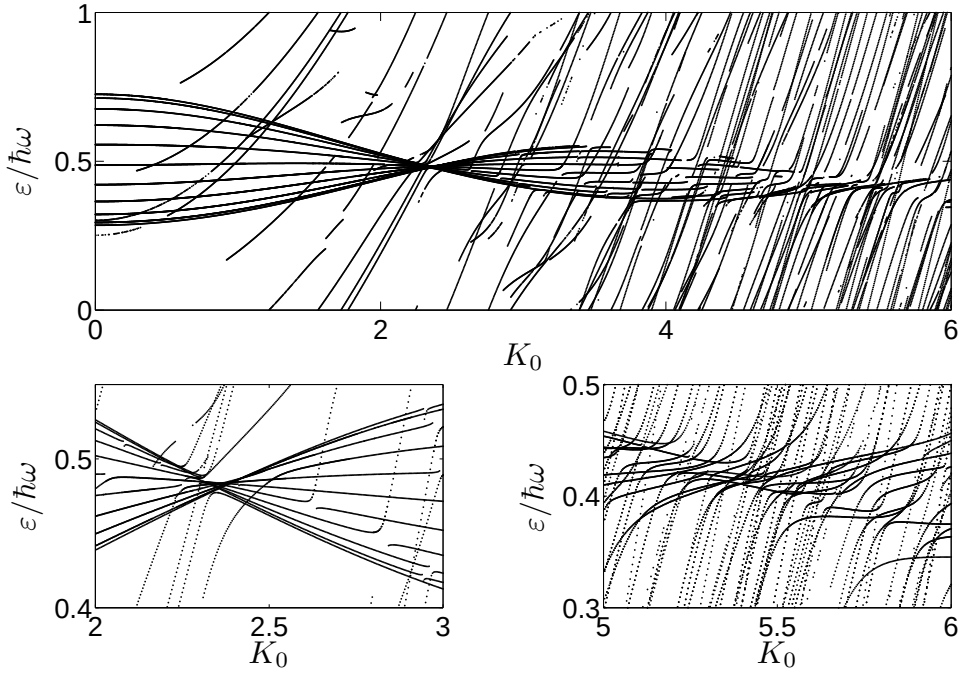

Figure 1.1: Above: One Brillouin zone of quasienergies for the optical lattice (1.22) with depth $V_0/E_{\rm rec} = 5.7$, driven with scaled frequency $\hbar\omega/E_{\rm rec} = 0.5$, vs. the scaled driving amplitude K_0. The lower left panel testifies that the first band collapse is almost perfect, whereas the second one, enlarged in the lower right panel, is already thwarted by multiphoton-like resonances.

parametrized in accordance with Eq. (1.9), and we have also admitted an arbitrary phase ϕ.

In all our model calculations we consider a lattice with depth $V_0/E_{\rm rec} = 5.7$, implying that the width of the lowest Bloch band is $W/E_{\rm rec} = 0.22$, whereas the gap between this lowest band and the first excited one figures as $\Delta/E_{\rm rec} = 2.76$. Even for such a comparatively shallow lattice, which is routinely being realized in current experiments [5], the dispersion of the lowest band already is reasonably well described by the tight-binding cosine approximation (1.3), setting $J = W/4$. In order to obtain dynamic localization, the driving frequency should then be chosen such that the quantum $\hbar\omega$ is significantly smaller than the gap Δ, so that, perturbatively speaking, interband transitions require higher-order multiphoton-like processes, which would be suppressed as long as the driving amplitude F_1

is not too strong [19]. On the other hand, it is reasonable to demand that $\hbar\omega$ be larger than the band width, so that the band fits into a single quasienergy Brillouin zone. A good choice of the driving frequency should therefore adhere to the chain $4J = W < \hbar\omega < \Delta$; we take $\hbar\omega/E_{\rm rec} = 0.5$ in all numerical scenarios depicted below. For ^{87}Rb atoms in a lattice with $\lambda = 842$ nm this choice fixes the frequency at $\omega/(2\pi) = 1.62$ kHz.

Figure 1.1 shows one Brillouin zone of quasienergies for these parameters vs. the scaled driving amplitude K_0, as defined by Eq. (1.16). Observe that the first quasimomentum Brillouin zone ranges from $-\hbar\pi/a = -\hbar k_{\rm L}$ to $+\hbar\pi/a = +\hbar k_{\rm L}$; the homogeneous force does not mix states with different wave numbers [10]. Hence, we combine quasienergies for states with $k = (i/10)\, k_{\rm L}$ in this plot, with $i = 0, 1, 2, \ldots, 10$. In this way, the comparison of the ideal quasienergy band (1.11) with the one appearing in the actual optical lattice is greatly facilitated. Evidently the first band collapse is almost perfect, although it is slightly shifted from $K_0 = 2.405$, the first zero of J_0, to $K_0 \approx 2.35$. In contrast, the second collapse, expected at $K_0 = 5.520$, already is significantly affected by a host of anticrossings, indicating multiphoton-like resonances. Thus, with $V_0/E_{\rm rec} = 5.7$ and $\hbar\omega/E_{\rm rec} = 0.5$ we may expect almost perfect dynamic localization at the first collapse point, whereas there will be strong disturbances of the ideal dynamics at the second one.

In Fig. 1.2 we depict the lowest quasienergy band for $K_0 = 0$, where it coincides with the original energy band; $K_0 = 1.18$, where its width is reduced by a factor of $\mathrm{J}_0(1.18) = 0.681$; and at the first collapse point, $K_0 = 2.35$. Ideally, a collapsed quasienergy band is completely flat, so that dynamic localization is associated with an infinite effective mass of the driven Bloch particle. Here we still observe some residual dispersion, probably resulting from both next-to-nearest neighbor couplings and couplings to higher bands, but the degree of band flattening achieved by the driving force is nonetheless impressive.

The ultimate demonstration of dynamic localization requires, of course, the inspection of wave-packet dynamics. To this end, we first compute the Bloch states $\langle x|\varphi_{1,k}\rangle$ of the lowest energy band of the lattice (1.22), and use them to design an initial wave packet

$$\langle x|\psi(t=0)\rangle = \int_{-k_{\rm L}}^{k_{\rm L}} {\rm d}k\, g_1(k, t=0)\, \langle x|\varphi_{1,k}\rangle \tag{1.27}$$

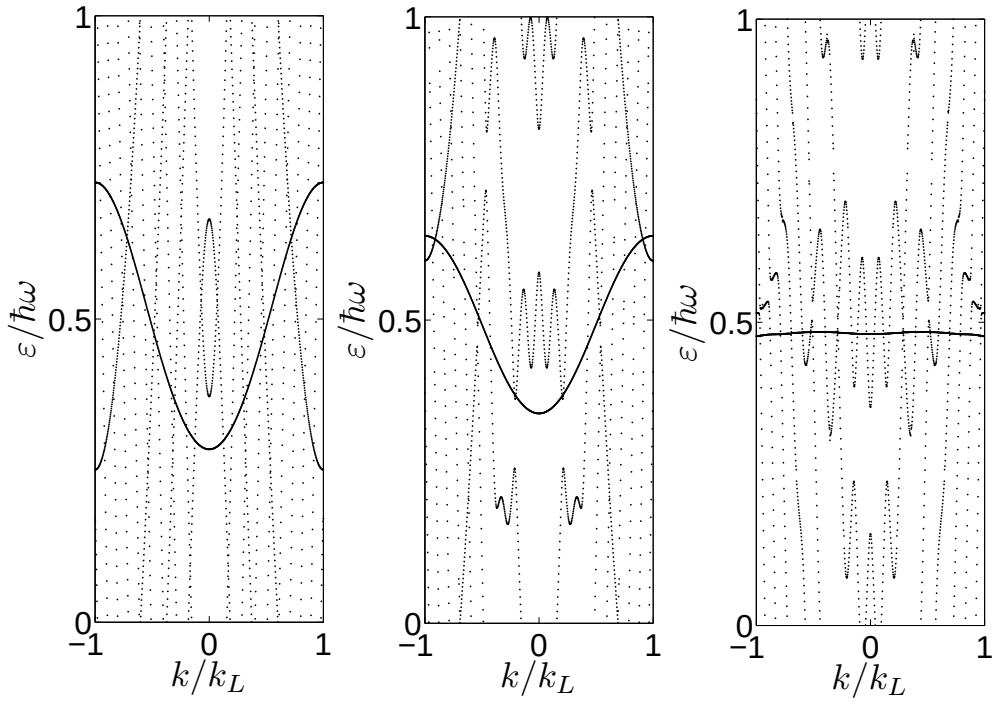

Figure 1.2: "Lowest" quasienergy band for the optical lattice (1.22) with depth $V_0/E_{\rm rec} = 5.7$, driven with scaled frequency $\hbar\omega/E_{\rm rec} = 0.5$, and scaled amplitudes $K_0 = 0$ (left), 1.18 (middle), and 2.35 (right). Additional curves result from higher bands.

with a Gaussian k-space distribution

$$g_1(k, t=0) = \frac{1}{\sqrt{2k_{\rm L}\sqrt{\pi}\Delta k}} \exp\left(-\frac{(k-k_{\rm c})^2}{2(\Delta k)^2}\right) \tag{1.28}$$

centered around some predetermined wave number $k_{\rm c}$, with width Δk. The corresponding probability density $|\langle x|\psi(t=0)\rangle|^2$ is concentrated in the wells of the lattice potential, equipped with a Gaussian envelope that varies the more slowly with x the narrower its distribution (1.28), that is, the smaller Δk. We then take this packet (1.27) as initial condition, and compute the wave function $\langle x|\psi(t)\rangle$ for $t > 0$ by solving the time-dependent Schrödinger equation numerically, fixing the phase ϕ in the Hamiltonian (1.26) at the value $\phi = \pi/2$. This means that the force $F(t) = F_1 \cos(\omega t + \phi)$ is instantaneously switched on at $t = 0$.

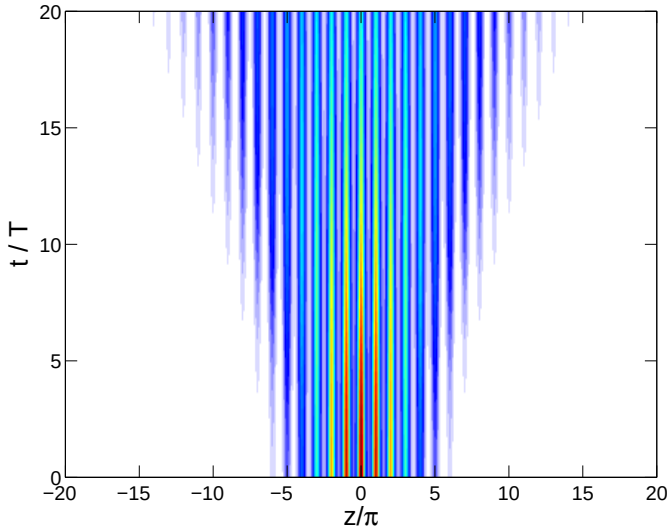

Figure 1.3: Spreading of the Bloch wave packet (1.27) with initial k-space width $\Delta k/k_{\mathrm{L}} = 0.1$, and initial momentum $k_{\mathrm{c}}/k_{\mathrm{L}} = 0$, in the unforced optical lattice. In this and the following figures, density is encoded in shades of gray.

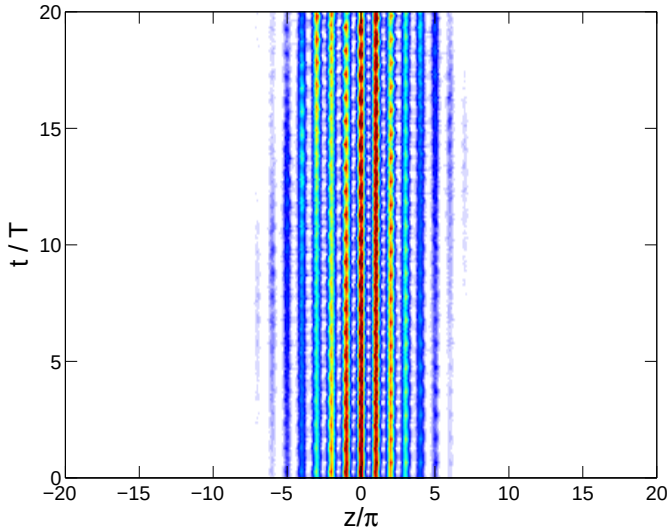

Figure 1.4: Evolution of the same initial wave packet as in Fig. 1.3 at the first band collapse ($K_0 = 2.35$): Here one encounters almost perfect dynamic localization; wave-packet spreading is disabled because the quasienergy band is dispersionless.

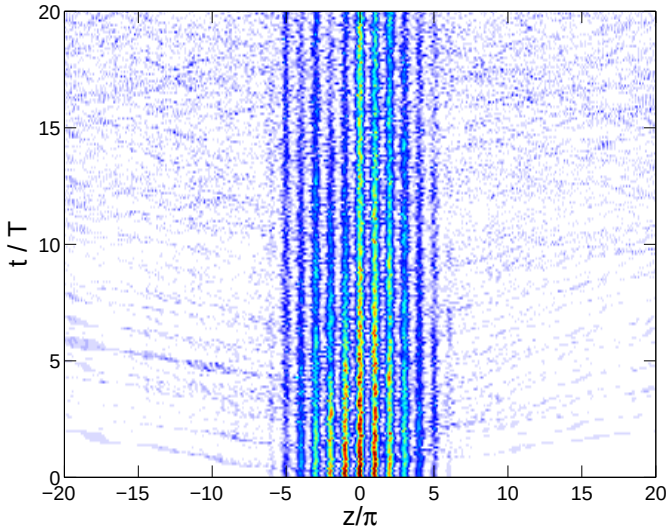

Figure 1.5: Evolution of the same inital wave packet as in Fig. 1.3 at the supposed second band collapse ($K_0 = 5.52$): Here the multiphoton-like resonances visible in Fig. 1.1 lead to a marked degradation of the localization.

Figure 1.3 shows a density plot of the wave packet when it evolves in the undriven lattice, that is, for $K_0 = 0$; the density is encoded in shades of gray. In this and the following figures, spatial extensions are measured in terms of the dimensionless coordinate $z = k_\mathrm{L} x$, so that a distance $\Delta z/\pi = 1$ corresponds to one lattice period; moreover, the time scale is set by the period $T = 2\pi/\omega$. With $k_\mathrm{c}/k_\mathrm{L} = 0$ the initial packet carries no net momentum; its width is chosen as $\Delta k/k_\mathrm{L} = 0.1$. As expected, the width of the packet then grows in the course of time by well-to-well tunneling.

In Fig. 1.4 we depict the density of the wave packet that evolves from the same initial condition when the driving amplitude is tuned to the first band collapse at $K_0 = 2.35$. Here we observe dynamic localization at its very best: The spreading has stopped, the packet is "frozen".

It is then also of interest to monitor the evolution at the supposed second collapse, at $K_0 = 5.52$; this is done in Fig. 1.5. While the "regular spreading" that has been prominent in Fig. 1.3 indeed seems to have stopped, small probability wavelets leak out of the initial packet almost immediately, spreading rapidly over the lattice. This is an effect of the multiphoton-

like resonances previously spotted in Fig. 1.1, which assist parts of the wave function in getting to higher bands, allowing them to escape on a short time scale.

As long as interband transitions remain negligible, the resulting single-band dynamics can often be regarded as "semiclassical" [22]: Namely, if an initial packet is strongly centered in k-space around some arbitrary wave number $k_{\mathrm{c}} \equiv k_{\mathrm{c}}(0)$, this center wave number evolves in time according to Bloch's famous "acceleration theorem"

$$\hbar \dot{k}_{\mathrm{c}}(t) = F(t) \,, \tag{1.29}$$

similar to the evolution (1.7) of the index of a single Houston state. The model Hamiltonian (1.26) specifies $F(t) = F_1 \cos(\omega t + \phi)$, so that in this case

$$k_{\mathrm{c}}(t) = k_{\mathrm{c}}(0) + \frac{F_1}{\hbar\omega}\Big(\sin(\omega t + \phi) - \sin(\phi)\Big) \,. \tag{1.30}$$

The packet's group velocity then is given by the derivative of the dispersion relation $E(k)$ of the band it lives in, evaluated at this moving center wave number (1.30):

$$v_{\mathrm{group}}(t) = \frac{1}{\hbar}\frac{\mathrm{d}E}{\mathrm{d}k}\bigg|_{k_{\mathrm{c}}(t)} \,. \tag{1.31}$$

Taking the tight-binding relation (1.3) as a good approximation for the actual lowest energy band of our model, this yields

$$v_{\mathrm{group}}(t) = \frac{2Ja}{\hbar}\sin\Big(k_{\mathrm{c}}(t)a\Big) \,. \tag{1.32}$$

Upon time-averaging, one is therefore left with

$$\overline{v}_{\mathrm{group}} = \frac{2J_{\mathrm{eff}}a}{\hbar}\sin\Big(k_{\mathrm{c}}(0)a - K_0\sin(\phi)\Big) \,, \tag{1.33}$$

where J_{eff} again is the driving-dependent effective hopping matrix element (1.12), and K_0 is the scaled amplitude (1.16). Thus, the initial phase ϕ may be utilized for imparting some momentum to the packet. Nonetheless, for any combination of $k_{\mathrm{c}}(0)$ and ϕ the average group velocity vanishes when $J_{\mathrm{eff}} = 0$, as corresponding to ideal dynamic localization.

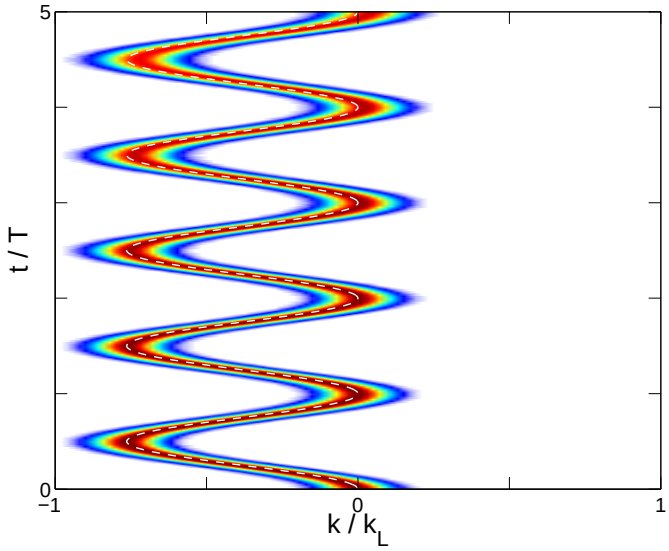

Figure 1.6: Evolution of the k-space distribution initially given by Eq. (1.28) with width $\Delta k/k_{\rm L} = 0.1$, for $K_0 = 1.2$ and $k_{\rm c}/k_{\rm L} = 0$. The white-dashed line indicates the "classical" solution (1.30).

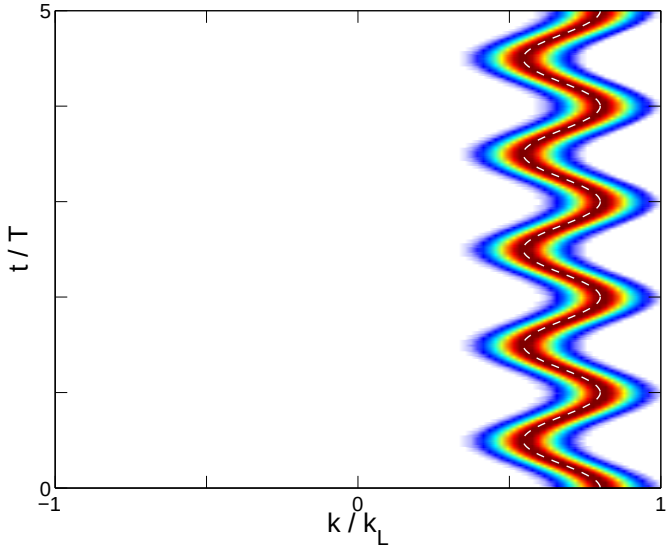

Figure 1.7: Evolution of the k-space distribution initially given by Eq. (1.28) with width $\Delta k/k_{\rm L} = 0.1$, but now for $K_0 = 0.4$ and $k_{\rm c}/k_{\rm L} = 0.8$, so that the white-dashed "classical" solution (1.30) starts from a non-zero value.

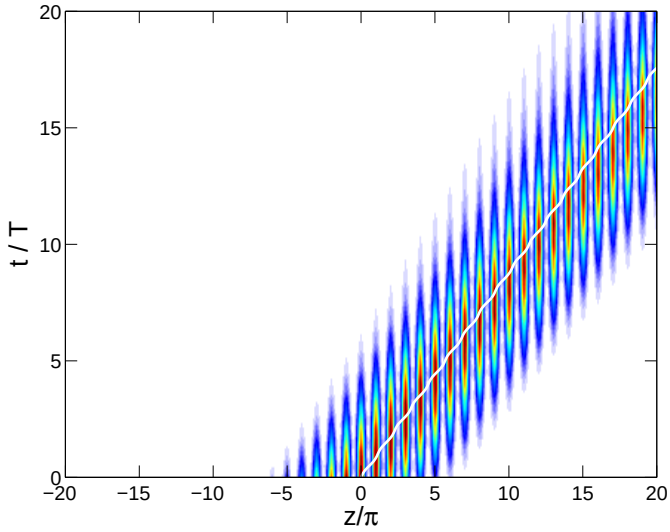

Figure 1.8: Evolution of the Bloch wave packet (1.27) with initial k-space width $\Delta k/k_{\mathrm{L}} = 0.1$ and initial momentum $k_{\mathrm{c}}/k_{\mathrm{L}} = 0.8$, driven with scaled amplitude $K_0 = 0.4$, as corresponding to the k-space distribution depicted in Fig. 1.7. The white line marks the trajectory obtained by integrating the oscillating group velocity (1.32).

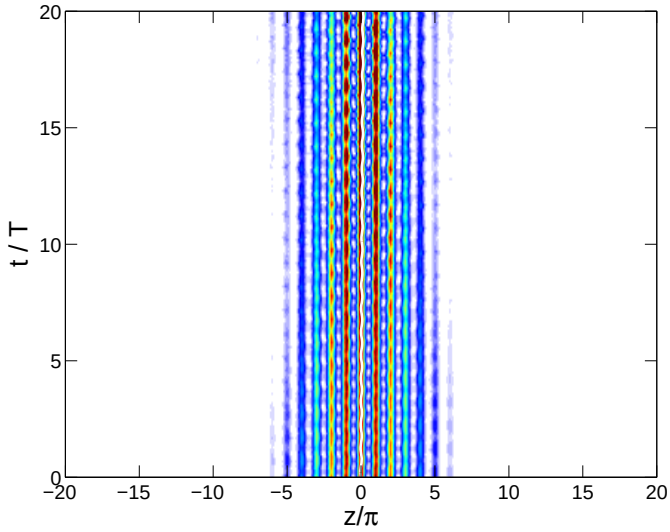

Figure 1.9: Evolution of the Bloch wave packet (1.27) with initial k-space width $\Delta k/k_{\mathrm{L}} = 0.1$ and initial momentum $k_{\mathrm{c}}/k_{\mathrm{L}} = 0.8$, now driven with scaled amplitude $K_0 = 2.35$: Despite the nonzero average momentum, the average group velocity vanishes because of the band collapse. The white line in the center is obtained as described in Fig. 1.8.

This semiclassical behavior is illustrated by a further set of figures. In Fig. 1.6 we plot the evolution of the exact k-space density that originates from the initial condition (1.28). Again we set $\Delta k/k_{\mathrm{L}} = 0.1$, meaning that the distribution is sufficiently narrow to ensure the validity of Eq. (1.31); moreover, $k_{\mathrm{c}}/k_{\mathrm{L}} = 0$ and $K_0 = 1.2$. Since $\phi = \pi/2$, the distribution then oscillates around $\overline{k} = -F_1/(\hbar\omega)$, or $\overline{k}/k_{\mathrm{L}} = -K_0/\pi$, following precisely the k-space trajectory predicted by Eq. (1.30).

A nonzero average momentum of the packet can likewise be achieved by selecting some suitable value of $k_{\mathrm{c}}/k_{\mathrm{L}}$. Figure 1.7 shows an example with $k_{\mathrm{c}}/k_{\mathrm{L}} = 0.8$, while $K_0 = 0.4$ and $\Delta k/k_{\mathrm{L}} = 0.1$. This obviously corresponds to a wave function $\langle x|\psi(t)\rangle$ which moves into the positive x-direction all the time; the density of this wave function is displayed in Fig. 1.8. Here the white line indicates the classical trajectory that results from integrating the group velocity (1.32); indeed, this trajectory describes the motion of the packet's center quite well. When adjusting the driving amplitude to the first collapse, as in Fig. 1.9, the average motion stops despite the nonzero average momentum, as it should; when increasing K_0 to still higher values, so that J_{eff} becomes negative, the packet's direction of motion can even be reversed.

While the semiclassical approach to dynamic localization may be helpful, insofar as it appeals to our intuition, its explanation in terms of "prohibited dephasing" resulting from a quasienergy band collapse is *much* more powerful: This view immediately reveals that not only does the average motion of a wave packet come to a complete standstill, but so does its spreading; moreover, prohibited dephasing applies to *any* initial condition, regardless whether or not its envelope varies suffiently slowly to justify the semiclassical approximation. As an extreme example of "nonclassical" motion we consider in Fig. 1.10 the undriven evolution of a wave function that coincides with a single Wannier function of the optical lattice [12] at $t = 0$, and therefore certainly does not possess a slowly varying envelope then, giving rise to a fairly complex spreading pattern which differs substantially from the semiclassical one previously visualized in Fig. 1.3. Nonetheless, when driven with the amplitude $K_0 = 2.35$ marking the first quasienergy band collapse, one observes another occurrence of dynamic localization, as witnessed by Fig. 1.11; the difference between the two evolution patterns depicted in Figs. 1.10 and 1.11 could hardly be more striking.

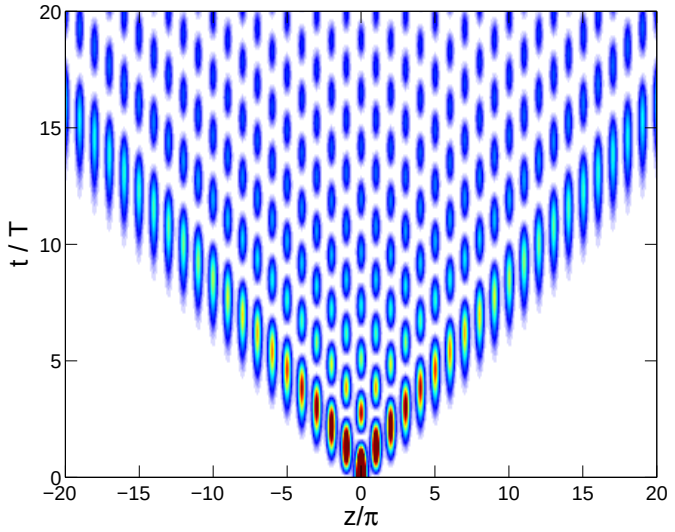

Figure 1.10: Evolution of the wave function that originates from an initial single Wannier state in the undriven lattice. This state does not possess a slowly varying envelope, and thus does not conform to semiclassical dynamics.

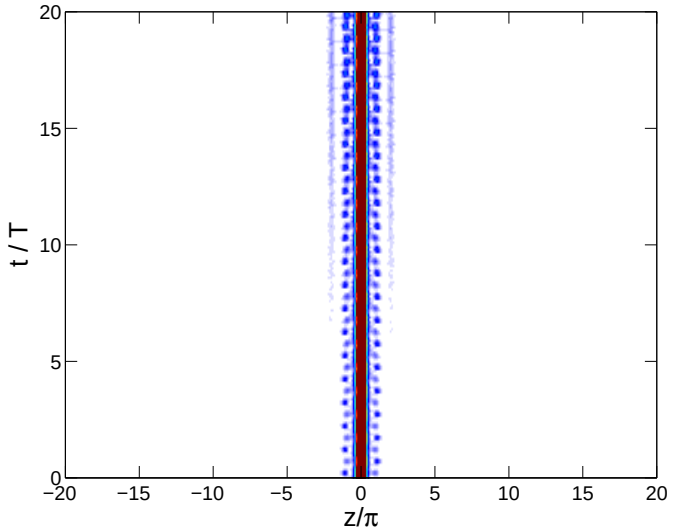

Figure 1.11: Evolution of the wave function that originates from an initial single Wannier state when driven with scaled amplitude $K_0 = 2.35$. The semiclassical approximation is not applicable here, but dynamic localization works nonetheless.

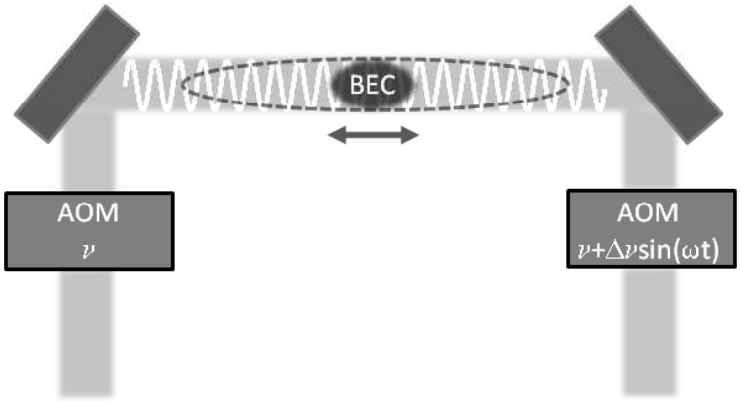

Figure 1.12: Experimental setup for *in-situ* measurement of dynamic localization of a Bose-Einstein condensate (BEC) in a driven optical lattice: The frequencies of two laser beams are shifted with the help of acousto-optic modulators (AOMs) by ν and by $\nu + \Delta\nu \sin(\omega t)$, respectively, before being directed against each other by mirrors. The resulting optical lattice then oscillates in the laboratory frame, giving rise to an oscillating inertial force in the frame of reference co-moving with the lattice. After the initial longitudinal confinement is switched off, the BEC expands by well-to-well tunneling; its final width (indicated by the dashed line) is recorded by imaging its shadow cast by a resonant flash onto a CCD chip. (Figure courtesy of O. Morsch.)

In actual laboratory experiments it is advantageous to work with a phase-coherent atomic Bose-Einstein condensate, rather than with individual atoms: If the density of the condensate is sufficiently low, or if the interatomic s-wave scattering length is tuned close to zero by means of a Feshbach resonance [13], the condensate is practically ideal, so that one effectively can perform a measurement on an ensemble of identically prepared noninteracting atoms in a single shot. Figure 1.12 shows a possible experimental setup [3, 4]: The optical lattice is formed by two laser beams of wavelength λ, which are directed against each other with the help of mirrors. Each beam passes through an acousto-optic modulator which shifts its frequency by ν and by $\nu+\Delta\nu(t)$, respectively. Because of the frequency difference $\Delta\nu(t)$ thus introduced between the counterpropagating beams, the condensate experiences the potential

$$V_{\mathrm{lab}}(x,t) = \frac{V_0}{2} \cos\left(2k_{\mathrm{L}}\left[x + \frac{\lambda}{2}\int_0^t \mathrm{d}\tau\, \Delta\nu(\tau)\right]\right) \tag{1.34}$$

in the laboratory frame, which means that the lattice position shifts in time according to the prescribed protocol $\Delta\nu(t)$. In a frame of reference co-moving with the lattice, this shift

translates into the inertial force

$$F(t) = M\,\frac{\lambda}{2}\,\frac{\mathrm{d}\Delta\nu(t)}{\mathrm{d}t}\;. \tag{1.35}$$

Therefore, choosing $\Delta\nu(t) = \Delta\nu_{\max}\sin(\omega t + \phi)$ leads to the desired Hamiltonian (1.26) in the co-moving frame, with the driving amplitude

$$F_1 = M\omega\,\frac{\lambda}{2}\,\Delta\nu_{\max}\;. \tag{1.36}$$

Now a Bose-Einstein condensate initially trapped in the center of the oscillating lattice is allowed to expand freely in the lattice direction by well-to-well tunneling after switching off the longitudinal confinement, while maintaining a weak transversal confinement in order to keep the condensate in the lattice. After a variable expansion time, the *in situ* width of the condensate is determined by a resonant flash, the shadow cast by which is imaged onto a CCD chip [3]. The measured expansion rate then is to a good approximation proportional to $|J_{\mathrm{eff}}|$, that is, to the absolute value of the effective hopping matrix element (1.12); in principle, even the sign of J_{eff} can be deduced from additional time-of-flight measurements [3]. In Fig. 1.13 we display data for the ratio J_{eff}/J acquired in this manner by the Pisa group with a condensate of ^{87}Rb atoms in a lattice of depth $V_0/E_{\mathrm{rec}} = 6.0$, driven with frequency $\omega/(2\pi) = 4.0$ kHz, after expansion times of 150 milliseconds. Evidently these data match the expected Bessel function $\mathrm{J}_0(K_0)$ quite well even up to the second zero. Note that here one has $\hbar\omega/E_{\mathrm{rec}} = 1.24$, so that the frequency employed in these measurements is significantly higher than in our model calculations. This means that the inequality $4J < \hbar\omega$ is satisfied in a stronger manner, while $\hbar\omega$ still remains reasonably small compared to the band gap. As a consequence, even the second band collapse can be quite well developed. In any case, this figure strikingly demonstrates that the concept of dynamic localization by now has crossed, in the context of mesoscopic matter waves, the threshold from an idealized theoretical concept to a well-controllable laboratory reality.

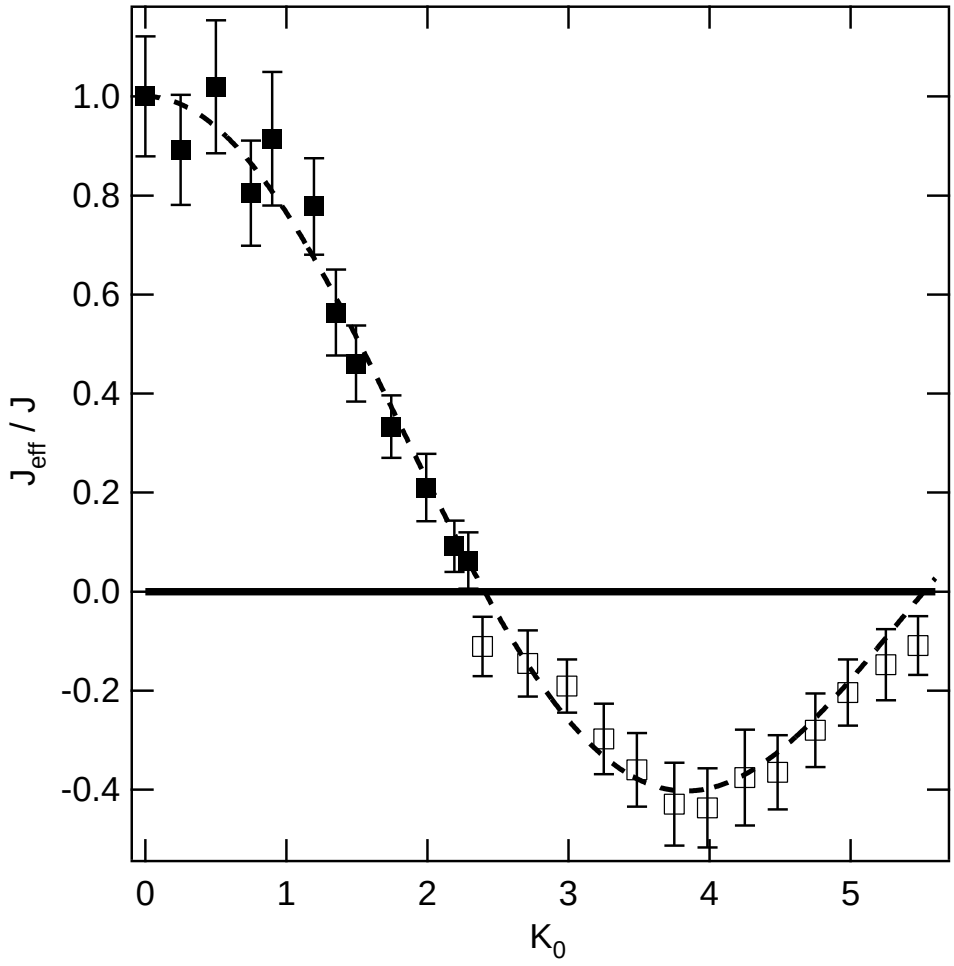

Figure 1.13: Experimental results for the ratio $J_{\rm eff}/J$ of the effective hopping matrix element (1.12) to the bare one as a function of the scaled driving amplitude (1.16), obtained with a Bose-Einstein condensate of ^{87}Rb atoms in an optical lattice with a depth of $V_0 = 6\,E_{\rm rec}$ ($\lambda = 842$ nm), driven with frequency $\omega/(2\pi) = 4.0$ kHz. The dashed line corresponds to the expected Bessel function $\mathrm{J}_0(K_0)$. (Figure courtesy of O. Morsch.)

1.3 What is it good for?

Up to this point we have considered no more than a possible realization of dynamic localization which comes fairly close to the theoretical ideal [1]. Apart from its observation with dilute Bose-Einstein condensates in time-periodically shifted optical lattices [3, 4], this type of quantum wave propagation has meanwhile also been made visible by means of an optical analog based on sinusoidally-curved lithium-niobate waveguide arrays [23]. This is certainly interesting, but it is not what one would call "deep"; the "prohibited dephasing"-view clearly reveals that the only physics entering here is summarized by stating that an initial state is "frozen" in time if the phase factors of all of its spectral components evolve at the same speed. Yet, the accompanying band collapse furnishes a strong hint that there may be more in stock. Namely, when the ideal dynamics is somehow perturbed it is the bandwidth which sets the scale with respect to which the strength of such a perturbation has to be gauged. A prominent example is provided by the repulsive interaction between ultracold atoms in an optical lattice; the strength of this interaction is expressed in terms of a parameter U which quantifies the repulsion energy of one pair of atoms occupying the same lattice site [21]. Accordingly, the characteristic dimensionless parameter then is the ratio U/J; here $J = W/4$ is taken instead of the bandwidth W. Indeed, it is this ratio U/J which decides which quantum phase a gas of ultracold, repulsively interacting atoms in an optical lattice adopts: For $U/J \ll 1$ the system is superfluid, but becomes a Mott insulator when this ratio exceeds a critical value [21]. Hence, when recalling that J is replaced by the effective hopping matrix element (1.12) when the system is driven with appropriate parameters, it is only natural to predict that this superfluid-to-Mott insulator transition can be induced in a time-periodically shifted optical lattice by varying the driving force [24, 25]: Assuming that one starts in the superfluid phase, $J_{\rm eff}$ can then virtually be made arbitrarily small by adjusting the scaled amplitude K_0 to a zero of J_0, resulting in a value of $U/J_{\rm eff}$ so large that the system is forced to enter the Mott regime. The experimental confirmation of this scenario, achieved by the Pisa group [5], probably constitutes the first known example of coherent control exerted by means of time-periodic forcing on a quantum phase transition.

There are other types of perturbations, associated with deviations from perfect transla-

tional symmetry, which affect even noninteracting ultracold atoms in optical lattices. Most notably, the system governed by the tight-binding Hamiltonian

$$H_{\mathrm{AA}} = -J \sum_{\ell} \Big(|\ell+1\rangle\langle\ell| + |\ell\rangle\langle\ell+1| \Big) + V \sum_{\ell} \cos(2\pi g \ell + \delta) |\ell\rangle\langle\ell| \,, \tag{1.37}$$

differing from its antecedent (1.1) through additional on-site energies which oscillate along the lattice with amplitude V, shows a quite peculiar behavior when the number g is irrational, so that this system becomes *quasiperiodic* [26, 27, 28]: As long as $|V/J| < 2$, so that the on-site perturbations are relatively weak, all of its energy eigenstates still remain extended over the entire lattice in a Bloch-like manner, whereas they are all exponentially localized, with one common localization length, when $|V/J| > 2$. Thus, there is a metal-insulator-like, incommensurability-induced transition at $|V/J| = 2$, originally studied by Harper [26] in the context of conduction electrons in a magnetic field, and later by Aubry and André [27]; this transition can be realized approximately with ultracold atoms in a *bichromatic* optical lattice described by the potential

$$V_{\mathrm{bic}}(x) = \frac{V_0}{2} \cos(2k_{\mathrm{L}} x) + V_1 \cos(2g k_{\mathrm{L}} x + \delta) \,. \tag{1.38}$$

The guiding idea here is to employ a primary lattice with depth V_0 for setting up the hosting tight-binding system (1.1), as before, and then to invoke a secondary lattice with much smaller depth $2V_1$ for achieving the required modulation of the local energies at the sites of the host [10, 11]. When the primary lattice is comparatively shallow, possessing a depth of only a few recoil energies, the transition occurs stepwise upon increasing V_1 [12], featuring pronounced mobility edges resulting mainly from the next-to-nearest neighbor couplings between the host's sites which are present in the full bichromatic potential (1.38), but do not occur in the Aubry-André model (1.37). When $V_0/E_{\mathrm{rec}} \gg 1$, so that the primary lattice is so deep that these additional couplings may be safely neglected, the transition occurring in the actual bichromatic lattice (1.38) is fairly sharp. The parameter J then again is given approximately by Eq. (1.25); moreover, one has

$$V/E_{\mathrm{rec}} \sim \frac{V_1}{E_{\mathrm{rec}}} \exp\left(-\frac{g^2}{\sqrt{V_0/E_{\mathrm{rec}}}} \right) \qquad \text{for} \quad V_0/E_{\mathrm{rec}} \gg 1 \tag{1.39}$$

with reasonably chosen g on the order of unity. Therefore, the equation $|V/J| = 2$ marking the metal-insulator-like transition in the ideal Aubry-André model now translates into the estimate [12]

$$\frac{V_1^{\mathrm{c}}}{E_{\mathrm{rec}}} \sim \frac{8}{\sqrt{\pi}} \left(\frac{V_0}{E_{\mathrm{rec}}}\right)^{3/4} \exp\left(-2\sqrt{\frac{V_0}{E_{\mathrm{rec}}}} + \frac{g^2}{\sqrt{V_0/E_{\mathrm{rec}}}}\right) \tag{1.40}$$

for the critical strength V_1^{c} of the secondary optical lattice, given a sufficient depth of the primary one. Indeed, this transiton has been observed with a Bose-Einstein condensate consisting of ^{39}K atoms, using a magnetically tunable Fesbach resonance for rendering these atoms practically noninteracting [13].

When ultracold atoms in such a bichromatic lattice (1.38) are subjected to time-periodic forcing, one obtains an additional knob which can be turned to induce the transition: Because J is replaced by the effective hopping strength (1.12) when the system is suitably driven, one can cross the critical border $|V/J_{\mathrm{eff}}| = 2$ by varying the parameters of the driving force; the critical parameters then are linked approximately by the relation

$$|\mathrm{J}_0(K_0)| \;\sim\; \frac{\sqrt{\pi}}{8} \frac{V_1}{E_{\mathrm{rec}}} \left(\frac{V_0}{E_{\mathrm{rec}}}\right)^{-3/4} \exp\left(+2\sqrt{\frac{V_0}{E_{\mathrm{rec}}}} - \frac{g^2}{\sqrt{V_0/E_{\mathrm{rec}}}}\right) . \tag{1.41}$$

Hence, it is feasible to coherently control the metal-insulator-like transition exhibited by noninteracting ultracold atoms in properly designed bichromatic optical potentials through time-periodic forcing [10, 11]. In order to substantiate this prediction, we now display the results of further numerical wave-packet calculations. In all of these we employ a primary lattice with depth $V_0/E_{\mathrm{rec}} = 5.7$, as in our preceding studies, and fix the incommensurability parameter at the golden mean $g = (\sqrt{5} - 1)/2$ up to numerical accuracy. With this choice, the above estimate (1.40) yields $V_1^{\mathrm{c}}/E_{\mathrm{rec}} \approx 0.165$ for the critical strength of the secondary lattice. The driving frequency is given by $\hbar\omega/E_{\mathrm{rec}} = 0.5$ throughout.

Figure 1.14 visualizes the evolution of a wave function that originates from the same Gaussian initial state as already employed in Fig. 1.3. Here the driving force is still absent, and the depth of the secondary lattice is $V_1/E_{\mathrm{rec}} = 0.10$, placing the system in its metallic phase; accordingly, the wave function readily explores the entire lattice. In contrast, when $V_1/E_{\mathrm{rec}} = 0.25$ and the drive is still switched off, the wave function remains localized as shown

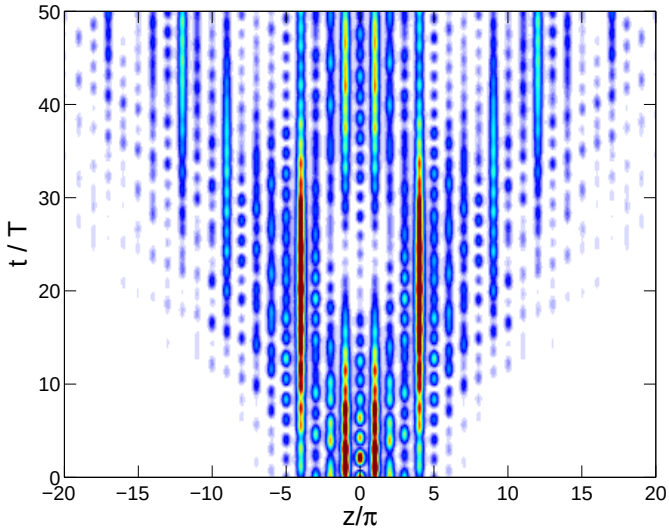

Figure 1.14: Evolution of the same initial wave packet as in Fig. 1.3 in an undriven bichromatic optical lattice (1.38). Here the strength of the secondary potential is $V_1/E_{\rm rec} = 0.10$, so that the system is in its mobile "metallic" phase, allowing the wave function to spread.

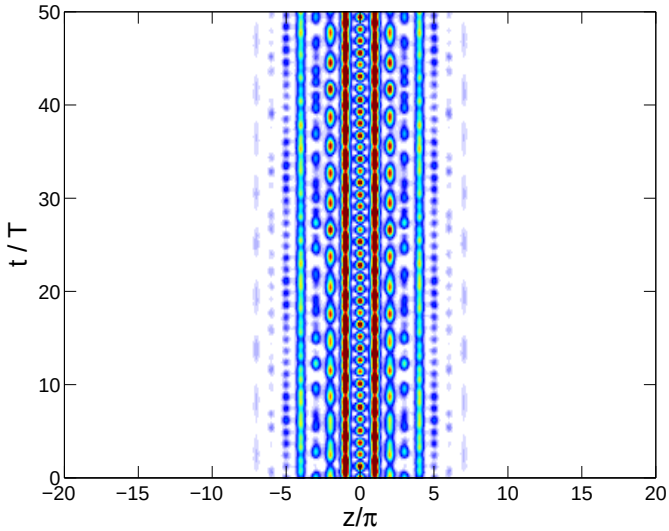

Figure 1.15: Evolution of the same initial wave packet as in Fig. 1.3 in an undriven bichromatic optical lattice (1.38). Here the strength of the secondary potential is $V_1/E_{\rm rec} = 0.25$, so that the system is in its "insulating" phase, keeping the wave function localized.

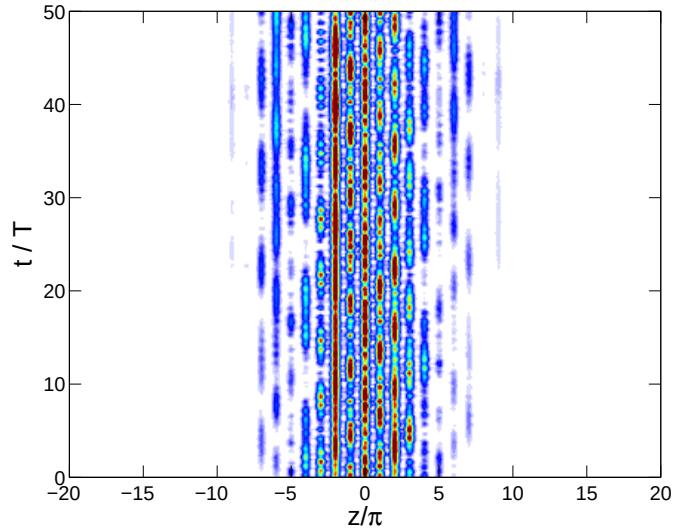

Figure 1.16: Evolution of the same initial wave packet as in Fig. 1.3 in a bichromatic optical lattice (1.38) driven with scaled amplitude $K_0 = 1.7$. The strength of the secondary lattice is $V_1/E_{\rm rec} = 0.10$, as in Fig. 1.14, so that the system would be in its "metallic" phase if there were no forcing.

in Fig. 1.15; this indicates that we are encountering the insulating phase now. But the wave function also remains localized when the secondary lattice is tuned back to $V_1/E_{\rm rec} = 0.10$ and the driving force acts with scaled amplitude $K_0 = 1.7$, as depicted in Fig. 1.16: The relation (1.41) predicts the transition from the metallic to the insulating phase to have occurred already at about $K_0 \approx 1.3$. It should be noted that there is a pronounced difference from the ideal dynamic localization reviewed in the preceding section: There the wave packet remains localized only when K_0 is exactly equal to a zero of J_0. In contrast, here one switches from the metallic into the insulating phase already when $|\mathrm{J}_0(K_0)|$ becomes sufficiently small.

Finally, we show a corresponding sequence of results for wave functions which evolve from an initial Wannier state of the primary lattice. In Fig. 1.17 we again consider an undriven bichromatic lattice with $V_1/E_{\rm rec} = 0.10$, so that the mobile metallic phase enables uninhibited spreading; in Fig. 1.18, where $V_1/E_{\rm rec} = 0.25$, the system's insulating character then keeps the wave function strongly localized. But that same high degree of localization may also be obtained when again resetting the strength of the secondary lattice to $V_1/E_{\rm rec} = 0.10$, and switching on the driving force with scaled amplitude $K_0 = 1.7$, as done in Fig. 1.19.

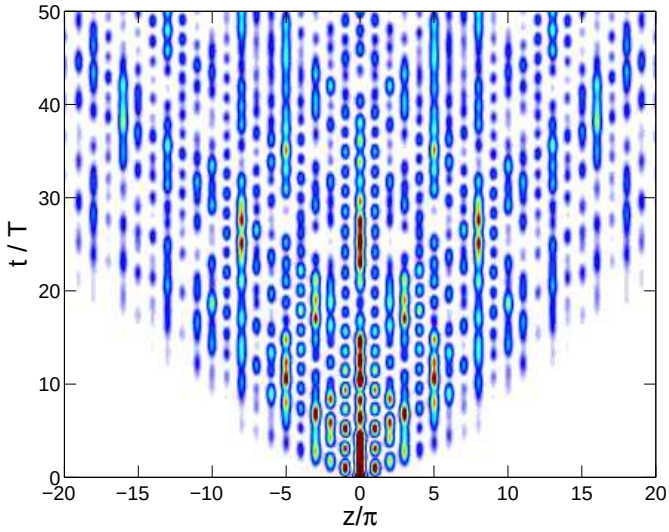

Figure 1.17: Evolution of the wave function originating from a single Wannier state of the primary lattice in an undriven bichromatic optical lattice (1.38). Here the strength of the secondary potential is $V_1/E_{\mathrm{rec}} = 0.10$, so that the system is in its "metallic" phase.

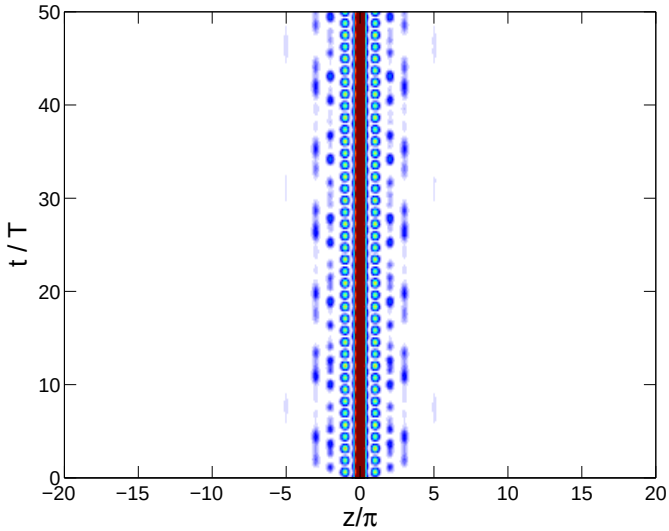

Figure 1.18: Evolution of the wave function originating from a single Wannier state of the primary lattice in an undriven bichromatic optical lattice (1.38). Here the strength of the secondary potential is $V_1/E_{\mathrm{rec}} = 0.25$, so that the system is in its "insulating" phase.

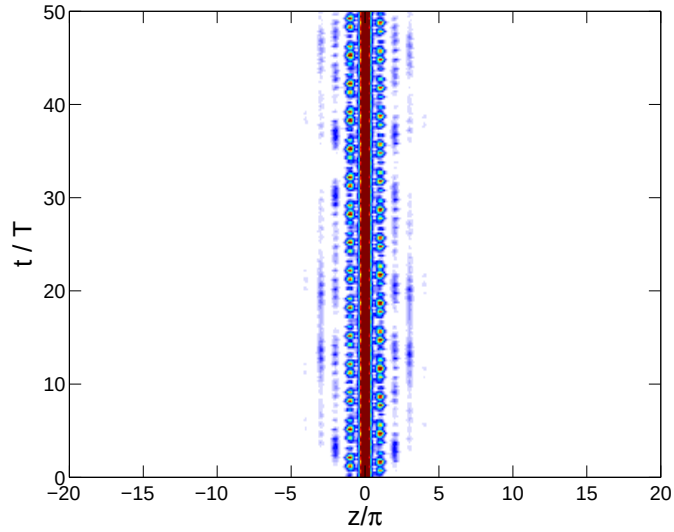

Figure 1.19: Evolution of the wave function originating from a single Wannier state of the primary lattice in a bichromatic optical lattice (1.38) driven with scaled amplitude $K_0 = 1.7$. The strength of the secondary lattice is $V_1/E_{\rm rec} = 0.10$, as in Fig. 1.17, so that the system would be in its "metallic" phase if there were no forcing.

These figures vividly illustrate the main message: In the presence of time-periodic forcing it is the width of the underlying quasienergy band which determines the effective strength of deviations from perfect spatial periodicity. In an ideal lattice without such deviations one encounters "only" dynamic localization, but in lattices with isolated, quasiperiodic, or random perturbations the strengths of these can be adjusted at will by suitably selecting the parameters of the drive. With regard to experimental tests, the enormous flexibility offered by ultracold atoms in optical potentials makes such systems far superior to electrons in ac-driven crystal lattices.

When the concept of controlling the incommensurability-induced metal-insulator transition exhibited by the Aubry-André model (1.37) by means of time-periodic forcing was conceived [10, 11] the experimental investigation of ultracold atoms in optical lattices was still in its infancies. But now that this transition has been unambiguously observed with a non-interacting Bose-Einstein condensate [13], the demonstration of its coherent control has come into immediate reach. Besides the already established coherent control of the interaction-induced superfluid-to-Mott insulator transition [5], this demonstration would constitute a

further milestone achievement in the on-going effort to explore the newly emerging prospects provided by dressed matter waves.

Acknowledgments

We thank O. Morsch and E. Arimondo for continuing discussions of their experiments [3, 4, 5], and O. Morsch in particular for providing Figs. 1.12 and 1.13. This work was supported by the Deutsche Forschungsgemeinschaft under Grant No. HO 1771/6.

References

[1] D. H. Dunlap and V. M. Kenkre, "Dynamic localization of a charged particle moving under the influence of an electric field", *Phys. Rev. B* **34**, 3625-3633 (1986).

[2] M. M. Dignam and C. M. de Sterke, "Conditions for dynamic localization in generalized ac electric fields", *Phys. Rev. Lett.* **88**, 046806 (2002).

[3] H. Lignier, C. Sias, D. Ciampini, Y. Singh, A. Zenesini, O. Morsch, and E. Arimondo, "Dynamical control of matter-wave tunneling in periodic potentials", *Phys. Rev. Lett.* **99**, 220403 (2007).

[4] A. Eckardt, M. Holthaus, H. Lignier, A. Zenesini, D. Ciampini, O. Morsch, and E. Arimondo, "Exploring dynamic localization with a Bose-Einstein condensate", *Phys. Rev. A* **79**, 013611 (2009).

[5] A. Zenesini, H. Lignier, D. Ciampini, O. Morsch, and E. Arimondo, "Coherent control of dressed matter waves", *Phys. Rev. Lett.* **102**, 100403 (2009).

[6] M. Holthaus, "Collapse of minibands in far-infrared irradiated superlattices", *Phys. Rev. Lett.* **69**, 351-354 (1992).

[7] M. Holthaus and D. Hone, "Quantum wells and superlattices in strong time-dependent fields", *Phys. Rev. B* **47**, 6499-6508 (1993).

[8] D. W. Hone and M. Holthaus, "Locally disordered lattices in strong ac electric fields", *Phys. Rev. B* **48**, 15123-15131 (1993).

[9] M. Holthaus, G.H. Ristow, and D.W. Hone, "ac-field-controlled Anderson localization in disordered semiconductor superlattices", *Phys. Rev. Lett.* **75**, 3914-3917 (1995).

[10] K. Drese and M. Holthaus, "Ultracold atoms in modulated standing light waves", *Chem. Phys.* **217** (Special issue: *Dynamics of Driven Quantum Systems*), 201-219 (1997).

[11] K. Drese and M. Holthaus, "Exploring a metal-insulator transition with ultracold atoms in standing light waves?", *Phys. Rev. Lett.* **78**, 2932-2935 (1997).

[12] D. J. Boers, B. Goedeke, D. Hinrichs, and M. Holthaus, "Mobility edges in bichromatic optical lattices", *Phys. Rev. A* **75**, 063404 (2007).

[13] G. Roati, C. D'Errico, L. Fallani, M. Fattori, C. Fort, M. Zaccanti, G. Modugno, M. Modugno, and M. Inguscio, "Anderson localization of a non-interacting Bose-Einstein condensate", *Nature* **453**, 895-898 (2008).

[14] W. V. Houston, "Acceleration of electrons in a crystal lattice", *Phys. Rev.* **57**, 184-186 (1940).

[15] J. H. Shirley, "Solution of the Schrödinger equation with a Hamiltonian periodic in time", *Phys. Rev.* **138**, B979-B987 (1965).

[16] Ya. B. Zel'dovich, "The quasienergy of a quantum-mechanical system subjected to a periodic action", *Zh. Eksp. Theor. Fiz.* **51**, 1492-1495 (1966) [*Sov. Phys. JETP* **24**, 1006-1008 (1967)].

[17] V. I. Ritus, "Shift and splitting of atomic energy levels by the field of an electromagnetic wave", *Zh. Eksp. Theor. Fiz.* **51**, 1544-1549 (1966) [*Sov. Phys. JETP* **24**, 1041-1044 (1967)].

[18] H. Sambe, "Steady states and quasienergies of a quantum-mechanical system in an oscillating field", *Phys. Rev. A* **7**, 2203-2213 (1973).

[19] S. Arlinghaus and M. Holthaus, "Driven optical lattices as strong-field simulators", *Phys. Rev. A* **81**, 063612 (2010).

[20] O. Morsch and M. Oberthaler, "Dynamics of Bose-Einstein condensates in optical lattices", *Rev. Mod. Phys.* **78**, 179-215 (2006).

[21] I. Bloch, J. Dalibard, and W. Zwerger, "Many-body physics with ultracold gases", *Rev. Mod. Phys.* **80**, 885-964 (2008).

[22] N. W. Ashcroft and N. D. Mermin, "Solid state physics", Harcourt College Publishers, Fort Worth, 1976 (see chapter 12 therein).

[23] S. Longhi, M. Marangoni, M. Lobino, R. Ramponi, P. Laporta, E. Cianci, and V. Foglietti, "Observation of dynamic localization in periodically curved waveguide arrays", *Phys. Rev. Lett.* **96**, 243901 (2006).

[24] A. Eckardt, C. Weiss, and M. Holthaus, "Superfluid-insulator transition in a periodically driven optical lattice", *Phys. Rev. Lett.* **95**, 260404 (2005).

[25] C. E. Creffield and T. S. Monteiro, "Tuning the Mott transition in a Bose-Einstein condensate by multiple photon absorption", *Phys. Rev. Lett.* **96**, 210403 (2006).

[26] P. G. Harper, "Single band motion of conduction electrons in a uniform magnetic field", *Proc. Phys. Soc. A* **68**, 874-878 (1955).

[27] S. Aubry and G. André, "Analyticity breaking and Anderson localization in incommensurate lattices", *Ann. Israel Phys. Soc.* **3**, 133-140 (1980).

[28] J. B. Sokoloff, "Unusual band structure, wave functions and electrical conductance in crystals with incommensurate periodic potentials", *Phys. Rep.* **126**, 189-244 (1985).

III

III. Generalized acceleration theorem for spatiotemporal Bloch waves

Stephan Arlinghaus and Martin Holthaus,
Generalized acceleration theorem for spatiotemporal Bloch waves,
Phys. Rev. B **84**, 054301 (2011).

PHYSICAL REVIEW B **84**, 054301 (2011)

Generalized acceleration theorem for spatiotemporal Bloch waves

Stephan Arlinghaus and Martin Holthaus
Institut für Physik, Carl von Ossietzky Universität, D-26111 Oldenburg, Germany
(Received 22 April 2011; published 8 August 2011)

A representation is put forward for wave functions of quantum particles in periodic lattice potentials subjected to homogeneous time-periodic forcing, based on an expansion with respect to Bloch-like states which embody both the spatial and the temporal periodicity. It is shown that there exists a generalization of Bloch's famous acceleration theorem which grows out of this representation and captures the effect of a weak probe force applied in addition to a strong dressing force. Taken together, these elements point at a "dressing and probing" strategy for coherent wave-packet manipulation, which could be implemented in present experiments with optical lattices.

DOI: 10.1103/PhysRevB.84.054301 PACS number(s): 72.10.Bg, 67.85.Hj, 42.50.Hz, 03.75.Lm

I. INTRODUCTION

The so-called acceleration theorem for wave-packet motion in periodic potentials, formulated already in 1928 by Bloch,[1] has proven to be of outstanding value to solid-state physics for understanding the dynamics of Bloch electrons within a semiclassical picture.[2,3] In its most-often used variant, this theorem states that if we consider an electronic wave packet in a spatially periodic lattice, which is centered in k space around some wave vector $\vec{k}_c$, and if an external electric field $\vec{E}(t)$ is applied under single-band conditions, then this center wave vector evolves in time according to $\hbar\dot{\vec{k}}_c(t) = -e\vec{E}(t)$, with $-e$ being the electronic charge. Perhaps its best-known application is the explanation of Bloch oscillations of particles exposed to a homogeneous, constant force,[4–16] which we recapitulate here in the simplest guise: Take a particle in a one-dimensional tight-binding energy band $E(k) = -(W/2)\cos(ka)$, where W is the band width and a denotes the lattice period. Assume that the particle's wave packet is centered around $k_c(0)$ initially and subjected to a homogeneous force of strength F. Then the acceleration theorem, now taking the form

$$\hbar\dot{k}_c(t) = F, \tag{1}$$

tells us $k_c(t) = k_c(0) + Ft/\hbar$, so that the packet moves through k space at a constant rate.[1] According to another classic work by Jones and Zener,[17] the particle's group velocity $v_g(t)$ in real space is determined, quite generally, by the derivative of $E(k)$ with respect to k when evaluated at the moving center $k_c(t)$,

$$v_g(t) = \frac{1}{\hbar}\left.\frac{dE}{dk}\right|_{k_c(t)}. \tag{2}$$

In our case, this relation immediately gives

$$v_g(t) = \frac{Wa}{2\hbar}\sin[k_c(0)a + \omega_B t], \tag{3}$$

implying that the particle's response to the constant force is an oscillating motion with the Bloch frequency[18] $\omega_B = Fa/\hbar$. This elementary example, to which we will come back later in Sec. IV, strikingly illustrates the power of this type of approach. But an obvious restriction stems from the necessity to remain within the scope of the single-band approximation; the above acceleration theorem (1) is put out of action when several Bloch bands are substantially coupled by the external force. Nonetheless, in the present work we demonstrate that there exists a generalization of the acceleration theorem which can be applied even under conditions of strong interband transitions. Specifically, we consider situations in which a Bloch particle is subjected to a strong oscillating force which possibly induces pronounced transitions between the unperturbed energy bands. By abandoning the customary crystal-momentum representation[19] and introducing an alternative Floquet representation instead, we show that the effect of an additional force then is well captured by another acceleration theorem which closely mimics the spirit of the original. We obtain two major results: The Floquet analog (32) of Bloch's acceleration theorem (1), and the Floquet analog (42) of the Jones-Zener expression (2) for the group velocity. These findings are particularly useful for control applications, when a strong oscillating field "dresses" the lattice and thus significantly alters its band structure, while a second, comparatively weak homogeneous force is employed to effectuate controlled population transfer. We first outline the formal mathematical arguments in Secs. II and III, and then we give two applications of topical interest, discussing "super" Bloch oscillations in Sec. IV and coherently controlled interband population transfer in Sec. V. Although we restrict ourselves here for notational simplicity to one-dimensional lattices, our results can be carried over to general, higher-dimensional settings.

II. THE FLOQUET REPRESENTATION

We consider a particle of mass m moving in a one-dimensional lattice potential $V(x) = V(x + a)$ with spatial period a under the influence of a homogeneous, time-dependent force $F(t)$, as described by the Hamiltonian

$$\widetilde{H}_0(x,t) = \frac{p^2}{2m} + V(x) - F(t)x. \tag{4}$$

Subjecting the particle's wave function $\widetilde{\psi}(x,t)$ to the unitary transformation

$$\widetilde{\psi}(x,t) = \exp\left(\frac{i}{\hbar}x\int_0^t d\tau\, F(\tau)\right)\psi(x,t), \tag{5}$$

the new function $\psi(x,t)$ obeys the Schrödinger equation

$$i\hbar\frac{\partial}{\partial t}\psi(x,t) = H_0(x,t)\psi(x,t), \tag{6}$$

with the transformed Hamiltonian

$$H_0(x,t) = \frac{1}{2m}\left(p + \int_0^t d\tau\, F(\tau)\right)^2 + V(x). \tag{7}$$

Now let us further assume that the force $F(t)$ is periodic in time with period T, such that its one-cycle integral either vanishes or equals an integer multiple of $\hbar$ times the reciprocal lattice wave number $2\pi/a$:

$$\int_0^T dt\, F(t) = r \times \hbar\frac{2\pi}{a}, \quad r = 0, \pm 1, \pm 2, \ldots. \tag{8}$$

For example, this is accomplished by a monochromatic oscillating force with an additional static bias,

$$F(t) = F_r + F_{\rm ac}\cos(\omega t), \tag{9}$$

provided the latter satisfies the condition $F_r a = r\hbar\omega$. Then the Floquet theorem guarantees that the time-dependent Schrödinger equation (6) admits a complete set of spatiotemporal Bloch waves,[20–22] that is, of solutions of the form

$$\psi_{n,k}(x,t) = \exp[ikx - i\varepsilon_n(k)t/\hbar]u_{n,k}(x,t), \tag{10}$$

with spatially *and* temporally periodic functions

$$u_{n,k}(x,t) = u_{n,k}(x+a,t) = u_{n,k}(x,t+T). \tag{11}$$

As usual, n is the band index and k a wave number; $\varepsilon_n(k)$ thus is the quasienergy dispersion relation for the nth band. If $r = 0$ in Eq. (8), the existence of these solutions is obvious, because then $H_0(x,t) = H_0(x+a,t) = H_0(x,t+T)$, so that the wave functions (10) generalize the customary Bloch waves[1] for particles in spatially periodic lattice potentials by also accounting for the temporal periodicity of the driving force. When $r \neq 0$, so that $H_0(x,t)$ itself is not periodic in time, spatiotemporal Bloch waves (10) emerge nonetheless because k is projected to the first quasimomentum Brillouin zone, as first discussed by Zak.[23] In any case, the quasienergies $\varepsilon_n(k)$ may depend in a complicated manner on the parameters of the driving force, and the wave functions $\psi_{n,k}(x,t)$ pertaining to a single quasienergy band may be nontrivial mixtures of several unperturbed energy bands. For later use, we observe that their spatial parts

$$\varphi_{n,k}(x,t) = \exp(ikx)u_{n,k}(x,t) \tag{12}$$

obey the quasienergy eigenvalue equation

$$\left(H_0(x,t) - i\hbar\frac{\partial}{\partial t}\right)\varphi_{n,k}(x,t) = \varepsilon_n(k)\varphi_{n,k}(x,t), \tag{13}$$

as follows immediately when plugging the solutions (10) into the Schrödinger equation (6). Throughout, we adopt the standard normalization

$$\int_{-\infty}^{\infty} dx\, \varphi^*_{n',k'}(x,t)\varphi_{n,k}(x,t) = \frac{2\pi}{a}\delta_{n,n'}\delta(k-k'). \tag{14}$$

An arbitrary wave packet $\psi(x,t)$ may now be expanded with respect to these spatiotemporal Bloch waves and written in the form

$$\psi(x,t) = \sum_n \sqrt{\frac{a}{2\pi}}\int_{\mathcal{B}} dk\, g_n(k,t)\varphi_{n,k}(x,t), \tag{15}$$

with $\mathcal{B} = [-\pi/a, \pi/a[$ denoting the fundamental Brillouin zone. The expansion coefficients $g_n(k,t)$ depend on the way the system has been prepared and on the way the driving force has been turned on, whereas the basis functions $\varphi_{n,k}(x,t)$ and their quasienergies $\varepsilon_n(k)$ are given by the eigenvalue equation (13) and obviously are independent of such details. Clearly, one has

$$g_n(k,t) = g_n(k,0)\exp[-i\varepsilon_n(k)t/\hbar], \tag{16}$$

so that the populations $|g_n(k,t)|^2$ remain constant in time. This expansion (15), referred to as the Floquet representation of the wave packet, is formally reminiscent of its customary crystal-momentum representation, that is, of an expansion with respect to the Bloch states of the unperturbed potential $V(x)$ which underlies the standard acceleration theorem.[19,24] There are, however, substantial differences which become most clear when considering a wave packet occupying a single quasienergy band,

$$\psi(x,t) = \sqrt{\frac{a}{2\pi}}\int_{\mathcal{B}} dk\, g(k,t)\varphi_k(x,t); \tag{17}$$

here and in the following, we omit the band index n for ease of notation. Now this wave packet (17) may describe, for instance, the dynamics in a situation where two unperturbed energy bands are resonantly coupled by the driving force $F(t)$; consequently, in a crystal-momentum representation one would have to account for Rabi-type oscillations between these two bands by coefficients which quantify the oscillating band populations. In the Floquet respresentation, on the other hand, the Rabi oscillations are already incorporated into the basis states (10), so that one merely encounters single quasienergy band dynamics, with the remaining time evolution of $g(k,t)$ simply given by Eq. (16). Thus, although the external force effectuates transitions between the unperturbed Bloch bands, there are no inter-quasienergy band transitions; $|g(k,t)|^2$ remains constant in time. Second, even in a situation where $F(t)$ does not couple different energy bands, the wave packet's center $k_{\rm c}(t)$ evolves according to the standard acceleration theorem $\hbar\dot{k}_{\rm c} = F$ in the crystal-momentum representation, whereas in the Floquet representation the moment

$$\langle k\rangle = \int_{\mathcal{B}} dk\, k|g(k,t)|^2 \tag{18}$$

obviously stays constant in time. In short, an expansion of the wave packet with respect to the spatiotemporal Bloch waves (10) implies constant coefficients, and hence constant occupation probabilities, if the external force $F(t)$ adheres to the specification (8). This formal shift of the dynamics from the occupation numbers to the basis states which is implied by the Floquet representation now allows for a clear and physically transparent description of the additional effects which emerge when the external force does *not* obey Eq. (8); these effects are captured by the generalized acceleration theorem exposed in the following.

III. THE FLOQUET ACCELERATION THEOREM

We take a wave packet occupying a single quasienergy band and stipulate that in addition to the possibly strong driving force $F(t)$ there is a second homogeneous force $F_{\rm p}(t)$ which

we denote as the *probe force*; this is assumed to be sufficiently weak so that it does not introduce transitions among different quasienergy bands. To be precise, the total Hamiltonian now reads

$$\widetilde{H}(x,t) = \frac{p^2}{2m} + V(x) - F(t)x - F_{\rm p}(t)x, \tag{19}$$

where the time-periodic force $F(t)$ is resonant in the sense of Eq. (8) and thus creates a basis of spatiotemporal Bloch waves (10), whereas the probe force $F_{\rm p}(t)$ also is spatially homogeneous, but not necessarily periodic in time. After performing the unitary transformation (5), we obtain the Hamiltonian in the form

$$H(x,t) = H_0(x,t) - F_{\rm p}(t)x, \tag{20}$$

with $H_0(x,t)$ given by Eq. (7). Moreover, we start from an initial wave packet of the form (17). Because of the additional probe force $F_{\rm p}(t)$, the time evolution of $g(k,t)$ is no longer given by Eq. (16); the aim now is to find an effective Hamiltonian $\mathcal{H}$ which governs the resulting dynamics of $g(k,t)$, under the proposition that this remains restricted to the single, initially occupied quasienergy band.

Exploiting the normalization (14), we have

$$g(k,t) = \sqrt{\frac{a}{2\pi}} \int dx\, \varphi_k^*(x,t)\psi(x,t). \tag{21}$$

This gives

$$\begin{aligned} i\hbar\frac{\partial g}{\partial t} &= \sqrt{\frac{a}{2\pi}} \int dx \left(i\hbar\frac{\partial \varphi_k^*}{\partial t}\psi + \varphi_k^* H\psi \right) \\ &= \sqrt{\frac{a}{2\pi}} \int dx \left(\left[H_0 - i\hbar\frac{\partial}{\partial t} \right] \varphi_k \right)^* \psi \\ &\quad - \sqrt{\frac{a}{2\pi}} F_{\rm p} \int dx\, \varphi_k^* x \psi, \end{aligned} \tag{22}$$

having suppressed the arguments x and t for better legibility; all integrals here are taken over the entire lattice. In the first term on the right-hand side of this equation we exploit the quasienergy eigenvalue equation, Eq. (13), yielding $\varepsilon(k)g(k,t)$. For rewriting the second term we use

$$\varphi_k^* x = i\,\partial_k \varphi_k^* - i\,{\rm e}^{-ikx}\partial_k u_k^*, \tag{23}$$

which is obtained by taking the derivative of the complex conjugate to Eq. (12) with respect to k, and leads to

$$\begin{aligned} \sqrt{\frac{a}{2\pi}} \int dx\, \varphi_k^* x \psi &= i\,\partial_k g - i\sqrt{\frac{a}{2\pi}} \int dx\, {\rm e}^{-ikx}\partial_k u_k^* \psi \\ &= i\,\partial_k g - i\,\langle \partial_k u_k | u_k \rangle g. \end{aligned} \tag{24}$$

For making the final step, we have resubstituted the expression (17) for ψ and have made use of the identity

$$\int dx\, {\rm e}^{i(k'-k)x} u_{k'} \partial_k u_k^* = \frac{2\pi}{a}\delta(k-k')\langle \partial_k u_k | u_k \rangle, \tag{25}$$

with the scalar product

$$\langle \partial_k u_k | u_k \rangle = \int_0^a dx\, u_k(x,t)\partial_k u_k^*(x,t) \tag{26}$$

being given by an integral over a single lattice period. Note that

$$\langle u_k | u_k \rangle = 1, \tag{27}$$

as an immediate consequence of Eq. (14), which implies

$$\langle \partial_k u_k | u_k \rangle + \langle \partial_k u_k | u_k \rangle^* = 0, \tag{28}$$

so that $\langle \partial_k u_k | u_k \rangle$ is purely imaginary. Collecting all the pieces, we obtain the desired evolution equation

$$i\hbar\frac{\partial}{\partial t} g(k,t) = \mathcal{H} g(k,t), \tag{29}$$

with the effective Hamiltonian for the Floquet representation,

$$\mathcal{H} = \varepsilon(k) - i\,F_{\rm p}\partial_k - F_{\rm p}\,{\rm Im}\langle \partial_k u_k | u_k \rangle. \tag{30}$$

From this expression we deduce the generalized acceleration theorem, that is, the acceleration theorem for the Floquet representation: Since the moment (18) obeys the the equation

$$\frac{d}{dt}\langle k \rangle = \frac{i}{\hbar}\langle [\mathcal{H}, k] \rangle \tag{31}$$

and the commutator appearing here on the right-hand side is easily evaluated, $i[\mathcal{H},k] = F_{\rm p}$, we are directly led to

$$\hbar\frac{d}{dt}\langle k \rangle(t) = F_{\rm p}(t). \tag{32}$$

This is the central result of the present work; its analogy to the standard acceleration theorem (1) for the crystal-momentum representation is evident. Observe that there is an intuitively clear reason for the appearance of the term proportional to $\langle \partial_k u_k | u_k \rangle$ in the effective Hamiltonian (30): The twofold periodic parts $u_k(x,t)$ of the spatiotemporal Bloch waves are obtained by solving the eigenvalue equation (13). This is done for each wave number k separately, so that one is free to bestow upon each eigensolution an arbitrary phase factor $\exp[i\theta(k)]$. On the other hand, the evolution equation (29) for the wave function $g(k,t)$ in the Floquet representation naturally establishes a "connection" between those different eigensolutions[25,26] and therefore requires information about the gauge function $\theta(k)$; this is provided by the expression $\langle \partial_k u_k | u_k \rangle$. Note further that when multiplying Eq. (29) by $g^*(k,t)$ and subtracting the complex conjugate of the resulting equation, this piece drops out, and one is left with

$$\left(\frac{\partial}{\partial t} + \frac{F_{\rm p}(t)}{\hbar}\frac{\partial}{\partial k} \right) |g(k,t)|^2 = 0. \tag{33}$$

Thus, $|g(k,t)|^2$ does not depend on k and t separately, but rather on the combination $k - \int_0^t d\tau\, F_{\rm p}(\tau)/\hbar$, so that the distribution $g(k,t)$ moves through the Floquet k space without change of shape, again in precise analogy to the classic behavior.[1] But we reemphasize that this seemingly simple dynamics might be unrecognizable in the usual crystal-momentum representation, because the system might undergo violent transitions between different energy bands when monitored in a basis of time-independent Bloch waves.

As the introductory example has shown, the standard (crystal momentum) acceleration theorem develops its main power in combination with the Jones-Zener expression (2) for the wave packet's group velocity in real space, and the question naturally arises whether there exists a similar

connection in the Floquet representation. Obviously, one can establish a relation corresponding to Eq. (2) by applying a stationary-phase argument to the expansion (15), but here we follow an alternative line of reasoning which may be found particularly enlightening. Considering a well-localized wave packet $\widetilde{\psi}(x,t)$ in the original frame of reference to which the Hamiltonian operators (4) and (19) pertain, that packet's group velocity is given by

$$\begin{aligned} v_{\mathrm{g}}(t) &= \frac{d}{dt}\langle\widetilde{\psi}(x,t)|x|\widetilde{\psi}(x,t)\rangle \\ &= \frac{1}{m}\langle\widetilde{\psi}(x,t)|p|\widetilde{\psi}(x,t)\rangle. \end{aligned} \tag{34}$$

On the other hand, exploiting the operator identity

$$\mathrm{e}^{-ikx}\,p\,\mathrm{e}^{ikx} = p + \hbar k, \tag{35}$$

the eigenvalue equation (13) transforms into the even more basic eigenvalue equation

$$\left(H_k(x,t) - i\hbar\frac{\partial}{\partial t}\right)u_{n,k}(x,t) = \varepsilon_n(k)u_{n,k}(x,t) \tag{36}$$

for the periodic core pieces $u_{n,k}(x,t)$ of the spatiotemporal Bloch waves (10), invoking the parametrically k-dependent operator

$$H_k(x,t) = \frac{1}{2m}\left(p + \hbar k + \int_0^t d\tau\, F(\tau)\right)^2 + V(x). \tag{37}$$

This eigenvalue problem can efficiently be implemented for numerical calculations.[21] It also manifestly contains the origin of the condition (8) imposed on the oscillating force $F(t)$, since k is reduced to fall within $\mathcal{B}$. Most importantly, this eigenvalue problem (36) poses itself in an extended Hilbert space made up of functions $u_{n,k}(x,t)$ which are periodic in both space and time, in accordance with Eq. (11). Consequently, "time" has to be regarded as a coordinate in this extended Hilbert space and therefore needs to be integrated over when forming a scalar product, just like any spatial coordinate. Thus, the natural scalar product in this extended Hilbert space is given by[27]

$$\langle\!\langle\cdot|\cdot\rangle\!\rangle \equiv \frac{1}{T}\int_0^T dt\,\langle\cdot|\cdot\rangle, \tag{38}$$

with $\langle\cdot|\cdot\rangle$ denoting the standard scalar product in the original, physical Hilbert space, as already employed in Eqs. (26) and (27). It follows that the quasienergies $\varepsilon_n(k)$ can be written as diagonal elements of the matrix of the quasienergy operator,

$$\varepsilon_n(k) = \langle\!\langle u_{n,k}|H_k - i\hbar\partial_t|u_{n,k}\rangle\!\rangle\ , \tag{39}$$

inviting us to make use of an analog of the Hellmann-Feynman theorem:[27]

$$\begin{aligned} \frac{d}{dk}\varepsilon_n(k) &= \langle\!\langle u_{n,k}|\frac{dH_k}{dk}|u_{n,k}\rangle\!\rangle \\ &= \frac{\hbar}{m}\langle\!\langle u_{n,k}|p + \hbar k + \int_0^t d\tau\ F(\tau)|u_{n,k}\rangle\!\rangle \\ &= \frac{\hbar}{m}\langle\!\langle\widetilde{\psi}_{n,k}|p|\widetilde{\psi}_{n,k}\rangle\!\rangle. \end{aligned} \tag{40}$$

In the final step we have undone the shift (35); the wave functions $\widetilde{\psi}_{n,k}(x,t)$ then denote the functions which are obtained from the spatiotemporal Bloch waves (10) by inverting the transformation (5). Comparison of Eqs. (34) and (40), keeping in mind the definition (38), now yields the desired relation: Supposing that $\widetilde{\psi}(x,t) = \widetilde{\psi}_{n,k_0}(x,t)$ were made up from a single spatiotemporal Bloch wave labeled by n and k_0, say, one would obtain the formal identity

$$\overline{v}_{\mathrm{g}} \equiv \frac{1}{T}\int_0^T dt\ v_{\mathrm{g}}(t) = \frac{1}{\hbar}\left.\frac{d\varepsilon_n}{dk}\right|_{k_0}. \tag{41}$$

But this is not what we want, because an individual spatiotemporal Bloch wave is uniformly extended over the lattice and thus does not correspond to a "group" which propagates in space. Rather, we require a wave packet (17) which is reasonably well centered in the Floquet k space, with a center $\langle k\rangle$ given by Eq. (18). Then we have

$$\overline{v}_{\mathrm{g}} = \frac{1}{\hbar}\left.\frac{d\varepsilon_n}{dk}\right|_{\langle k\rangle} \tag{42}$$

to good accuracy, so that the cycle-averaged group velocity of the Floquet wave packet is given by the derivative of its quasienergy dispersion relation, evaluated at its center $\langle k\rangle$. Again, this Floquet relation (42) closely mimics its historic crystal-momentum antecessor, given by Eq. (2). In contrast to the equation of motion (32) for $\langle k\rangle$ itself, which holds exactly within a single quasienergy band setting, this relation (42) is an approximation which holds the better, the narrower the packet's Floquet k-space distribution. Although it seems self-evident, it might be worthwhile to stress that the argument required to evaluate the derivative (42) is Floquet $\langle k\rangle$, not crystal momentum k_{c}.

IV. SUPER BLOCH OSCILLATIONS

The phenomenon termed "super" Bloch oscillations[28] arises when a Bloch particle is subjected to both a static (dc) and an oscillating (ac) force, such that an integer multiple of the ac frequency is only slightly detuned from the Bloch frequency associated with the dc component of the force.[28–31] Although the effect itself appears almost trivial from the mathematical point of view, we nonetheless dwell on this at some length, because it provides a particularly instructive example for juxtaposing the familiar crystal-momentum representation to the Floquet representation introduced in Sec. II and for demonstrating in detail how they match. To be definite, we consider the total force to be of the form

$$F(t) = \Theta(t - t_0)[F_{\mathrm{dc}} + F_{\mathrm{ac}}\cos(\omega t)], \tag{43}$$

where $\Theta(t)$ denotes the Heaviside function, so that both the dc and the ac component of the force are turned on instantaneously and simultaneously at t_0; that moment t_0 thus determines the relative phase between the Bloch oscillations caused by the dc component and the driving oscillations of the ac component.

The basic assumptions now are that (i) we are given an initial wave packet which occupies a single energy band, being centered around $k_{\mathrm{c}}(t_0)$ at the moment $t = t_0$ in the crystal-momentum representation, and that (ii) interband transitions remain negligible for $t > t_0$, despite the action of the force $F(t)$. We then encounter single-band dynamics which are

fully covered by the "old" acceleration theorem $\hbar\dot{k}_c(t) = F(t)$, giving

$$k_c(t) = k_c(t_0) + \frac{1}{\hbar}\left[F_{dc}(t-t_0) + \frac{F_{ac}}{\omega}\sin(\omega t) - \frac{F_{ac}}{\omega}\sin(\omega t_0)\right] \tag{44}$$

for $t > t_0$. As an archetypal example we now take a tight-binding cosine energy dispersion relation for the band considered,

$$E(k) = -\frac{W}{2}\cos(ka), \tag{45}$$

parametrized as in the Introduction. Utilizing Eq. (2), one then finds the packet's group velocity:

$$v_g(t) = \frac{1}{\hbar}\left.\frac{dE}{dk}\right|_{k_c(t)} = \frac{Wa}{2\hbar}\sin[k_c(t)a]. \tag{46}$$

This expression describes super Bloch oscillations if we assume further that the dc component of the force is almost resonant in the sense of Eq. (8). We therefore decompose this component according to

$$F_{dc} = F_r + \delta F, \tag{47}$$

where $F_r a = r\hbar\omega$ with some nonzero integer r as previously in Eq. (9), so that $r\omega$ equals the Bloch frequency $\omega_B = F_r a/\hbar$, while δF is quite small compared to F_r. We then have

$$F_{dc}a = r\hbar\omega + \hbar\delta\omega, \tag{48}$$

with frequency detuning $\delta\omega = \delta F a/\hbar$, so that the group velocity (46) takes the form

$$v_g(t) = \frac{Wa}{2\hbar}\sin(r\omega t + \delta\omega t + K\sin(\omega t) + \Phi), \tag{49}$$

having introduced the scaled driving amplitude

$$K = \frac{F_{ac}a}{\hbar\omega} \tag{50}$$

and a constant phase

$$\Phi = k_c(t_0)a - (r\omega + \delta\omega)t_0 - K\sin(\omega t_0), \tag{51}$$

which accounts for the initial conditions. Because $\delta\omega \ll \omega$ according to our specifications, the contribution $\delta\omega t$ to the argument of v_g does not vary appreciably during one single cycle $T = 2\pi/\omega$ of the ac component. Thus, when averaging the instantaneous group velocity over one such cycle, this "slow" time dependence may be ignored, meaning that $\delta\omega t$ may be considered as constant when taking the average.[31] Invoking the Jacobi-Anger indentity in the guise

$$e^{iK\sin(\omega t)} = \sum_{\ell=-\infty}^{\infty} J_\ell(K)e^{i\ell\omega t}, \tag{52}$$

where $J_\ell(K)$ denotes the Bessel functions of the first kind, one immediately obtains

$$\overline{v}_g(t) = \frac{1}{T}\int_0^T dt\, v_g(t) = (-1)^r J_r(K)\frac{Wa}{2\hbar}\sin(\delta\omega t + \Phi). \tag{53}$$

According to the above reasoning, here the "fast" time dependence is integrated out, but the slow dependence on $\delta\omega t$ remains.[31] Integrating, this yields the cycle-averaged drift motion of the packet, that is, its position $\overline{x}_g(t)$ without the fast ac quiver,

$$\overline{x}_g(t) = -(-1)^r J_r(K)\frac{W}{2\delta F}\cos(\delta\omega t + \Phi), \tag{54}$$

with a suitably chosen origin of the x axis. This result finally clarifies what is "super" with these dynamics: Because the residual force δF is quite small, the amplitude of this oscillation (54) can be fairly large; indeed, in a corresponding experiment with weakly interacting Bose-Einstein condensates in driven optical lattices Haller *et al.*[28] have observed giant center-of-mass oscillations with displacements across hundreds of lattice sites. As far as the phenomenon itself is concerned there is nothing more to add; because one requires single Bloch-band dynamics right from the outset, a Floquet treatment is not necessary. Nevertheless the Floquet approach is of its own intrinsic value even here, since it provides a somewhat different view which, in contrast to the above crystal-momentum calculation, is capable of some generalization.

The Floquet analysis starts from the spatiotemporal Bloch waves and their quasienergies. In a single-band setting with an external homogeneous force, these are exceptionally easy to obtain: Writing the Bloch waves of the undriven lattice in the form

$$\varphi_k(x) = \sum_\ell w_\ell(x)e^{ik\ell a}, \tag{55}$$

where $w_\ell(x)$ denotes a Wannier function localized around the ℓth lattice site,[32] the so-called Houston functions[33]

$$\widetilde{\psi}_k(x,t) = \sum_\ell w_\ell(x)e^{iq_k(t)\ell a}\exp\left(-\frac{i}{\hbar}\int_0^t d\tau\, E[q_k(\tau)]\right) \tag{56}$$

are solutions to the time-dependent Schrödinger equation in the original frame, for arbitrary $F(t)$, provided the "moving wave numbers" $q_k(t)$ are given by

$$q_k(t) = k + \frac{1}{\hbar}\int_0^t d\tau\, F(\tau), \tag{57}$$

always assuming the viability of the single-band approximation.[34] Taking a force of the particular form (9) with exactly resonant F_r obeying $F_r a = r\hbar\omega$, we have

$$q_k(t) = k + \frac{r\omega t}{a} + \frac{F_{ac}}{\hbar\omega}\sin(\omega t). \tag{58}$$

This implies that both the exponentials $\exp[iq_k(t)\ell a]$ and $E[q_k(t)]$ are T periodic in time, with $T = 2\pi/\omega$, whereas the integral over $E[q_k(t)]$ is not, because the Fourier expansion of $E[q_k(t)]$ contains a zero mode, so that its integral contains a linearly growing contribution. But this observation reveals that the "accelerated Bloch waves" (56) with resonant time-periodic forcing (9) are precisely the required spatiotemporal

Bloch waves in the original frame, with their quasienergies being determined by the zero mode:

$$\varepsilon(k) = \frac{1}{T}\int_0^T dt\, E[q_k(t)] = -(-1)^r J_r(K)\frac{W}{2}\cos(ka). \tag{59}$$

The remarkable fact that the quasienergy bands collapse, i.e., become flat when K is such that $J_r(K) = 0$, indicates that an oscillating force can effectively shut down the tunneling contact between neighboring wells; this "coherent destruction of tunneling" is a generic feature of driven single-band systems.[34–37] A bit of reflection then shows that the core pieces $u_k(x,t)$ of the spatiotemporal Bloch waves, that is, the solutions to the eigenvalue equation (36), are given by

$$u_k(x) = \sum_\ell w_\ell(x)\mathrm{e}^{ik\ell a} \times \exp\left(-\frac{i}{\hbar}\int_0^t d\tau\,\{E[q_k(\tau)] - \varepsilon(k)\}\right). \tag{60}$$

Although this has not been particularly emphasized, the above construction makes sure that any spatiotemporal Bloch wave (56) is labeled by the same wave number k as the ordinary Bloch wave to which it reduces when the external force vanishes.[34] Otherwise, there is nothing particular about the choice $t = 0$ for the lower bound of integration in Eq. (57) for $q_k(t)$: In contrast to Eq. (43), where $t = t_0$ has been singled out as the moment when the force is turned on, and which thus designates an initial-value problem for a particular wave packet, the solution of the eigenvalue problem (36) for the entire spatiotemporal Bloch basis requires a force $F(t)$ which is perfectly periodic in time; the resulting expression for $q_k(t)$ thus holds for both $t > 0$ and $t < 0$. Also note that it would be meaningless to include some additional constant phase into the argument of the ac component of the force (9): Because this expression holds for all times t, such a phase would merely amount to a shift of the origin of the time coordinate and thus is as irrelevant for the calculation of the quasienergy dispersion relation as would be a shift of the origin of the spatial coordinate system for the calculation of a crystal's energy band structure.

Knowing the quasienergy dispersion relation (59), the machinery established in Sec. III can be set to work: According to Eq. (42), the cycle-averaged group velocity of a Floquet wave packet (17) is given by

$$\overline{v}_\mathrm{g} = \frac{1}{\hbar}\left.\frac{d\varepsilon}{dk}\right|_{\langle k\rangle} = (-1)^r J_r(K)\frac{Wa}{2\hbar}\sin(\langle k\rangle a). \tag{61}$$

If we now turn back to the specific forcing (43), and thus consider exactly the same initial-value problem as in the previous crystal-momentum exercise, we can make operational use of the decomposition (47) of the dc force: Its resonant part F_r has already been incorporated into the spatiotemporal Bloch waves (56), which means that it has already been accounted for in "dressing" the lattice and changing its original energy dispersion $E(k)$ to the quasienergy dispersion $\varepsilon(k)$. Therefore, it is only the small residual part δF which enters into the equation of motion for $\langle k\rangle$, that is, into the generalized acceleration theorem (32); this part δF thus constitutes a particular, time-independent example of a probe force $F_\mathrm{p}(t)$ as considered in Sec. III. We now have

$$\hbar\frac{d}{dt}\langle k\rangle(t) = \frac{\hbar\delta\omega}{a}, \tag{62}$$

giving

$$\langle k\rangle(t) = \langle k\rangle(t_0) + \frac{\delta\omega}{a}(t - t_0). \tag{63}$$

All that remains to be done now is to express the initial Floquet center $\langle k\rangle(t_0)$ in terms of the initial wave packet's center $k_\mathrm{c}(t_0)$, which had been specified in the crystal-momentum representation. But this is an easy task, comparing the original Bloch waves (55) to their spatiotemporal descendents (56): At the moment t_0 when the force (43) is turned on, $k_\mathrm{c}(t_0)$ coincides with $q_k(t_0)$ for one particular k; this evidently is the desired $\langle k\rangle(t_0)$. The equality identifying $\langle k\rangle(t_0)$ thus is

$$k_\mathrm{c}(t_0) = q_{\langle k\rangle(t_0)}(t_0), \tag{64}$$

which, written out in full detail, reads

$$k_\mathrm{c}(t_0) = \langle k\rangle(t_0) + \frac{r\omega t_0}{a} + \frac{F_\mathrm{ac}}{\hbar\omega}\sin(\omega t_0). \tag{65}$$

Using this to eliminate $\langle k\rangle(t_0)$ from Eq. (63), we arrive at

$$\langle k\rangle(t)a = k_\mathrm{c}(t_0)a - r\omega t_0 - K\sin(\omega t_0) + \delta\omega(t - t_0) = \delta\omega t + \Phi \tag{66}$$

with precisely the same phase Φ as already defined in Eq. (51). Inserting this argument (66) into the cycle-averaged group velocity (61), and comparing with the previous expression (53), one confirms that the result of the Floquet analysis fully coincides with that of the more customary crystal-momentum calculation. The necessity to painstakingly distinguish between crystal momentum k_c and Floquet $\langle k\rangle$ at all stages may appear a bit mind-boggling; if this is not done with sufficient care, one might overlook a contribution to Φ.[31] But if respected properly, the mathematical structure of the Floquet picture unerringly leads to the correct answer.

If one strips the above reasoning to the bare essentials, that is, if one starts from the quasienergy dispersion relation (59), takes its derivative to obtain the formal expression (61) for the cycle-averaged group velocity, and then inserts the solution to the equation of motion (62) dictated by the generalized acceleration theorem in order to compute the group velocity of the wave packet actually considered, one sees that this procedure exactly parallels the explanation of the usual Bloch oscillations, as reviewed in the Introduction. Thus, super Bloch oscillations may be seen as ordinary Bloch oscillations arising in response to a weak probe force δF, but occurring in a spatiotemporal lattice, as created by dressing the original lattice through application of the strong force (9).

One might finally wish to get away from the particular, instantaneous onset of the forcing assumed in Eq. (43): The dc and the ac component might not be switched on simultaneously, or not abruptly, possibly involving two different turn-on functions for the two components. In any case, at some moment t_0 the final amplitudes will have been reached, so that the previous analysis goes through unaltered for $t > t_0$, if one only interprets $k_\mathrm{c}(t_0)$ correctly: This would no longer indicate the crystal-momentum wave number around which the initial wave

packet had been prepared, but rather that to which the latter had been shifted during the turn-on phase. Expressed differently, the phase Φ in Eqs. (53) and (54) depends significantly on the precise turn-on protocol: Not surprisingly, the way the external force has been turned on in the past crucially affects the coherent wave-packet motion after the turn-on is over.

Aside from its aesthetic value, the Floquet picture offers at least one further benefit: Bloch oscillations in dressed lattices may also occur under conditions such that the quasienergy bands are mixtures of several unperturbed energy bands, disabling a crystal-momentum treatment. A Floquet analysis, on the other hand, would merely require one to replace the single-band quasienergies (59) by the actual ones and then again invoke the generalized acceleration theorem (32), similar to the examples worked out in the next section.

V. COHERENT CONTROL OF INTERBAND POPULATION TRANSFER

A field of major current interest in which the Floquet picture may find possibly groundbreaking applications concerns ultracold atoms, or weakly interacting Bose-Einstein condensates, in time-periodically driven optical lattices.[21,28,30,34,38–40] As opposed to ordinary crystalline matter exposed to high-power laser fields, such systems offer the advantage that one can apply even nonperturbatively strong driving forces without inducing unwanted inhomogeneities, as caused by polarization effects or domain formation.[22] The issue at stake here is not merely redoing well-known condensed-matter physics in another setting, and thus selling old wine in new skins, but rather finding genuinely new ways of coherently controlling mesoscopic matter waves, such that target states are created which have not been accessible before and are manipulated according to some prescribed protocol. Here we point out that the generalized acceleration theorem (32) may be a valuable tool in this quest.

A standard one-dimensional (1D) optical lattice is described by a cosine potential,

$$V(x) = \frac{V_0}{2}\cos(2k_{\mathrm{L}}x), \tag{67}$$

where k_{L} is the wave number of the two counterpropagating laser beams generating the lattice.[41,42] Its depth V_0 is measured in multiples of the single-photon recoil energy

$$E_{\mathrm{r}} = \frac{\hbar^2 k_{\mathrm{L}}^2}{2m}. \tag{68}$$

For orientation, if one traps ^{87}Rb atoms in a lattice with k_{L} corresponding to the wavelength $\lambda = 842$ nm, as in a recent experiment by Zenesini *et al.*,[38] one finds $E_{\mathrm{r}} = 1.34 \times 10^{-11}$ eV; typical optical lattices are a few recoil energies deep.

Figure 1 shows quasienergy spectra for such a 1D cosine lattice (67) with depth $V_0/E_{\mathrm{r}} = 5.7$ under pure ac forcing, that is, for $F(t) = F_{\mathrm{ac}}\cos(\omega t)$ not containing a dc component, with driving frequency $\omega = 3.71\, E_{\mathrm{r}}/\hbar$. Under the laboratory conditions specified above (^{87}Rb at $\lambda = 842$ nm), this corresponds to $\omega/(2\pi) = 12$ kHz. Figure 1(a) results when the scaled driving amplitude (50) is set to zero; this subfigure therefore is obtained by projecting the lowest three unperturbed energy bands to the fundamental quasienergy Brillouin zone, which extends from $\varepsilon = -\hbar\omega/2$ to $\varepsilon = +\hbar\omega/2$ on the ordinate. Figure 1(b) displays the quasienergy band structure for the moderate driving strength $K = 0.5$; here avoided crossings show up which generally indicate multiphotonlike resonances.[22] Figure 1(c) then reveals pronounced ac Stark shifts (that is, shifts of the quasienergies against the zone-projected original energies) for $K = 3.0$, corresponding to truly strong forcing.

We now turn from the quasienergy spectrum to an exemplary initial-value problem: At $t = 0$ we prepare an initial wave packet (17) in the lowest Bloch band $n = 1$ with a Gaussian momentum distribution,

$$g_1(k,0) = (\sqrt{\pi}\,\Delta k)^{-1/2}\exp\left(-\frac{k^2}{2(\Delta k)^2}\right), \tag{69}$$

centered around $k_{\mathrm{c}}(0)/k_{\mathrm{L}} = 0$ with width $\Delta k/k_{\mathrm{L}} = 0.1$, and subject it to a pulse,

$$F(t) = F_{\max}s(t)\sin(\omega t), \tag{70}$$

starting at $t = 0$ and ending at $t = T_{\mathrm{p}}$, endowed with a smooth, squared-sine envelope function:

$$s(t) = \sin^2\left(\frac{\pi t}{T_{\mathrm{p}}}\right), \quad 0 \leqslant t \leqslant T_{\mathrm{p}}. \tag{71}$$

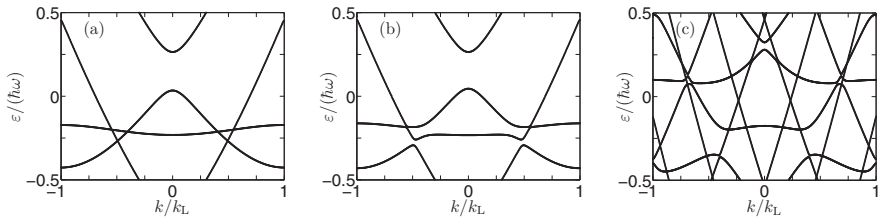

FIG. 1. (a) Quasienergy spectrum of an ac-driven 1D optical lattice (67) with depth $V_0/E_{\mathrm{r}} = 5.7$, scaled driving frequency $\hbar\omega/E_{\mathrm{r}} = 3.71$, and scaled driving amplitude $K = 0$. This figure is obtained by projecting the lowest three energy bands of the undriven lattice to the first quasienergy Brillouin zone, ranging from $\varepsilon/(\hbar\omega) = -1/2$ to $\varepsilon/(\hbar\omega) = +1/2$. (b) Quasienergy band structure for $K = 0.5$. Here the ac Stark shifts still are comparatively weak, but the time-periodic forcing introduces pronounced avoided crossings among the "lowest" three bands. (c) Quasienergy band structure for $K = 3.0$ for the "lowest" five bands, revealing substantial ac Stark shifts.

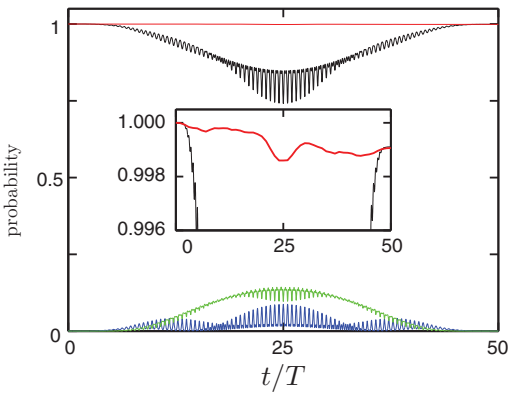

FIG. 2. (Color online) Time evolution of an initial wave packet (69) under the action of a driving pulse (70) with the smooth squared-sine envelope (71), with maximum scaled amplitude $K_{\max} = 3.0$, scaled driving frequency $\hbar\omega/E_r = 3.71$, and pulse length $T_p = 50\,T$, where $T = 2\pi/\omega$ is the duration of a single cycle. The main frame shows the occupation probabilities of the original Bloch energy bands during the pulse. Apart from the initially populated lowest band $n = 1$ (jagged line at the top), both bands $n = 2$ and $n = 3$ become significantly excited during the pulse (jagged lines at the bottom), the band $n = 3$ even to a higher extent than $n = 2$ at maximum driving strength. In contrast, when monitoring the same dynamics within the bases provided by the instantaneous spatiotemporal Bloch waves, *only* the corresponding Floquet band $n = 1$ is appreciably occupied, as shown by the horizontal line at the top and magnified in the inset. Observe the scale of the inset's ordinate!

We again set $\omega = 3.71\,E_r/\hbar$, as in Fig. 1; adjust the pulse length to 50 cycles, $T_p = 50 \times 2\pi/\omega$; and fix the maximum driving amplitude $F_{\max}$ such that $K_{\max} = F_{\max}a/(\hbar\omega) = 3.0$, corresponding to the conditions reached in Fig. 1(c). We then monitor the resulting wave-packet dynamics both in the basis of the unperturbed energy bands and in the bases provided by the instantaneous spatiotemporal Bloch waves, that is, in the family of Floquet bases which are obtained when the driving amplitude is kept fixed at any value $F_{ac} = F_{\max}s(t_0)$ reached during the pulse. Figure 2 displays the results: The jagged lines in the main frame show the occupation probabilities of the lowest three unperturbed Bloch bands $n = 1$, 2, and 3; in the middle of the pulse the band $n = 3$ contains even more population than the band $n = 2$. On the other hand, the horizontal line at the top depicts the occupation of the instantaneous Floquet band emerging from the lowest Bloch band: This Floquet band contains practically *all* the population during the entire pulse, which means that the wave function adjusts itself adiabatically to the changing morphology of its quasienergy band,[22] as previously sketched in Fig. 1, when the driving amplitude $F_{\max}s(t)$ is first increased and then decreased back to zero. To quantify the precise degree of adiabatic following, the inset in Fig. 2 shows the variation of the Floquet band population on a much finer scale. Observe that the final adiabaticity defect is on the order of merely 0.1%, even though the driving amplitude reaches its fairly high maximum strength within no more than 25 cycles.

With respect to the concepts developed in Sec. II, Fig. 2 strikingly demonstrates the advantages of the Floquet picture over the traditional crystal-momentum representation for the situation considered. If there were an additional probe force, its effect would have to be tediously disentangled from the fast oscillations of the Bloch band populations. When the same dynamics are seen from the Floquet viewpoint, essentially "nothing" happens, because practically all inter-Bloch-band transitions are already accounted for by continuously adapting the Floquet basis, so that the action of a probe force would stand out most clearly. Although, of course, the crystal-momentum representation is mathematically equivalent to the Floquet picture, there is no question which one is preferable here. Note also that Fig. 2 answers one further pertinent question: How do we prepare a wave packet which occupies merely a single quasienergy band, although it is undergoing rapid transitions between several Bloch bands at the same time? The recipe for achieving this is simple: Start with a wave packet occupying a single Bloch band and switch on the driving force smoothly, thereby enabling adiabatic following.

At this point an important issue needs to be stressed: The concept of adiabatic following, or parallel transport in a differential-geometric language, usually is applied to energy eigenstates;[25,26] in the context of optical lattices this has been exploited, e.g., by Fratalocchi and Assanto[43] for studying nonlinear adiabatic evolution and emission of coherent Bloch waves. In contrast, here we consider the adiabatic following of explicitly time-dependent *quasi*energy eigenstates, that is, of solutions to the quasienergy eigenvalue equation (13); this is what allows us to separate the fast, oscillating time dependence of the driving force from the slow, parametric time dependence of its envelope.

Having learned these lessons, we now set the generalized acceleration theorem (32) to work. Suppose that we are prompted to empty the ground-state energy band. Starting again from an initial wave packet (69), we then may proceed as follows: First we smoothly turn on an ac force which dresses the lattice, creating avoided quasienergy crossings initially not "seen" by the adiabatically following packet. For instance, we may wish to utilize the avoided crossings showing up in Fig. 1(b). To this end, we again take an ac force with frequency $\omega = 3.71\,E_r/\hbar$ and fix its scaled driving amplitude at the plateau value $K = 0.5$. This dressing force is switched on during 25 cycles with half a squared-sine envelope, maintained at maximum amplitude for 50 further cycles, and switched off again for another 25 cycles, as sketched in Fig. 3(a). If this were all we did, the wave packet would simply undergo adiabatic evolution and finally restore its initial condition, as previously observed in Fig. 2. Instead, once the maximum dressing amplitude has been reached, we now apply an additional weak probe force $F_p(t)$ in order to exploit Eq. (32) for moving the packet away from the Brillouin zone center, driving it over the avoided crossings that have opened up in Fig. 1(b). This probe force is implemented in the form of two smooth, squared-sine shaped dc pulses, one acting during the plateau of the dressing pulse, the other acting with reversed sign after the dressing pulse is over, as drawn in Fig. 3(a). The maximum strength of the probe force here is only 2.5% of that of the dressing force; for better visibility, the probe force is magnified in Fig. 3(a) by a factor of 10.

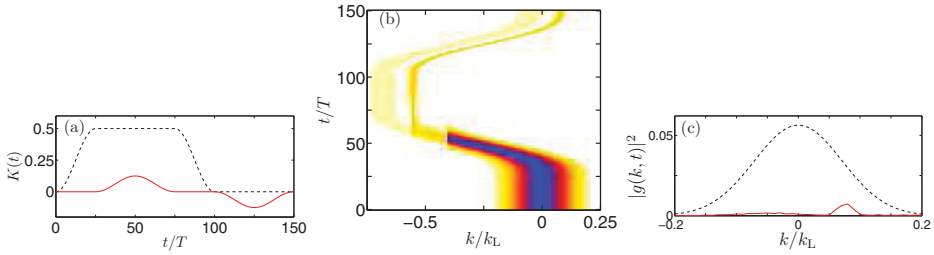

FIG. 3. (Color online) (a) Protocol for achieving almost complete interband population transfer in a dressed optical lattice by means of a weak probe force. The dashed line is the scaled envelope of the dressing ac force. The solid line is the negative, scaled probe force, amplified by a factor of 10. (b) Resulting wave-packet dynamics in the Floquet representation, shown as a contour plot of $|g_1(k,t)|^2$. Under the first action of the probe force the wave packet is shifted in accordance with the generalized acceleration theorem (32), until it undergoes Zener-type transitions to other quasienergy bands at the avoided crossings visible in Fig. 1(b). After the dressing force is switched off, the second, reversed action of the probe force shifts the remaining part of the packet back to the Brillouin zone center. (c) Comparison of the initial wave packet (dashed line) with the part of the wave function that remains in the lowest energy band at the end of the process (solid line).

It is now almost obvious how to describe the response of the wave packet within the Floquet picture: The initial state (69) first is adiabatically shifted into a single quasienergy-band packet during the turn-on of the dressing force. In contrast to a crystal-momentum representation, all dressing-induced fast oscillations are taken out of the dynamics of $g_1(k,t)$ in the Floquet representation, as shown in Fig. 3(b). When the first probe pulse acts at constant dressing amplitude, it forces the wave packet over the avoided crossing seen in Fig. 1(b), so that the packet undergoes Zener-type transitions to "higher" quasienergy bands,[18,22] splitting into individual subpackets associated with the different quasienergy bands involved. When the dressing force is switched off, each of these subpackets moves adiabatically on its own quasienergy surface, finally reaching the continuously connected Bloch bands. The second, reversed probe pulse, applied after the dressing pulse is over, then acts in accordance with Bloch's original acceleration theorem (1), shifting the various subpackets back to the Brillouin zone center. In the scenario displayed in Fig. 3, the lowest band is almost entirely depopulated by the probe-induced Zener transitions, so that only a marginal fraction of the initial packet returns, as depicted in Fig. 3(c). Thus, the main part of the initial packet has been placed in higher Bloch bands, as intended. We have also checked by explicit calculation that without the comparatively weak probe pulses the returning wave packet would be almost identical to the initial one.

The above example of our "dressing and probing" strategy immediately lends itself to a host of further modifications and extensions. To give but one further instance, if the probe pulse is still weaker, such that the wave packet does not pass over the avoided-crossing regime, but rather stops there, the Zener transitions are incomplete, so that a signifcant part of the initial state is recovered when the process is over. This is elaborated in Fig. 4 with the same dressing force as above, but now the maximum strength of the probe force amounts to only 1.7% of that of the dressing force. The final subpacket still occupying the lowest Bloch band then is no longer centered

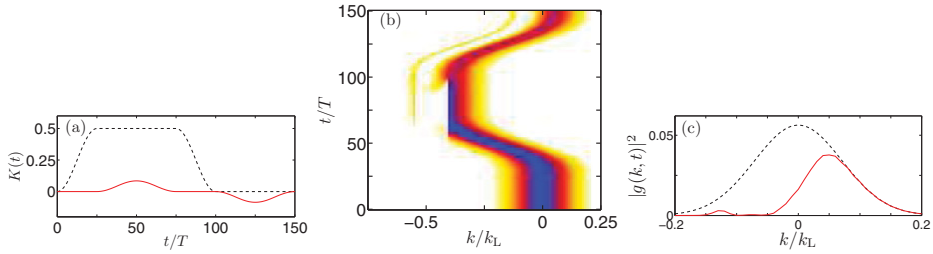

FIG. 4. (Color online) (a) Protocol for achieving partial interband population transfer in a dressed optical lattice by means of a weak probe force. The dashed line is the scaled envelope of the dressing ac force, which is the same as in Fig. 3. The solid line is the negative, scaled probe force, amplified by a factor of 10; this force is weaker than the one in Fig. 3. (b) Resulting wave-packet dynamics in the Floquet representation, shown as a contour plot of $|g_1(k,t)|^2$. Under the first action of the probe force the wave packet is shifted in accordance with the generalized acceleration theorem (32), but not as far as in Fig. 3, such that it undergoes only partial Zener transitions. After the dressing force is switched off, the second, reversed action of the probe force shifts the remaining part of the packet back to the Brillouin zone center. (c) Comparison of the initial wave packet (dashed line) with the part of the wave function that remains in the lowest energy band at the end of the process (solid line).

around $k/k_L = 0$, implying that this subpacket will move over the lattice. In a sense, the left wing of the initial wave packet has been cut out, so that Fig. 4 may be regarded as a particular paradigm of "wave-packet surgery."[44]

VI. CONCLUSIONS

Summarizing our line of reasoning, we have introduced in Sec. II a representation of wave packets of quantum particles in spatially periodic lattices subjected to homogeneous, time-periodic forcing which is based on an expansion with respect to spatiotemporal Bloch waves and reduces to the standard crystal-momentum representation when the forcing is turned off. It embodies forcing-induced oscillations into the basis, so that only the actually relevant dynamics remain to be dealt with. Within this Floquet representation one encounters many features already familiar from solid-state physics in time-independent lattice potentials, but here their scope is different. As a prominent example, the generalized acceleration theorem derived in Sec. III takes the same form as its historic antecessor formulated by Bloch,[1] but applies to single quasienergy band dynamics, which can be drastically different from single energy band behavior. There are further features which can be carried over from the crystal-momentum representation to the Floquet picture and acquire a modified meaning there, such as the expression for the group velocity of a wave packet or Zener transitions among different bands.

The super Bloch oscillations considered in Sec. IV provide a mainly pedagogical example which can be worked out in full detail analytically. Here the Floquet picture cannot exert its full strength, because one assumes *a priori* that the driving force does not induce transitions from the initially occupied energy band to other ones, so that the historic acceleration theorem remains capable of describing the entire dynamics. The Floquet approach leads to exactly the same result, but implies a different viewpoint, separating the dc component of the force into one part which is resonant with the ac component, and together with the latter dresses the lattice, creating a quasienergy band; the remaining residual part of the dc force then probes this new quasienergy band, rather than the original unperturbed energy band.

This theme of "dressing and probing" also prompts far-reaching strategies for achieving coherently controlled inter-band population transfer and even more. Two basic examples for this have been discussed in Sec. V, but the possibilities obviously extend much farther. Utilizing the generalized acceleration theorem, an initial wave packet may by split coherently into two components at an avoided quasienergy band crossing in a dressed lattice, and the lattice may then be redressed (that is, exposed to an ac force with different parameters) such that another quasienergy band structure is generated, possibly involving avoided crossings which affect only one of the daughter wave packets created in the first step, but not the other. Moreover, daughter wave packets can be made to move, possibly into different directions, and to interfere with other wavelets having been manipulated separately before in distant parts of the lattice. This vision apparently will be hard to realize with traditional solids, but it has come into immediate reach in current laboratory experiments with weakly interacting Bose-Einstein condensates in driven optical lattices. Seen against this background, the generalized acceleration theorem almost provides a blueprint for a wave-packet processor.

ACKNOWLEDGMENTS

M.H. thanks T. Monteiro for a thorough discussion of super Bloch oscillations. This work was supported by the Deutsche Forschungsgemeinschaft under Grant No. HO 1771/6.

[1] F. Bloch, Z. Phys. **52**, 555 (1929).
[2] N. W. Ashcroft and N. D. Mermin, *Solid State Physics* (Harcourt, Fort Worth, 1976), Chap. 12.
[3] C. Kittel, *Quantum Theory of Solids*, 2nd ed. (Wiley, New York, 1987).
[4] H. G. Roskos, M. C. Nuss, J. Shah, K. Leo, D. A. B. Miller, A. M. Fox, S. Schmitt-Rink, and K. Köhler, Phys. Rev. Lett. **68**, 2216 (1992).
[5] J. Feldmann, K. Leo, J. Shah, D. A. B. Miller, J. E. Cunningham, T. Meier, G. von Plessen, A. Schulze, P. Thomas, and S. Schmitt-Rink, Phys. Rev. B **46**, 7252 (1992).
[6] J. Feldmann, *Bloch Oscillations in a Semiconductor Superlattice*, in Festkörperprobleme, Advances in Solid State Physics Vol. 32, edited by U. Rössler (Vieweg, Braunschweig/Wiesbaden, 1992), p. 81.
[7] C. Waschke, H. G. Roskos, R. Schwedler, K. Leo, H. Kurz, and K. Köhler, Phys. Rev. Lett. **70**, 3319 (1993).
[8] A. A. Ignatov, E. Schomburg, K. F. Renk, W. Schatz, J. F. Palmier, and F. Mollot, Ann. Phys. **3**, 137 (1994).
[9] J. Rotvig, A.-P. Jauho, and H. Smith, Phys. Rev. Lett. **74**, 1831 (1995).
[10] A. A. Ignatov, E. Schomburg, J. Grenzer, K. F. Renk, and E. P. Dodin, Z. Phys. B **98**, 187 (1995).
[11] A. M. Bouchard and M. Luban, Phys. Rev. B **52**, 5105 (1995).
[12] K. Unterrainer, B. J. Keay, M. C. Wanke, S. J. Allen, D. Leonard, G. Medeiros-Ribeiro, U. Bhattacharya, and M. J. W. Rodwell, Phys. Rev. Lett. **76**, 2973 (1996).
[13] V. G. Lyssenko, G. Valušis, F. Löser, T. Hasche, K. Leo, M. M. Dignam, and K. Köhler, Phys. Rev. Lett. **79**, 301 (1997).
[14] G. Lenz, I. Talanina, and C. M. de Sterke, Phys. Rev. Lett. **83**, 963 (1999).
[15] M. Ben Dahan, E. Peik, J. Reichel, Y. Castin, and C. Salomon, Phys. Rev. Lett. **76**, 4508 (1996).
[16] O. Morsch, J. H. Müller, M. Cristiani, D. Ciampini, and E. Arimondo, Phys. Rev. Lett. **87**, 140402 (2001).
[17] H. Jones and C. Zener, Proc. R. Soc. London A **144**, 101 (1934).
[18] C. Zener, Proc. R. Soc. London A **145**, 523 (1934).
[19] J. Callaway, *Quantum Theory of the Solid State* (Academic Press, New York, 1976).
[20] M. Holthaus, Z. Phys. B **89**, 251 (1992).
[21] K. Drese and M. Holthaus, Chem. Phys. **217**, 201 (1997).
[22] S. Arlinghaus and M. Holthaus, Phys. Rev. A **81**, 063612 (2010).

[23] J. Zak, Phys. Rev. Lett. **71**, 2623 (1993).
[24] V. Grecchi and A. Sacchetti, Phys. Rev. B **63**, 212303 (2001).
[25] B. Simon, Phys. Rev. Lett. **51**, 2167 (1983).
[26] M. V. Berry, Proc. R. Soc. London A **392**, 45 (1984).
[27] H. Sambe, Phys. Rev. A **7**, 2203 (1973).
[28] E. Haller, R. Hart, M. J. Mark, J. G. Danzl, L. Reichsöllner, and H.-C. Nägerl, Phys. Rev. Lett. **104**, 200403 (2010).
[29] A. R. Kolovsky and H. J. Korsch, J. Sib. Fed. Univ.: Math. Phys. **3**, 311 (2010); e-print arXiv:0912.2587.
[30] A. Alberti, V. V. Ivanov, G. M. Tino, and G. Ferrari, Nat. Phys. **5**, 547 (2009).
[31] K. Kudo and T. S. Monteiro, Phys. Rev. A **83**, 053627 (2011).
[32] W. Kohn, Phys. Rev. **115**, 809 (1959).
[33] W. V. Houston, Phys. Rev. **57**, 184 (1940).
[34] A. Eckardt, M. Holthaus, H. Lignier, A. Zenesini, D. Ciampini, O. Morsch, and E. Arimondo, Phys. Rev. A **79**, 013611 (2009).
[35] M. Grifoni and P. Hänggi, Phys. Rep. **304**, 229 (1998).
[36] S. Longhi, Phys. Rev. A **71**, 065801 (2005).
[37] K. Kudo, T. Boness, and T. S. Monteiro, Phys. Rev. A **80**, 063409 (2009).
[38] A. Zenesini, H. Lignier, D. Ciampini, O. Morsch, and E. Arimondo, Phys. Rev. Lett. **102**, 100403 (2009).
[39] A. Eckardt, P. Hauke, P. Soltan-Panahi, C. Becker, K. Sengstock, and M. Lewenstein, Europhys. Lett. **89**, 10010 (2010).
[40] J. Struck, C. Ölschläger, R. Le Targat, P. Soltan-Panahi, A. Eckardt, M. Lewenstein, P. Windpassinger, and K. Sengstock, Science Express,doi:10.1126/science.1207239.
[41] O. Morsch and M. Oberthaler, Rev. Mod. Phys. **78**, 179 (2006).
[42] I. Bloch, J. Dalibard, and W. Zwerger, Rev. Mod. Phys. **80**, 885 (2008).
[43] A. Fratalocchi and G. Assanto, Phys. Rev. A **75**, 013626 (2007).
[44] S. Arlinghaus and M. Holthaus (unpublished).

IV

IV. Controlled wave-packet manipulation with driven optical lattices

Stephan Arlinghaus and Martin Holthaus,
Controlled wave-packet manipulation with driven optical lattices,
Phys. Rev. A **84**, 063617 (2011).

PHYSICAL REVIEW A **84**, 063617 (2011)

Controlled wave-packet manipulation with driven optical lattices

Stephan Arlinghaus and Martin Holthaus
Institut für Physik, Carl von Ossietzky Universität, D-26111 Oldenburg, Germany
(Received 24 August 2011; published 14 December 2011)

Motivated by recent experimental progress achieved with ultracold atoms in kilohertz-driven optical lattices, we provide a theoretical discussion of mechanisms governing the response of a particle in a cosine lattice potential to strong forcing pulses with smooth envelope. Such pulses effectuate adiabatic motion of a wave packet's momentum distribution on quasienergy surfaces created by spatiotemporal Bloch waves. Deviations from adiabaticity can then be deliberately exploited for exerting coherent control and for reaching target states which may not be accessible by other means. As one particular example, we consider an analog of the π pulses known from optical resonance. We also suggest adapting further techniques previously developed for controlling atomic and molecular dynamics by laser pulses to the coherent control of matter waves in shaken optical lattices.

DOI: 10.1103/PhysRevA.84.063617 PACS number(s): 67.85.Hj, 42.50.Hz, 32.80.Qk, 03.75.Lm

I. INTRODUCTION

Boosted by the seminal observation of the quantum phase transition from a superfluid to a Mott insulator in a gas of ultracold ^{87}Rb atoms trapped by an optical lattice potential [1], the experimental and theoretical study of ultracold atoms in optical lattices has matured into a major area of contemporary research [2–4]. To a large extent, this field is driven by the promise of simulating complex condensed-matter systems and obtaining novel insight into phenomena which hitherto are not understood, such as high-temperature superconductivity.

At present, evidence is accumulating which suggests that this field is developing a new branch, aiming at the coherent control of mesoscopic matter waves in optical lattices through the application of time-periodic forces, with driving frequencies in the lower kilohertz regime. While it had been pointed out earlier that a metal-insulator–like transition undergone by ultracold atoms in quasiperiodic optical lattices should be controllable by adjusting the amplitude of a sinusoidal drive [5], experimental work in this direction increased pace only in 2007, with the clear-cut observation of forcing-induced dynamical suppression of tunneling, and even reversal of the sign of the tunneling matrix elements, by Arimondo, Morsch, and co-workers [6,7]. This group also has documented an analog of photon-assisted tunneling with Bose-Einstein condensates in shaken optical lattices [8], and has verified that the superfluid–to–Mott-insulator transition can be coherently controlled by suitably "dressing" a matter wave in an optical lattice [9], taking up a theoretical proposal by Eckardt *et al.* [10]. The very same principle underlying this form of coherent control has quite recently been exploited successfully for emulating frustrated magnetism in driven triangular optical lattices [11], which may well be regarded as a guiding landmark example of quantum simulation. Moreover, there now exist first experimental results demonstrating active control of correlated tunneling in ac-driven optical lattices [12].

These experimental advances concerning time-periodically-driven matter waves are accompanied by growing theoretical efforts. For example, Kudo *et al.* have investigated the possibility of driving-induced control of bound-pair transport [13], while Tokuno and Giamarchi have studied a kind of spectroscopy for cold atoms in periodically phase-modulated optical lattices [14]. Moreover, Tsuji *et al.* have pointed out that ac forcing may even change the interparticle interaction from repulsive to attractive, possibly allowing one to simulate an effectively attractive Hubbard model with a temperature below the superconducting transition temperature [15]. So far, all these considerations merely involve strict ac forcing with a constant amplitude. In analogy to the physics of atoms and molecules interacting with laser pulses, here we suggest that many more control options should become available when ultracold atoms in optical lattices are subjected to forcing *pulses* with a deliberately shaped envelope.

Such attempts to gain coherent control over mesoscopic matter waves call for a systematic theory of the response of ultracold many-body systems to nonperturbatively strong external forcing. Although one may obtain some insight from drastically simplified model systems [16], and substantial progress is being made now with the help of advanced numerical schemes [17], this goal still is far from accomplishment. In this situation, an intermediate step suggests itself: In experiments with sufficiently dilute Bose-Einstein condensates in optical lattices, or with condensates for which the interparticle s-wave scattering length has been tuned close to zero by means of a Feshbach resonance, one may ignore interaction effects altogether, and can observe typical single-particle phenomena, such as ordinary or "super" Bloch oscillations, with condensates [18–21]. Thus, it seems advisable to undertake a comprehensive theoretical study of the possibilities of coherent control of single-particle dynamics in forced optical lattices. The results of such a study can then immediately be tested in "interaction-free" condensate experiments and may help one to disentangle genuine many-body effects at a later stage.

This is the step we are going to take in the present paper. Building on our previous work [22], here we provide a detailed picture of basic mechanisms which imply single-particle state control: We first demonstrate in Sec. II the feasibility of adiabatic transport of momentum distributions on quasienergy surfaces corresponding to time-periodically-forced optical lattices. This option is opened up by the existence of a basis of spatiotemporal Bloch waves, that is, of Bloch-like states which embody both the spatial periodicity of the lattice and the temporal periodicity of a driving force on equal footing;

such states constitute the foundation of our analysis [23]. We then establish in Sec. III an analog of the π pulses known from the theory of optical resonance [24] and outline how to utilize avoided crossings of quasienergy surfaces for "cutting out" parts of an initially given momentum distribution. Section IV briefly addresses effects connected to the phase of the driving force. Taken together, our findings indicate that there is a high potential for transferring well-established methods currently used for manipulating and controlling atoms and molecules by specifically designed laser pulses [25–29] to the newly emerging field of manipulating and coherently controlling mesoscopic matter waves in optical lattices by specifically tailored forces; this prospect is put forward in our conclusions.

II. ADIABATIC TRANSPORT OF MOMENTUM DISTRIBUTIONS

The starting point of our considerations is a single particle of mass m moving in a one-dimensional optical lattice potential [2–4]

$$V(x) = \frac{V_0}{2}\cos(2k_{\mathrm{L}}x), \tag{1}$$

where the lattice depth V_0 is proportional to the intensity of the laser radiation generating the lattice, and k_{L} denotes the corresponding wave number. Thus, the potential is periodic with lattice constant $a = \pi/k_{\mathrm{L}}$, so that $V(x) = V(x+a)$. Moreover, the particle is subjected to a spatially homogeneous inertial force $F(t)$, which can be applied by accelerating the lattice in the laboratory frame [30]. After transforming to a frame of reference comoving with the lattice, the Hamiltonian of the system is given by

$$\widetilde{H}(x,t) = \frac{p^2}{2m} + V(x) - F(t)x. \tag{2}$$

If we denote the solution to the Schrödinger equation pertaining to Eq. (2) by $\widetilde{\psi}(x,t)$ and perform the unitary transformation

$$\psi(x,t) = \exp\left(-\frac{i}{\hbar}x\int_0^t d\tau\, F(\tau)\right)\widetilde{\psi}(x,t), \tag{3}$$

the transformed functions $\psi(x,t)$ obey a Schrödinger equation with the new Hamiltonian

$$H(x,t) = \frac{1}{2m}\left(p + \int_0^t d\tau\, F(\tau)\right)^2 + V(x). \tag{4}$$

The traditional solid-state approach to monitoring the wave-packet dynamics now is as follows: The unforced lattice possesses improper energy eigenstates $\chi_{n,k}(x)$ which have the form of Bloch waves [31–33], that is, of plane waves which are modulated by lattice-periodic functions $v_{n,k}(x) = v_{n,k}(x+a)$, so that

$$\chi_{n,k}(x) = \mathrm{e}^{ikx}v_{n,k}(x); \tag{5}$$

these waves solve the time-independent Schrödinger equation

$$\left(\frac{p^2}{2m} + V(x)\right)\chi_{n,k}(x) = E_n(k)\chi_{n,k}(x). \tag{6}$$

Here n is a band index and k a wave number, so that $E_n(k)$ is the energy dispersion relation of the nth Bloch band. Owing to the periodicity of the lattice, the wave numbers can be restricted to the first quasimomentum Brillouin zone $\mathcal{B} = [-\pi/a, +\pi/a[$. In addition, we require the normalization

$$\int_{-\infty}^{+\infty} dx\, \chi^*_{n',k'}(x)\chi_{n,k}(x) = \frac{2\pi}{a}\delta_{n,n'}\delta(k-k'). \tag{7}$$

When an arbitrary given wave packet $\psi(x,t)$ is expanded with respect to the Bloch basis in the form

$$\psi(x,t) = \sum_n \sqrt{\frac{a}{2\pi}}\int_{\mathcal{B}} dk\, g^{\mathrm{B}}_n(k,t)\chi_{n,k}(x), \tag{8}$$

this convention (7) makes sure that the momentum distributions $|g^{\mathrm{B}}_n(k,t)|^2$ are normalized according to

$$\sum_n \int_{\mathcal{B}} dk\, \left|g^{\mathrm{B}}_n(k,t)\right|^2 = 1. \tag{9}$$

In solid-state physics, the expansion (8) is known as the crystal-momentum representation of the wave packet $\psi(x,t)$.

When there is no external forcing, $F(t) \equiv 0$, the time dependence of the expansion coefficients $g^{\mathrm{B}}_n(k,t)$ in Eq. (8) simply reads

$$g^{\mathrm{B}}_n(k,t) = g^{\mathrm{B}}_n(k,0)e^{-iE_n(k)t/\hbar}. \tag{10}$$

For studying the dynamics under the action of a force $F(t)$, let us at this point assume that the wave packet initially occupies only one band with a particular index n, and that the force remains so weak that it does not induce substantial interband transitions. Then Bloch's acceleration theorem [31–33] comes into play: The packet's center wave number in k space, given by the first moment

$$k_{\mathrm{c}}(t) = \int_{\mathcal{B}} dk\, k\left|g^{\mathrm{B}}_n(k,t)\right|^2, \tag{11}$$

then evolves according to the semiclassical law

$$\hbar\dot{k}_{\mathrm{c}}(t) = F(t). \tag{12}$$

For example, a constant force leads to a linearly increasing $k_{\mathrm{c}}(t)$, which, in its turn, gives rise to Bloch oscillations in real space.

Although this time-honored approach has many virtues, for our purposes it is advantageous to look at the wave-packet dynamics from a different angle. In view of the goal to exert coherent control on the lattice atom, it is quite natural to specifically consider sinusoidal forces $F(t) = F_{\mathrm{ac}}\sin(\omega t)$ in the first place, since then the Hamiltonian (2) is of the familiar form which also describes a charged particle in a monochromatic classical radiation field within the dipole approximation. The most conspicuous difference concerns the frequencies: Typical frequencies for driving optical lattices [6–12] fall into the lower kilohertz regime, about 11 orders of magnitude lower than optical frequencies. In the following, we merely require that the force be periodic in time with period T, so that $F(t) = F(t+T)$, and we assume that its one-cycle average vanishes, so that

$$\frac{1}{T}\int_0^T dt\, F(t) = 0. \tag{13}$$

With these specifications, the transformed Hamiltonian (4) is periodic in space as well as in time, $H(x,t) = H(x+a,t) = H(x,t+T)$. While the ordinary Bloch waves (5) account for

the spatial periodicity only, the mathematical Floquet theorem governing the structure of solutions to differential equations with periodic coefficients [34–36] can now be invoked to simultaneously incorporate *both* the spatial *and* the temporal periodicity, resulting in a set of solutions to the time-dependent Schrödinger equation of the suggestive form

$$\psi_{n,k}(x,t) = \exp[ikx - i\varepsilon_n(k)t/\hbar]u_{n,k}(x,t) \tag{14}$$

with biperiodic functions $u_{n,k}(x,t)$ which reflect the two translational symmetries, $u_{n,k}(x,t) = u_{n,k}(x+a,t) = u_{n,k}(x,t+T)$. We refer to these solutions (14) as *spatiotemporal Bloch waves* [23]. The quantities $\varepsilon_n(k)$ determining the linear growth of the phase factors with time are commonly known as quasienergies [37,38]. They are obtained by solving the eigenvalue problem

$$\left(H(x,t) - i\hbar\frac{\partial}{\partial t}\right)\varphi_{n,k}(x,t) = \varepsilon_n(k)\varphi_{n,k}(x,t), \tag{15}$$

where the functions $\varphi_{n,k}(x,t) = \exp(ikx)u_{n,k}(x,t)$ denote the spatial parts of the spatiotemporal Bloch waves (14). Fully in accordance with our rationale, this eigenvalue problem (15) is posed in an extended Hilbert space which puts position x and time t on equal footing [39]. Because of the periodicity of $H(x,t)$ in time, the eigenvalues $\varepsilon_n(k)$ are defined up to an integer multiple of $\hbar\omega$, with $\omega = 2\pi/T$, which means that there also is a Brillouin-zone scheme for the quasienergies, with the fundamental zone $\mathcal{Q} = [-\hbar\omega/2, +\hbar\omega/2[$, in analogy to the fundamental quasimomentum zone $\mathcal{B} = [-\pi/a, +\pi/a[$. Evidently, Eq. (15) now takes the place of the traditional eigenvalue equation (6), and the spatiotemporal Bloch waves (14) replace the ordinary Bloch waves (5). Consequently, we abandon the standard crystal-momentum representation (8) and instead perform expansions of given wave packets $\psi(x,t)$ in this new basis: Fixing, in analogy to the previous Eq. (7), the normalization

$$\int_{-\infty}^{\infty} dx\, \varphi^*_{n',k'}(x,t)\varphi_{n,k}(x,t) = \frac{2\pi}{a}\delta_{n,n'}\delta(k-k'), \tag{16}$$

we thus arrive at the Floquet representation [23]

$$\psi(x,t) = \sum_n \sqrt{\frac{a}{2\pi}} \int_{\mathcal{B}} dk\, g_n(k,t)\varphi_{n,k}(x,t). \tag{17}$$

When the amplitude of the driving force goes to zero, the functions $\varphi_{n,k}(x,t)$ reduce to the Bloch waves (5), and the quasienergies $\varepsilon_n(k)$ approach the energies $E_n(k)$, modulo $\hbar\omega$. Therefore, in this limit the Bloch expansion (8) coincides with the Floquet expansion (17). However, in the presence of a strictly T-periodic force, such as $F(t) = F_{\rm ac}\sin(\omega t)$, we now have two different pictures of the same wave-packet dynamics: Within the crystal-momentum approach, a single-band wave packet is described by a momentum distribution $|g^{\rm B}_n(k,t)|^2$; the center of this distribution moves in k space according to the acceleration theorem (12). In contrast, within the Floquet picture one merely has

$$g_n(k,t) = g_n(k,0)e^{-i\varepsilon_n(k)t/\hbar}, \tag{18}$$

so that the Floquet distribution $|g_n(k,t)|^2 = |g_n(k,0)|^2$ does not move at all, but stays perfectly constant in time, with the response to the oscillating force already being incorporated into the basis states (14).

Clearly, both approaches are mathematically equivalent. But it is the second one which allows us to make further contact with advanced techniques developed for studying the interaction of atoms and molecules with laser radiation, and for developing schemes for coherent control of ultracold atoms in driven optical lattices.

Such schemes naturally will involve *pulses* of driving forces, that is, nonperiodic forcing. As a simple case, we may consider pulses of the form

$$F(t) = F^{\rm max}_{\rm ac} s(t)\sin(\omega t), \tag{19}$$

where the dimensionless shape function $s(t)$ vanishes before and after the pulse, $s(t) = 0$ for both $t < 0$ and $t > T_{\rm P}$, say, and is normalized such that its maximum value is 1, implying that $F^{\rm max}_{\rm ac}$ is the maximum amplitude encountered during the pulse.

It is then of key importance to note that the Floquet picture is meaningful not only for perfectly time-periodic forces $F(t) = F(t+T)$, but also for situations in which one or more system parameters change slowly, that is, undergo only minor variations during one cycle T [40]. This is the case, for instance, if the pulse $F(t)$ is equipped with a "slowly" varying envelope $s(t)$. Then one considers not only one single-eigenvalue problem (15) corresponding to one particular amplitude $F_{\rm ac}$, but rather the family of all such eigenvalue problems with $0 \leqslant F_{\rm ac} \leqslant F^{\rm max}_{\rm ac}$. This gives a basis of spatiotemporal Bloch waves for each instantaneous value of the amplitude; taken together, these bases serve as a "moving frame of reference" with respect to which the wave packet can evolve adiabatically: Under pulse conditions enabling adiabaticity, the Floquet momentum distributions $|g_n(k,t)|^2$ remain almost constant in time, provided the expansion (17) refers at each moment to that basis of spatiotemporal Bloch waves which is obtained by fixing the slowly varying amplitude at its momentary value. Pictorially speaking, the instantaneous eigenvalues $\varepsilon_n^{F_{\rm ac}}(k)$, considered as functions of wave number k and driving amplitude $F_{\rm ac}$, form quasienergy surfaces on which the momentum distribution can move almost without change of shape in response to smooth variations of the envelope $s(t)$.

To see what this means in practice, we consider a cosine lattice (1) with depth $V_0 = 5.7E_{\rm r}$, where $E_{\rm r} = \hbar^2k_{\rm L}^2/(2m)$ denotes the single-photon recoil energy [2–4]; this depth is routinely being realized in current experiments [6–9,11,12]. The width of the lowest Bloch band then amounts to $E_1(k_{\rm L}) - E_1(0) = 0.220E_{\rm r}$, while the lowest band gap is $E_2(k_{\rm L}) - E_1(k_{\rm L}) = 2.763E_{\rm r}$. The maximum separation of the lowest two bands, encountered in the Brillouin-zone center, figures as $E_2(0) - E_1(0) = 4.690E_{\rm r}$ [22]. We then take a wave packet prepared at time $t = 0$ in the lowest Bloch band $n = 1$,

$$\psi(x,0) = \sqrt{\frac{a}{2\pi}} \int_{\mathcal{B}} dk\, g^{\rm B}_1(k,0)\chi_{1,k}(x), \tag{20}$$

with a Gaussian initial momentum distribution

$$g^{\rm B}_1(k,0) = (\sqrt{\pi}\Delta k)^{-1/2}\exp\left(-\frac{k^2}{2(\Delta k)^2}\right) \tag{21}$$

centered around $k_c(0)/k_L = 0$ with width $\Delta k/k_L = 0.1$. This wave packet is subjected to pulses (19) of length T_P with a squared-sine envelope,

$$s(t) = \sin^2\left(\pi \frac{t}{T_P}\right); \quad 0 \leqslant t \leqslant T_P. \tag{22}$$

The frequency selected for the model calculation discussed in the following is $\omega = 1.640E_r/\hbar$, well below the lowest band gap, while the maximum scaled driving amplitude

$$K_0^{\max} = \frac{F_{ac}^{\max} a}{\hbar\omega} \tag{23}$$

is set to $K_0^{\max} = 0.8$. The pulse length is fixed at $T_P = 10T$, so that the peak driving strength is reached within no more than five cycles. We then compute, on the one hand, the momentum distributions $|g_1^B(k,t)|^2$ in the crystal-momentum representation, and also perform the Floquet expansions

$$\psi(x,t) = \sum_n \sqrt{\frac{a}{2\pi}} \int_B dk\, g_n(k,t) \varphi_{n,k}^{F_{ac}(t)}(x,t) \tag{24}$$

with respect to the instantaneous solutions $\varphi_{n,k}^{F_{ac}}(x,t)$ to the quasienergy equation (15) in order to obtain the corresponding Floquet distributions $|g_1(k,t)|^2$, on the other.

Figure 1 juxtaposes the results of the two approaches. In Fig. 1(a) we show the evolution of the crystal-momentum density $|g_1^B(k,t)|^2$ under the pulse. Because interband transitions remain negligible for the parameters chosen, the packet's center moves in perfect accordance with Bloch's acceleration theorem (12). On the other hand, Fig. 1(b) depicts the evolution of the Floquet density $|g_1(k,t)|^2$. This density remains practically constant, indicating almost perfect adiabatic following of $\psi(x,t)$ with respect to the spatiotemporal Bloch waves: Despite the short duration of the pulse, the initial distribution merely makes an adiabatic excursion on its quasienergy surface, returning more or less unaltered.

Still, Fig. 1 is no more than a look at the same dynamics from two different viewpoints, and so far neither of these is better than the other. But now comes the crucial step: Control is exerted by utilizing interband transitions. While such transitions fall outside the scope of the semiclassical acceleration theorem, which explicitly requires a single-band setting, they can be monitored as deviations from adiabaticity, caused by near-degeneracies of quasienergy surfaces, within the Floquet approach. In order to locate the parameters for which such deviations occur, Fig. 2 shows the final escape probability from the lowest Bloch band in the amplitude-frequency plane [22], as resulting from the same initial wave packet as constructed above after pulses with the envelope (22), with greater length $T_P = 50T$. Most notably, the "single-photon resonance" with $\hbar\omega = E_2(0) - E_1(0)$ shows up already for quite small driving amplitudes around $\hbar\omega \approx 4.690E_r$; and one observes a sequence of multiphotonlike resonances at lower frequencies. Interestingly, there also is a pronounced frequency window between the two-photon resonance and the single-photon peak which allows for adiabatic response even to fairly strong pulses with $K_0^{\max} > 3$. This window appears to be most suitable for studying single-band phenomena associated with strong forcing, such as the driving-induced reversal of the sign of the effective hopping matrix element [6,7].

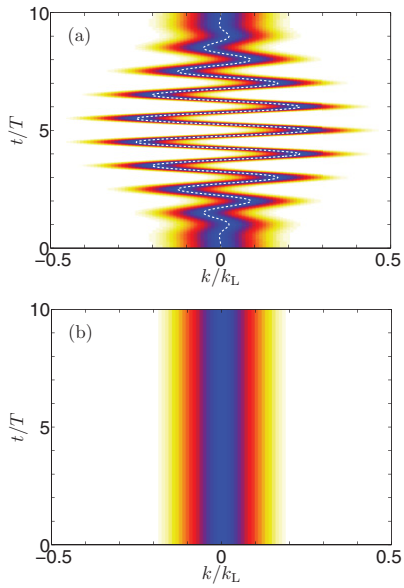

FIG. 1. (Color online) Response of the initial wave packet (20) with momentum distribution (21) in an optical lattice with depth $V_0/E_r = 5.7$ to a short pulse (19) with nonresonant scaled frequency $\hbar\omega/E_r = 1.640$, maximum scaled amplitude $K_0^{\max} = 0.8$, and pulse length $T_P/T = 10$. (a) shows the density $|g_1^B(k,t)|^2$ in the crystal-momentum representation. For comparison, the white-dashed line is the first moment $k_c(t)$, as predicted by the acceleration theorem (12). (b) depicts the Floquet density $|g_1(k,t)|^2$, obtained by expanding the same wave packet with respect to the instantaneous spatiotemporal Bloch waves.

The Floquet approach now enables one to look into the transition dynamics in great detail, and thus to understand basic principles allowing one to deliberately manipulate the momentum distribution and to create certain desired target states; this will be elaborated in the following section. Before closing the present section, we would like to draw an interesting comparison: Aside from degeneracies, the adiabatic motion of a wave packet's momentum distribution on its quasienergy surface, as visualized in Fig. 1(b), seems to resemble the adiabatic evolution of molecular states on their Born-Oppenheimer potential energy surfaces [41]. There is, however, an important difference: In the case of cold atoms in driven optical lattices the concept of adiabatic following [42,43] has to be applied to each wave number k in parallel, each one labeling a different spatiotemporal Bloch wave. Thus, here we are confronted not with adiabatic following of individual states, but rather with that of a density associated with a continuum of quasienergy eigenstates.

III. TAILORING THE MOMENTUM DISTRIBUTION

Nonadiabatic transitions, which prevent an initial momentum distribution from returning practically unchanged after a pulse, result from near-degeneracies of quasienergy surfaces.

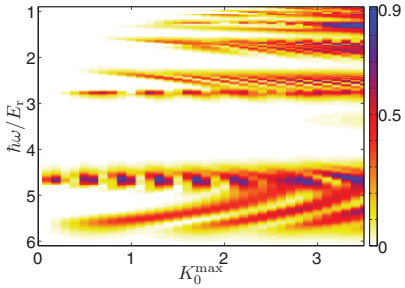

FIG. 2. (Color online) Final escape probabilities from the lowest Bloch band of an optical lattice with depth $V_0/E_r = 5.7$, calculated for the same initial wave packet as considered in Fig. 1, after pulses with squared-sine envelope (22) and length $T_P/T = 50$. Observe the window of almost adiabatic response appearing between the two-photon and the single-photon resonances.

Two different cases have to be distinguished: Either the near-degeneracy is induced already at small driving amplitudes by selecting a resonant frequency, or it shows up only under strong nonresonant driving, when the ac Stark shift forces two surfaces into an avoided crossing [22]. In this section we show that either of these scenarios can be exploited for controlling and reshaping the k-space distribution coherently. In all model calculations we consider an optical lattice with depth $V_0 = 5.7E_r$ and start from the initial Bloch wave packet (20) with Gaussian coefficients (21), again setting $\Delta k/k_L = 0.1$.

A. Resonant forcing

We now adjust the driving frequency such that $\hbar\omega = E_2(0) - E_1(0)$, so that the lowest two bands are coupled resonantly in the center of the quasimomentum Brillouin zone, at $k/k_L = 0$. The length of the pulses with squared-sine envelope (22) is $T_P = 50T$. Figure 3 shows the resulting final distributions $|g_1^B(k,T_P)|^2$ and $|g_2^B(k,T_P)|^2$ for the lowest and for the first excited Bloch band, respectively, in dependence on the maximum driving amplitude K_0^{max}. One observes a smooth, oscillating excitation pattern, the first indication of which was already visible in Fig. 2. In particular, for $K_0^{max} = 0.186$, which is the lowest peak amplitude leading to maximum population transfer to the band $n = 2$, the final excited-band distribution is substantially narrower than the original one, while the distribution remaining in the lowest band is bimodal, corresponding to a wave packet moving in two opposite directions.

With the help of the tools assembled in the preceding section, these results can be understood in an almost intuitive manner, without the need to invoke much formalism. Figure 4(a) depicts the two quasienergy surfaces involved in the dynamics, emerging from the two unperturbed Bloch bands $n = 1$ and 2. Because of the Brillouin-zone structure of the quasienergy spectrum, the "one-photon resonant" driving frequency causes a degeneracy of both surfaces for vanishing instantaneous scaled amplitude $K_0 = F_{ac}a/(\hbar\omega)$. As a consequence, the initial wave packet is not placed on an individual quasienergy surface under the action of a pulse,

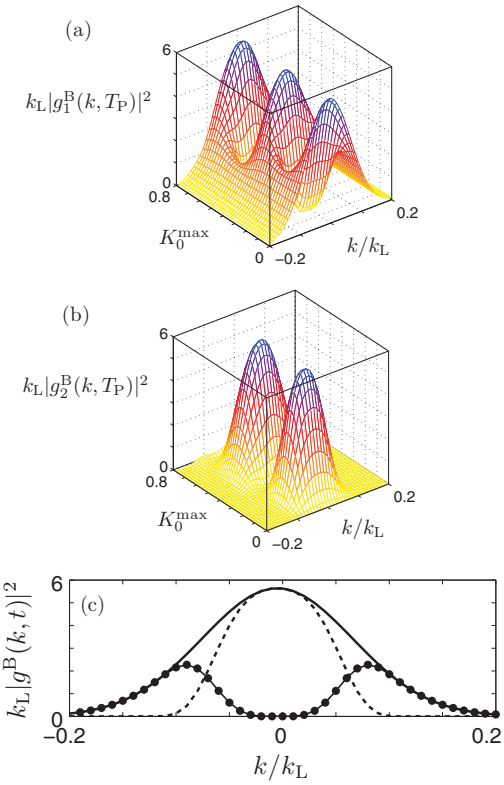

FIG. 3. (Color online) Final momentum distributions in the lowest (a) and in the first excited (b) Bloch bands after the initial state has been exposed to pulses with squared-sine envelope (22) and length $T_P/T = 50$, with varying maximum scaled amplitudes $0 \leqslant K_0^{max} \leqslant 0.8$. Here the scaled driving frequency is $\hbar\omega/E_r = 4.690$, implying $\hbar\omega = E_2(0) - E_1(0)$, so that both bands are exactly resonant at $k/k_L = 0$. (c) compares the final distributions in the first (dotted) and in the second (dashed) bands to the initial distribution (full line), for $K_0^{max} = 0.186$. This particular situation corresponds to a "π pulse."

but rather placed coherently on both surfaces: A Floquet expansion (17) yields contributions for both $n = 1$ and 2. Both parts of the wave function then react adiabatically to the slowly varying amplitude, each one picking up its own dynamical phase factors, given by the time integrals over the instantaneous quasienergies $\varepsilon_n^{F_{ac}}(k)$ encountered. When the driving amplitude goes to zero at the end of the pulse, both parts of the wave function produce an interference pattern which determines the final excitation probability: For each wave number k sufficiently close to resonance, the transition probability to the first excited band is proportional to the expression [44]

$$P_{1\to2}^{(k)} = \sin^2\left(\frac{1}{2\hbar}\int_0^{T_P} dt\left[\varepsilon_1^{F_{ac}(t)}(k) - \varepsilon_2^{F_{ac}(t)}(k)\right]\right). \quad (25)$$

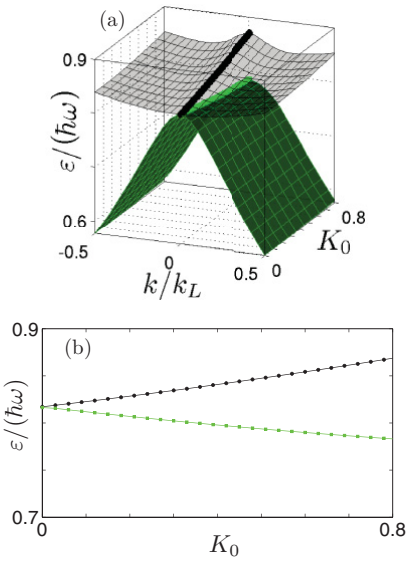

FIG. 4. (Color online) (a) Quasienergy surfaces underlying the excitation pattern observed in Fig. 3. The upper surface originates from the unperturbed Bloch band $n = 1$, the lower one from the band $n = 2$. Because of the resonant frequency, both surfaces are degenerate at $k/k_L = 0$ for vanishing instantaneous amplitude K_0. The quasienergy lines at $k/k_L = 0$ are emphasized for better visibility. (b) Section through the surfaces at $k/k_L = 0$, showing the removal of the initial degeneracy.

As seen in Fig. 4(b), for $k/k_L = 0$ the quasienergy difference $\varepsilon_1^{F_{ac}}(0) - \varepsilon_2^{F_{ac}}(0)$ increases linearly with the driving amplitude, as is typical for a single-photon resonance [44]. Maximum excitation then is obtained when the argument of the squared sine in Eq. (25) equals an odd-integer multiple of $\pi/2$, the first such maximum showing up for

$$\frac{1}{\hbar}\int_0^{T_P} dt\left[\varepsilon_1^{F_{ac}(t)}(k) - \varepsilon_2^{F_{ac}(t)}(k)\right] = \pm\pi. \tag{26}$$

This is reminiscent of the familiar π-pulse condition; indeed, when the quasienergies are calculated analytically within the rotating-wave approximation, Eq. (26) reduces to the customary area theorem known from optical resonance [24,44]. But here we are confronted with the fact that this condition (26) cannot be met simultaneously for all components k with one single pulse shape: When it is satisfied for $k/k_L = 0$, the other components of the wave packet experience slightly or even strongly different quasienergies, depending on its initial width in k space, as becomes evident when looking at Fig. 4(a). This is exactly what allows one to "cut out" a part of the momentum distribution, as was demonstrated in Fig. 3(c): Here the pulse shape is such that Eq. (26) indeed is satisfied for $k/k_L = 0$, leading to maximum transition probability in the center of the Brillouin zone. In contrast, the initial degeneracy at $k/k_L = 0$ has no effect on the wings of the initial distribution, so that these wings return adiabatically. As a result, the pulse transfers

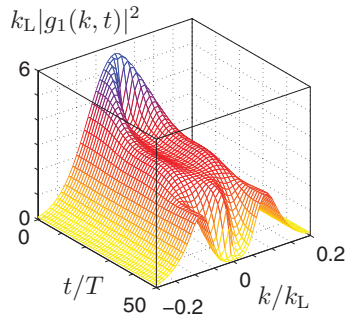

FIG. 5. (Color online) Floquet representation of the evolution of a wave packet initially prepared in the lowest Bloch band, under the action of a resonant π pulse with $K_0^{max} = 0.186$. This figure shows how the final bimodal distribution $|g_1(k,T_P)|^2$ depicted in Fig. 3(c) appears after an initial reduction of the original density, corresponding to the partial occupation of the other resonantly coupled quasienergy surface; and after a period of almost adiabatic motion during the middle of the pulse.

a relatively narrow central part of the initial distribution to the first excited Bloch band, leaving behind a symmetric bimodal distribution in the lowest one.

It is then of particular interest to monitor the dynamics during such a pulse in the Floquet representation, instead of merely looking at the final distributions in the usual crystal-momentum representation. One such example, visualizing the the action of the very "π pulse" considered above, is shown in Fig. 5. Observe how the evolution of $|g_1(k,t)|^2$ embodies the elements discussed before: The distribution soon is reduced to half its initial height, reflecting the occupation of the other quasienergy surface at the beginning of the pulse; then stays about constant during the pulses' middle part, reflecting approximately adiabatic motion; and develops the bimodal pattern only at its end, reflecting the final interference.

B. Nonresonant, strong forcing

For the following second example of wave-packet manipulation we again select the driving frequency $\omega = 1.640E_r/\hbar$, as in the previous calculations having led to Fig. 1, but now we also consider pulses with larger scaled amplitudes K_0^{max}. In Fig. 6 we display the final distributions $|g_1^B(k,T_P)|^2$ and $|g_2^B(k,T_P)|^2$ as resulting from pulses with $0.7 \leqslant K_0^{max} \leqslant 1.3$. Even for $K_0^{max} = 0.8$ the initial distribution returns still undistorted, but for $K_0^{max} \approx 0.9$ strong interband transitions set in, leading to a trimodal excited-band distribution when $K_0^{max} = 1.3$.

Once more the explanation for this response behavior is provided by the morphology of the quasienergy surfaces, shown in Fig. 7. The surface with comparatively low curvature originates from the Bloch band $n = 1$; this surface is penetrated by the one emerging from the Bloch band $n = 2$ along a parabola-shaped line with apex at $k/k_L = 0$ and $K_0 \approx 0.9$. Along this line the two surfaces exhibit a narrow avoided crossing. The quasienergy representatives plotted in Fig. 7 are shifted against those continuously connected to the original energy

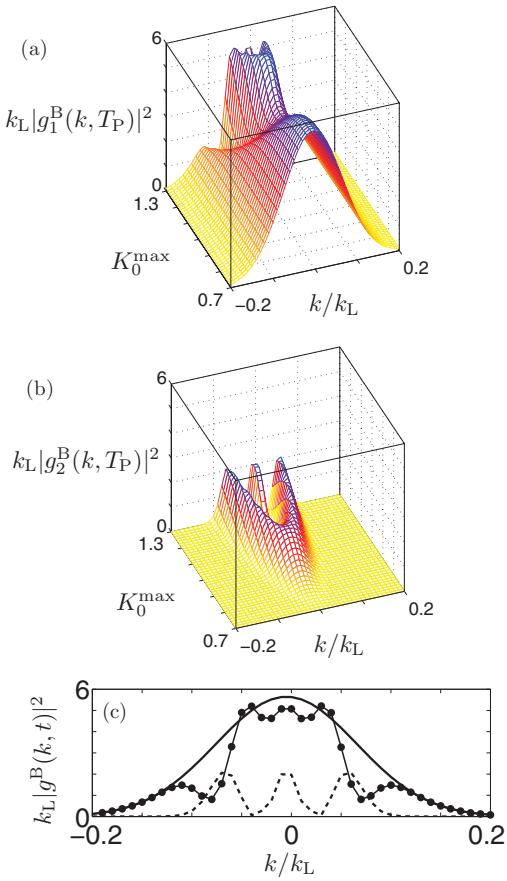

FIG. 6. (Color online) Final momentum distributions in the lowest (a) and in the first excited (b) Bloch bands after the initial state has been exposed to pulses with squared-sine envelope (22) and length $T_P/T = 50$, with varying maximum scaled amplitudes $0.7 \leqslant K_0^{max} \leqslant 1.3$. Here the nonresonant scaled driving frequency is $\hbar\omega/E_r = 1.640$, as in Fig. 1. (c) compares the final distributions in the first (dotted) and in the second (dashed) bands to the initial distribution (full line) for $K_0^{max} = 1.3$.

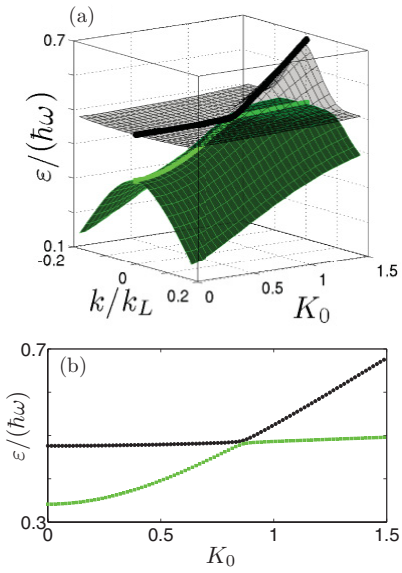

FIG. 7. (Color online) (a) Quasienergy surfaces underlying the excitation pattern observed in Fig. 6. The almost flat surface originates from the comparatively narrow Bloch band $n = 1$, the one with larger curvature from the band $n = 2$. Both surfaces undergo an avoided crossing along a parabola with apex at $k/k_L = 0$ and $K_0 \approx 0.9$. The quasienergy lines at $k/k_L = 0$ are emphasized for better visibility. (b) Section through the surfaces at $k/k_L = 0$, showing the narrow avoided crossing.

bands by $+\hbar\omega$ ($n = 1$) and by $-2\hbar\omega$ ($n = 2$), respectively, so that the anticrossing marks a "three-photon resonance." As long as the maximum pulse amplitude does not reach the apex of the anticrossing parabola, the momentum distribution merely moves adiabatically on its quasienergy surface, as already demonstrated in Fig. 1, and returns without notable modification. But when $K_0^{max} > 0.9$ the distribution has to pass the avoided-crossing line, resulting in partial Landau-Zener transitions to the other surface. Thus, the onset of excited-band population in the K_0^{max}-k/k_L plane, as observed in Fig. 6(b), precisely reflects the locus of the band intersection.

Considering a pulse with $K_0^{max} > 0.9$, the different k components thus encounter "their" respective avoided crossing at different amplitudes, and hence at different times. Therefore, the different components acquire quite different dynamical phase factors between their first passage through an avoided crossing during the rise of the pulse and the second passage taking place during the switch-off. Thus, for each k one finds Stückelberg oscillations [45] due to the interference of the parts having evolved on the two different surfaces, but their phases vary strongly within the Brillouin zone. This feature is the origin of the trimodal distribution $|g_2^B(k,T_P)|^2$ shown in Fig. 6(c). As can be clearly seen in Fig. 6(b), the center lobe of this distribution already corresponds to the second Stückelberg maximum, whereas the two outer lobes still are associated with the first.

In Fig. 8 we show the evolution of the Floquet distribution $|g_1(k,t)|^2$ during the pulse with maximum amplitude $K_0^{max} = 1.3$. Evidently the outer wings of this distribution move adiabatically, not encountering the avoided-crossing line, whereas the central part jumps to the anticrossing surface with high probability when passing this line, returning later when the line is hit a second time.

We remark that by suitable choices of the frequency one may likewise design pulses which involve higher quasienergy bands: If the Bloch band $n = 1$ is slightly detuned from a multiphoton resonance with a higher band, and if the ac Stark

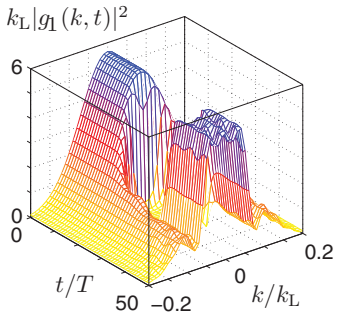

FIG. 8. (Color online) Floquet representation of the evolution of a wave packet initially prepared in the lowest Bloch band, under the action of a nonresonant pulse with $K_0^{\max} = 1.3$. After an initial period of almost adiabatic motion, the center of the distribution undergoes partial Landau-Zener transitions to the anticrossing surface depicted in Fig. 7, and later returns to the initial surface, subject to Stückelberg oscillations.

shift forces the quasienergy surfaces emerging from these two bands into an anticrossing, one can exploit the corresponding multiphotonlike Landau-Zener transitions in the same manner as in the example considered here.

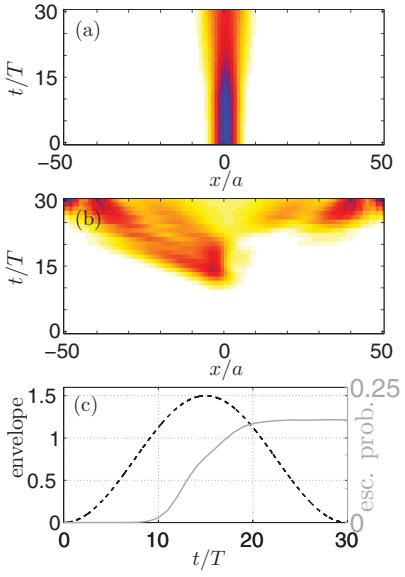

FIG. 9. (Color online) Contour plot of the real-space density $|\psi_1(x,t)|^2$ associated with the lowest Bloch energy band (a), and of the density $|\psi_2(x,t)|^2$ associated with the first excited band (b), as resulting from a pulse with $\hbar\omega/E_r = 1.640$, $K_0^{\max} = 1.5$, and $T/T_P = 30$. The phase φ in Eq. (27) has been set to zero. (c) shows the gradual loss of population from the lowest band.

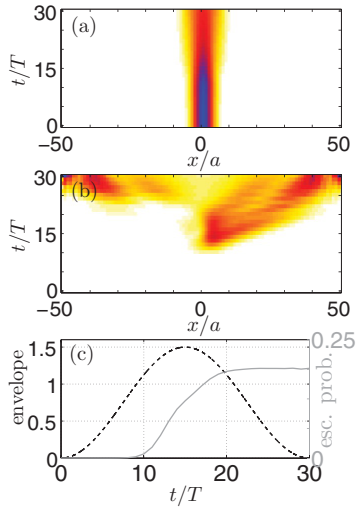

FIG. 10. (Color online) As Fig. 9, but for $\varphi = \pi$.

IV. PHASE EFFECTS

The solutions to the quasienergy eigenvalue equation (15) refer to perfectly periodic driving, and thus do not change when the force $F(t) = F_{ac}\sin(\omega t)$ is replaced by $F(t) = F_{ac}\sin(\omega t + \varphi)$, except for a trivial shift of the time coordinate. Accordingly, as long as the pulse dynamics are fully adiabatic they are not affected by the phase φ. This is different, however, under nonadiabatic conditions. Then the transitions effectuated by a pulse may strongly depend on φ, so that this phase offers an additional handle of control. For demonstration, we replace the previous pulses (19) by

$$F(t) = F_{ac}^{\max} s(t)\sin(\omega t + \varphi), \tag{27}$$

maintaining the interval $0 \leqslant t \leqslant T_P$ as the active pulse period and employing the same squared-sine envelope (22) as before. Having set $\omega = 1.640E_r/\hbar$, $K_0^{\max} = 1.5$, and $T = 30T_P$, Fig. 9 shows contour plots of the densities $|\psi_1(x,t)|^2$ and $|\psi_2(x,t)|^2$ associated with the lowest two Bloch bands, together with the transition dynamics, for $\varphi = 0$. Evidently the transfer of probability to the excited band does not proceed symmetrically in space.

Figure 10 then depicts the corresponding results for $\varphi = \pi$. While the distribution $|\psi_2(x,t)|^2$ here is the exact mirror image of that displayed in Fig. 9(b), the depopulation of the lowest band proceeds in exactly the same manner as before. This finding is easily explained: Replacing φ by $\varphi + \pi$, and simultaneously replacing x by $-x$, leaves the interaction term $-F(t)x$ in the Hamiltonian (2) invariant, so that a phase shift by π is equivalent to spatial inversion. Needless to say, one can also select other values of φ and produce results not predictable by simple symmetry considerations. For example, the outcome of a passage through an avoided crossing may depend on the particular instantaneous phase at which this anticrossing is met. More generally, the possible effects of the phase of the carrier frequency with respect to the pulse

envelope closely resemble corresponding effects encountered in laser-atom interaction [46].

V. CONCLUSIONS AND FURTHER VISIONS

In this paper we have discussed mechanisms which govern the response of a single particle in a cosine lattice to pulsed homogeneous forcing, with a view toward controlling weakly interacting Bose-Einstein condensates in shaken optical lattices. While several successful experiments with ultracold atoms in strongly ac-forced optical lattices have already been reported [6–9,11,12,20,21], the systematic exploration of the possibilities of coherent control opened up, e.g., by deliberate pulse shaping, is likely to break new ground in ultracold-atom physics.

This optimistic view is suggested by a simple parallel: Atomic and molecular physics in itself, not invoking the use of lasers, already is a fascinating and important subject, but it becomes infinitely more rich when lasers come into play, allowing one, on the one hand, to do precision spectroscopy, and to perform deliberate state manipulations on the other. By the same token, ultracold atoms in optical lattices offer access to much fundamental physics, but there is a host of further options when applying inertial forces, either in the form of an ac drive for creating dressed matter waves, or in the form of carefully designed pulses in order to exert active coherent control.

Here we have focused on elementary mechanisms of control deriving from pulses with a smooth envelope, leading to adiabatic motion of a wave packet's momentum distribution on quasienergy surfaces created by spatiotemporal Bloch waves and to deviations from adiabaticity which can be purposefully exploited for reaching target states which may not be accessible by other means. The accompanying Floquet picture offers the distinct advantage that it enables one to adapt many concepts developed for the theoretical description of laser-matter interaction, such as the notion of π pulses. In our opinion, the actual implementation and observation of such π pulses with dilute Bose-Einstein condensates in shaken optical lattices constitutes an *experimentum crucis*: If this can be done, many further related control scenarios will be equally viable, also involving variations of the driving frequency.

As a future perspective it seems particularly rewarding to also carry over advanced strategies devised for controlling molecular dynamics and even chemical reactions by specifically engineered laser pulses [25–29]. Such techniques often involve feedback loops for optimizing the pulse characteristics with the help of genetic learning algorithms; this approach is tantamount to "teaching lasers to control molecules" [25]. When working with Bose-Einstein condensates in optical lattices, control pulses can be applied by piezoelectrically juggling the position of a mirror which reflects the lattice-generating laser beam back into itself, thus giving rise to a moving standing light wave in the laboratory frame, and to a corresponding inertial force in the comoving frame of reference. By sheer analogy, one then would "teach mirrors to control condensates." In this manner one could assess the "reachability problem" for condensates in optical lattices and explore whether one can reach any preselected final-state distribution with the help of a proper pulse sequence. In particular, it would be of major interest to apply such strategies for creating mesoscopic Schrödinger-cat-like states, that is, quantum superposition states of condensates.

ACKNOWLEDGMENTS

This work was supported by the Deutsche Forschungsgemeinschaft under Grant No. Ho 1771/6.

[1] M. Greiner, O. Mandel, T. Esslinger, T. W. Hänsch, and I. Bloch, Nature (London) **415**, 39 (2002).
[2] O. Morsch and M. Oberthaler, Rev. Mod. Phys. **78**, 179 (2006).
[3] M. Lewenstein, A. Sanpera, V. Ahufinger, B. Damski, A. Sen, and U. Sen, Adv. Phys. **56**, 243 (2007).
[4] I. Bloch, J. Dalibard, and W. Zwerger, Rev. Mod. Phys. **80**, 885 (2008).
[5] K. Drese and M. Holthaus, Phys. Rev. Lett. **78**, 2932 (1997).
[6] H. Lignier, C. Sias, D. Ciampini, Y. Singh, A. Zenesini, O. Morsch, and E. Arimondo, Phys. Rev. Lett. **99**, 220403 (2007).
[7] A. Eckardt, M. Holthaus, H. Lignier, A. Zenesini, D. Ciampini, O. Morsch, and E. Arimondo, Phys. Rev. A **79**, 013611 (2009).
[8] C. Sias, H. Lignier, Y. P. Singh, A. Zenesini, D. Ciampini, O. Morsch, and E. Arimondo, Phys. Rev. Lett. **100**, 040404 (2008).
[9] A. Zenesini, H. Lignier, D. Ciampini, O. Morsch, and E. Arimondo, Phys. Rev. Lett. **102**, 100403 (2009).
[10] A. Eckardt, C. Weiss, and M. Holthaus, Phys. Rev. Lett. **95**, 260404 (2005).
[11] J. Struck, C. Ölschläger, R. Le Targat, P. Soltan-Panahi, A. Eckardt, M. Lewenstein, P. Windpassinger, and K. Sengstock, Science **333**, 996 (2011).
[12] Y.-A. Chen, S. Nascimbène, M. Aidelsburger, M. Atala, S. Trotzky, and I. Bloch, Phys. Rev. Lett. **107**, 210405 (2011).
[13] K. Kudo, T. Boness, and T. S. Monteiro, Phys. Rev. A **80**, 063409 (2009).
[14] A. Tokuno and T. Giamarchi, Phys. Rev. Lett. **106**, 205301 (2011).
[15] N. Tsuji, T. Oka, P. Werner, and H. Aoki, Phys. Rev. Lett. **106**, 236401 (2011).
[16] M. Holthaus, Phys. Rev. A **64**, 011601 (2001).
[17] D. Poletti and C. Kollath, Phys. Rev. A **84**, 013615 (2011).
[18] V. V. Ivanov, A. Alberti, M. Schioppo, G. Ferrari, M. Artoni, M. L. Chiofalo, and G. M. Tino, Phys. Rev. Lett. **100**, 043602 (2008).
[19] M. Gustavsson, E. Haller, M. J. Mark, J. G. Danzl, G. Rojas-Kopeinig, and H.-C. Nägerl, Phys. Rev. Lett. **100**, 080404 (2008).
[20] A. Alberti, V. V. Ivanov, G. M. Tino, and G. Ferrari, Nat. Phys. **5**, 547 (2009).

[21] E. Haller, R. Hart, M. J. Mark, J. G. Danzl, L. Reichsöllner, and H.-C. Nägerl, Phys. Rev. Lett. **104**, 200403 (2010).
[22] S. Arlinghaus and M. Holthaus, Phys. Rev. A **81**, 063612 (2010).
[23] S. Arlinghaus and M. Holthaus, Phys. Rev. B **84**, 054301 (2011).
[24] L. Allen and J. H. Eberly, *Optical Resonance and Two-Level Atoms* (Dover, New York, 1987).
[25] R. S. Judson and H. Rabitz, Phys. Rev. Lett. **68**, 1500 (1992).
[26] S. A. Rice, Science **258**, 412 (1992).
[27] A. Assion, T. Baumert, M. Bergt, T. Brixner, B. Kiefer, V. Seyfried, M. Strehle, and G. Gerber, Science **282**, 919 (1998).
[28] M. Shapiro and P. Brumer, Rep. Prog. Phys. **66**, 859 (2003).
[29] T. Baumert, Nat. Phys. **7**, 373 (2011).
[30] R. Graham, M. Schlautmann, and P. Zoller, Phys. Rev. A **45**, R19 (1992).
[31] J. Callaway, *Quantum Theory of the Solid State* (Academic Press, New York, 1976).
[32] N. W. Ashcroft and N. D. Mermin, *Solid State Physics* (Harcourt, Fort Worth, 1976), Chap. 12.
[33] C. Kittel, *Quantum Theory of Solids*, 2nd rev. ed. (Wiley, New York, 1987).
[34] G. Floquet, Ann. Scit. Ec. Normale Super. **12**, 47 (1883).
[35] M. S. P. Eastham, *The Spectral Theory of Periodic Differential Equations*, Texts in Mathematics (Scottish Academic Press, Edinburgh, 1973).
[36] P. Kuchment, *Floquet Theory for Partial Differential Equations* (Birkhäuser, Basel, 1993).
[37] Ya. B. Zel'dovich, Zh. Eksp. Teor. Fiz. **51**, 1492 (1966) [Sov. Phys. JETP **24**, 1006 (1967)].
[38] S. I. Chu and D. A. Telnov, Phys. Rep. **390**, 1 (2004).
[39] H. Sambe, Phys. Rev. A **7**, 2203 (1973).
[40] K. Drese and M. Holthaus, Eur. Phys. J. D **5**, 119 (1999).
[41] M. Born and R. Oppenheimer, Ann. Phys. **389**, 457 (1927).
[42] M. Born and V. Fock, Z. Phys. **51**, 165 (1928).
[43] M. V. Berry, Proc. R. Soc. London, Ser. A **392**, 45 (1984).
[44] M. Holthaus and B. Just, Phys. Rev. A **49**, 1950 (1994).
[45] E. C. G. Stückelberg, Helv. Phys. Acta **5**, 369 (1932).
[46] G. G. Paulus, F. Grasbon, H. Walther, P. Villoresi, M. Nisoli, S. Stagira, E. Priori, and S. De Silvestri, Nature (London) **414**, 182 (2001).

V

V. ac Stark shift and multiphoton-like resonances in low-frequency driven optical lattices

Stephan Arlinghaus and Martin Holthaus,
ac Stark shift and multiphoton-like resonances in low-frequency driven optical lattices,
Preprint.

ac Stark shift and multiphoton-like resonances in low-frequency driven optical lattices

Stephan Arlinghaus and Martin Holthaus
Institut für Physik, Carl von Ossietzky Universität, D-26111 Oldenburg, Germany
(Dated: March 11, 2012)

We suggest that Bose-Einstein condensates in pulsed optical lattices may provide detailed experimental access to multiphoton-like transitions between ac-Stark-shifted Bloch bands. Such transitions correspond to resonances described theoretically by avoided quasienergy crossings. We show that the width of such anticrossings can be inferred from measurements involving asymmetric pulses. We also introduce a pulse tracking strategy for locating the particular driving amplitudes for which resonances occur. Our numerical calculations refer to a currently existing experimental set-up [Haller *et al.*, PRL **104**, 200403 (2010)].

PACS numbers: 42.50.Hz, 67.85.Hj, 03.75.Kk

The study of multiphoton excitation and ionization processes so far has concerned the interaction of matter with strong electromagnetic fields [1–4]. In the present proposal we demonstrate that ideas and concepts developed in this field of research can also be applied for understanding the response of ultracold macroscopic matter waves in optical lattices to pulse-like forcing. Such systems offer additional handles of control which are not available in experiments with atoms or molecules exposed to pulses of laser radiation. Therefore, they can give novel insights into multiphoton dynamics in general, and in particular may also allow one to systematically investigate the effects of interparticle interactions on such dynamics.

The experimental investigation of Bose-Einstein condensates (BECs) in time-periodically forced optical lattices has been pushed forward with remarkable vigor within the last years, addressing quite diverse topics such as parametric amplification of matter waves [5], dynamic localization [6, 7], photon-assisted tunneling [8], coherent control of the superfluid-to-Mott insulator transition [9], quantum ratchets [10], super Bloch oscillations [11], quantum simulation of frustrated magnetism [12], controlled correlated tunneling [13, 14], and even the realization of tunable gauge potentials [15]. The present theoretical study of multiphoton-like condensate dynamics refers to conditions recently realized by Haller *et al.* [11]: These authors have loaded BECs of Cs atoms into a vertically oriented 1D optical lattice $V(x) = (V_0/2)\cos(2k_{\rm L}x)$. Here $k_{\rm L} = 2\pi/\lambda_{\rm L}$, where $\lambda_{\rm L} = 1064.49$ nm is the wavelength of the lattice-generating laser light, so that the lattice period is $d = \pi/k_{\rm L}$. We choose a comparatively shallow lattice with depth $V_0 = 2.3\,E_{\rm r}$, where $E_{\rm r} = (\hbar k_{\rm L})^2/(2m)$ is the single-photon recoil energy [16], with m denoting the mass of the Cs atoms. Using a magnetically induced Feshbach resonance, the s-wave scattering length of these atoms is tuned to zero [17], so that one is dealing with a condensate of effectively noninteracting particles. By means of a time-periodic modulation of the levitation gradient employed for compensating gravity, an external oscillating force is introduced which acts on the atoms with maximum amplitude $F_{\rm max}$ and frequency $\nu = \omega/(2\pi)$, such that their dynamics are governed by the Hamiltonian

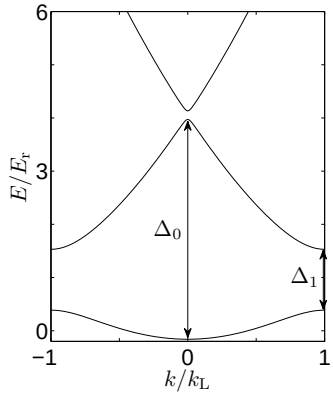

FIG. 1: Energy band structure of an unperturbed optical cosine lattice with depth $V_0 = 2.3\,E_{\rm r}$. Measured in terms of the photon energy $\hbar\omega = 0.23\,E_{\rm r}$, as corresponding to the driving frequency $\omega/(2\pi) = 300$ Hz, the gap between the lowest two bands is $\Delta_1 = 5.05\,\hbar\omega$ at the Brillouin zone edge, and $\Delta_0 = 18.24\,\hbar\omega$ at its center.

$$H(t) = \frac{p^2}{2m} + V(x) - s(t)F_{\rm max}x\cos(\omega t) \qquad (1)$$

with a dimensionless shape function $s(t)$ determining the envelope of the pulses applied. All calculations reported here are performed for the relatively low frequency $\omega/(2\pi) = 300$ Hz, so that $\hbar\omega = 0.23\,E_{\rm r}$. As indicated in Fig. 1, this means that the gap $\Delta_1 = 1.14\,E_{\rm r}$ between the lowest two Bloch bands $E_1(k)$ and $E_2(k)$ of the unperturbed optical lattice, which occurs at the Brillouin zone edge $k/k_{\rm L} = \pm 1$, amounts to $5.05\,\hbar\omega$: Exciting particles from the initially occupied lowest band to the first excited one requires the absorption of more than five "photons".

A first glimpse at the condensate dynamics under the action of a force $F(t)$ is provided by Bloch's acceleration

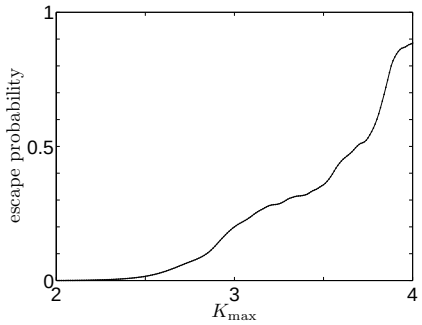

FIG. 2: Interband transition probabilities after pulses with the squared-sine envelope (3) and length $T_{\rm p} = 60 \times 2\pi/\omega$, obtained from numerical solutions of the Schrödinger equation. All atoms which are excited to bands $n > 1$ after a pulse are assumed to escape from the lattice.

theorem: The expectation value $\langle k \rangle(t)$ of an atomic wave packet in k-space evolves in time according to

$$\hbar \frac{\mathrm{d}}{\mathrm{d}t} \langle k \rangle(t) = F(t) \,, \tag{2}$$

provided interband transitions remain negligible [18]. Assuming a sinusoidal force $F(t) = F \cos(\omega t)\Theta(t)$ instantaneously switched on at time $t = 0$, this gives $\langle k \rangle(t)/k_{\rm L} = \langle k \rangle(0)/k_{\rm L} + (K/\pi)\sin(\omega t)$, where $K = Fd/(\hbar\omega)$ is a dimensionless measure of the driving amplitude. Thus, when considering a wave packet initially at rest in the lowest band, so that $\langle k \rangle(0)/k_{\rm L} = 0$, the packet's center $\langle k \rangle(t)$ just reaches the Brillouin zone edge when $K = \pi$. Because the zone edge gives rise to Zener-type transitions [19], one then expects pronounced excitation of higher bands. Therefore, one has $K \approx \pi$ as a rough order-of-magnitude estimate of the amplitude required for inducing multiphoton-like transitions.

This expectation is confirmed by the numerical calculations summarized in Fig. 2. Here we consider driving pulses $s(t)F_{\max}\cos(\omega t)$ as already incorporated into the Hamiltonian (1), with a smooth envelope

$$s(t) = \sin^2(\pi t/T_{\rm p}) \quad ; \quad 0 \le t \le T_{\rm p} \,. \tag{3}$$

The pulse length is fixed at 60 driving cycles, $T_{\rm p} = 60\,T$ with $T = 2\pi/\omega$. In order to model the dynamics of a noninteracting BEC responding to such pulses, we start with an initial state

$$\psi(x,0) = \sqrt{\frac{d}{2\pi}} \int \mathrm{d}k \, g_1(k,0) \chi_{1,k}(x) \tag{4}$$

made up from Bloch waves $\chi_{1,k}(x)$ of the lowest band, employing a Gaussian momentum distribution

$$g_1(k,0) = \left(\sqrt{\pi}\Delta k\right)^{-1/2} \exp\left(-\frac{[k - \langle k \rangle(0)]^2}{2\,(\Delta k)^2}\right) \tag{5}$$

centered around $\langle k \rangle(0)/k_{\rm L} = 0$ with width $\Delta k/k_{\rm L} = 0.1$, and then solve the single-particle Schrödinger equation by means of a Crank-Nicolson algorithm [20]. Varying the maximum scaled amplitude $K_{\max} = F_{\max}d/(\hbar\omega)$ from pulse to pulse, we plot the escape probability from the lattice at the end of each pulse, at $t = T_{\rm p}$. Here we assume that only atoms which finally still populate the lowest band remain in the lattice, since atoms which have been excited to higher bands tend to escape from the shallow lattice quite fast; for later comparison with actual experimental data it should be borne in mind that a part of the excited atoms may still be present in the lattice at $t = T_{\rm p}$. Evidently, interband transitions start to make themselves felt at $K_{\max} \approx 2.5$, and reach substantial strength when $K_{\max} \approx 3$, confirming the above rough estimate. Thus, proof-of-principle experiments performed along these lines should establish the feasibility of using BECs in driven optical lattices as novel probes for multiphoton-like transitions.

In a second step, this tool can be employed for getting more detailed insight into multiphoton dynamics. Namely, the single-band acceleration theorem (2) ignores an essential element: Not only does the wave packet's center $\langle k \rangle(t)$ move within its band in response to the external forcing, but also the bands themselves are "dressed" by the drive, and therefore experience an ac Stark shift [21]. Hence, initially nonresonant bands may be shifted such that their separation in energy approaches an integer multiple of $\hbar\omega$ for certain Bloch wavenumbers k, possibly leading to strong resonant interband coupling, that is, to a multiphoton resonance. Theoretically, such resonances are found by computing the quasienergy bands $\varepsilon_n(k)$ which emerge from the energy bands $E_n(k)$ in the presence of a drive with constant amplitude. These quasienergy bands reflect the ac-Stark-shifted energy bands, projected into an interval of width $\Delta\varepsilon = \hbar\omega$, so that a multiphoton resonance translates into an avoided quasienergy crossing [4, 21]. For example, Fig. 3 shows the quasienergies $\varepsilon_n(0)$ with $n = 1, 2, 3$ which pertain to the pulses considered in Fig. 2, plotted versus the scaled amplitude K. The quasienergy originating from the ground state $E_1(0)$ of the optical lattice undergoes two well-resolved avoided crossings when $K > 3$, signaling the presence of two individual multiphoton resonances. The observation that these "large" resonances begin to show up only for $K \approx \pi$ nicely relates the elaborate quasienergy approach to the previous elementary reasoning based on Eq. (2).

Inspecting that elementary reasoning once again, one expects multiphoton resonances to occur for smaller driving amplitudes when the initial packet is centered around a nonzero wavenumber, $\langle k \rangle(0)/k_{\rm L} \neq 0$, since then smaller amplitudes are required for reaching the Brillouin zone edge. This expectation is confirmed by Fig. 4, which depicts quasienergies $\varepsilon_n(k)$ for $k/k_{\rm L} = 0.8$, with the first resonance showing up already at $K \approx 0.9$. Ex-

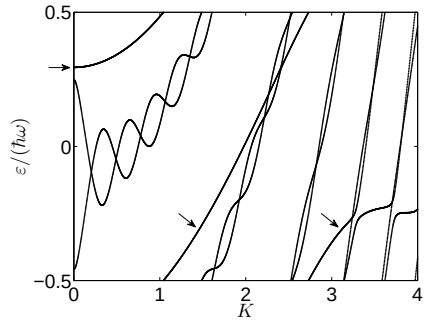

FIG. 3: Quasienergies $\varepsilon_n(0)$ at the center of the Brillouin zone for an optical lattice with depth $V_0/E_\mathrm{r} = 2.3$, driven with scaled frequency $\hbar\omega/E_\mathrm{r} = 0.23$. The quasienergy originating from the lowest band $n = 1$ is marked by the arrows. It exhibits a substantial ac Stark shift, and undergoes pronounced avoided crossings for $K > 3$.

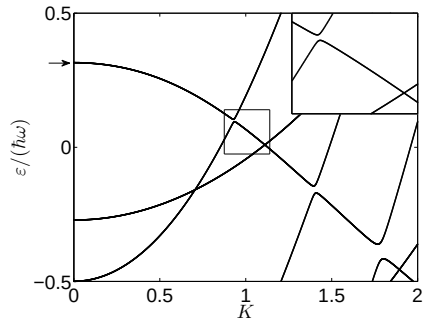

FIG. 4: Quasienergies $\varepsilon_n(k)$ for $k/k_\mathrm{L} = 0.8$ and $n = 1, 2, 3$. The arrow indicates the quasienergy originating from the lowest energy band $n = 1$.

perimentally, one can prepare an initial state with arbitrary $\langle k\rangle(0)$ by subjecting the condensate to a suitable "kick" [22]. Thus, one should also be able to detect the resonances predicted by Fig. 4. To this end, we propose a particular kind of "avoided-level-crossing spectroscopy" based on the use of *asymmetric* pulses $s(t)$. For illustration, we assume that the rising part of such pulses be given by the first half of the envelope (3), with fixed switch-on time $T_\mathrm{p}^{(1)}/2 = 5\,T$, while their decreasing part is described by the second half of a squared-sine envelope, but with a different switch-off time $T_\mathrm{p}^{(2)}/2$. The maximum scaled amplitude is $K_\mathrm{max} = 1.2$. During the rising part of such a pulse, a wave packet initially centered around $\langle k\rangle(0)/k_\mathrm{L} = 0.8$ then follows its quasienergy states adiabatically, until the instantaneous amplitude reaches the multiphoton resonance at $K \approx 0.9$ visible in

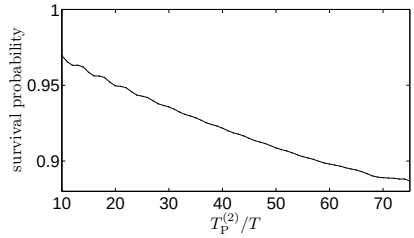

FIG. 5: Survival probability of atoms in the lowest band after asymmetric pulses with fast switch-on time $T_\mathrm{p}^{(1)}/2 = 5\,T$, and with varying switch-off durations $T_\mathrm{p}^{(2)}/2$. The initial packets were centered around $\langle k\rangle(0)/k_\mathrm{L} = 0.8$, so that the dynamics are determined by the spectrum shown in Fig. 4; $K_\mathrm{max} = 1.2$ for all pulses.

Fig. 4. Then the packet undergoes a Landau-Zener transition to the anticrossing quasienergy states [23]. Due to the rapid switch-on of the pulse, and to the narrow quasienergy separation $\delta\varepsilon$ at the avoided crossing, that transition is almost complete. Thereafter, the packet again adiabatically follows the pulse envelope, until the resonance is encountered a second time when the amplitude decreases. If then $T_\mathrm{p}^{(2)} \gg T_\mathrm{p}^{(1)}$, a major part of the wave function does not "jump over" the avoided crossing back to the initial state, but rather stays in the continuously connected quasienergy states. This implies that a major fraction of the condensate atoms is excited at the end of the pulse, escaping out of the lattice. When such an experiment is performed repeatedly with fixed rise time $T_\mathrm{p}^{(1)}/2$ while varying the switch-off duration $T_\mathrm{p}^{(2)}/2$, one should observe survival probabilities which drop exponentially with increasing $T_\mathrm{p}^{(2)}$, allowing one to extract the quasienergy separation $\delta\varepsilon$ at the avoided crossing from the drop rate by means of the known Landau-Zener formula for quasienergy states [23].

The results of a series of solutions to the Schrödinger equation corresponding to this scenario are plotted in Fig. 5. From the slope of the numerical data we deduce a quasienergy gap $\delta\varepsilon/(\hbar\omega) = 0.0099$, in perfect agreement with the value 0.01 read off from Fig. 4. These findings clearly underline that this quasienergy gap $\delta\varepsilon \ll \hbar\omega$ is the actually relevant energy scale for the multiphoton transitions under scrutiny here, *not* the band separation $\Delta_1 = 5.05\,\hbar\omega$ indicated in Fig. 1.

There are further options offered by BECs in driven optical lattices which have no match in laser-based multiphoton studies. For example, one can switch off the driving force abruptly at any moment, and analyze the state of the wave packet at that particular instant. Specifically, we again utilize envelopes of the form (3), and let the amplitude rapidly drop to zero at some instant T_out, with $0 < T_\mathrm{out} < T_\mathrm{p}/2$. We set $T_\mathrm{p} = 60\,T$ and take initial wave packets with $\langle k\rangle(0)/k_\mathrm{L} = 0$, as for the previous calcula-

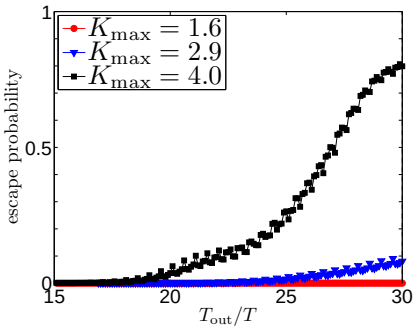

FIG. 6: (color online) Pulse tracking realized by switching off the squared-sine envelope (3) with $T_{\rm p} = 60\,T$ abruptly at $t = T_{\rm out}$, and recording the escape probability at this moment. The onset of interband transitions then reveals the presence of a multiphoton resonance at the instantaneous amplitude reached at $t = T_{\rm out}$.

tions shown in Fig. 2, and plot the escape probabilities versus switch-off time $T_{\rm out}$ in Fig. 6. For $K_{\max} = 1.6$ the wave packet simply follows its quasienergy states adiabatically, not encountering any of the resonances observed in Fig. 3. However, for $K_{\max} = 2.9$ interband transitions set in at $T_{\rm out} \approx 25\,T$, that is, when the instantaneous amplitude reaches $K = K_{\max} s(T_{\rm out}) \approx 2.7$; this is due to a tiny resonance not resolved in Fig. 3. When $K_{\max} = 4.0$, pronounced interband transitions occur at $T_{\rm out} \approx 20\,T$, corresponding to the instantaneous amplitude $K \approx 3$: This is already in the regime of influence of the first of the two "large" resonances seen in Fig. 3. Thus, this "pulse tracking" strategy allows one to experimentally detect multiphoton resonances, that is, to find those values of the driving amplitude for which strong resonant interband transitions occur.

To summarize, we have argued that BECs in pulsed optical lattices can be employed for mimicking multiphoton processes. The enormous degree of controllability realizable with pulsed optical lattices enables one to obtain information not reachable with laser-irradiated crystalline solids; in particular, we have suggested the use of asymmetric pulses for performing avoided quasienergy crossing spectroscopy. Moreover, we have shown how pulse tracking by abruptly switching off the driving amplitude allows one to monitor the dynamics at each moment during an individual pulse, and thus to locate multiphoton resonances between ac-Stark-shifted Bloch bands. Obviously, our approach also lends itself to systematic explorations of the effects of pulse shaping. Even more interestingly, one can activate interparticle interactions by suitably tuning the s-wave scattering length of the Cs atoms [17]. Hence, the detailed experimental investigation of the influence of such interactions on multiphoton transitions has come into immediate reach.

We are indebted to E. Haller for detailed discussions, and for performing preliminary measurements confirming the viability of our suggestions. We also acknowledge support from the Deutsche Forschungsgemeinschaft under grant No. HO 1771/6.

[1] G. Mainfray and G. Manus, Rep. Prog. Phys. **54**, 1333 (1991).
[2] C. Cohen-Tannoudji, J. Dupont-Roc, and G. Grynberg, *Atom-Photon Interactions* (Wiley-Interscience, New York, 1992).
[3] N. B. Delone and V. P. Krainov, *Multiphoton Processes in Atoms* (Springer-Verlag, Berlin, 2000).
[4] S. I. Chu and D. A. Telnov, Phys. Rep. **390**, 1 (2004).
[5] N. Gemelke, E. Sarajlic, Y. Bidel, S. Hong, and S. Chu, Phys. Rev. Lett. **95**, 170404 (2005).
[6] H. Lignier, C. Sias, D. Ciampini, Y. Singh, A. Zenesini, O. Morsch, and E. Arimondo, Phys. Rev. Lett. **99**, 220403 (2007).
[7] A. Eckardt, M. Holthaus, H. Lignier, A. Zenesini, D. Ciampini, O. Morsch, and E. Arimondo, Phys. Rev. A **79**, 013611 (2009).
[8] C. Sias, H. Lignier, Y. P. Singh, A. Zenesini, D. Ciampini, O. Morsch, and E. Arimondo, Phys. Rev. Lett. **100**, 040404 (2008).
[9] A. Zenesini, H. Lignier, D. Ciampini, O. Morsch, and E. Arimondo, Phys. Rev. Lett. **102**, 100403 (2009).
[10] T. Salger, S. Kling, T. Hecking, C. Geckeler, L. Morales-Molina, and M. Weitz, Science **326**, 1241 (2009).
[11] E. Haller, R. Hart, M. J. Mark, J. G. Danzl, L. Reichsöllner, and H.-C. Nägerl, Phys. Rev. Lett. **104**, 200403 (2010).
[12] J. Struck, C. Ölschläger, R. Le Targat, P. Soltan-Panahi, A. Eckardt, M. Lewenstein, P. Windpassinger, and K. Sengstock, Science **333**, 996 (2011).
[13] R. Ma, M. E. Tai, P. M. Preiss, W. S. Bakr, J. Simon, and M. Greiner, Phys. Rev. Lett. **107**, 095301 (2011).
[14] Y.-A. Chen, S. Nascimbène, M. Aidelsburger, M. Atala, S. Trotzky, and I. Bloch, Phys. Rev. Lett. **107**, 210405 (2011).
[15] J. Struck, C. Ölschläger, M. Weinberg, P. Hauke, J. Simonet, A. Eckardt, M. Lewenstein, K. Sengstock, and P. Windpassinger, arXiv:1203.0049.
[16] O. Morsch and M. K. Oberthaler, Rev. Mod. Phys. **78**, 179 (2006).
[17] T. Köhler, K. Góral, and P. S. Julienne, Rev. Mod. Phys. **78**, 1311 (2006).
[18] F. Bloch, Z. Phys. **52**, 555 (1929).
[19] C. Zener, Proc. R. Soc. Lond. A **145**, 523 (1934).
[20] J. Crank and P. Nicolson, Proc. Camb. Phil. Soc. **43**, 50 (1947).
[21] S. Arlinghaus and M. Holthaus, Phys. Rev. B **84**, 054301 (2011).
[22] E. Haller, private communication.
[23] K. Drese and M. Holthaus, Eur. Phys. J. D **5**, 119 (1999).

Accuracy of Statement

Hereby I certify that the information provided by the author regarding his contributions to the publications (see pages 121–124) is correct.

(Date) (Prof. Dr. M. Holthaus)

Declaration

Hereby I certify that this dissertation has been composed by me alone and is based on my own work, unless stated otherwise. Material from published or unpublished work of others, which is referred to in the dissertation, is credited to the author in the text.

(Date) (S. Arlinghaus)

Curriculum Vitae

Education

2009–Current **Doctoral Student, Physics**, *University of Oldenburg, Germany*,
Area of research: Coherent control of time-periodically driven quantum systems
Expected time of receiving the Doctoral degree: April 2012.

2009 **Diploma (equivalent to Masters degree), Physics**,
University of Oldenburg, Germany, *Condensed matter theory group*.
Thesis: "Bose-Einstein-Kondensate in einer Doppelmulde: Kohärente Kontrolle des Tunneleffektes" (Translation: "Bose-Einstein condensates in a double-well: Coherent control of quantum tunnelling").

Publications – Peer Reviewed

2011 **Stephan Arlinghaus** and Martin Holthaus: *Controlled wave-packet manipulation with driven optical lattices*, Phys. Rev. A **84**, 063617 (2011).

2011 **Stephan Arlinghaus** and Martin Holthaus: *Generalized acceleration theorem for spatiotemporal Bloch waves*, Phys. Rev. B **84**, 054301 (2011).

2010 **Stephan Arlinghaus** and Martin Holthaus: *Driven optical lattices as strong-field simulators*, Phys. Rev. A **81**, 063612 (2010).

2010 Bettina Gertjerenken, **Stephan Arlinghaus**, Niklas Teichmann, and Christoph Weiss: *Reproducible mesoscopic superpositions of Bose-Einstein condensates and mean-field chaos*, Phys. Rev. A **82**, 023620 (2010).

Other Publications

2012 **Stephan Arlinghaus** and Martin Holthaus: *ac Stark shift and multiphoton-like resonances in low-frequency driven optical lattices*, Preprint.

2011 **Stephan Arlinghaus**, Matthias Langemeyer, and Martin Holthaus: *Dynamic localization in optical lattices* in: Dynamical Tunneling - Theory and Experiment, (S. Keshavamurthy and P. Schlagheck, eds.), Chapter 12 (Taylor and Francis CRC, 2011).

Professional Presentations

2011 **Wave-packet surgery in driven optical lattices**, *Spring meeting of the German Physical Society*, March 2011, Dresden, Germany.

2010 **Angetriebene optische Gitter als Starkfeld-Simulatoren**, *Theoretical Physics Colloquium*, May 2010, Oldenburg, Germany.
(Translation: Driven optical lattices as strong-field simulators)

2010 **Multiphoton-like transitions in driven optical lattices**, *Spring meeting of the German Physical Society*, March 2010, Hannover, Germany.

Professional Memberships

Member of the German Physical Society

Trainings And Courses

2011 **Workshop "How to publish in peer-reviewed journals"**,
Oldenburg, Germany.

2010 **Summer School "Quo vadis Bose-Einstein condensation?"**,
Max-Planck-Institut Dresden, Germany.

2009 **Summer School "Introductory Course on Ultracold Quantum Gases"**,
University of Innsbruck, Austria.

Acknowledgments

First and foremost, I would like to thank my supervisor Prof. Dr. Martin Holthaus for his constant support. His intuitive understanding of physics, his passion for his work, and his gift to explain complex subjects in a simple yet precise way, greatly encouraged me in my work. I consider myself fortunate to have an adviser who granted me the freedom to explore my own ideas and who at the same time provided the guidance I needed not to veer off course.

My special thanks go to my colleagues Bettina Gertjerenken, Matthias Langemeyer, Dr. Felix Rüting, Kirsten Stiebler, Dr. Svend-Age Biehs, Dennis Hinrichs, and Maria Tschikin, who it was always fun to work with. The pleasant yet productive working atmosphere surely contributed to the success of this work. Stimulating scientific discussions but also the occasional movie nights make me look back with pleasure on these last few years in the Condensed Matter Theory Group.

For their efforts to carefully proofread parts of this thesis and for providing valuable comments, I am indebted to Matthias Langemeyer, Bettina Gertjerenken, and Dr. Anna Wirtz. In addition, I would like to thank Stefan Krautwald and Frauke Ahrens: Their speedy and competent support in any administrative issues surely helped me to stay focused on my research.

This thesis would not have been possible without the assistance and constant support of my parents, who greatly encouraged me on my way

and always listened to my problems. They are the reason why I am a physicist today.

Last but not least, I wish to express my deep gratitude to Anna for her loving encouragement and strong support over the past years. She endured my incessant ramblings on physics and without her, this thesis would not have been possible.